New specimens and species of the Oligocene toothed baleen whale *Coronodon* from South Carolina and the origin of Neoceti (#78092)

First submission

Guidance from your Editor

Please submit by 24 Oct 2022 for the benefit of the authors (and your token reward) .



Structure and Criteria

Please read the 'Structure and Criteria' page for general guidance.



Custom checks

Make sure you include the custom checks shown below, in your review.



Author notes

Have you read the author notes on the guidance page?



Raw data check

Review the raw data.



Image check

Check that figures and images have not been inappropriately manipulated.

Privacy reminder: If uploading an annotated PDF, remove identifiable information to remain anonymous.

Files

Download and review all files from the <u>materials page</u>.

40 Figure file(s)

- 11 Table file(s)
- 1 Raw data file(s)
- 2 Other file(s)



New species checks

- ! Have you checked our <u>new species policies</u>?
- Do you agree that it is a new species?
- Is it correctly described e.g. meets ICZN standard?

Structure and Criteria



Structure your review

The review form is divided into 5 sections. Please consider these when composing your review:

- 1. BASIC REPORTING
- 2. EXPERIMENTAL DESIGN
- 3. VALIDITY OF THE FINDINGS
- 4. General comments
- 5. Confidential notes to the editor
- You can also annotate this PDF and upload it as part of your review

When ready submit online.

Editorial Criteria

Use these criteria points to structure your review. The full detailed editorial criteria is on your guidance page.

BASIC REPORTING

- Clear, unambiguous, professional English language used throughout.
- Intro & background to show context.
 Literature well referenced & relevant.
- Structure conforms to <u>PeerJ standards</u>, discipline norm, or improved for clarity.
- Figures are relevant, high quality, well labelled & described.
- Raw data supplied (see <u>PeerJ policy</u>).

EXPERIMENTAL DESIGN

- Original primary research within Scope of the journal.
- Research question well defined, relevant & meaningful. It is stated how the research fills an identified knowledge gap.
- Rigorous investigation performed to a high technical & ethical standard.
- Methods described with sufficient detail & information to replicate.

VALIDITY OF THE FINDINGS

- Impact and novelty not assessed.

 Meaningful replication encouraged where rationale & benefit to literature is clearly stated.
- All underlying data have been provided; they are robust, statistically sound, & controlled.



Conclusions are well stated, linked to original research question & limited to supporting results.



Standout reviewing tips



The best reviewers use these techniques

Τ	p

Support criticisms with evidence from the text or from other sources

Give specific suggestions on how to improve the manuscript

Comment on language and grammar issues

Organize by importance of the issues, and number your points

Please provide constructive criticism, and avoid personal opinions

Comment on strengths (as well as weaknesses) of the manuscript

Example

Smith et al (J of Methodology, 2005, V3, pp 123) have shown that the analysis you use in Lines 241-250 is not the most appropriate for this situation. Please explain why you used this method.

Your introduction needs more detail. I suggest that you improve the description at lines 57-86 to provide more justification for your study (specifically, you should expand upon the knowledge gap being filled).

The English language should be improved to ensure that an international audience can clearly understand your text. Some examples where the language could be improved include lines 23, 77, 121, 128 – the current phrasing makes comprehension difficult. I suggest you have a colleague who is proficient in English and familiar with the subject matter review your manuscript, or contact a professional editing service.

- 1. Your most important issue
- 2. The next most important item
- 3. ...
- 4. The least important points

I thank you for providing the raw data, however your supplemental files need more descriptive metadata identifiers to be useful to future readers. Although your results are compelling, the data analysis should be improved in the following ways: AA, BB, CC

I commend the authors for their extensive data set, compiled over many years of detailed fieldwork. In addition, the manuscript is clearly written in professional, unambiguous language. If there is a weakness, it is in the statistical analysis (as I have noted above) which should be improved upon before Acceptance.



New specimens and species of the Oligocene toothed baleen whale *Coronodon* from South Carolina and the origin of Neoceti

Robert W Boessenecker Corresp., 1, 2, Brian L Beatty 3, 4, Jonathan H Geisler 3, 4

Corresponding Author: Robert W Boessenecker Email address: boesseneckerrw@cofc.edu

Baleen whales (Mysticeti) are gigantic filter-feeding cetaceans possessing the unique soft tissue structure baleen and lacking adult teeth; Oligocene fossils have revealed a wealth of early diverging tooth-bearing mysticetes highlighting the transition from archaeocete ancestors to early toothless baleen-bearing eomysticetid whales. The archaeocete-like, toothed mysticete Coronodon havensteini from the lower Oligocene Ashley Formation of South Carolina possesses a number of peculiar aspects of feeding morphology suggesting dental filter-feeding in the earliest diverging mysticete lineage. New fossils of *Coronodon* are described in detail, including 1) supplementary description of the holotype skull and skeleton of Coronodon havensteini; 2) description of two new juvenile skulls of C. havensteini and a partial skull and postcranial skeleton of an adult; 3) description of the new species Coronodon planifrons n.sp.; and 4) description of the new species Coronodon newtoni. New specimens of Coronodon havensteini include a partial adult skeleton preserving new elements for the species including incisors, numerous upper premolars and molars, lower m4, scapula, lumbar, and caudal vertebrae, and two juvenile skulls with tympanoperiotics and teeth. Fossils from the overlying unit, the Chandler Bridge Formation, represent two new species: Coronodon newtoni n. sp. and Coronodon planifrons n. sp. *Coronodon newtoni* possesses a concave-up alveolar profile, a mandibular condyle elevated far above the toothrow, and a gracile periotic resembling those of juvenile C. havensteini. Coronodon planifrons n. sp. possesses a horizontal supraorbital process, successively smaller upper molars, massively inflated periotic, and longer intertemporal region. Coronodon planifrons n. sp. preserves one of the most complete vertebral columns among toothed mysticetes, indicating nine thoracic vertebrae, ten lumbar vertebrae, and at least 20 caudal vertebrae. The column exhibits a somewhat stabilized caudal peduncle

¹ Mace Brown Museum of Natural History, College of Charleston, Charleston, SC, United States

² University of California Museum of Paleontology, University of California, Berkeley, Berkeley, California, United States

³ Department of Anatomy, New York Institute of Technology, Old Westbury, New York, United States

 $^{^{}m 4}$ Department of Paleobiology, National Museum of Natural History, Washington, D.C., USA



with enlarged lumbocaudal vertebrae, and rectangular terminal caudals indicate the presence of tail flukes. Juvenile skulls reveal several ontogenetic trends in *Coronodon havensteini*, including the anterior migration of the orbitotemporal crest, anteroposterior elongation of the intertemporal region, inflation of the body of the periotic, enlargement of the tympanic bulla, and continued postnatal emergence of the premolars and molars from their alveoli. Disarticulated skulls suggest a degree of rostral kinesis in this genus. Phylogenetic analysis of the largest assembled supermatrix of Mysticeti (n=138 OTUs; four archaeocetes, ten odontocetes, 124 mysticetes; 391 morphological and 27225 molecular characters) confirms placement of *Coronodon* as the earliest diverging lineage of Mysticeti under equally weighted analyses whereas implied weighting places *Coronodon* and similar taxa outside Neoceti, prompting a review of character transformations at the base of Neoceti.



- 1 New specimens and species of the Oligocene toothed baleen whale Coronodon from South
- 2 Carolina and the origin of Neoceti
- 3 Robert W. Boessenecker^{1,2}
- 4 Brian L. Beatty^{3,4}
- 5 Jonathan H. Geisler^{3,4}
- 6 ¹Mace Brown Museum of Natural History, College of Charleston, Charleston, SC, USA 29414
- ²University of California Museum of Paleontology, University of California, Berkeley, CA, USA
- 8 94720
- 9 ³Department of Anatomy, New York Institute of Technology College of Osteopathic Medicine,
- 10 Old Westbury, NY, USA 11568
- ⁴Department of Paleobiology, National Museum of Natural History, Smithsonian Institution, PO
- 12 Box 37012, Washington, DC, USA 20013
- 13 Corresponding Author:
- 14 Robert W. Boessenecker^{1,2}
- 15 Email address: boesseneckerrw@cofc.edu



ABSTRACT

18	Baleen whales (Mysticeti) are gigantic filter-feeding cetaceans possessing the unique soft tissue
19	structure baleen and lacking adult teeth; Oligocene fossils have revealed a wealth of early
20	diverging tooth-bearing mysticetes highlighting the transition from archaeocete ancestors to early
21	toothless baleen-bearing eomysticetid whales. The archaeocete-like, toothed mysticete
22	Coronodon havensteini from the lower Oligocene Ashley Formation of South Carolina possesses
23	a number of peculiar aspects of feeding morphology suggesting dental filter-feeding in the
24	earliest diverging mysticete lineage. New fossils of Coronodon are described in detail, including
25	1) supplementary description of the holotype skull and skeleton of Coronodon havensteini; 2)
26	description of two new juvenile skulls of C. havensteini and a partial skull and postcranial
27	skeleton of an adult; 3) description of the new species Coronodon planifrons n.sp.; and 4)
28	description of the new species <i>Coronodon newtoni</i> . New specimens of <i>Coronodon havensteini</i>
29	include a partial adult skeleton preserving new elements for the species including incisors,
30	numerous upper premolars and molars, lower m4, scapula, lumbar, and caudal vertebrae, and two
31	juvenile skulls with tympanoperiotics and teeth. Fossils from the overlying unit, the Chandler
32	Bridge Formation, represent two new species: Coronodon newtoni n. sp. and Coronodon
33	planifrons n. sp. Coronodon newtoni possesses a concave-up alveolar profile, a mandibular
34	condyle elevated far above the toothrow, and a gracile periotic resembling those of juvenile C .
35	havensteini. Coronodon planifrons n. sp. possesses a horizontal supraorbital process,
36	successively smaller upper molars, massively inflated periotic, and longer intertemporal region.
37	Coronodon planifrons n. sp. preserves one of the most complete vertebral columns among
38	toothed mysticetes, indicating nine thoracic vertebrae, ten lumbar vertebrae, and at least 20
39	caudal vertebrae. The column exhibits a somewhat stabilized caudal peduncle with enlarged



lumbocaudal vertebrae, and rectangular terminal caudals indicate the presence of tail flukes. Juvenile skulls reveal several ontogenetic trends in *Coronodon havensteini*, including the anterior migration of the orbitotemporal crest, anteroposterior elongation of the intertemporal region, inflation of the body of the periotic, enlargement of the tympanic bulla, and continued postnatal emergence of the premolars and molars from their alveoli. Disarticulated skulls suggest a degree of rostral kinesis in this genus. Phylogenetic analysis of the largest assembled supermatrix of Mysticeti (n=138 OTUs; four archaeocetes, ten odontocetes, 124 mysticetes; 391 morphological and 27225 molecular characters) confirms placement of *Coronodon* as the earliest diverging lineage of Mysticeti under equally weighted analyses whereas implied weighting places *Coronodon* and similar taxa outside Neoceti, prompting a review of character transformations at the base of Neoceti.

INTRODUCTION

The terrestrial to aquatic transition in whales is one of the most dramatic and compelling examples of macroevolution, and a series of well-preserved skulls and skeletons of Eocene archaeocete whales have illuminated changes in brain size, hearing, olfaction, locomotion, feeding morphology, and even reproduction (Gingerich et al., 1990, 1994, 2001, 2009; Godfrey et al., 2012; Marino et al., 2004; Nummela et al., 2007; Thewissen et al. 1994, 2001; Uhen, 2004). While many gaps in our knowledge have been filled, the divergence of the Neoceti – the clade including modern and extinct toothed whales (Odontoceti) and baleen whales (Mysticeti) and their common ancestor- is relatively understudied. The origin of toothed whales has been the focus of some studies evaluating the early adaptations (or lack thereof) for echolocation (Geisler et al., 2014; Churchill et al., 2016; Racicot et al., 2019), feeding morphology (Boessenecker et



66

67

68

69

70

71

72

73

74

75

76

77

78

79

80

81

82

83

84

85

al., 2017) and locomotion (Boessenecker et al., 2020), although the earliest odontocetes remain unnamed and only partially described (Barnes et al., 2001).

The transition from archaeocetes to early mysticetes, on the other hand, has attracted extensive study in recent years. Early discoveries of toothed mysticetes were formerly confused with or considered to be archaeocetes (Pritchard, 1939; Emlong, 1966; Russell, 1968), or known from poorly preserved material too incomplete to reveal morphological transformations in the earliest members of the group (Mitchell, 1989). The recognition of aetiocetids as toothed mysticetes was a key development in this field of study (Barnes et al., 1995), followed later by the recognition of small, large-eyed raptorial feeding forms like *Janjucetus* (Fitzgerald, 2006). These discoveries suggested a degree of diversity among toothed mysticetes that had not been previously appreciated. The identification of lateral palatal foramina in Aetiocetus weltoni by Deméré et al. (2008), thereby suggesting the simultaneous presence of baleen and teeth, proved to be surprisingly provocative and triggered a number of critical responses (Fitzgerald, 2010; Fordyce and Marx, 2018; Marx, 2011; Marx et al., 2016; Peredo et al., 2017, 2018B, 2022). Among the flurry of research published in the wake of Fitzgerald (2006) and Deméré et al. (2008), is research on the diverse feeding adaptations in the dentition, mandibles, and skulls of toothed mysticetes including papers proposing 1) benthic suction feeding (Fitzgerald, 2010; Marx et al., 2016; Fordyce and Marx, 2016; Lambert et al., 2017); 2) macrophagy (Fitzgerald, 2006; Marx et al., 2015; Hocking et al., 2017); 3) filter feeding using baleen (Ekdale and Deméré, 2022) or even 4) dental filtering (Geisler et al., 2017); the 5) possible retention of teeth in the early chaeomysticete clade Eomysticetidae (Boessenecker and Fordyce, 2015A); 6) recognition of a mammalodontid clade (Fitzgerald, 2010; Marx, 2011); 7) the early evolution of baleen and associated neurovascular plumbing (Ekdale and Deméré, 2022; Peredo et al., 2022) or





alternatively 8) thickened gums (Marx et al., 2016; Fordyce and Marx, 2018); 9) the evolution of 86 tooth loss (Meredith et al., 2009, 2011; Peredo et al., 2017; Mu et al., 2021; Randall et al., 2022; 87 Gatesy et al., 2022), and 10) the origin of low frequency hearing (Ekdale and Racicot, 2014; Park 88 et al., 2018). In addition, two long-standing but (until recently) unpublished toothed mysticetes – 89 *Llanocetus* and *Coronodon* – were finally described (Geisler et al., 2017; Fordyce and Marx, 90 91 2018). 92 Despite this research effort, many disagreements remain over the origin and interpretation 93 of baleen, dental filtration, and the phylogenetic placement of various toothed mysticetes. Virtually every published matrix resolves different topologies at the base of Mysticeti (e.g. 94 mammalodontids as the earliest diverging clade, followed by Coronodonidae and *Llanocetus*, 95 Marx et al., 2015; Coronodonidae most basal, followed by *Llanocetus* and then 96 Mammalodontidae, Fitzgerald, 2010; Fordyce and Marx, 2018; Coronodonids most basal, 97 followed by mammalodontids, and then *Llanocetus*, Geisler et al., 2017). Otherwise, little has 98 99 advanced regarding the evolution of rostral kinesis and mandibular kinesis (but see Gatesy et al., 2022), locomotor adaptations, taphonomic patterns, ontogenetic changes, or the divergence of 100 101 mysticetes from odontocetes from their archaeocete ancestors. More recently, one phylogenetic 102 analysis even suggested that many toothed mysticetes (including Coronodon, Llanocetus, Mystacodon, and mammalodontids) may be placed outside the odontocete-mysticete clade, 103 suggesting that only the Aetiocetidae are actually toothed mysticetes (Corrie and Fordyce, 2022). 104 A consensus has yet to emerge for even the most intensely studied aspects of early 105 mysticete evolution, and many questions remain to be answered – and others have not yet been 106 107 asked. Likely contributing to these disagreements is the fossil record of toothed mysticetes, 108 which chiefly consists of isolated skulls, occasionally preserved with the phylogenetically



110

111

112

113

114

115

116

117

118

119

120

121

122

123

124

125

126

127

128

129

130

131

informative earbones, teeth, and mandibles. Few specimens preserve postcrania, with some exceptions (e.g. *Mystacodon*; Lambert et al., 2017; Muizon et al., 2019), and virtually all nominal toothed mysticete species are represented solely by a holotype skull, with only a single exception – *Fucaia goedertorum*, also known from a paratype skull (Barnes et al., 1995). Biases in the mysticete fossil record limit phylogenetic coding, assessment of locomotion, and in particular, assessment of individual variation and ontogenetic variation – both of which are virtually unstudied amongst early Neoceti.

Archaeocete-like fossils with some features of Neoceti and Mysticeti were first discovered from Oligocene sediments (Ashley and Chandler Bridge formations) in the vicinity of Charleston, South Carolina (USA) in the 1970s, and first formally studied in the 1990s (Barnes and Sanders, 1996A, 1996B). These specimens housed in The Charleston Museum (ChM PV 2778, 4745, and 5720) were widely acknowledged and studied by mysticete specialists and colloquially referred to as 'archaeomysticetes' or the 'Charleston toothed mysticetes', though they remained unpublished. Early conference presentations remarked that these fossils were more archaic than previously discovered toothed mysticetes and demonstrated the derivation of early mysticetes from "dorudontine" basilosaurids (Barnes and Sanders, 1996A, 1996B). A virtually complete skull (CCNHM 108), clearly closely related to ChM PV2788, 4745, and 5720, was collected from exposures of the Ashley Formation (late Rupelian) in 2002 and subsequently became the holotype of Coronodon havensteini (Geisler et al., 2017). Coronodon havensteini possesses large, basilosaurid-like teeth, a wide and somewhat flattened, partly kinetic rostrum, large basioccipital crests, and a veritable mix of basilosaurid-like and mysticete-like features, though admittedly more plesiomorphic than all other described toothed mysticetes (Geisler et al., 2017). A number of strange craniomandibular features, unique amongst toothed mysticetes, led



to the novel proposal that *Coronodon* represented an early stage of toothed mysticetes that evolved the ability to filter feed with their cheek teeth (Geisler et al., 2017). This interpretation was based on worn, mesially-facing cusps; a lack of apical wear on many of the highest cusps on the cheek teeth; highly emergent lower cheek teeth that overlapped labiolingually to form posterolaterally-directed, interdental slots, and a near homodont battery of cheekteeth with accessory cusps subequal to the primary cusp (Geisler et al., 2017).

New material of *Coronodon* includes partial skeletons of two new species of *Coronodon* from the younger Chandler Bridge Formation as well as new specimens, including young juveniles, of *Coronodon havensteini* from the Ashley Formation that, for the first time, shed light on the ontogeny, individual variation, and locomotor adaptations of a single species of early mysticete. This bountiful sample of an early neocete includes virtually complete skulls, earbones, teeth, mandibles, and postcrania of multiple individuals, permitting evaluation of many characters identified as synapomorphies of Neoceti and Mysticeti, as well as the hypothesis that *Coronodon* and other toothed mysticetes might fall outside crown Cetacea.

MATERIALS AND METHODS

Phylogenetic Methods

We revisited the phylogenetic position of *Coronodon havensteini*, as well as determined the positions of the new species *Coronodon newtoni* and *C. planifrons*, using a supermatrix of 27,617 characters. The morphological partition of this supermatrix was based on the dataset of Boessenecker and Fordyce (2017), to which we added 29 new morphological characters, ordered



154	81 multistate characters (Boessenecker and Fordyce, 2017 treated all multistate characters as
155	unordered), and added 53 taxa. Ordering allows for similarity among character states to be
156	included as data in phylogenetic analyses (Wilkinson, 1992), and multistate characters that had
157	equally dissimilar states were left unordered. The number of odontocete outgroups was increased
158	from two to 10, now including Olympicetus, Ashleycetus, Ankylorhiza tiedemani, the
159	xenorophids Echovenator and Albertocetus, and two extant odontocetes (Ziphiidae, based
160	primarily on Tasmacetus shepherdi, and Physeter macrocephalus). The enigmatic and recently
161	redescribed Kekenodon onamata, which is either a basal neocete or a late-surviving archaeocete,
162	was also added (Corrie and Fordyce, 2022). Five specimens in the genus Coronodon were coded
163	separately in the matrix. Three (i.e. CCNHM 108, CCNHM 164, ChM PV4775) represent <i>C</i> .
164	havensteini, and were combined to create a species-level operational taxonomic unit (OTU).
165	Differences among the three specimens were coded as polymorphisms for the composite OTU,
166	but majority-rule coding was employed where PV4775 was different from the other two and the
167	difference could be explained by its young ontogenetic stage. Other noteworthy additions
168	(citations indicate taxa coded from the literature or photographs, otherwise specimens were
169	examined directly) to the matrix of Boessenecker and Fordyce (2017) include the toothed
170	mysticetes Aetiocetus tomitai (Barnes et al., 1995), Borealodon osedax, Chonecetus sookensis,
171	Fucaia buelli, Kaaucetus thesaurus (Cisneros Hernandez, 2022), Llanocetus denticrenatus,
172	Mammalodon hakataramea (Fordyce and Marx, 2016), Metasqualodon symmetricus (Okazaki,
173	1982), Mystacodon selenensis (Muizon et al., 2019), Morawanocetus yabukii (Barnes et al.,
174	1995, Niparajacetus palmadentis (Solis-Anorve et al., 2019), Salishicetus meadi (Peredo and
175	Pyenson, 2018), and the basal toothless or nearly toothless mysticetes Maiabalaena nesbittae and
176	Sitsqwayk cornishorum. Several additional crown mysticetes were also coded. This



180

181

182

183

184

185

186

187

188

189

190

191

192

193

194

195

196

197

198

199

morphological matrix was then combined with the molecular partition published by Deméré et al. (2008).

The morphological dataset was constructed in the application Mesquite (Maddison and Maddison, 2021), exported to TNT format (Goloboff et al., 2008), and then manually combined with the molecular partition in a text editor. Most parsimonious trees were discovered using a "new technology search" in the computer application TNT. Two separate analyses were conducted; one with all characters equally weighted, referred to as the equal weight analysis (EW), and another using implied weighting (IW analysis), with the constant k=3 (Goloboff, 1993). The shortest or best-fit trees from these analyses are referred throughout the text as the EW trees and the IW trees, respectively. Default settings were used in both analyses except that the search was ended after the most parsimonious trees were found 1000 times and the memory was set to save up to 10,000 shortest trees. The phylogenetic analysis without implied weighting found more than 10,000 trees, and it is unclear if the strict consensus from those trees is representative of the strict consensus of all most parsimonious trees, both saved and unsaved. Thus, the strict consensus was compared to an estimated consensus that was derived from a driven search, which used default settings except that the consensus was stabilized 10 times. Nodal support was measured using the bootstrap in TNT. Default search settings were used except for the following: 1) bootstraps were done with replacement, 2) absolute frequencies were reported, and 3) each replicate included a new technology search with the search ended after the shortest tree for that replicate was recovered five times. Optimization of characters on individual trees was explored in Mesquite, but summaries of all synapomorphies were saved to output files using TNT (Optimize > List common synapomorphies). To investigate the lengths of individual characters on all trees from both analyses (10,015 trees), all but the character of interest was



excluded the calculation of tree length, all trees were sorted by length (Trees > Tree buffer > Sort trees), and then the longest and shortest trees were viewed to get the range of length across all trees from a given analysis. If the range of lengths for a specific character from trees obtained with implied weights overlapped the range from trees obtained without implied weighting, then we considered this character to support both sets of trees equally.

Descriptive Methods and Anatomical Terminology

Anatomical terminology follows Mead and Fordyce (2009) with additions from Boessenecker and Fordyce (2015B). Photographs were taken with a Canon Rebel Eos T5 and a 18-55mm zoom lens or a 100mm f/2.8 macro lens. Measurements were recorded using large calipers to the nearest millimeter and digital calipers for smaller (<30 cm) measurements to the nearest tenth of a millimeter.

We estimated the body length of *Coronodon* by using three methods: the bizygomatic skull width and partial least square equations from Pyenson and Sponberg (2011) for stem Mysticeti, and using a composite skeletal length using the holotype skull and cervical vertebrae of *Coronodon havensteini*, the thoracic vertebrae of the referred *Coronodon havensteini* specimen CCNHM 164, and the holotype lumbocaudal vertebrae *Coronodon planifrons*, along with estimated intervertebral disc lengths based on Long et al. (1997).

Taxonomy



The electronic version of this article in Portable Document Format (PDF) will represent a published work according to the International Commission on Zoological Nomenclature (ICZN), and hence the new names contained in the electronic version are effectively published under that Code from the electronic edition alone. This published work and the nomenclatural acts it contains have been registered in ZooBank, the online registration system for the ICZN. The ZooBank LSIDs (Life Science Identifiers) can be resolved and the associated information viewed through any standard web browser by appending the LSID to the prefix http://zoobank.org/. The LSID for this publication is: urn:lsid:zoobank.org:pub:796ED3F3-33A1-46E3-A6A0-F3898EA5C094. The online version of this work is archived and available from the following digital repositories: PeerJ, PubMed Central SCIE and CLOCKSS.

Geologic Background

Fossils of *Coronodon* have only been discovered in the Oligocene Ashley and Chandler Bridge formations of the Charleston embayment in South Carolina, USA (Figure 1). The Ashley Formation is a lightly consolidated, quartzose to phosphatic calcarenite ranging from yellow to tan, light gray, and olive brown in color (Weems et al., 2016). The Ashley Formation is up to 38 m thick, and unconformably overlies the uppermost Eocene Harleyville Formation. The Ashley Formation is sparsely to richly fossiliferous and frequently contains isolated mollusks and barnacles, occasionally concentrated into pavements. Phosphatic molds of small solitary corals (*Flabellum*, *Balanophyllia*) as well as steinkerns and phosphate pebbles are common; common invertebrates include the wentletrap *Epitonium*, the oyster *Cubitostrea*, and the barnacle *Concavus* (Fallon and Boessenecker, 2020). Vertebrate fossils are uncommon within the Ashley Formation, but include sharks (Miller et al., 2021), bony fish (Fierstine and Weems, 2009), sea



244

245

246

247

248

249

250

251

252

253

254

255

256

257

258

259

260

261

262

263

264

265

turtles (Weems and Sanders, 2014; Fallon and Boessenecker, 2020), sirenians (Domning, 1989. 1997; Domning and Beatty, 2018; Velez-Juarbe and Domning, 2014), toothed whales (Albright et al., 2018, 2019; Boessenecker et al., 2017, 2020; Churchill et al., 2016; Geisler et al., 2014; Godfrey et al., 2016; Kellogg, 1923; Sanders and Geisler, 2015), eomysticetid baleen whales (Sanders and Barnes, 2002A), and *Coronodon* (Geisler et al., 2017). Extensive bioturbation, grain size (fine-medium sand), and phosphatic bonebeds indicate middle shelf deposition (Fallon and Boessenecker, 2020). Fossils of the billfish Aglyptorhynchus suggest relatively warm conditions, with sea surface temperatures ranging 20-24°C, similar to the overlying Chandler Bridge Formation (Fierstine and Weems, 2009). The Ashley Formation has produced microfossils corresponding to calcareous nannofossil zone NP24 (29.63-26.84 Ma; Gradstein et al., 2012) and foraminiferal zone P21 (29.18-26.93 Ma; Gradstein et al., 2012), as well as ⁸⁷Sr/⁸⁶Sr dates of 28.4-29.0 Ma for the Runnymede Marl and Givhan's Ferry members (Weems et al., 2016), summarized here as 29-27 Ma. These dates indicate that the unconformity separating Oligocene rocks and cetaceans from the uppermost Eocene Harleyville Formation represents approximately 5 my, given that the basilosaurid-producing Harleyville Formation has produced microfossils corresponding to the Eocene portion of calcareous nannofossil zone NP21 (34.44-33.9 Ma; Weems et al., 2016). The Chandler Bridge Formation unconformably overlies the Ashley Formation; it is

The Chandler Bridge Formation unconformably overlies the Ashley Formation; it is patchy in distribution, apparently being eroded away or only deposited along paleotopographic highs (Katuna et al., 1997). It consists of under one meter (typically 40-60 cm thick, and rarely up to 2.5 meters thick) of massive poorly lithified siltstone with some sand and is rich in phosphatic pebbles; the siltstone is typically khaki to olive green at the base (Bed 0-1) and brown to tan in the upper part (Bed 2); where exposed, the rare uppermost bed (Bed 3) is gray to tan and



266	lightly consolidated and yields scattered discoidal quartz pebbles (Sanders et al., 1982). The
267	Chandler Bridge Formation is in turn unconformably overlain by the even thinner and patchier
268	Edisto Formation, which straddles the Oligocene-Miocene boundary (Weems et al., 2016). Fossi
269	vertebrates from the Chandler Bridge Formation have been more intensely studied, relative to the
270	Ashley Formation, and include sharks (Cicimurri and Knight, 2009, Miller et al., 2021), bony
271	fish (Fierstine and Weems, 2009; McCuen et al., 2020), sea turtles (Hay, 1923; Weems and
272	Sanders, 2014, Weems and Brown, 2017; Fallon and Boessenecker, 2020), sea birds (Ksepka,
273	2014), toothed whales (Geisler et al., 2014; Churchill et al., 2016; Boessenecker and Geisler,
274	2018; Boessenecker et al., 2020), eomysticetid baleen whales (Sanders and Barnes, 2002B), and
275	sirenians (Domning, 1997; Velez-Juarbe and Domning, 2014). Dinoflagellates and vertebrate
276	taphonomy initially suggested that Bed 1 represented fully marine conditions followed by
277	shallower deposition within a protected embayment or estuary with Beds 2 and 3 (Katuna et al.,
278	1997). Studies of the ichthyofauna suggest continuous open marine conditions throughout
279	deposition (Cicimurri and Knight, 2009), though these authors did not report sharks from
280	individual beds. The occurrence of warm water sharks and the billfish Aglyptorhynchus indicates
281	sea surface temperatures of approximately 20-24°C (Fierstine and Weems, 2009).
282	Dinoflagellates from the Chandler Bridge Formation indicate assignment to zones NP24-25,
283	indicating an age of 29.6-23.1 Ma (Gradstein et al., 2012), and ⁸⁷ Sr/ ⁸⁶ Sr ratios from oyster shells
284	ranging from 24.7-24.5 Ma (Weems et al., 2016). A minimum age is provided by ⁸⁷ Sr/ ⁸⁶ Sr dates
285	of 23.5 Ma from the overlying Edisto Formation (Weems et al., 2016) indicates an age range of
286	24.7-23.5 Ma (e.g. McCuen et al., 2020).

288

RESULTS



PeerJ

289	Systematic Paleontology
290	Mammalia Linnaeus, 1758
291	Cetacea Brisson, 1762
292	Neoceti Fordyce and Muizon, 2001
293	Mysticeti Gray, 1864
294 295	Coronodonidae New Family LSID urn:lsid:zoobank.org:act:1FE35563-5AD1-447E-A3AC-280C4A9BB2D0
296	
297	Diagnosis
298	Large toothed mysticetes (BZW=40-60 cm, estimated body length 5-8 meters) with incipient
299	polydonty (11 upper, 12 lower teeth); wide rostra with loose premaxilla-maxilla and
300	maxillofrontal sutures; edentulous and transversely narrow blade-like premaxilla anterior to I1;
301	dorsally curved nasal apex; long intertemporal constriction with high sagittal crest and parallel
302	margins; nearly vertical occipital shield and occipital apex thrust to level of supramastoid crest
303	tall and vertical nuchal crest; squamosal with short, dorsoventrally deep zygomatic process
304	bearing facet for jugal, enlarged squamosal prominence, large sternomastoid fossa; amastoid
305	periotic with triangular anterodorsal and posterodorsal angles but highly reduced superior ridge
306	low and anteriorly narrow pars cochlearis separated from anterior process by obtuse angle (160
307	180°); wide non-rotated bulla with flat ventral surface and median furrow, step-like profile of
308	involucrum with flat medial face; dentition with thin smooth enamel (some lingual ridging on
309	caniniform teeth and p1-2 only), incipient serrations on proportionally large postcanine teeth;

double rooted postcanines (P3-M3) with long root isthmus, demi-roots (except C. newtoni),

310





311	overlapping lower cheek teeth, five or more mesial denticles on premolars; posterior upper cheek
312	teeth distally inclined; mandible with faint sutural surface for symphysis, elevated molars, lobate
313	but subtriangular and vertical coronoid process and a mandibular condyle separated far from
314	coronoid.
315	Included Taxa
316	Coronodon; unnamed genera represented by ChM PV 5720 (and CCNHM 214), and CCNHM
317	8745.
318	Remarks
319	The name Coronodontidae is unavailable as it is preoccupied by Coronodontidae Harris 1951. In
320	accordance with ICZN articles 29.2 and 29.6, Coronodonidae is available. At present this clade
321	includes only one genus, Coronodon. However, naming this clade is warranted as an unnamed
322	toothed mysticete, ChM PV 5720, has been used in a number of cladistic analyses (Geisler and
323	Sanders, 2003; Geisler et al., 2011; Fitzgerald, 2006, 2010; Boessenecker and Fordyce, 2015A,
324	2015B, 2015C, 2017; Marx and Fordyce, 2015; Sanders and Geisler, 2015; Lambert et al., 2017;
325	Martinez-Caceres et al., 2017; Fordyce and Marx, 2018; Peredo et al., 2018B; Muizon et al.,
326	2019). Unpublished specimen CCNHM 214 appears to represent a juvenile of the same taxon as
327	ChM PV 5720. CCNHM 8745 is described below. A comparative diagnostic table for different
328	coronodonid taxa is presented in Table 1.
329	
330	Coronodonidae indeterminate
331	



337

338

339

340

341

342

343

344

345

346

347

348

349

350

351

352

Referred Specimen

- 333 CCNHM 8745, a partial braincase loose from the Cooper River, Ashley Formation, Berkeley
- County, South Carolina, USA, discovered in the early 2000s by an unknown amateur collector.
- Additional locality data is available on file at CCNHM.

336 **Description**

Frontal, Nares, and Orbit

CCNHM 8745 (Figure 2; Table 2) generally resembles *Coronodon* spp. and Basilosauridae in possessing a narrow and posteriorly positioned vertex, long intertemporal constriction, and a supraorbital process of the frontal that is only slightly wider than long. CCNHM 8745 has a nearly complete and rectangular supraorbital process of the frontal on the right side, missing just the postorbital process. Judging from a preorbital width of 340 mm, CCNHM 8745 is approximately the same size as Coronodon havensteini and Coronodon planifrons, likely having a bizygomatic width of around 450-460 mm. The supraorbital process is dorsoventrally shallow and delicate at the orbital margin, and the preorbital process is dorsoventrally thin (23 mm) compared to *Coronodon havensteini* 41 mm). The preorbital process is squared off and the anterior edge of the supraorbital process is transversely oriented; the posterior margin of the supraorbital process is concave like *Coronodon* spp. The orbitotemporal crest is positioned dorsally to the postorbital ridge so that the frontal between these is vertical and faces posteriorly (intermediate between Basilosauridae and Kinetomenta). A single large ?diploic foramen is positioned 1 cm ventral to the orbitotemporal crest and 7.5 cm lateral to the midline on this posterior face of the frontal, as in *Coronodon* spp. and some Basilosauridae.



The dorsal surface of the supraorbital process faces somewhat anterodorsally (like *Coronodon* spp.) but is otherwise planar. The middle of the frontal, where it bears sutural articulations with the nasals, premaxilla, and maxilla, is transversely arched and raised 5 cm above the supraorbital process. This is more greatly arched than in *Coronodon*. At the base of this arch is a deep triangular fossa for the ascending process of the maxilla on the right side; on the more incomplete left side, much of the ascending process of the maxilla is preserved in articulation with the frontal. It is triangular and covers the anterior 50% of the frontal, terminating at the anteroposterior midpoint. The maxillofrontal suture is mortised with a four to five parallel longitudinal grooves/ridges (on the right side), unlike the flat butt joint in *Coronodon*. These ridges are discontinuous and about 3-4 cm long.

The ascending process of the maxilla contacts the frontal ventrally but not medially; there is a transversely narrow gap between these elements occupied by a thin vertical sheet of the nasal process of the premaxilla separating the maxilla from the medial 'arched' portion of the frontal. The premaxilla and maxilla share a slightly mortised suture. The nasal process of the premaxilla extended about 3 cm posterior to the maxilla, sharing a direct contact with the frontal posteriorly, like *Coronodon* (and differing from Protocetidae and Basilosauridae).

Both nasals are preserved and the left is nearly complete; the nasal is dorsally flat and has a straight dorsal margin, lacking the upturned anterior tip seen in *Coronodon* spp. and ChM PV 5720. The nasal is triangular in dorsal view, and slightly transversely convex in cross-section, though generally conforming to the transverse arching of the underlying frontal. The nasal is small, only 85 mm long and 18.5 mm wide, v. 140 mm and 31.8 mm in *Coronodon* (CCNHM 108) despite nearly identical absolute skull size. The nasal gradually narrows posteriorly, and it is unclear if the nasals contacted medially or were separated along their entire length owing to





incompleteness. Judging from articular sutures on the underlying frontal, the nasals most likely contacted medially only along the anterior 30-40 mm of their length, and at least the posterior half of the nasals were separated by a triangular exposure of the frontal as in Basilosauridae and ChM PV 5720 (differing from *Coronodon*). Posterior to the terminations of the premaxilla are paired 2 cm wide, 4 cm long shallow troughs on the frontal flanked by a low, longitudinal ridge that extends posteriorly from the premaxilla-maxilla suture; such a pair of median troughs and/or ridges characterizes some Basilosauridae (*Basilosaurus cetoides*; *Dorudon atrox*; *Zygorhiza kochii*; Boessenecker, pers. obs.).

The anterior part of the frontal bears a triangular prenarial process on either side of the internal nares, which serves as an articular buttress for the nasals and premaxilla; the process is transversely narrow and near vertical with the lateral surface formed by the premaxilla-frontal suture and the dorsal surface overlapped by the nasals. The prenarial process extends at least 4 cm anterior to the nasal. Each nasal bears a longitudinal trough leading to the common fissure for the dorsal nasal meatus (dorsal end) and the ethmoid labyrinth (ventral end). These fissures (Figure 2) are sigmoidal in shape, and the dorsal nasal meati are close to the midline and separated by only 12 mm. Ventrally and medially to the common fissures is the highly cancellous presphenoid, which is dorsoventrally thick, transversely narrow, oval in cross-section and narrowing somewhat dorsally. The presphenoid is flanked on either side by the choanae, which descend posteroventrally 25° from the horizontal plane. The choana is separated from the ethmoid labyrinth by a thin subhorizontal shelf. A deep laterally facing fossa is present dorsal to the choana but ventral to the optic groove.

The optic groove is exposed along its entire length from the braincase, forming a Y-shape; the grooves are never confluent but separate gradually just posterior to the frontoparietal



suture and curve anterolaterally; the groove widens into a broad anterolaterally directed furrow on the ventral side of the supraorbital process. Two laterally directed ethmoid foramina are present within the optic groove. The postorbital ridge is low and formed as a corner in cross-section; the opening of the optic canal is positioned posteriorly on the frontal. Small diploic foramina are present lateral to the optic canal; a few scattered diploic foramina are also present dorsally within 5 cm of the midline near the apices of the premaxillae and maxilla.

Posteriorly, each optic foramen is 13 mm wide and separated from one another by a 21 mm wide gap. Dorsomedial to these is a long olfactory nerve tract with a thin (~1 mm) median bony septum; the combined olfactory nerve tracts are 9mm wide and 10 mm deep. If the cribriform plate is positioned at approximately the level of the ethmoid foramen, the entire olfactory nerve tract would be at least 200 mm long.

Intertemporal Constriction and Vertex

The intertemporal constriction is long, measuring approximately 183 mm and constituting 54% of preorbital width, compared with a maximum of 49% in *Coronodon havensteini*; the constriction is quite narrow and measures approximately 65 mm or 19.1% of preorbital width, compared to 25% in *Coronodon havensteini*. In each of these regards CCNHM 8745 is plesiomorphic relative to *Coronodon*. Like *Coronodon* the sagittal crest is tall and sharp; the dorsal margin of the crest is concave where it rises abruptly in its posterior third towards the highly elevated vertex, unlike in *Coronodon* where the crest has a straight dorsal margin.

The frontoparietal suture appears approximately transverse owing to breakage, though grooves on the frontal suggest the presence of anterolateral wings of the parietal that would overlap the frontal on the anterior part of the constriction; these wings give the frontoparietal



suture the posteriorly pointing V shape in *Coronodon* and this condition likely occurred in CCNHM 8745. If true, sutures on the frontal suggest that the frontal would penetrate 2-3 cm between the parietals in this specimen. The intertemporal portion of the parietal is laterally flat and nearly vertical, and broadly concave posteriorly. Like *Coronodon*, and differing from Basilosauridae, no postparietal foramina are developed.

The vertex is elevated by 3 cm above the sagittal crest; in dorsal view, the nuchal crests diverge at approximately 77-80°. The occipital shield is obscured by matrix but appears to have been flat to slightly concave, and faces posterodorsally at approximately a 45-50° angle from horizontal. The nuchal crests are tall, vertical, and do not overhang the braincase in dorsal view. The occipital shield is triangular and narrow, with a triangular rather than rounded apex.

Braincase

The squamosal is mostly missing but nearly the entire suture with the parietal is preserved. The suture is laterally more convex than in *Coronodon* and the lateral apex of the suture is positioned about halfway up the side of the braincase, whereas in *Coronodon* spp. it is low and just posterodorsal to the subtemporal crest. The dorsal half of the suture is nearly transverse in CCNHM 8745 whereas it is approximately anteroposterior in *Coronodon*. A small fragment of the squamosal is preserved ventrally, and bears a smooth lunate trough as in CCNHM 164 (*Coronodon havensteini*) and CCNHM 166 (*Coronodon planifrons*), identified as receiving the dorsal part of the alisphenoid.

The endocranial cavity is similar to *Coronodon* (e.g. CCNHM 164), being broadly pyramidal in shape with a deep fissure anterodorsally for the posterior terminus of the olfactory nerve tract. The fossae for the cerebral hemispheres are 12 cm wide and posteriorly flanked by a





large fossa for an endocranial rete situated dorsal to the cerebellum; these fossae suggest a posterior cranial fossa that is 155 mm across. A low median ridge subdivides the dorsal side of the posterio cranial fossa.

Identification and Remarks

CCNHM 8745 is seemingly slightly more plesiomorphic than *Coronodon*, with a slightly longer and narrower intertemporal constriction and prenarial exposure of the frontal between the nasals. Despite these features, it does not represent a basilosaurid as it possesses several features of typical of basal neocetes, including dorsal contact of the premaxilla and frontal, a triangular apex of the occipital shield, as well as a somewhat telescoped vertex that is at the approximate level of the subtemporal crest with an occipital shield facing posterodorsally (e.g. Martinez-Caceres et al., 2017). Amongst all nominal Neoceti, the shape of the supraorbital process and length and width of the intertemporal constriction in CCNHM 8745 are present only in the Coronodonidae. Owing to incompleteness it is not coded into our cladistic matrix, but is similar enough to *Coronodon* to warrant referral to the Coronodonidae.

This specimen exhibits adhering matrix most consistent with derivation from one of the members of the Ashley Formation. This specimen was either collected from the Cooper River along with CCNHM 552, an isolated lower beak of the sea turtle *Euclastes* sp. described by Weems and Brown (2017) and CCNHM 4294, an isolated atlas vertebra of *Ankylorhiza*, or perhaps from the Wando River in the vicinity of the type locality of *Coronodon havensteini* (M. Brown, pers. commun. 2016 and 2022). Weems and Brown (2017:6), influenced by the archaic morphology of CCNHM 552 and its association with fossils identified as *Dorudon serratus*,



Ferry Formation. However, no fossils of *Dorudon serratus* exist in CCNHM collections aside from those collected in situ from quarries in the Harleyville region further inland. It is possible that, owing to the incomplete nature of CCNHM 8745, this braincase was initially misidentified as *Dorudon serratus*. Regardless, the Cooper River in the vicinity plotted by Weems and Brown (2017: fig. 1) bottoms out in the Ashley Formation (Weems et al., 1985; Weems and Lemon, 1993), and these specimens (CCNHM 552, CCNHM 4294, and CCNHM 8745) are best interpreted as being derived from the Ashley Formation. This is surprising at it would extend the already surprisingly young late Eocene age for the archaic *Euclastes* lineage proposed by Weems and Brown (2017) well into the Oligocene epoch.

CCNHM 8745 differs from *Coronodon* spp. and ChM PV 5720 in having absolutely and proportionally tiny and flat nasals, parallel troughs and ridges on the frontal posterior to the nasals and premaxillae (shared with some Basilosauridae), a concave dorsal margin of the sagittal crest, a longer sagittal crest (much longer than in ChM PV 5720), and a dorsally shallow preorbital process (Tables 1-2). CCNHM 8745 shares with Basilosauridae and ChM PV 5720 a triangular median wedge of frontal separating the nasals, differing from continuous medial contact in *Coronodon* spp. The apex of the occipital shield is narrower and more acutely triangular than in *Coronodon*, ChM PV 5720, or CCNHM 214. Based on the small and flat nasals and other basilosaurid-like symplesiomorphies, CCNHM 8745 may lie as sister to the *Coronodon* + ChM PV 5720 clade rather than sister to either coronodonid. Regardless, probable derivation from the Ashley Formation indicates that at least two coronodonids are present in the Rupelian, paralleling three in the Chattian based on the assemblage from the Chandler Bridge Formation (*Coronodon newtoni*, *Coronodon planifrons*, and ChM PV 5720).



488	
489	Coronodon Geisler et al., 2017
490	Type Species
491	Coronodon havensteini, Geisler et al., 2017
492	Amended Diagnosis
493	Species of <i>Coronodon</i> are large toothed mysticetes (ca. BZW = 460 mm) possessing elongate
494	intertemporal constriction with tall sagittal crest (length of crest= 34% of BZW), longer than in
495	ChM PV 5720 (20% of BZW), wider and dorsoventrally shallower maxilla than ChM PV 5720
496	with straight (rather than concave) lateral edge; periotic with multiple (rather than single)
497	posteroexternal foramina.
498	
499	Coronodon havensteini Geisler et al., 2017
500	Type Specimen
501	CCNHM 108, partial skeleton including virtually complete skull with left and right periotics and
502	tympanic bullae, left and right mandibles, 16 teeth, seven cervical vertebrae, seven thoracic
503	vertebrae, and eight ribs, collected by Mark Havenstein and others, summer 2002.
504	Referred Specimens
505	CCNHM 164, partial skeleton including rostrum fragments, braincase, fragmentary periotic, 19
506	teeth, five cervical vertebrae, nine thoracic vertebrae, three lumbar vertebrae, rib fragments, and
507	partial scapula, collected summer 2007 by Paul Bailey from the Ashley Formation in the vicinity



of North Charleston, Dorchester County, South Carolina; CCNHM 8722, partial skull including partial maxilla and braincase, left periotic, and right tympanic bulla, collected spring 2019 by Jeremmiah Volcko from the vicinity of North Charleston, Dorchester County, South Carolina; ChM PV 4745, nearly complete skull, four teeth, periotics, right tympanic bulla, collected May 1986 by Steve Faust from a drainage ditch exposure of the Ashley Formation in the vicinity of Summerville, Dorchester County, South Carolina, USA. Detailed locality data on file at CCNHM and ChM.

Type Locality

515

519

521

522

523

524

525

526

527

528

The holotype of *Coronodon havensteini* was collected from subaqueous exposures of the Ashley
Formation in the Wando River, Charleston/Berkeley County, South Carolina. Detailed locality
data on file at CCNHM.

Horizon and Age

520 Ashley Formation, late early Oligocene (28-30 Ma).

Amended Diagnosis

A species of *Coronodon* possessing frontal with preorbital and postorbital processes of equal depth, ventrolaterally sloping supraorbital processes of the frontal in anterior view (horizontal in *C. planifrons*), a periotic with a distally widening posterior bullar facet with large spurs on distal edge, upper molars of identical size (differing from *C. planifrons*), lack of overlapping of the upper cheek teeth (differing from *C. newtoni*), maxilla with embrasure pits along length of toothrow and straight ventral edge (differing from *C. newtoni*), mandible with straight ventral edge and condyle not elevated above m4 alveolus (differing from *C. newtoni*).



Description

A complete description of the holotype specimen of *Coronodon havensteini* was provided by Geisler et al. (2017: supporting information). Accordingly, this description will emphasize new aspects of the morphology of *C. havensteini* revealed by the new specimens rather than repeating the published description. New details fall into three categories: 1) features not preserved in the holotype or details reinterpreted in light of insights gained from new specimens; 2) polymorphic features; and 3) morphological differences between juvenile and adult specimens that represent ontogenetic changes.

Rostrum

The left and right maxillae and a partial vomer are preserved in juvenile ChM PV 4745 (Figures 3-5; Table 2), including the alveoli for C1-M2. This specimen was collected long before the *Coronodon havensteini* holotype and prepared as best as was possible at the time, with the descending processes of the maxillae meeting at the midline. The more complete rostrum of CCNHM 108 (Figures 4-6) indicates that the maxillae did not medially contact and that there was a continuous strip of vomer present; owing to this, and to the curvature of the medial margin of the maxilla, the rostrum of ChM PV 4745 is likely too narrow. A corrected reconstruction is shown in Figure 9.

The right premaxilla is nearly completely preserved in CCNHM 164 (Figure 6; Table 2), and is missing only the incisor-bearing portion. The premaxilla is nearly longitudinally straight in dorsal view, lacking the slight lateral bowing in the reconstructed holotype. The posterior half of the premaxilla is nearly identical to the loose premaxilla of *Coronodon planifrons*. The lateral surface is undulatory in places and anteriorly bears a sharp horizontal ridge that descends





anteroventrally; ventral to this is a deep longitudinal furrow to receive the anterodorsal edge of the maxilla.

The lateral edge of the maxilla is straight in CCNHM 8722, ChM PV 4745, and CCNHM 108 (Figures 3-4, 6). CCNHM 8722 appears to have had a triangular rostrum of nearly identical proportions to the adult, based on the length of the maxilla from the P1 alveolus to the antorbital notch relative to postorbital width; the length of the maxilla posterior to P1 is approximately 90% of postorbital width in all specimens of *Coronodon havensteini*.

In CCNHM 8722 the maxilla is dorsoventrally deeper than and lacks the dorsal, horizontal surface on the posterior half of the maxilla of the holotype (Figure 5); instead, the maxilla is gently sloping along its entire length with a small subhorizontal platform adjacent to the dorsal infraorbital foramina. This platform is somewhat larger in ChM PV 4745 and more similar to the holotype, and is present along the posterior half; it bears three dorsal to dorsolaterally opening dorsal infraorbital foramina at the level of M1. The maximum depth of the maxilla is equivalent to 18-19% of antorbital width in the juvenile skulls compared to 13% in the holotype. The external nares seem to have been present at the level of P4 in these juveniles.

The premaxilla-maxilla contact is obscured in the holotype by the vomer and premaxilla, but the medial side of the maxilla (Figure 7) is well preserved in juvenile specimens (ChM PV 4745, CCNHM 8722) and the lateral edge of the premaxilla is exposed in the referred adult (CCNHM 164). The medial surface of the maxilla in juvenile specimens (Figure 7) preserves four major surfaces – two ventral surfaces below a horizontal ridge that underlies the premaxilla, and two dorsally positioned surfaces above this ridge. The first is a deep trough for the premaxilla positioned along the posterior 2/3 of the maxilla; this trough is deepest anteriorly and posteriorly but shallows around the level of the P4. The sutural surface is smooth and lacks a



mortised articulation. Anteriorly, the second surface is developed along the anterior 2/3 of the maxilla; this surface is a vertical, flat butt joint articulation between the premaxilla and maxilla. The third is a long, smoothly concave ventromedial trough for the palatal part of the vomer, positioned on the dorsomedial surface of the descending plate of the maxilla. The fourth is a fossa for the wing of the vomer; it is dorsoventrally deep posteriorly, transversely concave and smooth; this accommodates the choanae and would have been lined by the vomerine wing when complete. The maxillae of each juvenile specimen (CCNHM 8722, ChM PV 4745) preserve a delicate dorsomedial ridge that forms a lip along the lateral edge of the premaxilla (Figures 3, 7); medial to the dorsal infraorbital foramina this ridge overhangs laterally somewhat.

Demi-alveoli for the 'demi-roots' are present in juvenile specimens (Figures 4, 7), but fewer than in the adult holotype, where demi-roots or alveoli for them are present on P3 through M2. In juvenile CCNHM 8722, there are only alveoli for demi roots in M1 and M2. In ChM PV 4745 there are quadrate to circular pedestals in between the root alveoli for P3 through M2, which may correspond to demi-root alveoli later in ontogeny.

In the juvenile specimen CCNHM 8722, embrasure pits are present on the palate labially between P1 and P2 (for p1), and medial to P4, M1, and M2, but not medial to P3 (Figure 7). These pits are much shallower than in CCNHM 108. In ChM PV 4745, more embrasure pits are present and are deeper than in CCNHM 8722, but fewer and shallower than in the holotype. These include labial pits for the p1 (between C1/P1), p2 (between P1/P2), and lingual pits for the p3 (anteromedial to P2), p4 (just medial to P3/P4), m1 medial to the anterior root of M1), and m2 (medial to anterior root of m2). The m2 embrasure pit is the deepest. Fragments of the maxilla in CCNHM 164 include labially-facing embrasure pits anterior to P1 and P2, and lingual embrasure pits medial to the P3-M2 alveoli. The well-preserved palate of the holotype (CCNHM 108)



preserves labial embrasure pits between teeth from I1 to P1, a deep embrasure pit in line with the toothrow between P1 and P2, and deep lingual embrasure pits medial to the anterior roots of P3, P4, M1, and M2 (Figure 4B); the pits medial to P3-M1 (P4 in particular) are the deepest. Each of these is shallowly conical and of sufficient anteroposterior diameter to accommodate the entire crown length of the corresponding mandibular tooth, with the bony bridges between the pits corresponding to the gaps between crown apices of the mandibular cheek teeth. Bone remodeling on the labial edge of these pits has broadly exposed the lingual side of the roots of P3-M2. The same is likely true of M3, but the medial part of the maxilla is missing and only the lateral edge of the reduced infraorbital plate is present.

Orbit, Supraorbital Process, and Interorbital Region

In CCNHM 8722 the orbitotemporal crest overhangs the temporal fossa much more than in the adult holotype, forming a clear medial shelf in ventral view (Figure 7). In anterior view, the supraorbital process of the frontal descends ventrolaterally (Figure 8). The postorbital process is longer and more acutely pointed in ChM PV 4745 and CCNHM 164 than in the holotype, though CCNHM 8722 is similar to the holotype. The median frontal suture is open and planar to slightly sinuous in juvenile specimen CCNHM 8722, whereas it is closed and partially obliterated in ChM PV 4745; it is completely obliterated in CCNHM 108. A furrow is present at the frontal midline in CCNHM 164, but owing to poor preservation, it is unclear whether or not the suture was persistent or obliterated. The supraorbital process of the frontal is anteroposteriorly shorter in the juvenile specimens than in the holotype (Figures 3, 6, 9; Table 2), approximately 26.5% of postorbital width in CCNHM 8722, 26.4% in ChM PV 4745, and 31.5% in the holotype. However, the supraorbital process is somewhat shorter in adult specimen



621

622

623

624

625

626

627

628

629

630

631

632

633

634

635

636

637

638

639

640

641

642

more concave (Figure 3) and there is a stronger angle between the orbitotemporal crest and the postorbital process. The preorbital and postorbital processes of CCNHM 8722, ChM PV 4745, CCNHM 108, and 164 are nearly equivalent in dorsoventral depth (Figure 5, Table 1), unlike *Coronodon newtoni* and *Coronodon planifrons*.

The frontonasal and frontal-premaxilla sutures are anteroposteriorly shorter in juvenile specimens, measuring approximately 55% of anteroposterior supraorbital length in CCNHM 8722 and 54% in ChM PV 4745 v. 70% in the holotype. In ChM PV 4745, a median triangular extension of the frontal was present between the posterior ends of the nasals (Figure 3B); a similar condition is present in CCNHM 8722, though the frontal extended less far anteriorly (Figure 3A). In adult specimens CCHM 108 and 164, the frontonasal sutures are too elongated to tell and no smooth triangular surface is evident (Figure 6). The fossa for the ascending process of the maxilla Is slightly more excavated in CCNHM 8722 and ChM PV 4745, whereas this surface is nearly flat in CCNHM 108. In CCNHM 164, the articular fossa is somewhat more defined, and based on this feature the ascending maxilla overlapped the anterior 48mm of the frontal (45% of the length of the frontal). Lateral to the sutures for the premaxilla there are scattered diploic foramina in all specimens. In CCNHM 8722, ChM PV 4745, and CCNHM 108 they are small dorsally to posterodorsally opening pores. However, in CCNHM 164, they are confluent with roughly transversely oriented, shallow, 1.5-2mm wide sulci. Some anteroposteriorly oriented sulci cross-cut these. In the holotype there are an additional pair of diploic foramina positioned near the posterior margin and open posteriorly but lack sulci.

The orbit is 67mm long in CCNHM 8722 and corresponding to 21% of postorbital width, which is proportionally smaller than in the adult holotype (25% of postorbital width); however, in ChM PV 4745 the orbit is proportionally larger, approximately 85 mm and 28% of postorbital



width. Scattered diploic foramina are present in the optic canal of all specimens halfway from the midline to the orbital margin. In both juveniles there is a low curved ridge on the dorsal surface of the supraorbital process that extends from the middle of the orbit to the medial part of the orbitotemporal crest; it is more clearly defined in ChM PV 4745, but diffuse and nearly absent adult specimens CCNHM 108 and 164. In CCNHM 8722, a shallow fossa parallels the posterior margin of this low crest medial to the postorbital process. In CCNHM 8722, a pathological fossa is present medial to the middle of the orbit on the right frontal, and is floored by cancellous bone. In CCNHM 8722 the postorbital ridge is low, medially sharp and positioned further anteriorly so that the orbitotemporal crest roofs over the anteromedial part of the temporal fossa more extremely than in ChM PV 4745 and CCNHM 108, resembling the condition in basilosaurids. In both CCNHM 8722 and ChM PV 4745, the supraorbital process is anteroposteriorly shorter (~25% of postorbital width at mid-frontal) than in the holotype; in CCNHM 164, it is longer than in the juveniles, but still somewhat shorter than the holotype. Juvenile specimens possess the longest and narrowest postorbital processes.

The frontoparietal suture is V-shaped and posteriorly-pointing in all specimens, but in ChM PV 4745 there is a transversely narrow median process of the parietal or separate midline ossification that extends anteriorly between the frontals; the parietals of CCNHM 8722 are incomplete, but the frontals possess a narrow median embayment and likely received a projection of the parietal. In CCNHM 108, the suture is V-shaped without a median parietal process; this region is fractured in CCNHM 164. Upon closer examination of the holotype, a similar condition is present in CCNHM 108 that eluded the initial description. An oval-shaped median ossification is present just anterior to the frontoparietal suture (and separated from the parietal by the frontoparietal suture), corresponding to the complete element in ChM PV 4745 and the gap in the



667

668

669

670

671

672

673

674

675

676

677

678

679

680

681

682

683

684

685

686

frontal in CCNHM 8722. This element is not fused to the parietal and has clear sutures laterally for the frontal, and anteriorly is fused to the frontal at the midline. Whether or not this element represents the interparietal or a separate ossification is the subject of a separate study (Roston et al., unpublished data).

Lateral to the sutural surface for the premaxilla, the dorsal surface of the frontal is smooth and shallowly concave, corresponding to the articulation for the ascending process of the maxilla. The exact shape is unclear, and only the holotype preserves a partial ascending process, which is approximately 31 mm wide. Preserved articular surfaces on the frontal in all specimens suggests that it terminated anterior to the posterior apex of the premaxilla. A clue lies in the coloration and staining of the frontal in CCNHM 108; if this is a stain from the ascending maxilla, it would indicate a roughly triangular ascending process with a blunt or lobate apex extending to nearly the posterior edge of the preserved part of the premaxilla and nasal, and terminating just anterior to the preserved articular grooves on the frontal for these elements. Medially there is a triangular prong of frontal in ChM PV 4745, CCNHM 108, and CCNHM 164; this feature is not developed in CCNHM 8722. This structure forms the articular buttress ventral to the nasal and premaxilla. The olfactory region of the holotype is exposed (Figure 10) and is broadly similar to that of CCNHM 8745, possessing proportionally larger and straight (rather than sigmoidal) common fissures for the dorsal meatus and ethmoid labyrinth. Unlike CCNHM 8745, the fissure is expanded rather than transversely constricted at mid-height. Unlike CCNHM 8745, the nasal passages curve anterodorsally after emanating anteriorly from the dorsal meatus, conforming to the anterodorsally flaring profile of the nasal bone.

687

688

Intertemporal Region



690

691

692

693

694

695

696

697

698

699

700

701

702

703

704

705

706

707

708

The intertemporal region is transversely narrow and anteroposteriorly elongate in all specimens of Coronodon havensteini, generally resembling basilosaurids (Figures 3, 6; Table 2). A tall sagittal crest is developed in all specimens, though in the ontogenetically youngest the apex of the crest is flat but narrow, with a minimum width of 4.1 mm, widening slightly anteriorly and posteriorly; the crest is narrow in the larger juvenile ChM PV 4745 and both adult specimens (CCNHM 108 and 164). However, in ChM PV 4745, it is only sharp along its posterior half and it dissipates anteriorly toward the frontoparietal suture. The length of the intertemporal constriction (gap between the supraoccipital apex and the anteriormost point on the orbitotemporal crest) is relatively shorter in CCCNHM 8722, where it measures only 33% of postorbital width; in ChM PV 4745, it measures 31% of postorbital width. In adult specimens, it measures 46% (CCNHM 108) and 40% (CCNHM 164). However, owing to some uncertainty with reassembled fractures in the intertemporal region, the intertemporal constriction could have been somewhat longer as in CCNHM 108; 40% of postorbital width should therefore be viewed as a minimum value in CCNHM 164. In all specimens the median parietal suture is obliterated and there is no sign of it in broken specimens (CCNHM 164, 8722). The medial wall of the temporal fossa is continuously concave in CCNHM 8722, unlike the straight margin in the holotype; larger juvenile ChM PV 4745 is intermediate, with a slightly longer intertemporal region with a short parasagittal margin anteriorly. Despite breakage in CCNHM 164, the medial wall of the intertemporal constriction was straight-sided and parallel for at least the anterior 2/3 of its length and likely no wider than 90 mm.

709

710

Vertex, Dorsal Braincase, and Occiput





The apex of the supraoccipital is triangular in CCNHM 8722, ChM PV 4745, and CCNHM 108, and is incompletely preserved in CCNHM 164 (Figures 3, 6). The apex of the occipital is positioned at the level of the subtemporal crest in CCNHM 108, 8722, and slightly anterior to the crest in ChM PV 4745, and far anterior in CCNHM 164. This condition is sensitive to skull orientation, but in CCNHM 164, it is possible that the intertemporal constriction was reconstructed too far ventrally, and a condition closer to the holotype is possible.

The occipital/parietal suture is open but mortised in CCNHM 8722 and ChM PV 4745, and more tightly mortised in the holotype. The contact is dorsoventrally extensive and at least 5-6 cm long dorsoventrally in CCNHM 8722. The nuchal crests diverge posteriorly at an 82° angle in CCNHM 8722 and 95° in ChM PV 4745, similar to the holotype (85°); this angle may be affected by some deformation of the vertex in ChM PV 4745. The occipital shield (Figure 12) of the holotype is nearly vertical, whereas in the juvenile specimens it is slightly more anterodorsally sloping. The more completely preserved nuchal crests of ChM PV 4745 slightly overhang the lateral wall of the braincase than in the holotype, a result of the more sloping occipital shield earlier in ontogeny. Such a degree of nuchal crest overlap can be duplicated in the holotype by viewing in posterodorsal view, instead of dorsal view. In the juveniles (CCNHM 8722, ChM PV 4745) the shield bears a short (albeit lower) external occipital crest like the adult; such a crest is absent in *Coronodon planifrons*. Lateral to the crest, the supraoccipital bears faintly rugose surface for the attachment of neck muscles, likely the semispinalis (Schulte, 1916).

The squamosal-parietal suture in all specimens of *Coronodon havensteini* is sinusoidal in dorsal view with an anterolaterally convex curve anteriorly, differing from the sharp corner present in *Coronodon planifrons* and *Coronodon newtoni*; juvenile specimens CCNHM 8722



and ChM PV 4745 exhibit a more sinuous suture than the holotype. The subtemporal crest is sharp and approximately transverse in CCNHM 8722, but trends anteromedially in larger juvenile ChM PV 4745 and adults (CCNHM 108, 164). The subtemporal crest is sharp laterally near the base of the zygomatic process but medially becomes rounded in cross-section.

Ventromedially the parietal of CCNHM 8722 bears a smooth and somewhat rectangular facet for the alisphenoid; the alisphenoid-parietal suture seems to be an open fissure in the larger juvenile (ChM PV 4745). In CCNHM 166, the facet is instead crescentic and unlike the juveniles, the articular surface is somewhat rugose indicating postnatal transition from a planar butt joint to a more firm suture. The anterior half of the parietal in CCNHM 8722 is composed entirely of bone with a strong longitudinal grain. The incomplete condition of CCNHM 8722 permits some observations of the endocranial cavity. Internally there is a smooth (possibly eroded) impression of the right cerebral hemisphere and a low ridge, perhaps the location where the tentorium cerebelli attaches, that differentiates the cerebral hemisphere from the cerebellum.

Basicranium

The squamosal in *Coronodon* is distinctive in possessing an unusually deep and anteroposteriorly shortened zygomatic process (Figures 3-6, 11). The zygomatic process is laterally inflated, medially excavated, and triangular in lateral view. It bears an enlarged squamosal prominence, much larger than in all other toothed mysticetes. The squamosal bears a dorsoventrally deep and proportionally large sternomastoid fossa that faces posterolaterally (Figure 11; Table 2). The squamosals of juvenile specimens CCNHM 8722 and ChM PV 4745 are similar to the adult, though these specimens bear zygomatics that are dorsoventrally



shallower at mid-length (19% of bizygomatic width in CCNHM 8722, 17% of BZW in ChM PV 4745, compared with 26% in CCNHM 108). In ChM PV 4745, the zygomatic processes are much closer (less than 1 cm) to the postorbital processes of the frontals than in the holotype where they are separated by a large gap (8-9 cm); although some of this difference could be ontogenetic, part is due to the tips of the zygomatic processes being broken off in CCNHM 108. The zygomatic processes in ChM PV 4745 are pinched anteriorly giving the entire process a 'spindle' shape in lateral view like in Basilosauridae, *Llanocetus*, and *Coronodon planifrons*. Anteroventrally the zygomatic of ChM PV 4745 further possesses a clear facet for the posterior end of the jugal as in *Coronodon planifrons*. The zygomatic of CCNHM 8722 is composed of more extremely cancellous bone than the rest of the squamosal and in lateral view it is more rectangular; this cancellous bone is preferentially worn away in CCNHM 8722, the holotype, and CCNHM 164, but unabraded in CCNHM 8722. In CCNHM 8722 and ChM PV 4745, the squamosal prominence is proportionally smaller than the holotype and positioned further laterally from the squamosal-parietal suture.

The sternomastoid fossa in the juvenile skulls is large but slightly smaller than the holotype (Figure 5); its depth is 52% of the maximum depth of the squamosal, v. 60% in the holotype (measured from the squamosal prominence to the postglenoid process). In CCNHM 164, the sternomastoid fossa is larger even than the holotype, and extends further anteriorly; the maximum length of the fossa is equivalent to 20% of bizygomatic width, v. 12% in the holotype. In the juvenile specimens, the fossa faces more laterally than in the holotype and CCNHM 164. The fossa is shallowly concave and faintly rugose with a somewhat cancellous and radiating surface texture in CCNHM 8722; in the holotype and CCNHM 164 the surface is more deeply pitted and composed entirely of cortical bone at the surface. It is unclear how far dorsally the



780

781

782

783

784

785

786

787

788

789

790

791

792

793

794

795

796

797

798

799

800

801

fossa extended in CCNHM 8722, but does not appear to have extended dorsally as a thin strip along the lateral edge of the nuchal crest as in *Coronodon planifrons* n. sp. In ChM PV 4745, it terminates at the base of the nuchal crest as in CCNHM 108 and 164, and lacks a dorsal extension like *Coronodon planifrons*. Ventrally the fossa transitions into a rugose and deeply fissured postmeatic process; these deep fissures are not present in ontogenetically older specimens.

The pit for the periotic (Figure 13) is oval in juvenile specimens and approximately twice as long as transversely wide, and bilobate as in adults. In juveniles CCNHM 8722 and ChM PV 4745, the pit for the periotic is oriented nearly parasagittally whereas in both adult specimens (CCNHM 108, 164) the pit is oriented anteromedially and deviates ~30° from the sagittal plane. A smooth, low transverse ridge is present in the juvenile specimens, but is lower than in the holotype; in CCNHM 164, this transverse ridge is higher and sharp. In CCNHM 8722, the fossa posterior to this ridge is punctate. A foramen spinosum is not present in any specimen. The spiny process is broken in CCNHM 8722, but the pit for the periotic was excavated dorsomedial to the process; a shallow oval fossa for the sigmoid process of the bulla is present laterally. There is a 10 mm gap between the spiny process and the falciform process to accommodate the lateral tuberosity of the periotic. When placed in articulation, nearly the entire lateral surface of the periotic is separated from the wall of the pit for the periotic by a gap, nearly 1 cm wide at the base of the anterior process. In this juvenile, the transverse ridge does not conform to the morphology of the lateral surface of the periotic. The posterodorsal angle of the periotic articulates with a dorsally ascending triangular furrow opposite from the spiny process; a sheet of parietal appears to have been received by the trough-like suprameatal fossa as in some early odontocetes (e.g. Xenorophidae; CCNHM 1838). The medial edge of the pit for the periotic is



defined by a sharp ridge formed by the squamosal at the squamosal-parietal suture. The tip of the anterodorsal angle appears to have articulated with the squamosal at the anteriormost end of the pit for the periotic; most of the surface contact for the periotic-squamosal articulation appears to be where the epitympanic recess received the spiny process of the squamosal as well as the gap between the spiny process and the falciform process, which received the lateral tuberosity of the periotic. Despite breakage there seems to have been a 1.5-2cm gap between the posterior process of the periotic and the lateral edge of the postmeatic process, indicating that *Coronodon havensteini* possessed an amastoid condition at all stages of ontogeny. The pit for the posterior process of the periotic is much larger in CCNHM 164 to accommodate the larger posterior process; the ridge between this and the main pit for the periotic is sharper than in CCNHM 108. The periotic of CCNHM 164 articulates tightly with the pit for the periotic along the posterior half of the body and the posterior process, but the anterior process is separated from the lateral wall by an anteriorly widening gap.

The glenoid fossa (Figures 4, 12) is smoothly concave in CCNHM 8722, ChM PV 4745, and CCNHM 108, but in CCNHM 164 the fossa is bilobate and consists of a smooth posterolateral fossa and a smaller, highly rugose anteromedially positioned pit. The secondary pit is positioned just lateral to the falciform process; each side is broken but the left secondary fossa is 30mm wide and 35mm long on the right. The postglenoid process is dorsoventrally shorter in juvenile specimens CCNHM 8722 and ChM PV 4745, and it does not curve anteroventrally at its apex.

The medial wall of the periotic fossa is formed by the basioccipital, and in ChM PV 4745, the lateral surface of that bone is nearly planar, differing from the dorsolateral swelling in the holotype that, in concert with the spiny process, constricts the periotic fossa forming a



bilobate outline in ventral view. Instead, the periotic fossa of ChM PV 4745 is oval. In ChM PV 4745 the dorsal fissure of the periotic fossa (=cranial hiatus of some authors) is widely open and extends anterior to the anterior process of the periotic, whereas in the holotype it terminates at the anterior margin of the pars cochlearis and is developed only as a transversely narrow fissure between the basioccipital and parietal. Dorsal to the periotic fossa in ChM PV 4745 the medial wall of the parietal is vertical whereas it is ventrolaterally sloping in the holotype. The basioccipital crests are more widely set apart in CCNHM 108 than in ChM PV 4745; in the juvenile, the crests are only slightly wider than the occipital condyles. The basioccipital crest in ChM PV 4745 has-a sharp posteroventral and anteroventral edges and is deeply concave laterally; in CCNHM 108, the crest is more transversely inflated and smoothly convex, and the lateral surface is planar. The paroccipital concavity in CCNHM 164 is deeper than in the holotype and bears two deep pits on the left side.

The pterygoid is more completely preserved in ChM PV 4745. The lateral lamina arises from the region of the foramen pseudovale, which is located just lateral to the squamosal-alisphenoid suture. A narrow rectangular and horizontal band of the alisphenoid is exposed ventrally in the temporal fossa of this specimen. The medial lamina of the pterygoid extends posteriorly toward the basioccipital crest and posterior to the anterior edge of the periotic fossa. The foramen ovale is incised into the posterior margin of the alisphenoid in ChM PV 4745; this margin is irregular and bears pits and posterolaterally directed finger-like nodules of bone. The basisphenoid-basioccipital suture is anterodorsally trending and open but partly obscured by the vomer. The pterygoid sinus fossa is deeply concave, smooth, and proportionally small relative to Basilosauridae, being roughly smaller than the periotic fossa.





The occipital condyles are set out on a more distinct neck in CCNHM 164 than in the holotype specimen, where the articular edges are nearly flush with the posterior surface of the exoccipital. The occipital condyles of ChM PV 4745 are proportionally much larger than in the holotype, constituting 33% of bizygomatic width v. 24% in CCNHM 108.

Periotic

The periotics of *Coronodon havensteini* (Figures 14-15; Table 3), as well as *Coronodon newtoni*, *Coronodon planifrons*, and the unnamed coronodonids ChM PV 5720 and CCNHM 214 share the following combination of unique features, to the exclusion of all other cetaceans: low pars cochlearis with triangular outline in ventral view, apex of which positioned just anterior to fenestra rotunda; anterior pars cochlearis narrowed into a cochlear ridge; bladelike anterior process with sharply pointed anterodorsal angle and sharp anterior crest, but anteroventral angle not developed; medial tubercle present anterior to pars cochlearis; anteroposteriorly long, transversely narrow trough-like suprameatal fossa and completely excavated superior ridge; spine-like posterodorsal angle; distally widening posterior bullar facet with flat distal edge; pair of tubercles on body near posteroexternal foramen. Some of these features (low triangular pars cochlearis, cochlear ridge, suprameatal fossa developed as long trough) are shared with *Kekenodon onamata*, and others (bladelike anterior process with spine-like anterodorsal angle, spine like posterodorsal angle, and trapezoidal posteriorly widening posterior bullar facet with flat posterior end) are further shared with cf. *Kekenodon* (OU 22294).

Partial or complete periotics are known for all specimens of *Coronodon havensteini*. The anterior process, body, and pars cochlearis are all approximately the same anteroposterior length,



but the periotic becomes transversely inflated, dorsal structures become more elaborated, and the posterior process lengthens and enlarges during postnatal ontogeny. For example, the distance from the anterior process to the fenestra ovalis is 44.3 mm in juvenile CCNHM 8722 and 44.6 mm in adult CCNHM 108. Periotics of *Coronodon havensteini* (and indeed, *Coronodon* spp.) are highly unusual in lacking a continuous superior ridge, possessing dorsoventrally deep anterodorsal and posterodorsal angles, an obtuse (~160-180°) angle between the pars cochlearis and the anterior process, an elongate pars cochlearis that is dorsoventrally shallow anteriorly, forming a cochlear ridge, a trough-like suprameatal fossa. The dorsal side of the periotic looks dramatically different in these specimens, as ossification begins ventrally within Cetacea and progresses dorsally during postnatal growth (Bisconti, 2001). Amongst all Cetacea, these periotics most closely resemble *Kekenodon onamata* and the Eomysticetidae, and to a lesser extent, Aetiocetidae and Mammalodontidae.

The ontogenetically youngest specimen, CCNHM 8722, has the most gracile periotic. The posterior process is missing, but it is otherwise well-preserved; it and somewhat larger juvenile ChM PV 4745 have a more gracile, transversely narrow anterior process and a lateral tuberosity that extends laterally beyond the margin of the body. In ChM PV 4745, the body is more inflated and the lateral tuberosity extends only slightly beyond the lateral margin. The anteroexternal sulcus is broader and deeper in CCNHM 8722 and ChM PV 4745 than in adult specimens; in CCNHM 108 and 164, the sulcus is more narrowly (and shallowly) incised, where it is pinched between the body and swollen anterior process. The anterior process is transversely thicker in each specimen, having a width of 16.4 mm at anteroposterior midpoint in CCNHM 8722, 17.1 mm in ChM PV 4745, 16.5 mm in the holotype, and 23.1 mm in CCNHM 164. The mallear fossa is larger in CCNHM 164 than in the holotype, measuring 10mm wide v. 7mm in



893

894

895

896

897

898

899

900

901

902

903

904

905

906

907

908

909

910

911

912

913

914

the holotype; the fossa incudis is deeper and more defined, perhaps a result of the anomalous surficial wear in the holotype periotics.

The anterior incisure is more deeply incised in the juveniles and accommodates a trough for the tensor tympani; just medial to this trough is a longitudinal ridge on the anteroventral surface of the pars cochlearis. In CCNHM 108 and 164 the inflation of the anterior process has resulted in ossification that overlaps and fills this trough, obscuring the ridge on the pars cochlearis. The incisure itself is an obtuse angle in all specimens of Coronodon, but in juvenile specimens CCNHM 8722 and ChM PV 4745 the incisure forms an angle of 143° and 145° (respectively), as opposed to 173° in the holotype. An anterointernal sulcus is present in older specimens; in CCNHM 164 the sulcus is finely incised, runs along the ventral margin, and bifurcates into a dorsal and ventral branch. The dorsal part of the anterointernal sulcus runs toward the anterodorsal angle and the ventral branch runs along the ventral margin. The anterodorsal angle is dorsally higher and more acute in the holotype, and relatively lowerin CCNHM 8722, and slightly higher in ChM PV 4745; it is prominent in CCNHM 164. In ChM PV 4745, the anterodorsal angle is positioned further anteriorly than in CCNHM 8722 or 108. In CCNHM 8722, there is a secondary spur just posterior to the dorsal terminus of the anteroexternal sulcus; a pair of foramina are present at the ventral end of the sulcus. In CCNHM 164, two anteroexternal sulci are present: the primary sulcus that runs anterodorsally and a shorter vertically oriented sulcus just posterior. A fissure-like transverse sulcus, not connected to the anteroexternal sulcus, is present posterior to the anteroexternal sulcus at the anterior margin of the suprameatal fossa in both CCNHM 8722 and ChM PV 4745; it crosses the low superior ridge and trends posteromedially into the fossa. In CCNHM 108, this sulcus is only developed medial to the crest and defines a highly rugose and inflated segment of the crest. The



anteroventral angle of the periotic is more defined and corner-like in CCNHM 164, and it forms a vertical crest along the anterior margin of the anterior process. The anterior process is dorsoventrally deeper in CCNHM 164, being 37.5mm deep v. 34.2mm deep in the holotype. The anterodorsal angle is more greatly developed and lacks a dorsomedial fossa seen in CCNHM 8722, ChM PV 4745, and CCNHM 108. Anteriorly within the suprameatal fossa of the juvenile specimens, just anterior to the facial canal, are irregular fissures, corresponding to a 4 x 9mm region of cancellous or micronodular bone in the holotype.

In both juveniles (CCNHM 8722 and ChM PV 4745) the facial canal opening is oval shaped and dorsomedially oriented, and lacks an elongated fissure-like hiatus fallopii like the holotype specimen, which measures 9.5 mm in length. The crista transversa is deeply recessed in these specimens so that the facial canal occurs within the meatus, as opposed to the separate canal and meatus in CCNHM 108. The foramen for the superior vestibular area (=foramen singulare of earlier studies) occurs laterally within the meatus in these juveniles.

Juvenile periotics (CCNHM 8722, ChM PV 4745) lack a secondary spur medial and adjacent to the posterodorsal angle, and a longitudinal sulcus is absent in CCNHM 8722; this sulcus is present anterior to the angle in ChM PV 4745, but does not separate this secondary spur from the posterodorsal angle as in CCNHM 108. This secondary spur is conical in CCNHM 108 and is equivalent to the "pyramidal process" of Marx et al. (2015). The posterodorsal angle is low in CCNHM 8722, somewhat more prominent in ChM PV 4745, and much higher in CCNHM 108; the condition in CCNHM 164 is unclear owing to breakage but appears to have been at least as well-developed as in the holotype.

The ventral side of the pars cochlearis in the holotype is anomalously polished but well-preserved in CCNHM 8722 and ChM PV 4745; in these specimens, and especially CCNHM



8722, there is a low longitudinal crest immediately lateral to the fenestra ovalis. Deep promontorial grooves are present in all specimens; the dorsal groove is present just medial to the meatus, and the ventral groove is positioned just ventral to the medial edge of the pars cochlearis. In CCNH 8722, the groove is floored by finely laminated and apparently fibrolamellar bone indicating rapid growth.

The lateral surface of the body is not inflated in CCNHM 8722, and bears a smooth and punctate surface texture; the lateral tuberosity is long (21.9mm from fenestra ovalis, v. 18.3mm in ChM PV 4745 and 19.5mm in CCNHM 108) and projects far beyond (7 mm) the lateral margin of the body in ventral view. In ChM PV 4745 it is slightly more inflated and projects only 2 mm beyond the lateral margin. In CCNHM 108 and 164 the lateral edge of the lateral tuberosity does not project beyond the lateral edge of the body and instead the body extends 4mm and 2mm (respectively) past the tuberosity. In CCNHM 108 and 164, the lateral surface is swollen and bears a rugose surface texture, especially posteriorly near the posteroexternal foramina.

Only a single posteroexternal foramen is present in CCNHM 8722 and ChM PV 4745; in CCNHM 108 there are three posteroexternal foramina. Though damaged in the more complete left periotic of CCNHM 164, a fragment of the right periotic confirms the presence of three posteroexternal foramina. Only a single posteroexternal foramen is present in *Coronodon newtoni*, *Coronodon planifrons*, and all other toothed mysticetes.

The aperture for the vestibular aqueduct is wider in CCNHM 8722 (10.7mm v. 7mm in CCNHM 108); the other juvenile specimen, ChM PV 4745, has a narrow fissure-like aperture as in the holotype. The lateral wall of the meatus extends further dorsally than the medial wall in all specimens, but posterolateral meatal spurs are absent in the juveniles (CCNHM 8722, ChM PV



962

963

964

965

966

967

968

969

970

971

972

973

974

975

976

977

978

979

4745), instead bearing a smoothly convex posterolateral meatal rim in medial view. A large tubercle is present in CCNHM 8722 posterodorsal to the fenestra rotundum, and bears several short sulci; this tubercle is less prominent in CCNHM 108, 164, and ChM PV 4745.

The posterior process of the periotic is anteroposteriorly short in ChM PV 4745 and bears a nearly diamond-shaped posterior bullar facet, differing from the posteriorly expanding facet in CCNHM 108 and 164. It lacks pits or a facet for the postmeatic process seen in CCNHM 108 and 164. In CCNHM 164, the posterior bullar facet differs from the trapezoidal facet in the left periotic of the holotype, and instead resembles the slightly diamond shaped facet in the right periotic of the holotype; the posterior margin, while being slightly pointed, still exhibits a nearly flat posterior margin and the entire facet widens posteriorly. The posterior process is longer as well, being 52mm in CCNHM 164 v. 42.6 mm in the holotype and only 28.2 mm in ChM PV 4745. The facet in CCNHM 164 is transversely convex and bears subtle striations, but more obviously developed than in the holotype. The facet is 42.6mm long at the middle v. 38.4mm in the holotype. The posterior process extends a further 11mm past the termination of the facet, forming a posteroventrally facing secondary articular facet for the postmeatic process of the squamosal. This means that in late postnatal ontogeny, the postmeatic ridge/process began to anteriorly overlap the posteriormost end of the posterior process of the periotic – the latter of which appears to have grown posterodorsally. The entire periotic of CCNHM 164 is 102.9mm v. 94.7mm in CCNHM 108.

980

981

Tympanic Bulla



A tympanic bulla is preserved in the holotype and both juvenile specimens (Figure 16; Table 4). Juvenile bullae are similar to the adult but are absolutely smaller; CCNHM 8722 is 75mm long, ChM PV 4745 is 76.7 mm long, and CCNHM 108 is 85mm long. The bulla of CCNHM 8722 is slightly proportionally narrower, the width being 61% of length whereas the width is 66% of the length in CCNHM 108.

The medial margin of the involucrum is more concave in CCNHM 8722 than the holotype and bears an oblique furrow on the medial side of the involucrum. This surface is flat in the holotype. Anterior to the inner posterior pedicle there is a small fossa on the dorsal side of the involucrum in CCNHM 8722 as compared to a prominent bulge in the holotype. Both the inner and outer posterior pedicles are more delicate in CCNHM 8722. The medial lobe is proportionally smaller than in the holotype, constituting 50% of transverse width, rather than 60% as in the holotype. CCNHM 8722 bears a very short median furrow that terminates into a low ventral prominence, as in Basilosauridae and Llanocetus; in ChM PV 4745, CCNHM 108, and 164, *Coronodon newtoni*, *Coronodon planifrons*, and virtually all other toothed mysticetes, this ventral convexity is absent and the surface is instead flat to shallowly concave.

Dentition

Juvenile CCNHM 8722 preserves no teeth, but ChM PV 4745 preserves two caniniform teeth and the upper left M1 and M2 (Figure 17; Table 5). CCNHM 108 preserves the upper P3 and M1/2 and nearly the entire lower dentition (Figures 18-19; Table 5), missing only the incisors, canines, and m4. CCNHM 164 has a more incomplete lower dentition (n=6; p2-m4), but preserves numerous upper teeth (n=9, P3-M3).





For dental descriptions besides the caniniform teeth, cusps are identified as either the central cusp or those mesial or distal to it, each denticle identified as being first, second, third, and so forth, with respect to their distance from the central cusp. The central cusp is determined by being the largest cusp and is typically at or near the mesiodistal center of the tooth. Each of these denticles, including the central cusp, are united by a crown base. As these teeth slightly resemble a hand, the analogy could be carried out to make the denticles and central cusp the fingers and the crown base the palm. Each of the rows of denticles follow an axis along the mesiodistal length of the tooth and are sloped in labial and lingual view with respect to the crown base. The differences in slopes with respect to the crown base are noted, as is the curvature of that slope, which always tend to be arched (but to lesser and greater degrees).

Regarding enamel texture and smaller details, it should be noted that none of the teeth of *Coronodon* have cingula, yet they all have carinae. The carinae follow mesiodistally along the edge of each denticle and the central cusp, and tend to be more pronounced at the base of each denticle, resulting in the base of each denticle being slightly pinched in, making them all appear a bit "plump". This coincides with a depression of the crown base in between each denticle that can carry down to the basal-most edge of the crown, forming a shallow trough. These apicobasal crown base troughs usually result in clustering the more mesial or distal denticles on one side, and those denticles closer to the central cusp on the other. A central apicobasal crown base trough typically lies basal to the central cusp itself (possibly making the teeth prone to taphonomic breakage along the central cusp), usually found to be deeper on the lingual than the labial side of the tooth.

The enamel is thinner than that found in *Basilosaurus*, and typically covered with undulating oblong bumps and depressions at a very small scale, much less than a millimeter in



size. These bumps and depressions can be found everywhere on the enamel besides polished surfaces of the apices of some cusps and denticles and the surfaces of shear facets.

Regarding the roots, for those teeth (both upper and lower) for which both roots are preserved, it is readily notable that the mesial root is thicker, straighter, and more vertically oriented than the distal root of the same tooth. Distal roots tend to be tilted more distally and slightly narrower, not only in the thick part nearest the crown base, but the distal roots also taper more than the mesial roots.

Caniniform teeth

All of the caniniform teeth (by definition), have a single, pointed cusp (Figure 17). The caniniform teeth appear to have apicobasal lengths greater than their mesiodistal lengths, with roots approximately twice the length of the apicobasal length of the crown. Subtle carinae can be seen on all cusps of these teeth as well as some minor apicobasal ridges extending from the base of the crown to very near the apices. All of them appear to have had a thicker root at some point, with a layer of cementum that thickened within a centimeter of the crown's base.

Upper dentition

The third upper left premolar (CCNHM 164.37) exhibits the same palmate cusp structure found in the holotype CCNHM 108 (Figure 18). The upper right P3 has four denticles mesial to the central cusp, and three distal to the central cusp. The mesial row of denticles get smaller mesially, whereas the distal row of denticles are more subequal in size and do not get as



progressively smaller distally. The slope of the mesial row of denticles appears to dip toward the base of the crown more steeply than does the distal row of denticles, though this illusion seems due to the increased number denticles on the mesial row, making it extend further basally, as well as the greater change in size of the denticles along the mesial row as compared to the distal row of denticles.

The upper left P4 (CCNHM 164.3) has four mesial and four distal denticles surrounding the central cusp (Figure 18). The denticles of the mesial and distal rows get smaller the further away from the central cusp, but they do not seem to do so in an appreciably different degree way. The slopes of the mesial and distal rows of denticles also do not seem to differ from each other. Ultimately, this makes the crown of the P4 more symmetrical, with the roots primarily indicating mesial and distal ends of the tooth.

The upper M1 (CCNHM 164.8) is only known from the right side for CCNHM 164, and several denticles are broken or worn, but it clearly had three mesial and three distal denticles when intact (Figure 18). The most mesial and most distal denticles are more similar in size to the central cusp than those of either the P3 or P4. The slopes of the mesial and distal denticle rows appear to be less than the same slopes on the P4, but this, too, could be because of the smaller denticle count and greater similarity of denticle size within rows.

CCNHM 164.39 could either be a distal fragment of the upper right M2 or M3 (Figure 18). Based on the tendency for the shallow apicobasal groove to lie basal to the central cusp, it seems that the large cusp preserved here is the central cusp. Distal to it are four progressively smaller distal denticles. These denticles differ in size more than the distal denticles of the M1 or P4, and are more similar in decreasing proportions like the distal denticles of the right P3 (CCNHM 164.7).



The most complete M3 is from the right (CCNHM 164.6) and is missing much of its mesial edge (only preserving two denticles), though its distal side retains four well-preserved distal denticles (as does the left M3, CCNHM 164.4) (Figure 18). The apices of the central cusp and denticles of the M3 have a more triangular profile than do the equivalent denticles of the more mesial teeth (which appear more rounded in profile). This more triangular profile makes the tips of each denticle narrower than their base, which resembles the denticles of *Borealodon* and *Metasqualodon* more than the rounded profiles of the denticles of the more mesial teeth of *Coronodon*.

Lower dentition

CCNHM 164.5 is a right lower p2 (Figure 19), and has a large central cusp surrounded by two much smaller mesial denticles and three distal denticles. The equivalent tooth in the holotype (CCNHM 108) has only one mesial denticle and three distal denticles. The mesial denticles are half the size of the distal denticles. This tooth looks very similar to the Nishiyama specimen of *Metasqualodon* from the Ashiya Group (Okazaki, 1982), except that the Nishiyama tooth lacks mesial denticles altogether and the distal denticle arises off a location closer to the apex of the central cusp. In addition, the lower right p2 of CCNHM 164 has some waviness in the profile of its carinae for the mesial and distal denticle adjacent to the central cusp, as well as the carinae of the central cusp itself.

The right lower third premolar (CCNHM 164.2) (Figure 19) has three mesial denticles and five distal denticles. The mesial denticles are approximately the same size as the distalmost three denticles of the distal row, with only the distal denticle adjacent to the central cusp being



larger than all of the other denticles (mesial and distal). This asymmetry in number and size creates an asymmetry in the central cusp that makes the slope of the mesial denticle row appear steeper than the distal row. The central cusp is also shifted a few millimeters mesially, and its distal edge and carina is apicobasally shorter than its mesial edge.

CCNHM 164.10 and CCNHM 164.9 are both identified as a right lower m1 or m2 (Figure 19). It is unclear which one is which. CCNHM 164.10 has five mesial and five distal denticles on either side of the central cusp. The denticles are approximately the same size and the denticle rows are almost at the same slope. The only minor difference between the two denticle rows is that the mesial row is arranged in a slightly straighter line and the distal row's profile is more rounded, like an arc (this is especially notable from the lingual view). CCNHM 164.9 has four mesial and four distal denticles, though the denticles of the distal row are larger than those of the mesial row. Like CCNHM 164.10, the mesial row of denticles has a steeper and straighter slope and the distal row appears to have a more rounded profile (like an arc), in contrast to the mesial denticle row, which is a bit straighter.

The lower left m3 is represented by CCNHM 164.41 (Figure 19), though this identification is tentative because this tooth is incomplete. This partial tooth consists of the mesial row of denticles, the mesial root, and the majority of the crown base, with evidence of five mesial denticles aligned at an angle that is steep like in the other lower molars. The preserved part of the labial side of the crown base includes shallow apicobasal grooves indicative of the presence of at least two distal denticles, though there were surely more.

CCNHM 164.4 is the lower right m4 and has four mesial and four distal denticles (Figure 19). The mesial denticles are approximately the same size as their respective opposite on the distal denticle row, but the mesial row itself is longer and more steeply sloped than the distal





row. Like the lower molars mesial to the m4, the mesial denticle row's profile appears straighter than the slightly more arced profile of the distal denticle row.

Four teeth are preserved in juvenile specimen ChM PV 4745, including two loose caniniform teeth likely representing I³ or C¹ and C¹ or P¹, as well as the upper left M¹-², both of which are in situ within the maxilla (Figure 17). All teeth are hollow with voluminous pulp cavities, only ~2 mm thick dentine, and relatively short roots, no longer than about 21 mm in the larger caniniform tooth. Both caniniform teeth possess erect subconical crowns with sharp, smooth mesial and distal carinae. The labial enamel is smooth but lingually there are low, parallel apicobasal ridges. The M¹-² are similar to the preserved M² in the holotype (CCNHM 108) but differ in possessing four mesial and four distal accessory cusps (rather than five of each in CCNHM 108). These molars are only partly erupted, with the mesial and distal edges of the enamel crown base still in the labial part of the alveolus (and obscured by the maxilla) in lateral view. Unlike the anteroposteriorly aligned alveoli of the holotype, the molars are posterolaterally imbricated and overlap by 9.5mm in ChM PV 4745, with the distal edge of M1 positioned labial to the mesial edge of M2, forming a posterolaterally directed interdental slot like the mandibular postcanine dentition in the holotype (Geisler et al., 2017).

Mandible

Mandibles are only preserved in the adult specimens, including the nearly complete left and right mandibles in the holotype and a partial right mandible in CCNHM 164 (Figures 20-21; Table 6). The posterior half of the right mandible in CCNHM 164 is partially preserved with partial alveoli for p3-m2, a well-preserved coronoid process and mandibular condyle, though the



angular process and entire medial surface is missing ventral to the m4 and coronoid process, so that the morphology of the mandibular foramen is unclear. Like the holotype, the ventral margin is roughly straight, and a slight curvature around the p4-m1 may be due to accumulated minor inaccuracies created when gluing many fragments of the mandible together. It is slightly longitudinally sinuous, and lacks the more extreme ventral curvature seen in *Coronodon newtoni*.

The m4 alveolus is elevated approximately 3-4 cm dorsal to the mandibular condyle in CCNHM 164, somewhat higher than in the holotype, though this part of the mandible is damaged. The coronoid process is complete in the right mandible of the holotype and CCNHM 164; it is intermediate in morphology between the triangular condition in Basilosauridae and the elongate tongue-shaped process in Aetiocetidae: it is somewhat lobate with convex and equally sloping anterior and posterior margins, whereas in Basilosauridae the posterior margin is nearly vertical. The coronoid is slightly thicker anteriorly and is transversely thickened at the apex. A pre-coronoid trough is present medially along the anterior margin of the coronoid, in line with the m4 and posterior toothrow. In CCNHM 164 there is a low but well-developed tubercle posteromedially along the posterior margin of the coronoid, 35mm dorsal to the margin of the mandibular foramen.

The mandibular foramen of CCNHM 164 is voluminous and approximately 10 cm deep dorsoventrally; unlike the holotype, the margins are unknown. This breakage reveals that the mandibular canal is similarly large and continues anteriorly to at least the level of the p4; the walls of the mandible increase in thickness anteriorly. The mandibular condyle is separated from the coronoid process by an 8 cm long neck; the condyle is planoconvex in articular view, shallowly excavated medially by the mandibular fossa, and it faces posterodorsally. The articular surface is deeply pitted and rugose.

Atlas

Complete atlases are preserved in ChM PV 4745 and the holotype; a fragmentary atlas is present in CCNHM 164 (Figures 22-24; Table 7). The atlas of CCNHM 164 is similar in size and proportions to CCNHM 108 but the transverse process is dorsoventrally shallower. The atlas of ChM PV 4745 differs from the holotype in being anteroposteriorly somewhat flatter and having an oval-shaped neural foramen that does not narrow ventrally. Like the holotype and unlike *Coronodon planifrons* (CCNHM 166), a hypapophysis is not developed. ChM PV 4745 possesses the only complete transverse process in *Coronodon*; it is transversely directed and rectangular in anterior view with a vertical lateral margin, unlike the bifurcated posterolaterally directed condition in Basilosauridae and some stem odontocetes.

Axis

A complete axis is preserved in CCNHM 108 and a partial axis is present in CCNHM 164 (Figures 22-24; Table 7). The more complete axis of CCNHM 108 is noteworthy for exhibiting a transverse foramen. The axis of CCNHM 164 possesses a more projecting odontoid process and larger hypapophysis and a less dorsally arched ventral margin in anterior view. The anterior part of the neural spine is preserved and is massive, stout, and pyramidal; the neural spine is proportionally wide.

C3-C7



Two partial mid-cervicals are present in CCNHM 164, C3 and C4 based on comparison with CCNHM 108 (Figures 22-24; Table 8). They do not differ from CCNHM 108 except in possessing centra with more rounded ventral margins, whereas the mid-cervical centra in the holotype are all nearly rectangular.

1186

1187

1188

1189

1190

1191

1192

1193

1194

1195

1196

1197

1198

1199

1200

1201

1202

1203

1204

1182

1183

1184

1185

Thoracic Vertebrae

An apparently complete set of nine thoracic vertebrae are preserved in CCNHM 164, whereas in CCNHM 108, only seven are preserved (Figures 22-24; Table 9). Based on measurements these form a continuous series in CCNHM 164 (T1 to T9). The anteriormost thoracics (T1-2) are dorsoventrally shallow and possess oval centra bearing shallow notochordal pits posteriorly. Pore-like notochordal pits are present anteriorly in T1-7 and small fissure-like pits are present in T8-9. T1-2 bear anterior costal facets at the dorsolateral edge of the centrum but T3 does not. Small posterior costal facets are present in T1-5, whereas in T6-7 they are large and concave, small again in T8, and absent in T9. T3-5 are successively longer than T1-2, and length increases steadily throughout the thoracics; centrum depth increases from T1 to T5, and depth is consistent throughout the remaining thoracics (T6-9). In the posterior thoracics (T6-9) the dorsal edge of the centrum becomes more flattened; all thoracics bear a rounded ventral margin and lack a ventral keel. In T7-9 the costal articulations transition rapidly. T6-7 bear a facet for the tubercle on the pedicle of the vertebra but in T8 the tubercular facet is further ventrally at the base of the pedicle at its junction with the centrum; the capitular facet is located only 15mm ventrally. In T9 there is only a single capitular facet for a rib lacking a tubercle; it is positioned laterally on a short transverse process positioned at the level of the dorsal half of the centrum.



Lumbar Vertebrae

Lumbar vertebrae are preserved only in CCNHM 164, which preserves three recognized here as LA, LB, and LC (Figures 22-24; Table 10); these are of nearly identical centrum length but are arrayed in anteroposterior sequence based on increasing centrum width and decreasing neural foramen diameter. LA has a subpentagonal anterior centrum with a flat dorsal edge and somewhat pointed median ventral margin; the ventral surface has a sharp median keel. LA also exhibits a long (but partial) ventrolaterally projecting transverse process, oriented 26° from horizontal. LB has a more circular centrum as well as a sharp ventral keel. LC is quite abraded and weathered but had a circular to oval posterior centrum with an arthritic pathology forming a ventral lip along the ventralmost margin and somewhat on the left side. All three lumbars possess 3-4mm deep fissure-like notochordal pits.

Ribs

Several partial ribs are preserved in the holotype (CCNHM 108; Geisler et al., 2017: fig. S3) and rib fragments are preserved in CCNHM 164. See Geisler et al. (2017: supporting information) for a description of the holotype ribs.

Scapula

A partial right scapula is preserved in CCNHM 164 (Fig. 23), including the distal end and the inferior border. The scapula appears to have been more strongly fan-shaped relative to the





anteroposteriorly narrow scapula of most Basilosauridae, and widens more abruptly immediately proximal to the glenoid fossa. The inferior border seems straight but it is unclear if a posteroventral hook was present. The glenoid fossa is large and oval in shape, measuring 60 mm wide and 80 mm long; the fossa is shallowly concave and bears a slightly pointed anterior end. In lateral view the anterior part of the glenoid fossa extends anteroventrally. The broken base of the coracoid process is present, measuring 18 mm in diameter and is circular in shape. Based on the broken cross-section the anterior border of the scapula was transversely thick, about 3 cm just dorsal to the distal end.



1234	
1235	
1236	
1237 1238	Coronodon newtoni n. sp. LSID urn:lsid:zoobank.org:act:987DE600-70D1-426B-9F6E-4FE477E3387D
1239	
1240	Type Specimen
1241	ChM PV 2778, partial skeleton including nearly the entire left side of a skull, three teeth,
1242	periotic, bulla, nearly complete left mandible, three vertebrae, and one rib, collected October
1243	1978 by Claude and Albert Newton, Albert Sanders, and Peter Coleman from the Chandler
1244	Bridge Formation in the vicinity of North Charleston, Charleston County, South Carolina, USA.
1245	Type Locality
1245 1246	Type Locality The holotype specimen of <i>Coronodon newtoni</i> was collected from a manmade exposure of the
1246	The holotype specimen of <i>Coronodon newtoni</i> was collected from a manmade exposure of the
1246 1247	The holotype specimen of <i>Coronodon newtoni</i> was collected from a manmade exposure of the Chandler Bridge Formation in the vicinity of North Charleston, Charleston County, South
1246 1247 1248	The holotype specimen of <i>Coronodon newtoni</i> was collected from a manmade exposure of the Chandler Bridge Formation in the vicinity of North Charleston, Charleston County, South Carolina, USA. Detailed locality information on file at ChM.
1246 1247 1248 1249	The holotype specimen of <i>Coronodon newtoni</i> was collected from a manmade exposure of the Chandler Bridge Formation in the vicinity of North Charleston, Charleston County, South Carolina, USA. Detailed locality information on file at ChM. Horizon and Age
1246 1247 1248 1249 1250	The holotype specimen of <i>Coronodon newtoni</i> was collected from a manmade exposure of the Chandler Bridge Formation in the vicinity of North Charleston, Charleston County, South Carolina, USA. Detailed locality information on file at ChM. Horizon and Age Chandler Bridge Formation, late Oligocene (24.7-23.5 Ma).
1246 1247 1248 1249 1250	The holotype specimen of <i>Coronodon newtoni</i> was collected from a manmade exposure of the Chandler Bridge Formation in the vicinity of North Charleston, Charleston County, South Carolina, USA. Detailed locality information on file at ChM. Horizon and Age Chandler Bridge Formation, late Oligocene (24.7-23.5 Ma). Diagnosis



with lower accessory cusps, shorter roots, and a shorter crown (70% lower relative to anteroposterior crown length), and absence of maxillary embrasure pits posterior to P2; from both *Coronodon havensteini* and *Coronodon planifrons* n. sp. in possessing a ventrally convex ventral margin of the mandible, a mandibular condyle elevated far above the m4 alveolus, and possessing a more dorsoventrally inflated preorbital process of the frontal that is deeper than the postorbital process, possessing a gracile periotic with transversely narrow anterior process, short posterior process, a less inflated lateral surface of the body and a lateral tuberosity that is much longer and laterally prominent in medial view, possessing periotic with proportionally larger spiral cribriform tract and crista transversa recessed shallowly within external acoustic meatus; from *Coronodon planifrons* n. sp. in having a ventrolaterally sloping supraorbital process of the frontal, possessing periotic with transversely narrow fissure-like endocranial opening of facial canal (shared with *C. havensteini*), and suprameatal fossa developed as a narrow trough along its entire length.

Description

Rostrum

ChM PV 2778 is unique amongst specimens of *Coronodon* in preserving the maxilla in articulation with the frontal, albeit imperfectly (Figure 25; Table 2). The frontal seems to be tilted so that the medial part is anteroventrally deflected and the rostrum is deflected medially and to the right side; a corrected reconstruction is shown in Figure 26. A ventral sliver of the left premaxilla is preserved in articulation with the maxilla, and preserves alveoli for somewhat





procumbent I1-3. The premaxilla is transversely narrow and bears shallow pits on its lateral surface between alveoli for teeth.

The maxilla has a straight lateral edge; in cross-section it is flat dorsally and dorsoventrally thick (~5 cm medially) but thins laterally and becomes dorsolaterally convex in cross section. Anteriorly the entire surface of the maxilla slopes laterally. The antorbital process is developed as a steep face anterior to the lacrimal in all specimens (partial in CCNHM 8722 and 164), with a thin flange of maxilla buttressing the anterior margin of the lacrimal. The fossa for the lacrimal is well-preserved in ChM PV 4745 and CCNHM 108; the fossa is smooth, dorsoventrally shallow, oval, and anteromedially trending. The maxilla-lacrimal suture was unfused at all ontogenetic stages. Sutures between the frontal and maxilla are not mortised. The lacrimal occupies a gap between the frontal and maxilla, and extends medially for about 6-8 cm; flexion between the rostrum and frontal likely occurred at the frontal-lacrimal joint. The antorbital notch is developed as a shallow inclined groove below the antorbital process and presumably transmitted the facial nerve. This groove faces anteroventrally and somewhat laterally. A short, but incomplete infraorbital process of the maxilla extends ventral to the preorbital process of the frontal, but does not underlie the orbit as in archaeocetes.

In lateral view, the alveolar margin of the maxilla is slightly convex ventrally, conforming to the curvature of the alveolar margin of the mandible (Figure 26). Ventrally, alveoli are present for C1, P1-4, and M1-3; only the C1-P1 are single rooted. P2 has closely appressed alveoli for the roots; they are slightly more widely separated in P3, and widely separated in P4-M3. Large diastemata are present between C1-P2; small (~1cm) diastemata are present between P2-4. P2 and P3 are aligned parallel with the maxillary edge, but all alveoli posterior to this (P4-M3) are rotated with the mesial root alveolus shifted labially and the distal



anterolaterally (rather than anteriorly or even anteromedially to be parallel with the maxillary edge). Further, the overlapping of the alveoli indicates that these teeth would have overlapped with the distal root lying anterolabial to the mesial root lobe of the tooth immediately posterior to it, with posterolaterally oriented interdental slots like the mandibular cheek teeth of *Coronodon havensteini*. Accessory alveoli for 'demi-roots' are not present, unlike *Coronodon havensteini*.

Embrasure pits are present between C1 and P1 and between P1 and P2, but there is only a shallow embrasure pit posteromedial to P2. Other pits present further posteriorly in *Coronodon havensteini* (CCNHM 108), such as those medial to the M1 and M2, are not obviously developed in ChM PV 2778. The palate is similar to *Coronodon havensteini* but appears less excavated medial to the molars; like the holotype of *Coronodon havensteini*, there appears to have been a broad triangular exposure of the vomer posteriorly. A deeply excavated and medially convex greater palatine sulcus is developed along the medial edge of the maxilla. The lateral edge of the maxilla descends ventrally to form a vertical lip along the labial edge of the teeth.

Frontal

The frontal is similar to *Coronodon havensteini* and *Coronodon planifrons* n. sp. in dorsal and ventral view and shares a similar articulation with the rostral elements. In lateral view, the preorbital process is massive and dorsoventrally thick, and deeper than the postorbital process; this differs from the condition in *Coronodon havensteini*, where the pre- and postorbital processes are equivalent in depth, and from *Coronodon planifrons* n. sp. where the postorbital process is deeper. The postorbital process has a rectangular outline in lateral view. The preorbital





process shares a concavo-convex ball joint with the lacrimal. The orbitotemporal crest was positioned posterodorsally with a subvertical posterior surface, like CCNHM 108, though it notably overhangs the temporal fossa more than in CCNHM 108.

Squamosal

The left squamosal is well preserved, and does not differ much from *Coronodon havensteini*, but has a lower squamosal prominence and a dorsoventrally deeper postglenoid process. The lateral edge of the zygomatic process is more convex in dorsal and ventral view. The squamosal prominence is positioned further anteromedially than in *Coronodon havensteini*. The squamosal-parietal suture bears a sharp anterolateral corner in dorsal view, so that the anteriormost part of the suture jogs laterally; in *Coronodon havensteini* this forms a smoothly convex arc.

Periotic

The periotic (Figure 27; Table 3) is well-preserved and similar in size and anteroposterior length to *Coronodon havensteini* and *Coronodon planifrons* n. sp., but differs chiefly in being much more gracile in overall proportions and most closely resembles the periotics of juvenile *Coronodon havensteini* (ChM PV 4745, CCNHM 8722). The anterior process is transversely narrow and the body of the periotic is not laterally inflated; the distance between the fenestra ovalis and the lateral margin is close to the transverse width of the pars cochlearis (150%), whereas it is slightly thicker (approximately 170% of the pars cochlearis width) in *Coronodon havensteini* and *Coronodon planifrons* n. sp. The anterior process is dorsoventrally shallower



than other species of *Coronodon*, with a flat medial margin in ventral view as opposed to the slightly convex margin in other *Coronodon* spp. The angle between the anterior process and pars cochlearis in ventral view is 152°, similar to juveniles of *Coronodon havensteini* (143-145°). The suprameatal fossa is transversely narrow and the superior process is so reduced that the medial wall of the fossa is visible in lateral view.

The mallear fossa is proportionally large and circular. The lateral tuberosity has a sharp transverse crest and protrudes far beyond the lateral margin of the periotic body, a result of the lack of inflation of the periotic body. Even so, the lateral tuberosity is large as in *Coronodon planifrons* n. sp., differing strongly from the tubercle-like tuberosity in *Coronodon havensteini*. The internal acoustic meatus is distinctive; the spiral cribriform tract and facial canal are not aligned as in other *Coronodon* spp. Instead, the spiral cribriform tract is anterolaterally divergent and forms an obtuse angle medially with the opening of the facial canal.

The posterior process is short, equidimensional, and leaf-shaped, similar to juvenile *Coronodon havensteini* specimen ChM PV 4745; it is approximately as long as the pars cochlearis, whereas it is 150% of pars cochlearis length in the *Coronodon havensteini* holotype. The posterior bullar facet is more deeply grooved than in the holotype of *Coronodon havensteini*. The posterior process does not widen posteriorly and lacks the spurs on the posterior margin characteristic of the *Coronodon havensteini* holotype.

Tympanic Bulla

The tympanic bulla (Figure 28; Table 4) is very similar to *Coronodon havensteini* and approximately the same size as the adult holotype (CCNHM 108). The bulla differs from



Coronodon havensteini in possessing a more deeply excavated concavity on the medial margin of the involucrum in dorsal view; in medial view, the involucrum has a more even dorsal margin with a less prominent step. Further, in medial view the ventral edge of the involucrum is evenly convex whereas in Coronodon havensteini the margin is straight. The sigmoid process is imperfectly reassembled in the Coronodon havensteini holotype, and ChM PV 2778 clarifies the morphology in Coronodon. The sigmoid process is erect and canted about 20 degrees posterolaterally from the transverse plane, and the tip of the sigmoid is elevated above the level of the inner posterior pedicle. This suggests that the unusual position in the Coronodon havensteini holotype is caused by improper gluing, and that the sigmoid process has been artificially rotated dorsally and medially. The conical process is dorsoventrally deep and hemispherical.

Dentition

The p1 and M1 are preserved in ChM PV 2778 (Figures 25, 29). The p1 is similar to that of the *Coronodon havensteini* holotype but the tooth is slightly smaller and has an apicobasally shorter crown (70% of crown height in CCNHM 108), smaller mesial and distal denticles, and an apicobasally shorter isthmus between the roots, with the roots being slightly more split in ChM PV 2778.

The M1 is not preserved in the *Coronodon havensteini* holotype but this position is preserved in ChM PV 2778. It compares well with the M1 of *Coronodon planifrons* n. sp. and the M1-M2 of *Coronodon havensteini* (CCNHM 164). The M1 is higher crowned than in CCNHM 166, and the base of the enamel is more dorsally arched. It differs from the M1 of



CCNHM 164 in possessing 5 rather than 4 distal denticles; the M2 of CCNHM 108 also has five but the basal denticle is minute. Five distal denticles are present in CCNHM 166. The M1 of ChM PV 2778 possesses four mesial denticles, unlike the M1 of CCNHM 166 (five mesial denticles) and the M2 of CCNHM 108.

1391

1392

1393

1394

1395

1396

1397

1398

1399

1400

1401

1402

1403

1404

1405

1406

1407

1408

1387

1388

1389

1390

Mandible

The partial left mandible (Figure 29; Table 6) is missing the angular process, ventral half of the "pan bone" and lateral wall adjacent to the molars. Otherwise, aside from some Osedax bioerosion, the mandible is well-preserved. The mandible is notable for possessing alveoli for eight (p1-m4) rather than seven postcanine teeth as originally identified in *Coronodon* havensteini (see Revised Tooth Count in Coronodon and Implications for Polydonty in Neoceti, below). The mandible has a similarly shaped coronoid process to Coronodon havensteini, but the mandibular condyle is elevated far above the m4 alveolus; in Coronodon havensteini and Coronodon planifrons n. sp., the condyle is at the level of the m4 alveolus. The ventral margin is also convex, whereas it is straight in both Coronodon havensteini and Coronodon planifrons n. sp. The mandible of Coronodon newtoni n. sp. further differs from Coronodon havensteini in possessing a more dorsoventrally tapered anterior tip. The mandibular foramen is partly preserved, and its anterior margin seems to have been entirely posterior to the coronoid apex. The coronoid process is subtriangular and separated from the condyle by an 92 mmm long neck. Like Coronodon havensteini, the mandibular symphysis is unfused and the symphyseal surface is smooth and flat to slightly undulatory; it is anteroposteriorly short, extending only to the level of the C1.



Postcrania

Three vertebrae and one rib are preserved in ChM PV 2778 (Figure 29). The vertebrae include a mid thoracic, a vertebra representing the last thoracic (T9) or first lumbar (L1), and a mid-caudal vertebra, likely Ca5, 6, or 7 (based on comparison with CCNHM 164 and 166). The mid-thoracic vertebra has a deep centrum with a flat dorsal edge, a capitular facet on the dorsolateral edge of the anterior (but not posterior) epiphysis, a robust pedicle, and a swollen transverse process. The T9/L1 has a dorsoventrally shallow and small (compared to posterior lumbars in CCNHM 166) centrum with a truncated dorsal margin (more closely resembling the T9 rather than L1 of CCNHM 166 in this regard), and a dorsoventrally deep, horizontal, and dorsally positioned transverse process. The mid-caudal vertebra is large with a circular anterior epiphysis and slightly transversely narrowed posterior epiphysis, a low neural arch with a small and low neural spine, small, short, and ventrally deflected transverse processes, and large subtriangular haemal facets anteriorly and posteriorly.

Coronodon planifrons n. sp. LSID urn:lsid:zoobank.org:act:445DF386-7800-453F-ACA7-1425 3D3EE8143149

Type Specimen

CCNHM 166, partial skeleton including rostrum fragments, braincase, left and right periotics, 24 teeth, left mandible, four cervical vertebrae, seven thoracic vertebrae, ten lumbar vertebrae, 11 caudal vertebrae, and at least 13 ribs, discovered and collected by Jeremmiah Volcko, Taffie



Chapman, and Mark Havenstein, November 2010 from an exposure of the Chandler Bridge 1431 Formation in the vicinity of North Charleston, Dorchester County, South Carolina. 1432 **Referred Specimen** 1433 CCNHM 8732, an isolated upper right M3, collected by an unknown collector from the vicinity 1434 of Summerville, South Carolina, USA. 1435 1436 **Type Locality** The type specimen of *Coronodon planifrons* was collected from an exposure of the Chandler 1437 Bridge Formation in a drainage ditch in North Charleston, Charleston County, South Carolina, 1438 USA. More detailed locality records available on file at CCNHM. 1439 1440 Horizon and Age Chandler Bridge Formation, likely, but uncertainly from Bed 2, late Oligocene (24.7-23.5 Ma). 1441 1442 **Diagnosis** Coronodon n. sp. is a large toothed mysticete (BZW = 460 mm) differing from Coronodon 1443 havensteini and Coronodon newtoni in possessing a horizontal (rather than ventrolaterally 1444 sloping) supraorbital process of the frontal (sloping 4°, v. 14-15° in C. havensteini); possessing a 1445 dorsoventrally deep postorbital process that is deeper than the preorbital process; possessing a 1446 crescentic dorsal extension of the sternomastoid fossa, nearly to the posterior apex of the nuchal 1447 crest (fossa in *C. havensteini* is approximately 1/3 this length); frontals penetrating further 1448 posteriorly into the interorbital region, 13% of postorbital width v. 8% in C. havensteini; 1449 zygomatic process dorsoventrally deeper than in C. havensteini, relative to height at vertex (not 1450 possible to evaluate in C. newtoni n. sp.); larger lateral tuberosity of the petrosal, with 1451



rectangular outline, and projecting beyond lateral margin of petrosal; medially excavated and undercut basioccipital crest that protrudes further ventrally than *C. havensteini*; longer intertemporal region (distance from anteriormost point of orbitotemporal crest to supraoccipital apex 54% of postorbital width v. 34-36% in *C. havensteini*); more deeply excavated dorsal condyloid fossae; dorsoventrally thicker postorbital process (9.5% of postorbital width v. 5% in *C. havensteini*); lower m3 has six rather than five mesial denticles as in *C. havensteini*; upper M2 slightly smaller and lower crowned than in *C. havensteini*; upper M3 dramatically smaller than M2. *Coronodon* n.sp. further differs from *Coronodon newtoni* in possessing a straight ventral margin of the mandible, a mandibular condyle not elevated above the toothrow, and absolutely larger teeth and petrosal.

Description

General Remarks on Skull

CCNHM 166 preserves a partial, somewhat fractured braincase (Figure 30; Table 2), right posterior premaxilla, right nasal, fragments of the maxilla, left and right periotics, and numerous teeth.

This description will emphasize features differing from *Coronodon havensteini* and morphology either not preserved in the *Coronodon havensteini* holotype or not detailed in the original description (Geisler et al., 2017: supporting information).

Premaxilla



The premaxilla is disarticulated from the maxilla (Figure 30), permitting description of morphology obscured in the holotype of *Coronodon havensteini*. It is mostly damaged, but the posterior half of the right premaxilla is well preserved and isolated; it is rod-like, somewhat dorsoventrally deeper than wide, and the dorsal surface steeply slopes medially into the bony nares. The dorsal surfaces is flattened to slightly convex, becoming more horizontal anterior to the nares. In dorsal view, the entire element is laterally bowed around the nares. There is a longitudinal groove along the ventromedial margin of the premaxilla, likely for a simple premaxilla-vomer articulation.

Several vascular channels ascend from a common sulcus on the lateral side of the bony nares, curving posterodorsally towards the nasal. Four or more grooves and at least three ridges form a deeply mortised but unfused and open frontal-premaxilla articulation; this articular surface is at least 10 cm long and faces dorsomedially. The nasal-premaxilla articulation is similar, at least 9 cm long, 15 mm wide, but bears a deep dorsomedially facing trough with discontinuous ridges and grooves recessed within.

The ventral margin of the rod-like middle part of the premaxilla is rounded and convex in cross-section. The lateral surface is somewhat flat, smooth, and bears a shallow discontinuous trough; this trough receives the medial edge of the maxilla and, posteriorly, the ascending process of the maxilla. Just lateral to the nasals, the trough bears a median longitudinal ridge measuring 45x8mm. Aside from this, the entire premaxilla-maxilla articulation is developed as a slightly undulating butt joint.

Maxilla





Fragments of the maxilla are preserved (Figure 30) but are too incomplete to make any meaningful comparisons with *Coronodon newtoni* n.sp. or *Coronodon havensteini*.

Nasal

The right nasal is preserved and similar to the *Coronodon havensteini* holotype in being anterodorsally flaring, rectangular in dorsal view, and shallowing towards a flat posterior end (Figure 30). Scattered diploic foramina are present on the posterior half; these are about 1-1.5mm in diameter and bear short posteriorly directed sulci. The medial surface bears deep longitudinal grooves for the internasal suture – five ridges and grooves, anteroventrally directed, and towards the anterior tip this surface gives way to a flat articular surface without grooves.

The nasal is dorsally sloped laterally with a median ridge, which becomes more prominent anteriorly and gives the nasal a triangular cross section. The ventral surface bears a prominent ventromedial ridge to articulate with the groove on the medial side of the prenarial process of the frontal; the lateral edge of the nasal instead overlaps onto the premaxilla to articulate with its posterodorsal surface. The anteromedial face of the nasal has an anterodorsally curving, anteriorly widening trough for the nasal passage, and appears to have been vertical like the holotype of *Coronodon havensteini*.

Frontal

Most of the frontal forms the somewhat rectangular supraorbital process; the supraorbital process is approximately horizontal (Figure 30; Tables 1-2). The frontal bears a narrowly



triangular prenarial process to articulate with the premaxilla and nasal; the prenarial process is dorsoventrally deeper than the supraorbital process and bears longitudinal ridges and grooves. Lateral to this the frontal is dorsoventrally thin and excavated into a shallow fossa to receive the ascending process of the maxilla. The preserved parts of this fossa are smooth and lack the deep parallel ridges and grooves that characterize the frontal-premaxilla and frontal-nasal articulations. Based on changes in bone texture and the edges of this fossa, the ascending maxilla was subtriangular with a convex posterolateral margin and covering a region of the frontal approximately 50mm wide and 50 mm long. The prenarial process is laterally undercut by a groove for the medial edge of the ascending maxilla.

The frontonasal sutures occupy approximately ¾ of the anteroposterior length of the supraorbital process (not including the prenarial process) and transition into a rough, slightly rugose bone texture. This zone of rough texture forms a 90mm wide parabolic 'halo' surrounding the articular grooves for the nasal and premaxilla and terminating nearly at the posterior margin of the supraorbital process. Diploic foramina are present dorsally in two sets; the first are posterolaterally opening, radially oriented, 1 mm wide foramina with 5-40mm long sulci, and the second are a cluster of larger 1-2mm wide foramina lateral to the posterior tip of the nasals and 40mm from the midline. There is a fissure at the median frontal suture, suggesting a persistent unfused suture into adulthood, but is more likely the result of breakage during collecting along a zone of weakness (as in CCNHM 164). The postorbital process is triangular, posterolaterally flaring, and tapers to a point. It is rectangular in lateral view and dorsoventrally thick; the orbit is moderately concave in lateral view. The frontoparietal suture is deeply V-shaped with the frontals penetrating 55mm posterior to the anterior margin of the temporal fossa. In lateral view, the frontoparietal suture descends posteroventrally.



The orbitotemporal crest forms the posterior edge of the supraorbital process of the frontal, which has a concave posterior margin. The postorbital process extends far posterolaterally to the anteromedial margin of the temporal fossa. The orbitotemporal crest slightly overhangs the postorbital ridge medially, and the posterior surface of the frontal is approximately vertical, intermediate between the condition in basilosaurids and chaeomysticetes. This surface is concave and slightly excavated and bears a single large laterally opening foramen on the posteromedial surface.

The frontal groove is laterally shallow and triangular in ventral view, rapidly narrowing medially; it bears laterally opening diploic foramina within. The optic canal is posteriorly placed within the supraorbital process and shallow, curving posteromedially. Anterior to the optic canal and medial to the preorbital process is a shallow fossa of uncertain homology, and not clearly associated with the maxilla. One large diploic foramen is present at the boundary between the optic canal and this fossa.

Intertemporal Constriction, Parietal, and Vertex

The intertemporal constriction is dorsoventrally deep and transversely narrow but is broken ventrally; the preserved part is acutely triangular in cross-section and narrows dorsally (Figure 30; Table 2). The sagittal crest is sharp along most of its length and is proportionally longer than in *Coronodon havensteini*. A single dorsally convex, roughly horizontal sulcus emanates from the broken region of the frontoparietal suture, approximately 4 cm long on right and 7cm long on left.





Like the *Coronodon havensteini* holotype, the vertex is at the level of the posterior third of the temporal fossa; though the nuchal crests are broken, the supraoccipital apex was triangular. Breakage artificially makes the occipital shield appear more triangular than it likely was when complete. In dorsal view the anterolateral 75% of the nuchal crest is composed of parietal and the posterior 25% is composed of the supraoccipital. A faint external occipital crest is developed on the dorsal third of the occipital shield.

Squamosal

The apex of the zygomatic is more completely preserved in CCNHM 166 (Figure 30) than in the *Coronodon havensteini* holotype (Figure 6, 8), and in lateral view it thickens dorsoventrally at mid-length and tapers abruptly into an acutely triangular apex, giving the process an overall 'spindle' shape. In dorsal view, the apex curves slightly anteromedially; ventrally there is a poorly defined facet for the jugal along the anterior 30 mm of the zygomatic. The zygomatic process is composed of highly cancellous bone and is likely damaged in all other known specimens of *Coronodon*, including the otherwise well-preserved juvenile ChM PV 4745 and holotype (CCNHM 108) of *Coronodon havensteini*.

The squamosal prominence is developed as a transversely thickened and blunt knob on the supramastoid crest; it is medially situated, emarginates the squamosal fossa in dorsal view, and is dorsally adjacent to the sternomastoid fossa. The sternomastoid fossa is large and rectangular to crescentic in shape, faces posterolaterally, and is approximately 90mm deep and 80mm wide. The fossa has a concave posterior margin where it is emarginated by the exoccipital. The fossa is smooth anteriorly but deeply pitted close to the exoccipital;



dorsomedially the fossa ascends as a trough along the lateral edge of the nuchal crest. Ventrally the fossa continues onto the posterior meatal crest.

The postglenoid process is tongue-shaped and transversely narrow, and laterally is anteroposteriorly thickened at its ventral apex. The anterior meatal crest is short but sharp and leads to the broken base of the spiny process, which bears a pit for the sigmoid process of the bulla. The glenoid fossa is developed as a pair of shallow fossae separated by a low convexity; the lateral fossa bears a cluster of vascular foramina, and the medial fossa bears cancellous bone. The medial fossa is bordered by a sharp ridge that transitions anteriorly into the falciform process.

The periotic fossa is solid, smooth, and transversely bowl-shaped – but developed as an anteroposteriorly oriented trough with a slight reniform outline, being medially concave and conforming to the shape of the lateral surface of the periotic. A low tubercle is present on the dorsal side of the periotic fossa, corresponding to a gap on the superior process of the periotic between the anterodorsal and posterodorsal angles. Dorsal to this, the medial wall of the squamosal is flat with faint dorsoventrally oriented striations of presumed vascular origin, perhaps corresponding to a rete.

As in *Coronodon havensteini*, there is a gap between the anterior process of the periotic and squamosal, and the periotic only seems to tightly articulate with the pit for the periotic posteriorly and at the lateral tuberosity. A low ridge is present between the periotic fossa and the pit for the posterior process. The skull is amastoid, and the postmeatic crest is formed from cancellous bone and separates the posterior process of the periotic from the lateral edge of the skull by approximately 35 mm. The postmeatic process abuts the truncated margin of the



posterior process of the periotic; on the left side, the postmeatic process is partly fused to the pathological posterior process of the periotic.

Exoccipital and Basioccipital

The exoccipital is anteroposteriorly thick ventrally and shares a closed suture with the squamosal (Figure 30). Laterally both bones are composed of porous, cancellous bone. The paroccipital process bears a circular to oval paroccipital concavity; it is deeper and circular on the right side, and shallow and oval on the left. The paroccipital concavity is posterior to the lateral edge of the posterior process of the periotic. Medially, the anterior face of the exoccipital is smooth and bears a trough for the jugular notch.

Posteriorly the exoccipital is dorsoventrally low and projects ventrolaterally; the posterior surface is smooth. The occipital condyles are set out on a short neck, projecting somewhat further than in *Coronodon havensteini*; each is nearly rectangular, perhaps a consequence of incompleteness. The foramen magnum is dorsoventrally deep, transversely narrow, and oval shaped. Deep dorsal condyloid fossae are preserved on the right side and the ventral condyloid fossa is deeper, and positioned lateral to the ventral third of the condyle.

The basioccipital crest is large, transversely wide, and composed of cancellous bone. The medial side is slightly more excavated than in the holotype of *Coronodon havensteini*. The ventral margin forms a continuous pharyngeal crest. The medial part of the basioccipital is smooth; a long sulcus separates the crest from the medial trough for the vomer. The posteromedial part of the right basioccipital crest edge forms a spur; this is instead rounded on the left side.

Periotic

The periotic of *Coronodon planifrons* n. sp. (Figure 31; Table 3) differs from *Coronodon havensteini* in possessing a more transversely inflated anterior process with a more elongated anterodorsal angle, a better defined anterior bullar facet, a flatter posterior bullar facet, a more shallowly excavated suprameatal fossa, a roofed over hiatus fallopii, and a larger, longer lateral tuberosity that projects beyond the lateral margin of the body.

The anterior process is grossly inflated transversely, as is the body, so that there is a deep crease separating the anterior process and lateral tuberosity. An incisural flange (*sensu* Boessenecker and Fordyce 2014) is present on the right but not the left periotic. The flange is demarcated by a short anterointernal sulcus which bifurcates closer to the anteroventral angle. The anterior incisure is a deep groove between the pars cochlearis and anterior process; more broadly, the angle between the anterior process and pars cochlearis at the incisure is 173° in the left periotic and 179° in the right periotic.

The lateral tuberosity is large (relative to other toothed mysticetes) and bears a pointed tip and a chisel-shaped apex in ventral view; there is a prominent continuous ridge forming the anterior margin of the mallear fossa that is laterally contiguous with the posterior edge of the lateral tuberosity. Anterior to the mallear fossa is a small broken nodule of bone where the accessory ossicle was partially fused to the anterior process and broken; the fracture is clearer in the right periotic. This structure is worn in the holotype of *Coronodon havensteini*, but appears to have been partly fused as well.



The endocranial opening of the facial canal is partly subdivided, forming a hiatus fallopii; this structure is instead developed a long fissure in the *C. havensteini* holotype. The aperture for the cochlear aqueduct is elevated further dorsally (and further separated from the fenestra rotundum) than in *C. havensteini*. In the *C. havensteini* holotype, the suprameatal fossa has a deep anteroposterior trough within its posterior half; this is absent in *C. planifrons* n. sp., and instead the suprameatal fossa is bowl-shaped. In *C. havensteini* this trough bifurcates the posterodorsal angle, forming a more medial tuberosity referred to as the pyramidal process *sensu stricto* by Marx et al. (2015). This sulcus is absent in *C. planifrons* and the pyramidal process and the posterodorsal angle are essentially the same structure.

The lateral surface of the periotic is more rugose and cancellous than in the *C*. *havensteini* holotype. Posterolaterally, near the posteroexternal foramen, paired rugose tubercles are developed anteroventrally to the posteroexternal foramen. The posteroexternal foramen is actually a cluster of three foramina just lateral to the stylomastoid fossa, like the *C. havensteini* and *C. newtoni* holotypes; in juvenile *Coronodon havensteini* (ChM PV 4745, CCNHM 8722) as well as unnamed coronodonid ChM PV 5720, there is a single foramen, like other stem mysticetes.

The posterior process has a flatter and less transversely convex posterior bullar facet; the medial half is partly concave. The posterior process is also dorsoventrally thicker in *C. planifrons* n.sp. The posterior process lacks the conspicuous posterior spurs on the posterior margin, as in the periotic of the *Coronodon havensteini* holotype, instead having a smooth subrectangular margin. Unlike the *C. havensteini* holotype, there is a groove separating the epitympanic hiatus from the posterior process.



The left periotic has a pathologically fused posterior process of the bulla, periotic, and postmeatic process of the squamosal. The combined process is massively inflated, bluntly conical in shape, and appears to be composed nearly entirely of cancellous bone. A thin bullaperiotic suture is present just dorsal to the facial sulcus, but is difficult to trace on the cancellous external (posterior) surface of the compound process. Articulation of the left periotic with the skull is difficult, and breakage suggests that the compound posterior process was fused anterolaterally with the postmeatic process.

Tympanic Bulla

The posterior process of the right tympanic bulla is isolated and well preserved (Figure 31I-J). It is quite dense with some cancellous bone developed laterally, and is triangular in shape with a flat articular facet and transversely convex ventral surface. The ventral surface bears fine sulci but is otherwise smooth; the articular facet bears shallow longitudinal grooves, corresponding to the ridges on the posterior bullar facet. Near the posterior pedicle there is an oval-shaped ridge with a fossa, which is the broken base of the outer and inner posterior pedicles, the fossa representing an excavation by part of the peribullary sinus.

Dentition

The teeth of *Coronodon planifrons* (CCNHM 166) have no cingula and all have carinae, just like *C. havensteini* (Figure 32; Table 5). The carinae are virtually identical in size and have a similar effect on denticle shape and notch formation as seen in *C. havensteini*. Likewise, the depression on the crown base in between each denticle forms the shallow troughs as those seen



in *C. havensteini*. The enamel is similarly thin in *C. planifrons* and, like *C. havensteini*, is covered in undulating oblong bumps and depressions less than a millimeter in size. Root morphology of *C. planifrons* is also essentially identical to *C. havensteini*, the mesial root is thicker, straighter, and more vertically oriented than the distal root of the same tooth.

Caniniform teeth

The caniniform teeth of CCNHM 166 all have a carina and very shallow apicobasal ridges and grooves along the surface, just like in *C. havensteini*. Like *C. havensteini*, the crowns of these teeth have a greater apicobasal height than their mesiodistal length. But the mesiodistal lengths of the caniniform teeth of CCNHM 166 are greater in length than that of *C. havensteini* (CCNHM 164).

Upper dentition

The upper left third premolar (CCNHM 166.45) is partly broken, missing most of the distal denticles besides the one adjacent to the central cusp. This first distal denticle is almost as large as the central cusp, and is slightly larger than the first mesial denticle. The mesial denticle row retains four large denticles and a fifth that is negligible in size and lacks a point. Though the distal denticle row is mostly missing and therefore not comparable, the mesial denticle row exhibits a similar straight and steeply sloped arch as seen in other premolars of *Coronodon*.

Both left (CCNHM 166.29) and right (CCNHM 166.48) upper fourth premolars are preserved. The right P4 (CCNHM 166.48) lacks the distal denticle row, but the left P4 (CCNHM



166.29) retains all of the denticles, including four mesial and four distal denticles. The distal denticles are slightly larger than their respective counterparts on the mesial denticle row, though the two denticle rows themselves appear to be similarly arched and equally sloped.

Both left (CCNHM 166.49) and right (CCNHM 166.34) upper first molars are preserved. The left M1 (CCNHM 166.49) has all of its cusps preserved, but the right M1 (CCNHM 166.34) is missing its mesial denticle row completely. The mesial denticles are mostly equal in size to their respective distal denticles, with five on each denticle row. Of these, the distalmost and mesialmost denticles are small and lack a point, they are borderline denticles but have the pinched edge of their adjacent denticle (like those described above for other *Coronodon* teeth). The mesial and distal denticle rows are both similarly arched, yet the mesial denticle row appears to extend more basally than the distal denticle row. Even though the mesial denticles are missing on the right M1, the crown base is preserved on the labial side, indicating that it, too, had a more basally-extended mesial side.

The second upper molar is represented by CCNHM 166.50, which exhibits an extreme amount of wear and damage to the lingual side of the mesial denticles and central cusp. This makes it challenging, but not impossible, to recognize its four mesial and four distal denticles. The four mesial denticles are of similar size to their respective distal denticles, but the mesial denticle row is more steeply sloped and straighter than the more arched and shallowly sloped distal denticle row. The mesial denticle row extends further basally than the distal denticle row does, just like as in the first molar.

CCNHM 166.51 is a right upper third molar that has partial damage to its central cusp and the mesial denticle just adjacent to it. It has three mesial denticles and four distal denticles.

The central cusp is broken, but from what remains of it, it was most likely larger than its adjacent





denticles, like in other teeth. The mesialmost denticle is also broken, so it is unclear whether it was of similar size or smaller than the first distal denticle. The second and third mesial denticles are smaller than their respective distal denticles, hinting that the first mesial denticle was probably smaller than the first distal denticle as well. Both denticle rows appear to be similarly arched and sloped.

Lower dentition

The second premolar, possibly a lower (CCNHM 166.44), has a large central cusp and one mesial denticle preserved. There may have been a distal denticle or an additional mesial denticle, but the specimen is incomplete. The mesial denticle is curved toward the central cusp and is 1/3 the size of it, similar to the proportions of the central cusp and first mesial denticle of *C. havensteini* (CCNHM 164), in which the first distal denticle is approximately half the size of the central cusp. The mesial denticle of the first premolar of the holotype of *C. havensteini* is much smaller than in the second premolar, approximately ½ or 1/5 the size of the central cusp.

CCNHM 166.47 (left) and CCNHM 166.32 (right) are lower third premolars. CCNHM 166.47 has only three cusps preserved: the central cusp and the mesial and distal denticles on either side of it. CCNHM 166.32 has one mesial denticle preserved (although there were certainly more), a central cusp, and five distal denticles.. For both specimens, the first mesial denticle is slightly smaller than the first distal denticle, making the apicobasal height of the distal carina of the central cusp a bit shorter than the mesial carina of the central cusp. This is the same pattern found in the lower p3 denticles adjacent to the central cusp of *C. havensteini* (CCNHM



164). The mesial carina of the central cusp is not completely smooth, but has some jagged edges forming pseudoserrations like that seen in lower right p2 of *C. havensteini* (CCNHM 164).

The lower fourth premolar is preserved as CCNHM 166.46, which is only the distal half of the tooth, including a central cusp, five denticles, and the distal root. It is unclear whether this is the left or right, though the curvature of the crown seems to indicate it is a left. The distalmost denticle is extremely small, sitting at the base of the fourth distal denticle. The crown base is smaller in this specimen, with virtually no crown base basal to the fourth and fifth distal denticles.

The left first molar is CCNHM 166.30 and has preserved evidence of five mesial denticles (though the two closest to the central cusp are broken/worn away) and five distal denticles. The mesial denticle row extends further basally than does the distal row and has a steeper and more extreme slope than the arched distal denticle row. The central cusp and all preserved denticles exhibit the same sort of kink in the carina that forms a pseuodserration on their mesial and distal sides.

CCNHM 166.27 is the lower left m2, which has six mesial and five distal denticles. The mesialmost denticle is extremely small and lacks a proper point, but instead resembles the bulge of the crown base. Like the first molar, the mesial denticle row is more steeply inclined and less arced than the distal denticle row. The central cusp and all preserved denticles retain the same pseudoserrations as the first molar.

The lower left m3 is represented by CCNHM 166.28, and it also has six mesial and five distal denticles. Likewise, the mesialmost denticle is extremely small and lacks a point, like that seen in the m2. Also like the first molar, the mesial denticle row is more steeply inclined and less



arced than the distal denticle row. Like the first and second molars, the central cusp and denticles have carinas with pseudoserrations on their mesial and distal sides.

CCNHM 166.33 is the lower left m4. The m4 has six mesial and four distal denticles. This tooth exhibits the most extreme form of the steeply sloped mesial denticle row that extends further basally than the distal denticle row. The mesial half of the tooth is longer than the distal half, including the root. The central cusp has a pseudoserration on the mesial side, but not the distal side, whereas the two distal denticles closest to the central cusp have prominent single pseudoserrations on their distal sides.

Mandible

The posterior half of the left mandible is well preserved (Figure 33; Table 6) and includes complete alveoli for M2-4 and partial alveoli for M4, and P4, Anteriorly the mandible has a rectangular outline with parallel ventral and dorsal margins; the ventral margin is straight to slightly concave along the preserved length of the mandible. The M2-4 are positioned posteriorly along the inclined part of the toothrow, each more dorsal than the prior tooth, with M4 positioned on the anterior margin of the coronoid process (alveolar margin of this tooth 1/3 of the distance from the condyle to the coronoid apex). All molars are double-rooted and the M2-3 have small alveoli for a labially positioned demi-root. The alveolar margins are similar in height for M2-3 but the labial margin is raised dorsally about 2 cm relative to the lingual margin at the level of M4. Posterior to the M4, there is a shallow longitudinal furrow positioned medially along the anterior edge of the coronoid process. The posterior margin of the coronoid process is damaged but appears to have been dorsally rounded with a straight, inclined anterior margin and a near



1801

1802

1803

1804

1805

1806

1807

1808

1809

1810

1811

1812

1813

1814

1815

1816

1817

1818

1819

1820

1821

1822

vertical posterior margin; this shape is intermediate between the triangular coronoid of basilosaurid archaeocetes and the elongate tongue-shaped coronoid of later diverging aetiocetid mysticetes. The coronoid compares well with *Llanocetus denticrenatus* but is less lobate and less posteriorly directed. Posteriorly, the base of the coronoid widens and descends posteroventrally towards the mandibular neck.

About 3-5 cm anterior to the condyle there is a 12mm long, 8-9mm wide, dorsally facing foramen that perforates the neck; it has smooth, round margins. It is likely pathological or congenital in origin (a similar fenestra is present in the posterior mandible of *Tohoraata* raekohao; Boessenecker and Fordyce, 2015A). A similar, but smaller anteroposteriorly directed foramen is also present in the same location on the neck of the right holotype mandible of Coronodon havensteini (CCNHM 108) but is absent in the left. The condyle is relatively small, dorsoventrally shallow, and bears a triangular articular surface. The surface is pathological, bearing deep pits and transverse sulci and rows of deep foramina separated by smooth compact bone; this rugose surface texture is also present anterodorsally in the secondary glenoid fossa of the squamosal, also observed in Coronodon havensteini (CCNHM 164; see above). The medial side of the condyle is deeply excavated by the mandibular fossa. The condyle faces posteriorly but bears a horizontal transverse 'corner' in medial/lateral view. The mandibular fossa is large and the cavernous mandibular canal dominates the entire preserved section of mandible, becoming somewhat narrower with thicker walls anteriorly at the level of the M2. The angular process is missing, but preserved bone indicates that the posteroventral margin was slightly concave below the condyle. Laterally the coronoid process bears a shallow but large masseteric fossa, which is most deeply excavated anterodorsally where it defines a robust ridge along the anterior margin of the coronoid process. A horizontal, longitudinal, and broadly convex ridge at



the level of the condyle defines the ventral margin of the fossa. A shallow medial masseteric fossa, approximately 50x50mm, is present posteroventral to the M4 and is positioned anterodorsally to the mandibular fossa.

1826

1827

1828

1829

1830

1831

1832

1833

1834

1835

1836

1837

1838

1839

1840

1841

1842

1843

1844

1845

1823

1824

1825

Cervical Vertebrae

The atlas (Figure 34; Table 7) is well-preserved but lightly bioeroded in places; it is missing the apices of the transverse processes. The atlas is anteroposteriorly flattened and dorsoventrally deep relative to basilosaurids and has a nearly circular outline in anterior view. The atlas bears several pathologies. The left ventrolateral margin is swollen 8-10 mm more than the right. There is a low convex bulge on the left condylar facet near the dorsal margin, corresponding to a pit in the same location on the left occipital condyle. Lastly, the anterior part of the lamina, anterior to the right transverse foramen, is completely resorbed; on the right side it is dorsoventrally thicker, albeit bioeroded. The condylar facets are shallowly concave, dorsoventrally deep, and separated by a shallow median furrow ventrally. The hypapophysis is low and robust, ventrally positioned, and posteroventrally directed. In lateral view, the centrum is approximately rectangular. The transverse process is anteroposteriorly flattened. posterolaterally directed, and dorsoventrally deep (~45-50% of atlas depth). There is no evidence of a foramen penetrating the process, though the lateral edge is missing. The neural arch is robust and dorsoventrally deeper anteriorly. It bears a low, pyramidal neural spine. The neural foramen is teardrop shaped and widens slightly dorsally; it is not bilobate. The axial facets are flat, lunate in shape, and expand dorsally; they are separated by a 30x30mm circular, posterodorsally facing odontoid fossa. The transverse foramen in the neural arch is approximately 10mm in diameter and transversely oriented.



One isolated cervical vertebra represents C4 based on comparison with the *Coronodon havensteini* holotype (Table 8). A less complete C3 centrum fragment is also present, being slightly thinner than C4. The C4 centrum is anteroposteriorly flattened (23mm in length) and subcircular to oval in shape; at the center of the centrum is a shallow fossa. A large lateral vertebral foramen is developed and incompletely encircled by bone. It is oval, dorsomedially sloping in anterior view, and measures 4.5 cm wide and 2 cm deep. Ventral to this foramen is a robust parapophysis that projects ventrolaterally and expands into a subrectangular end with three apices: a dorsally pointing apex that is the remnant of the lateral branch to the diapophysis, a ventrolateral apex that points posteriorly, and a ventromedial tubercle. The diapophysis is small, triangular, and ventrolaterally projecting; the pedicle is rectangular and anteroposteriorly flattened. The pre- and postzygapophyses are aligned, near vertical, and anteroposteriorly short. The lamina is short and surrounds the oval neural foramen. The lamina is delicate and culminates in a small, 2 cm high neural spine that is triangular in lateral view.

A partial C7 bears an oval centrum 3 cm in length and exhibits large and deeply excavated notochordal pits. A minute hypapophysis is present and parapophyses are absent; a small costal tubercle is present just below the flattened and dorsoventrally deep (1/2 of centrum depth) transverse process.

Thoracic Vertebrae

Both T1 and T2 are preserved (Figure 34; Table 9), and quite similar in morphology. They possess longer centra than C7 (40 and 45 mm, respectively) that are oval, slightly flatter dorsally, and bear costal facets at the lateral apex of the centrum; the anterior facets are slightly



more strongly defined. The pedicle is elevated and directed dorsolaterally and anteriorly; the transverse process is positioned anterior to the centrum and widens distally. The transverse process bears a tubercular facet ventrally and a short shelf-like prezygapophysis dorsally.

Based on centrum lengths, only T3 is absent; T4 has a centrum that is slightly deeper and flatter dorsally than T2. Costal facets are only present posteriorly. There is a subtle, shelf-like prezygapophysis, and an anteroposteriorly long, posteriorly shifted postzygapophysis. The neural spine has a wide base and is anteroposteriorly long and bears a vertical groove posteriorly at the midline. The neural foramen is subtriangular. Only a fragmentary centrum of T5 is preserved.

Four additional posterior thoracic vertebrae are present and constitute a continuous series, likely corresponding to T6-T9 based on measurements and comparisons with *Coronodon havensteini* (CCNHM 164). These vertebrae are roughly similar to T4 but possess successively longer, deeper, and wider centra and anteroposteriorly longer laminae; TB possesses a wider neural spine base. Posterior costal facets become larger further posteriorly within these vertebrae.

Lumbar Vertebrae

Ten lumbar vertebrae are preserved (Figure 34; Table 10) and presumed to represent L1-10 based on the ancestral lumbar count of 10 for Neoceti (Buchholtz and Gee, 2017). None preserve spines or complete arches, and only two preserve partial transverse processes. The centra become larger in all dimensions (length, width, depth) from anterior to posterior and maintain similar proportions, with L10 being the largest. The centra are circular throughout most of the series (e.g. L3-L10) but the L1 is still slightly shallower than wide like the posterior



thoracics. The ventral side of L1 is transversely convex, but in L3-L10 there is a well-defined median ventral keel, a purported synapomorphy of Neoceti (Davydenko et al., 2021). The pedicles are transversely narrow and become even more closely positioned to the midline posteriorly (e.g. L6-L10). The transverse process slopes ventrolaterally in L4 and L8 (22°), but is closer to horizontal in L10 (14°); in no case do the transverse processes slope as extremely ventrally as in Basilosauridae (e.g. 30° in *Dorudon atrox*).

Caudal Vertebrae

Nine nearly complete and two partial caudal vertebrae are preserved (Figure 34; Table 11), including Ca1-4, Ca6, Ca8, and two posterior caudals. The anterior caudals (Ca1-3) are similar to L10 in size and centrum proportions but possess wider-set haemal facets, weak anterior haemal facets, and paired longitudinal dorsolateral ridges medial to the transverse process. In Ca2 there is a ventrolateral ridge present. The transverse process in Ca2 is short (6 cm long), triangular, and positioned anteriorly with a straight, transverse anterior margin. All anterior and mid caudal vertebrae (Ca1-8) possess a vertical fissure-like notochordal pit.

The mid-caudals (Ca4-8) are of similar height but possess successively shorter transverse processes, shorter centra, dorsoventrally flattened neural arches with smaller canal-like neural foramina, larger haemal facets raised on inflated tubercles, and more dorsally positioned dorsolateral ridges. In Ca6 and 8, the anterior part of the arch bears paired tubercles aside a narrow 10-12mm wide neural foramen instead of prezygapophyses. The transverse process in Ca5 appears bifurcated, apparently pierced by the vertebrarterial foramen, and the transverse process \$1-2 cm long, In Ca6 it is triangular, anteriorly shifted with a dorsoventrally deep



tubercle present anteriorly at its base. In Ca8, the transverse process is reduced to a low ridge with a ventrally directed tubercle. In Ca5-8, the process is slightly narrower than deep.

The posterior caudals are represented by CaC, a circular anteroposteriorly flattened vertebra, and CaD, a wide and slightly rectangular terminal caudal vertebra. CaC is pierced by vertical vertebrarterial canals that are positioned laterally. Ventrally, a deep transverse sulcus emanates from these canals and continues ventrally; it is contiguous with a deep longitudinal trough at the ventral midline. Dorsally a short sulcus is present with an additional transverse sulcus that connects to a minute neural foramen. A small pit is present laterally. CaD is similar but lacks a neural foramen entirely, instead possessing a continuous transverse sulcus and ventral parasagittal fissures emanating dorsally onto the anterior side from the ventral opening of the vertebrarterial canal.

Ribs

Fourteen complete and partial ribs are preserved in CCNHM 166 (Figure 35), including the left rib 1 and several other positions throughout the series. Left rib 1 is the shortest and most highly curved rib; dorsally it is dorsoventrally deep with a small anteroposteriorly flattened tubercle set far (4 cm) from the similarly small and triangular capitulum. The tubercle bears a posteromedially facing articular facet; the rib shaft is anteroposteriorly flattened and gradually tapers distally. The dorsal ¼ of the rib shaft has a longitudinal furrow anteriorly. This rib articulates well with the first thoracic vertebra.

Mid-thoracic ribs have a more proximally positioned tubercle, a short neck, and a more robust shaft that is anteroposteriorly thicker; the shaft is less transversely bowed. One proximal





fragment of a mid-thoracic rib has a possibly pathological pit distally but is too fragmentary to evaluate. Posterior thoracic ribs are straighter and longer than the anterior ribs, and possess tubercles positioned close to the capitulum; the capitulum increases in diameter posteriorly throughout the rib series. One of the posteriormost ribs, likely the eight rib, has a large hemispherical capitulum, a reduced tubercle positioned on the posterior face and not dorsally elevated; it has a nearly round cross-section, and bears a shallow longitudinal furrow dorsally on the anterior surface of the shaft. A circular anteromedial facet on the capitulum may represent an articular pathology.

Coronodon sp.

Referred Specimens

ChM GPV 2029 (also bearing number ChM PV 9162), lower left P3 or P4 and associated fragment of a second molariform tooth, collected from the vicinity of Chandler Bridge Creek in Ladson, SC, by S. Deal and J. Chapman fall 1974; ChM PV 9161, partial lower left m4 or perhaps upper left M3, collector, locality and collection date unknown; ChM PV 9163, upper posterior molariform tooth, likely P4 or M1, collector, locality and collection date unknown; ChM PV 9177, partial lower right molar, collector, locality and collection date unknown; ChM PV 9584, associated caniniform tooth and posterior molariform tooth (P4 or M1), likely but uncertainly from the Chandler Bridge excavation site in Bed 3 of the Chandler Bridge Formation, unknown collector; CCNHM 556 a partial lower right molariform, likely P3-M2, collected by C. Kaufman from the bank of the Ashley River in August 2015; CCNHM 1839, upper left posterior molariform tooth (likely M1 or M2), collected from the Edisto River by J.



1957

1958

1959

1960

1961

1962

1963

1964

1965

1966

1967

1968

1969

1970

1971

1972

1973

1974

1975

1976

1977

1978

Kiser in July 2016; CCNHM 8729, caniniform tooth, perhaps lower right I3 or C1 or upper left I3 or C1, collector, locality and collection date unknown; CCNHM 8739, upper left M2 or M3, collector, locality and collection date unknown. CCNHM 8731, isolated C1 or P1, collector, locality and collection date unknown.

Remarks

These teeth all conform to the range of variation seen in *Coronodon* spp. (Figure 36), but generally lack stratigraphic context, collector data, or locality data, all of these owing to poor record keeping. One of these, ChM PV 2029 (=9162), was collected in 1974, representing one of the earliest discoveries of *Coronodon*. Another specimen that lacks data was stored with the rest of the collection of cetaceans from the Chandler Bridge excavation (Sanders, 1980), most of which were derived from Bed 3 of the Chandler Bridge Formation. Though some specimens such as ChM PV 9161 must represent the small posteriormost molar and resemble Coronodon planifrons, the lack of stratigraphic context suggests identification to only the species level at present. Others, such as CCNHM 1830, also resemble the M2 or M1 of Coronodon planifrons. The somewhat broad and low crowns of ChM PV 2029 and PV 5854 resemble the M1 of Coronodon newtoni. As is clear from the sample available for Coronodon havensteini, there is a degree of variation in cusp count and dimensions in the molariform teeth, precluding ready identification past the genus level. At present these teeth seem smaller than those of the larger coronodonid taxon represented by ChM PV 5720 and CCNHM 214, but detailed comparisons may be warranted once this larger taxon is described. In the absence of stratigraphic context, locality data is usually helpful in permitting provisional assignment to stratum; for example, most specimens found in Charleston area river bottoms, riverbanks, and spoil piles are likely derived from the Ashley Formation, whereas fossils in shallowly incised streams further inland



produce specimens more clearly from the overlying Chandler Bridge Formation. This rough approximation is not possible here, however, since no data was recorded for most of these specimens. ChM PV 2029, however, was collected from a stream with known exposures of the Chandler Bridge Formation, and likely represents *Coronodon planifrons* or *Coronodon newtoni* – but lacks clear diagnostic features of either species. This specimen does possess some mesial serrations on the principal cusp; such serrations are more prevalent in the unnamed taxon represented by ChM PV 5720, but do occur in some specimens of *Coronodon*. Isolated coronodonid teeth are rare, and unfortunately some of the data and paperwork associated with several of these isolated teeth from The Charleston Museum were misplaced after the passing of Albert Sanders (M. Gibson, pers. comm., 2020), former Curator of Natural History. Likewise, many 'minor' specimens at CCNHM were acquired without collector or locality data prior to 2015 (S.J. Boessenecker, pers. comm.). Curiously, isolated discoveries of the highly distinctive periotics or tympanic bullae have not yet been made.

Results of Phylogenetic Analysis

The equal weights (EW) phylogenetic analysis recovered 10,000 shortest trees, each 14013 steps in length. Additional trees were found but not saved because the allocated memory was exceeded, and based on the ratio of trees to be swapped to saved trees, the actual number of most parsimonious trees is considerably higher. Fortunately, the strict consensus of these 10,000 trees is identical to the consensus obtained by the driven search (Figure 37), thus we are reasonably confident that the strict consensus summarizes the common topologies among the total population of trees of this length. As is typically the case, the implied weighting (IW) analysis recovered far fewer trees: 15 trees with a fit of 1113.20656.





2003

2004

2005

2006

2007

2008

2009

2010

2011

2012

2013

2014

2015

2016

2017

2018

2019

2020

2021

2022

2023

2024

Both phylogenetic analyses (EW and IW) supported monophyly of Coronodonidae and the genus Coronodon (Figures 37, 38). Bootstrap support for Coronodonidae, which includes the undescribed taxon ChM PV5720, is quite high at 97% (MP) or 92% (IW). Although the Family Coronodonidae is named in the present study, OTU's consisting of individual specimens of coronodonids have been included in phylogenetic studies for more than 20 years, and they have always formed a clade (e.g. Geisler and Sanders, 2003; Fitzgerald, 2006; Boessenecker and Fordyce, 2015). Support for *Coronodon* is somewhat lower than that for Coronodonidae, but still fairly high in one analysis, 67% (MP), but not the other, >50% (IW). Both species of Coronodon from the Chandler Bridge Formation (i.e. C. newtoni and C. planifrons) are sister-groups in both analyses, also with relatively high bootstrap support (74% EW or 61% IW). Coronodonidae is diagnosed by five synapomorphies, including overlapping cheek teeth (character 294: state 1 > state 0); premolars, on average, with five or more mesial denticles (305:0>2), tooth enamel lacking longitudinal fluting (307:1>2), cheek teeth possessing wide and low crowns (308:1>2), and cusps of upper molars that are reclined distally (318:0>1). The genus Coronodon is characterized by three synapomorphies, including posterior end of premaxilla faces anteromedially (14:0>2), endocranial foramina on periotic aligned (160:0>1), and mandible slightly bowed (267:0>1). The clade of C. planifrons and C. newtoni is supported by the presence of a conical lateral tuberosity of the periotic (158:0>1) and an oval fenestra rotunda (206:1>0).

Somewhat surprisingly, both analyses supported the poorly known *Metasqualodon* and *Borealodon* as sequential stem taxa to Coronodonidae. A close relationship between Coronodonidae and *Metasqualodon* is relatively well supported, 63% EW or 70% IW, whereas the clade with *Borealodon* is less so, 51% EW or 55% IW. Previously, *Borealodon* was



positioned as the sister-group to a clade including Aetiocetidae and Chaeomysticeti, diverging off of the mysticete stem one node higher than Mammalodontidae (Shipps et al., 2019), whereas *Metasqualodon* was positioned as the second lineage to diverge off the mysticete stem, one node higher than *Coronodon* (Geisler et al., 2017). The close relationship between *Metasqualodon* and Coronodonidae is diagnosed by just a single feature: basal cusps on mesial side of cheekteeth point mesially (150:0>1). By contrast, the larger clade including *Borealodon* is supported by five synapomorphies in both analyses, including maxilla terminates anterior to posterior edge of nasal (38:0>1), nasal terminates at posterior half of supraorbital process of frontal (64:1>2), anterior end of pars cochlearis is a curved ridge in medial view (175:0>1), dorsal and posterior margins of periotic meet at right angle (188:0>1), and distal thirds of cheekteeth labially deflected in occlusal view (316: 0>1). There are three additional synapomorphies for this clade in the EW analysis: teardrop-shaped fenestra rotunda (206:0>1), presence of crest between stylomastoid and suprameatal fossae of periotic (216:0>1), and fluting of enamel restricted to lingual sides of teeth (307:0>1).

Several other aspects of the strict consensus trees from both analyses are similar. Like Corrie and Fordyce (2022), we found *Kekenodon* to be the sister-group to a clade that include odontocetes, mysticetes, and the putative mysticetes *Mystacodon* and Coronodonidae. If we apply a crown-based definition for Neoceti, as advocated by Fordyce (2009), then *Kekenodon* would be excluded from Neoceti. Synapomorphies of the clade of Neoceti and *Kekenodon*, but excluding basilosaurids, are: premaxilla terminates over anterior half of supraorbital process of frontal (8:0>1), mallear fossa of periotic medial to lateral tuberosity (180:0>1), anteromedial corner of pars cochlearis is rounded (184:0>1), medial lobe of bulla terminates as a blunt corner (245:0>1), roots of double-rooted teeth partially merged (304:0>1), upper cheekteeth lack a



2049

2050

2051

2052

2053

2054

2055

2056

2057

2058

2059

2060

2061

2062

2063

2064

2065

2066

2067

2068

2069

2070

lingual cingulum (310:0>1), lower molars lack reentrant grooves (313:0>1), and lower molars bear accessory cusps on mesial carina (314:0>1).

Odontoceti is monophyletic in both analyses, as is the recently named Kinetomenta (Gatesy et al., 2022) within Mysticeti. However, application of the phylogenetic definition of Gatesy et al. (2022) for Kinetomenta to our EW trees would exclude Fucaia, Morawanocetus, and *Kaaucetus* from this clade, and would shift some key features of this clade (e.g. loose mandibular symphysis, laterally bowed mandibles) to a more basal node. Otherwise, most aetiocetids form a clade in each analysis, although Niparajacetus is more closely related to Chaeomysticeti in the IW trees. Llanocetus is closely related to the unnamed taxon represented by ZMT-62 (Fordyce, 1989) in both analyses, similar to some of the implied weighting analyses of Geisler et al. (2017), and Chaeomysticeti is monophyletic, a result consistent with nearly all phylogenetic studies that include fossil mysticetes (Deméré et al., 2008; Marx and Fordyce, 2015; Boessenecker and Fordyce, 2017; Geisler et al., 2017; Peredo et al., 2018B; Muizon et al., 2019; Bisconti et al., 2019). Unlike Peredo et al. (2018B), we found *Maiabalaena* and *Sitsqwayk* to be within Eomysticetidae. Those authors placed these genera as the sole members of a lineage diverging just crownward to Aetiocetidae but immediately before the Eomysticetidae. In our EW trees Maiabalaena is the second most basal eomysticetid and Sitsqwayk is the sister-group to Eomysticetus, whereas in our IW trees, Maiabalaena is the sister-group to Yamatocetus and Sitsqwayk is the most basal eomysticetid. Support for Eomysticetidae, including Maiabalaena and Sitsqwayk, is quite strong, with a bootstrap value of 90% (MP) or 70% (IW) and a total of seven supporting synapomorphies common to both analyses, including supramastoid crest terminating posterior to the temporal fossa (123:0>2), margins of zygomatic process parallel in dorsal view (130:0>1), presence of a secondary squamosal fossa (132:0>1), squamosal



prominence forms a large cylindrical tubercle (135:1>2), presence of a ventral fossa on apex of zygomatic process (136:0>1), squamosal medially bowed in dorsal view (138:0>1), and sharp involucral ridge of bulla (241:1>0). Differences in tree topology can be accounted for by a number of mis-codings in the matrices of Peredo et al. (2018B) that pulled these taxa further stemward. As such, although *Maiabalaena* is an important taxon for understanding the early evolution of Mysticeti, the insights it provides are largely aligned with those outlined in previous studies of eomysticetids (e.g. Sanders and Barnes, 2002A, 2002B; Boessenecker and Fordyce, 2015B, 2015C). The purported toothlessness and absence of baleen in *Maiabalaena* has been challenged (Ekdale and Deméré, 2022; Gatesy et al., 2022), and recognition of its phylogenetic placement within Eomysticetidae suggests it is no more relevant to discussions of the origin of baleen and loss of teeth than other eomysticetids with better rostral and mandibular preservation with evidence of vestigial dentition and palatal vasculature best interpreted as associated with baleen (e.g. *Tokarahia*, *Waharoa*, *Yamatocetus*, Boessenecker and Fordyce, 2015A, 2015B, 2015C; Okazaki, 2012).

Despite the many similarities among the trees from our EW and IW analyses, there are important differences, particularly with respect to the position of Coronodonidae. As in most previous studies (e.g. Geisler and Sanders, 2003; Fitzgerald, 2010; Boessenecker and Fordyce, 2017; Geisler et al., 2017) our EW trees found Coronodonidae to be the most basal lineage within Mysticeti. The mysticete clade excluding Coronodonidae, *Metasqualodon*, and *Borealodon* has a bootstrap value < 50% but is diagnosed by five synapomorphies, including presence of an infraorbital plate (27:0>1), two dorsal infraorbital foramina (36:2>1), nuchal crest elevated above occipital apex (115:0>1), loss of transverse foramen in axis vertebra (329:0>1), and crescent-shaped neural canal of axis (331:0>1). By contrast, our IW trees exclude



Coronodonidae from Mysticeti and a crown-based definition for Neoceti. The same is true for the putative mysticete *Mystacodon*, which is in an even more basal position. Corrie and Fordyce (2022) also recovered *Coronodon* and *Mystacodon* as outside Mysticeti and Neoceti, although the exact relationships among these and other taxa differ. They found that *Mystacodon* and *Coronodon* were members of a toothed "mysticete" clade outside of Neoceti or that *Mystacodon* was more basal than *Coronodon*, depending on whether they used implied weighting in their cladistic analysis. In our IW trees, support for excluding *Coronodon* from Mysticeti and Neoceti is low, both relevant nodes have bootstrap values < 50%.

Lambert et al. (2017) described the toothed mysticete *Mystacodon selenensis*; their phylogenetic analysis recovered it as the most basal mysticete, and this is aligned with it being the oldest mysticete, at 36.4 Ma. This basal position was later corroborated by Muizon et al. (2019), although as described above, the majority of phylogenetic studies have positioned *Mystacodon* as more nested within Mysticeti than coronodonids. Our EW trees recovered a sister-group relationship between *Mystacodon* and *Llanocetus*, the second oldest mysticete, although bootstrap support is <50%. A close relationship between these taxa was first found by Fordyce and Marx (2018), and then later in the implied weighting analysis of Corrie and Fordyce (2022). Intriguingly, when *Mystacodon* is positioned outside of Mysticeti and Neoceti, as occurs in our IW trees, then a clade of Southern Ocean mysticetes emerges including *Llanocetus*, ZMT-62, and mammalodontids. Synapomorphies of this Southern Ocean clade include: rostrum has a gradually sloping profile anterior to nares (49:0>1); presence of channel for the lacrimal canal (60:1>0); orbital margin deeply notched in dorsal view (73:0>1); a nuchal crest higher than the occipital apex (115:0>1); and, on average, 4.5 to 5 distal cusps on premolars (306:1>0). A more



detailed discussion on the characters that support the conflicting clades in our EW and IW analyses can be found in the Discussion.

2118

2119

2120

2121

2122

2123

2124

2125

2126

2127

2128

2129

2130

2131

2132

2133

2134

2135

2136

2137

2116

2117

DISCUSSION

Toothed Mysticete Diversity in the Western North Atlantic

Toothed mysticetes from the Oligocene of Charleston have been informally recognized since the 1990s (Barnes and Sanders, 1996A, 1996B), and isolated, but previously unpublished teeth have been collected as early as the initial excavation of the Chandler Bridge Formation in 1970-1972 (e.g. ChM PV 2029). The morphology of the "archaeomysticetes" has finally been illuminated with the publication of Coronodon havensteini, Coronodon newtoni, and Coronodon planifrons (Geisler et al., 2017; this study). Two of these (Coronodon newtoni, Coronodon planifrons) are the first toothed mysticetes from the Chandler Bridge Formation. In addition to Coronodon spp. there is at least one other poorly known coronodonid represented by CCNHM 8745, and a second, much larger *Basilosaurus*-sized genus of Coronodonidae represented by ChM PV 5720 and CCNHM 214 from the Chandler Bridge Formation. Altogether, this sample suggests a total of five species of toothed mysticetes from the Oligocene of the western North Atlantic. In addition, the Ashley and Chandler Bridge formations have also produced purportedly toothless eomysticetids Micromysticetus and Eomysticetus. Eomysticetids, and potentially five species of toothed mysticetes constitute the entire mysticete assemblage, whereas the odontocete assemblage is substantially more diverse. Odontocetes from these strata include 9-10 species of Xenorophidae (five of which are named; Kellogg, 1922; Whitmore and Sanders, 1977; Geisler et al., 2014; Churchill et al., 2016; Boessenecker et al., 2017), Agorophius (Godfrey et al., 2016), at



least two species of *Ankylorhiza* (Boessenecker et al., 2020), *Ediscetus* and several other waipatiid-grade odontocetes (Albright et al., 2018; Boessenecker, pers. obs.), and several other taxa (Geisler and Sanders, 2003; Albright et al., 2019). With the exception of *Ankylorhiza* (body length 4.8 meters), no Oligocene odontocetes approached *Coronodon* in body length. *Coronodon* was originally interpreted as an ecologically flexible taxon capable of dental filtration and raptorial feeding, similar to extant leopard seals (Hocking et al., 2013; Geisler et al., 2017). Such a capability may have supported a degree of niche differentiation and eased competition with early giant dolphins like *Ankylorhiza*. However, subsequent studies have called into question the filter feeding adaptations of *Coronodon* based on a single metric (Hocking et al., 2017).

Regardless of the feeding morphology of *Coronodon*, the fossil record of toothed mysticetes in the North Atlantic contrasts strongly with that of the North Pacific, where smaller aetiocetid whales are numerically common and surprisingly diverse (Barnes et al., 1995; Cisneros-Hernandez and Velez-Juarbe, 2021). Aetiocetid whales are typically small (BZW=22-32 cm; estimated body length 2-4 m) with some exceptions (e.g. 65 cm BZW, 8 meter body length; Tsai and Ando, 2015) relative to *Coronodon* (BZW=46 cm, estimated body length 5 meters). While the feeding morphology of aetiocetids is hotly contested, at least some have been interpreted as raptorial (e.g. *Fucaia buelli*; Marx et al., 2015), benthic suction feeders (Marx et al., 2016), and "protobaleen"-bearing filter feeders capable of raptorial fish eating (Aetiocetus; Deméré et al., 2008; Deméré and Berta, 2008). The excessive diversity of aetiocetids is not recognized in any single stratum, where typically 2-3 species may be present; however, the bulk assemblage from the North Pacific preserves 21 species (Hernandez Cisneros and Velez-Juarbe et al., 2021). Few species are documented in coeval strata at different localities, raising the possibility that local mysticete diversity in Oligocene North Pacific marine basins was equivalent



to the toothed mysticete diversity in the Charleston embayment (n=2-3) and that extreme North Pacific richness is exaggerated by pooling of distant localities. Regardless, virtually all aetiocetid taxa are based on single type specimens and frequently lack overlapping parts, raising the possibility of diversity inflation through taxonomic splitting. Further study of ontogenetic and individual variation within toothed mysticetes, such as in this study, is clearly warranted, given the possibility of taxonomic synonyms and rare examples of identification of referred specimens in the past study of Aetiocetidae.

Taxonomic Unity of *Coronodon* specimens from the Ashley Formation

Specimens of *Coronodon* from the Ashley Formation seem to share common morphological features and lack the autapomorphies of *Coronodon newtoni* and *Coronodon planifrons*. Features uniting specimens from the Ashley Formation include preorbital and postorbital processes of approximately equal depth, upper molars of similar anteroposterior length and a ventrolaterally sloping posterior edge of the supraorbital process of the frontal (Table 1). These specimens (where preserved) have a straight lateral edge of the maxilla, differing from the concave-up margin in *Coronodon newtoni*. While CCNHM 164 does not preserve a complete enough rostrum to evaluate this feature, the m4 alveolus is not elevated so high above the mandibular condyle and the ventral margin of the mandible is nearly straight, differing from *Coronodon newtoni*. These specimens all possess a sternomastoid fossa that does not extend far up the lateral side of the nuchal crest, differing from *Coronodon planifrons*. The lateral tuberosity of the periotic is generally short in *Coronodon havensteini*, measuring up to 18-20 mm in length in CCNHM 108, 8722, and ChM PV 4745 (ChM PV 4745 is an exception,





measuring 24.5 mm), and in adults the lateral tuberosity does not extend beyond the lateral margin of the swollen periotic.

Because there are two distinct species of *Coronodon* in the Chandler Bridge Formation, it is possible that a second species of *Coronodon* may eventually be discovered in the Ashley Formation. However, given the available sample, differences between specimens from the Ashley Formation seem minor and best attributed to individual variation within *Coronodon havensteini*.

Ontogeny in Coronodon havensteini

A number of cranial features in *Coronodon havensteini* change during postnatal ontogeny; most of these changes relate to the proportions of the rostrum, intertemporal region, squamosal, periotic, bulla, and eruption of the dentition. Many minor changes are mentioned in the description, including for example the dorsoventrally deeper maxilla in juveniles, and are not discussed further.

Juvenile specimens of *Coronodon havensteini* possess relatively short intertemporal constrictions, constituting 33.6% of bizygomatic width in CCNHM 8722 and 29.2% in ChM PV 4745. In comparison, the intertemporal region of the adult holotype is 57.9% of bizygomatic width. In this case, the juvenile condition is not the plesiomorphic condition, and the adult condition instead converges on the archaic long intertemporal region of basilosaurids.

Several changes are evident in the taxonomically and phylogenetically informative periotic. Most obvious is the transverse inflation of the anterior process and body of the periotic; in this regard, there is a clear increase in the transverse thickness of the anterior process and the



body. As a result, the lateral tuberosity extends beyond the body in juveniles and the body extends beyond the lateral tuberosity in adults; likewise, the inflation becomes so great that in an old adult (CCNHM 164) a deep crease forms between the body and the anterior process. The posterior process increases in length during postnatal ontogeny, being shortest in ChM PV 4745 and increasingly longer in CCNHM 108 and 164; this parallels the growth of the posterior process in Crown Mysticeti (Bisconti, 2001).

The tympanic bulla of *Coronodon havensteini* is not fully developed at birth, as the youngest specimen (CCNHM 8722) possesses a bulla that is 74.9 mm long; the bulla in the slightly older juvenile (ChM PV 4745) is slightly larger (76.7 mm), and the adult holotype has a bulla measuring 83.2-85 mm in length. This postnatal increase in bulla size parallels that of the basilosaurid archaeocete *Dorudon atrox* (Uhen, 2004: appendix IVB) as well as the eomysticetid whale *Waharoa ruwhenua* (Boessenecker and Fordyce, 2015C). In contrast, the bulla of odontocetes is already full size at birth and does not grow postnatally (Buffrenil et al., 2004; Lancaster et al., 2015).

Maxillary postcanine teeth are less emergent in juveniles, with the base of the molar crowns at least 6 mm below the lateral edge of the maxilla in ChM PV 4745. In the *Coronodon havensteini* holotype the crowns are highly emergent, the enamel base of which is 13.6-17 mm ventral to the edge of the maxilla. Accordingly, the embrasure pits of juvenile specimens CCNHM 8722 and ChM PV 4745 are more poorly developed and restricted anteriorly. This indicates that the embrasure pits in *Coronodon* are only remodeled after the crowns have erupted more extensively. *Coronodon* differs from basilosaurid whales and most other toothed mysticetes in the extreme degree of tooth eruption.



The upper cheek teeth of adult *Coronodon havensteini* are aligned anteroposteriorly, unlike the p3-m4 in the lower dentition that are posterolabially slanted and overlap one another (Geisler et al., 2017). However, the upper M1 and M2 in juvenile *Coronodon havensteini* (e.g. ChM PV 4745) overlap by 18 mm (measured obliquely along axis of interdental notch). This overlap appears to be a result of the large size of the teeth erupting in an absolutely small juvenile maxilla; as the maxilla increases in length later in growth the overlap is lost by adulthood. Curiously, in the adult holotype of *Coronodon newtoni* the upper cheek teeth overlap with the posterior root of each cheek tooth lying labial to the anterior root of the tooth just posterior to it. Given the overlapping teeth in juvenile *Coronodon havensteini*, it is likely that dental overlap is neotenically retained in *Coronodon newtoni*.

Some features notably do not change during postnatal ontogeny. For example, the proportional length of the rostrum is static in all specimens, with the maxilla measuring approximately 85-105% of bizygomatic width. Juvenile specimen ChM PV 4745 has minimum rostral length of 104% of bizygomatic width, whereas the holotype has a proportionally shorter rostrum measuring 85% of bizygomatic width. In comparison, that value is 96% in juvenile CCNHM 8722 and 105% in adult CCNHM 164, which we interpret to be individual non-ontogenetic variation. Thus, the shape of the palate is approximately the same at all ontogenetic stages and it does not appear that the rostrum proportionally lengthened (or shortened) during ontogeny. This differs from the postnatal lengthening of the rostrum in odontocetes and later diverging mysticetes (e.g. Boessenecker and Fordyce, 2015C), and implies that rostrum proportions are critical to the feeding ecology of *Coronodon*.

Revised Tooth Count in Coronodon and Implications for Polydonty in Neoceti



Geisler et al. (2017) stated that *Coronodon havensteini* had eleven upper and lower teeth with all teeth, or their corresponding alveoli, preserved in the holotype skull. This interpretation was consistent with its fairly basal position in mysticete phylogeny, and implies that it diverged before polydonty evolved among stem mysticetes. However, further study of the holotype (CCNHM 108), in combination with the new specimens described in the present paper, indicates that *C. havensteini* had four lower molars (a total of twelve lower teeth), and that the mandibles are missing the anterior tips and the i1 alveoli. Several lines of evidence support this, including 1) new observations from the *Coronodon havensteini* holotype, 2) mandibular evidence from *Coronodon newtoni* n. sp., 3) the lack of wear on the last lower molars in new specimens of *Coronodon*, and 4) supplementary observations on the mandible of ChM PV 5720, the unnamed sister taxon of *Coronodon*.

When fitting the *Coronodon havensteini* holotype mandibles into "occlusion" with the embrasure pits in the skull, it is not possible to articulate the dentition so that the anteriormost lower incisor lies mesial (anterior) to the anteriormost upper incisor, as is the conserved occlusal relationship in mammals; when attempted, there is a 3 cm gap between the mandibular condyle and the glenoid fossa. When the mandible is in articulation with the squamosal, the posteriormost molar lies just distal (posterior) to the upper M3 – but the anteriormost mandibular tooth, identified as the i1 by Geisler et al. (2017), instead is positioned near the upper I2. This suggests that an additional tooth was present, and that the i1 is actually the i2, and that there were four lower molars instead of three. In addition, the spacing in the embrasure pits does not align under the interpretation of Geisler et al. (2017), either the anterior lower teeth fit in their corresponding embrasure pits or the posterior teeth fit, but not both. If the mandible is shifted posteriorly one tooth position, then the entire series of embrasure pits in the skull match the apices of the lower



2274

2275

2276

2277

2278

2279

2280

2281

2282

2283

2284

2285

2286

2287

2288

2289

2290

2291

2292

2293

2294

2295

dentition. Furthermore, our new position resolves some observations that we had assumed were the result of taphonomic distortion. In our original occlusal interpretation (i.e. Geisler et al., 2017) it appeared that the coronoid process might contact the supraorbital process and M3 might impact the mandible. Shifting the mandible posteriorly, relative to the skull, solves both of these problems; for the M3, the mandibular body shallows anteriorly so that there is now ample space for this tooth during occlusion, and shifting the coronoid process posteriorly provides plenty of clearance between it and the supraorbital process of the frontal. Finally, our new interpretation results in the upper and lower teeth of the holotype (CCNHM 108) being more similar in morphology. This is most evident among the anterior premolars, where the toothrow transitions from caniniform anterior teeth to multi-cusped posterior teeth. Under the arrangement suggested by Geisler et al. (2017), the "P2" had two mesial and four distal denticles. By contrast their "p2" had three mesial and five distal denticles, and the "P2" was about 60% the length of the "p2". Our new arrangement results in the upper and lower second premolars being nearly identical in length and much more similar in morphology. Both teeth have three distal denticles, and the P2 has two mesial denticles whereas the p2 has one mesial denticle. On both teeth the mesial denticles are much smaller than the distal denticles.

Having a different number of upper and lower molars means that the m4 would not occlude with another tooth. The new specimen of *C. havensteini* (CCNHM 164) and the holotype of *C. planifrons* (CCNHM 166) both preserve the m4, and shear facets are absent on the m4 of each specimen. The right and left mandibular bodies of the holotype of *C. havensteini* were missing their anterior tips. What was preserved indicated only a single alveolus, and the anterior ends of the mandibular bodies were reconstructed with only 11 lower teeth. It is possible that the *C. havensteini* had only two lower molars, but we suspect that more of the mandible was missing



than we originally realized and that there were in fact twelve lower teeth on each side. The complete left mandible of *Coronodon newtoni* confirms this and possesses alveoli for twelve mandibular teeth. Though the mandible of the unnamed large toothed mysticete ChM PV 5720 has a damaged anterior end, there is a difficult to observe partial alveolus for a procumbent long-rooted first incisor, in addition to eleven better preserved alveoli for the i2-m4. In sum, *Coronodon havensteini*, *Coronodon newtoni*, and ChM PV 5720 all possessed eleven upper and twelve lower teeth, accommodated by differing numbers of molars: three upper molars and four lower molars. These observations on ChM PV 2776 and 5720 were published in early conference abstracts by Barnes and Sanders (1996A, 1996B), and we should have given this possibility more consideration prior to our original description (i.e. Geisler et al., 2017).

When superimposed onto a line drawing of the mandible of *Coronodon havensteini*, the posteriormost molar in *Coronodon planifrons* – identified conservatively in the description above as the m4 – lies entirely posterior to the m4 of *Coronodon havensteini*, and the m3 of *Coronodon planifrons* is in the same position as the m4 in *Coronodon havensteini*. Two possibilities exist: first, and most conservatively, is that the entire toothrow of *Coronodon planifrons* is simply shifted posteriorly along the mandible. The second, and more speculative possibility, is that *Coronodon planifrons* possessed an additional molar (m5), relative to other species of *Coronodon*. Testing this hypothesis will require the discovery of a complete mandible (or dentition) of *Coronodon planifrons*.

Mandibular Kinesis in Coronodon





2318

2319

2320

2321

2322

2323

2324

2325

2326

2327

2328

2329

2330

2331

2332

2333

2334

2335

2336

2337

2338

2339

plesiomorphic features, it possesses an anteroposteriorly short and unfused mandibular symphysis that has only a low-relief articular surface and lacks the planar, rugose facet seen in archaeocetes and most terrestrial mammals (e.g. Coronodon havensteini, CCNHM 108; Coronodon newtoni n. sp., ChM PV 2778). A condition similar to basilosaurids is also present in Mystacodon selenensis (Muizon et al., 2019), and inferred for Janjucetus and Mammalodon based on isolated mammalodontid mandibles (Fitzgerald, 2010, 2012). The symphyseal morphology of *Coronodon* is instead more similar to that of the north Pacific toothed mysticetes, the Aetiocetidae, as well as Chaeomysticeti, and the lack of a tight articular suture indicates flexibility at the intramandibular joint. Coronodon seems to lack a symphyseal groove, present in the Aetiocetidae + Chaeomysticeti clade, which was recently named the Kinetomenta by Gatesy et al. (2022). A shallow furrow is present ventrally in Coronodon (CCNHM 108, ChM PV 2778), and this may be the homolog of the more deeply incised groove in the Kinetomenta. This groove appears to be an ontogenetic remnant of the groove for the Meckel's cartilage (Mead and Fordyce, 2009) which persists into early postnatal ontogeny in some early chaeomysticetes (Boessenecker and Fordyce, 2015C). Intramandibular kinesis is generally interpreted as an adaptation for filter feeding in mysticetes (Lambertsen et al., 1995; Deméré et al., 2008; Gatesy et al., 2022). It would permit longitudinal rotation of the mandible as well as slight lateral abduction of the tips of the mandibles, both motions of which serve to increase the volume of the oral cavity during feeding in extant mysticetes (Lambertsen et al., 1995; Goldbogen et al., 2007; Potvin et al., 2009). Accordingly, loss of a firm mandibular joint in *Coronodon*, though not initially cited, would

further support the filter feeding interpretation for Coronodon (Geisler et al., 2017). Like the

The mandible of *Coronodon* resembles that of Basilosauridae and despite many



Actiocetidae, *Coronodon* possesses straight mandibles that are not laterally bowed like those of Chaeomysticeti, which suggests only an incipient increase in oral volume during filter feeding. Other hypotheses that have not yet been proposed might be worth exploring; for example, mandibular fusion versus the retention of a suture (analogous to basilosaurids) in terrestrial and aquatic Carnivora is related to bilateral biting (fusion) or unilateral chewing and gnawing of even harder food items (Scapino, 1981; Scott et al., 2012; Tseng et al. 2016). Complete loss of mandibular articulation is rare in mammals and aside from cetaceans, seems to occur only in anteaters (Ferreira Cardoso et al., 2020). It is perhaps not a coincidence that anteaters, like baleen whales, have also lost their dentition (Ferreira-Cardosa et al., 2019). A loose mandibular symphysis in *Coronodon* seems best associated with filter feeding (e.g. Gatesy et al., 2022).

In addition to intramandibular kinesis, the glenoid fossa of the referred adult skull of *Coronodon havensteini* (CCNHM 164) and the holotype of *Coronodon planifrons* (CCNHM 166) both possess a bilobate glenoid fossa. In these specimens, a secondary fossa with a deeply pitted rugose texture matching the rugose texture of the mandibular condyles of all known specimens of *Coronodon* is present dorsomedially to the glenoid fossa proper. This secondary fossa suggests the presence of an unusual articulation, and perhaps indicates a movable craniomandibular joint permitting the longitudinal rotation and/or medial adduction of the posterior mandible by a few centimeters as in extant mysticetes (Lambertsen et al., 1995). This secondary glenoid fossa was not observed in the *Coronodon havensteini* holotype as this surface is completely smooth. Because the secondary fossa in CCNHM 164 and 166 bears similarly rugose, somewhat vermiform pattern of ridges matching the surface texture of the mandibular condyle, the secondary glenoid fossa cannot be dismissed as a sinus (such as the tympanosquamosal recess of odontocetes).



2364

2365

2366

2367

2368

2369

2370

2371

2372

2373

2374

2375

2376

2377

2378

2379

2380

2381

2382

2383

2384

2385

Rostral Kinesis in Coronodon

Extant mysticetes possess sutures between the rostral elements and between the rostrum and frontal that are completely or partially open (Bouetel, 2005). Most Chaeomysticeti possess a completely unfused premaxilla-maxilla suture and slight mortising (reciprocal ridges and grooves) of the premaxilla-frontal and maxilla-frontal joints, the latter of which is confined to the ascending process of the maxilla. Eomysticetids possess an intermediate morphology with premaxillae that are somewhat firmly articulated with the prenarial process of the frontal and share a firm sutured joint with the lateral edge of the nasal, but lack any sutural grooves or rough articular surfaces for the maxilla-frontal suture, suggesting that the maxilla was movable (Boessenecker and Fordyce, 2015C). Toothed mysticetes such as the Aetiocetidae, Mammalodontidae, and *Llanocetus* have typically been inferred to have firm (akinetic) rostral and rostro-frontal sutures (Fitzgerald, 2010). Among these, Mammalodon exhibits some postmortem splaying of the maxilla and premaxilla, revealing an open suture and only a lightly mortised maxilla-frontal and premaxilla-frontal joint, generally resembling chaeomysticetes. Advanced dental wear indicates that this cannot simply be dismissed as representing an early ontogenetic stage prior to suture closure. Kinetic rostra have not been reported in the Aetiocetidae, though many of these are collected and physically prepared from highly indurated concretions and observation of features of kinetic rostra would require acid preparation or CT imaging. Some toothed mysticetes exhibit rostral sutures that are clearly firmly closed, including Llanocetus denticrenatus, Mystacodon selenensis, Janjucetus hunderi, and Fucaia goedertorum, all of which possess a closed maxilla-premaxilla and/or maxilla-frontal suture. For example, in Fucaia goedertorum, loss of parts of the ascending process of the maxilla reveals a lightly rugose



frontomaxillary sutural surface (Boessenecker, pers. obs.), differing from the planar surface of the frontal in Coronodon. Regardless, limits of study imposed by preservation and preparation methods suggest that the assumption of akinetic rostra in most toothed mysticetes has not been substantiated by careful observation.

Coronodon spp., on the other hand, possess a premaxilla-maxilla suture with only faint topography that instead is developed more like a planar 'butt joint'. The maxilla-frontal articulation bears no sutural ridges or grooves. In contrast, the frontal bears deep grooves and ridges for an anteroposteriorly short premaxilla-frontal and nasofrontal articulation, and the premaxilla also articulates with a similar surface on the ventrolateral edge of the nasal. This condition is similar to that of the Eomysticetidae, with firm premaxillae buttressed by short triangular prenarial processes of the frontal that underlie the posteriormost premaxilla, accompanied by apparently mobile maxillae.

These sutures suggest a greater degree of kinesis in the rostrum of *Coronodon* than other toothed mysticetes, and differs strongly from the rigid rostra of basilosaurids. Rostral kinesis has received relatively little attention in the highly contested debates over the origin of filter feeding in stem mysticetes (e.g. Boessenecker and Fordyce, 2015C). Kinesis is poorly understood even in extant mysticetes, but is hypothesized to permit some flexibility of the rostrum during bulk filter feeding (Bouetel, 2005). It is unknown whether rostral kinesis is simply passive during filter feeding (e.g. accommodating hydrodynamic forces imposed upon the rostrum and palate during filter feeding) or actively controlled; it is hard to imagine the latter scenario, given the lack of muscles that insert onto the rostrum in extant mysticetes (Schulte 1916). Several possibilities could explain rostral kinesis in *Coronodon*. Kinesis could passively permit slight deformation of the rostrum by hydrodynamic forces during filter feeding; active movement of



the maxilla could further permit adjustment to the alignment of upper and lower teeth to control the dental filtering process. It is also possible that this loss of a firm articulation may be non-functional, paralleling the loss of a median premaxillary articulation and development of the mesorostral groove in Neoceti. If a reduced premaxilla-maxilla articulation parallels the mesorostral groove, perhaps this open suture might rather represent an exaptation in later filter feeding mysticetes.

Tympanoperiotic Fusion in Coronodon planifrons

Fusion of the posterior processes into a compound process is a key character in mysticete phylogeny, at present considered to diagnose a somewhat more exclusive clade of Chaeomysticeti excluding the Eomysticetidae and other archaic chaeomysticetes like *Horopeta*, *Toipahautea*, and *Whakakai* (Boessenecker and Fordyce, 2015C, Tsai and Fordyce, 2015, 2016, 2018) but including *Mauicetus* (Tsai and Fordyce, 2015; Marx and Fordyce, 2015). The derived condition also characterizes all extant species of mysticetes. Initially, a fused and long posterior process was considered a mysticete synapomorphy, prior to the discovery of toothed mysticetes and eomysticetids with unfused posterior processes (e.g. Geisler and Sanders, 2003).

The holotype of *Coronodon planifrons* is distinctive in possessing fused posterior processes of the bulla and periotic, but only on the left side. Owing to the asymmetry of this structure in the *Coronodon planifrons* holotype (CCNHM 166) and absence of fusion in any other toothed mysticetes, this condition can be dismissed as a pathology. However, if the *Coronodon planifrons* holotype had been discovered prior to *Coronodon havensteini*, and only with the fused periotic, such a condition could be misinterpreted as indicating a more crownward



position of *Coronodon* along the mysticete stem. More practically, the asymmetrical morphology of the periotics of *Coronodon planifrons* indicates that the periotic morphology of stem mysticete taxa known by only a left or right periotic from a single specimen (e.g. *Fucaia buelli*, *Mammalodon colliveri*, *Salishicetus meadi*, *Tohoraata raekohao*) should be interpreted carefully.

Postcranial Morphology and Locomotor Adaptations in Coronodon

The holotype skeleton of *Coronodon havensteini* possesses a complete set of cervical vertebrae and a nearly complete thoracic series. Extensive postcrania in the newly referred skeleton of *C. havensteini* CCNHM 164 and the holotype of *Coronodon planifrons* (CCNHM 166) reveal much of the remaining postcranial morphology, vertebral count, and locomotor adaptations in the earliest diverging toothed mysticetes (Figure 39; Tables 7-11).

No single specimen of *Coronodon* possesses a complete series of thoracic and lumbar vertebrae, however, CCNHM 166 preserves the posteriormost thoracics and a complete set of lumbars. CCNHM 164 preserves three isolated lumbars and nine thoracics. Centrum measurements of the thoracic vertebrae indicate that these constitute a continuous series from the T1 through the T9; the T9, critically, matches the posteriormost thoracic vertebra and presumed T9 in CCNHM 166. Based on these two specimens, a count of 9 thoracics is most likely for the genus, though a count of 10 may be possible. CCNHM 166 preserves 10 lumbar vertebrae, and a jump in measurements between the anteriormost (L1) and the next preserved vertebra may suggest that L1 or L2 is missing, and that a total of 11 lumbar vertebrae were present; a count of ten is conservatively estimated. Nine (more fragments?) caudal vertebrae are preserved, and the total likely exceeded 20 caudals in CCNHM 166, consistent with the primitive number of 21



caudals reconstructed by Buchholtz and Gee (2017). Comparison of the holotype vertebrae with those of CCNHM 164 and *Coronodon planifrons* n. sp. (CCNHM 166) and measurements of the holotype vertebrae indicate that only T5 and T9 are missing. Initially, Geisler et al. (2017) assumed a higher thoracic count for basal Neoceti (e.g. Buchholtz and Gee, 2017), and under the assumption that the thoracic series was too incomplete to identify further, only identified T1-2.

Like other toothed mysticetes and chaeomysticetes, the vertebral column of *Coronodon* includes relatively flattened disk-like cervical vertebrae, thoracic and lumbar vertebrae with wide centra, and gradually increasing length, depth, and width in the lumbar series peaking around the lumbocaudal boundary. Centrum length peaks in the mid-lumbars, whereas centrum height peaks in the anterior caudals; this suggests incipient development of a stiffened tail stock. However, the caudals are all relatively wide, suggesting that, like early odontocetes (*Albertocetus*, *Ankylorhiza*; Boessenecker et al., 2017, 2020), *Coronodon* did not possess a transversely narrowed caudal peduncle and that this feature evolved independently within Odontoceti and Mysticeti (Boessenecker et al., 2020). The posteriormost caudal, Ca D, of CCNHM 166 is rectangular and somewhat dorsoventrally shallower than wide, indicating the presence of a caudal fluke like Basilosauridae and all other Neoceti for which caudal vertebrae are known (Uhen, 2004).

Gradual changes in vertebral dimensions and the lack of clear regionalization of the vertebral column (Tables 8-11) indicates that *Coronodon* can be assigned to "Pattern 1" swimmers, like basilosaurid whales and other mysticetes (Buchholtz, 2001). Though of similar size, the giant dolphin *Ankylorhiza* (from the same Oligocene strata as *Coronodon* spp.) was a "Pattern 2" swimmer (similar to Ziphiidae and the beluga, *Delphinapterus*; Boessenecker et al., 2020) and was apparently a somewhat more efficient swimmer than *Coronodon* (E. Buchholtz, pers. comm.). The vertebral profile of *Coronodon* is relatively similar to the small basilosaurid





Zygorhiza as well as the toothed mysticete *Aetiocetus cotylalveus* (Buchholtz, 2001). If *Coronodon* was an apex predator as proposed by Hocking et al. (2017), it possessed no postcranial specializations for it (unlike *Ankylorhiza*; Boessenecker et al., 2020).

Body length and skull proportions of Coronodon

Estimation of body length using the equations of Pyenson and Sponberg (2011) resulted in a length of 4.22 meters using the bizygomatic skull width and 4.41 meters using the partial least squares method. Estimation of the body length of *Coronodon* used the skull length of CCNHM 108 (=99 cm), the cumulative cervical length of CCNHM (=24 cm), cumulative thoracic length of CCNHM 164 (=53 cm), the cumulative lumbar length of CCNHM 166 (=91 cm), and the cumulative caudal length with missing vertebrae estimated (=140 cm) to fill the ancestral count of 13 anterior caudals and 9 fluke caudals from Buchholtz and Gee (2017), for a skeletal length of 4.08 meters. To estimate the length of the vertebral column constituted by cartilaginous intervertebral disks, we applied the average disk:vertebra length ratio of 24:100 from Long et al. (1997) to the average vertebra length within each region and multiplied by the vertebra count from each region, resulting in a total additional length of 76.8 cm. Altogether, this yields a body length of 4.8-5.0 meters, depending upon the exact count of caudal vertebrae.

Pyenson and Sponberg (2011) did not indicate the unit of skull measurements to be entered into their equations, and if in millimeters rather than centimeters are used, the bizygomatic width equation provides a much smaller body length estimate of 3.55 meters for *Coronodon havensteini*. We are confident that the correct units are centimeters; we plugged in bizygomatic width (in cm) into their equations and were able to replicate values they provided in



2499

2500

2501

2502

2503

2504

2505

2506

2507

2508

2509

2510

2511

2512

2513

2514

2515

2516

2517

2518

2519

2520

their table 4 for several taxa. For further comparability/repeatability, it would be ideal if the dataset used for the analysis by Pyenson & Sponberg (2011) were published. It is important to determine if the difference between the lengths calculated from BZW and PLS equations, and the length estimated from the vertebral column, which we consider to be more reliable, are just expected errors or a sign that fundamental proportions between the skull and the vertebral column have changed over time, and cannot be easily inferred from equations derived from extant taxa only.

Geisler et al. (2017) predicted that if *Coronodon* engaged in dental filtration, then the relative skull length, and size of the oral cavity in particular, would increase at the origin of Mysticeti. Extant mysticetes have enormous heads, which allow for a larger oral cavity and greater efficiency for filter-feeding, and thus there is clear functional link between behavior and relative head size. Using our length estimate from the preserved vertebral columns of Coronodon spp., we estimate that the skull of *Coronodon* comprised approximately 20% of body length. This is much greater than the relative skull size in basilosaurids (Uhen, 2004; Muizon et al., 2019) and at first glance would appear to support the prediction of Geisler et al. (2017). However, protocetids have a skull that comprises a much greater proportion of the body length, as compared to basilosaurids, and also have fewer lumbar vertebrae (Gingerich et al., 2009; Uhen, 2014). In addition, the basal odontocete Ankylorhiza (Boessenecker et al., 2020) has a head that also comprises about 20% of body length. Thus to clarify the evolution of head length, relative to body length, across the archaeocete to neocete transition will require a better understanding of the relationships of stem neocetes to basilosaurids and other members of Pelagiceti, as well as how proportions are influenced by changes in length of the rostrum, vertebral count, and vertebral length.



2522

2523

2524

2525

2526

2527

2528

2529

2530

2531

2532

2533

2534

2535

2536

2537

2538

2539

2540

2541

2542

Do Neoceti and Mysticeti include Coronodonidae and Mystacodon?

As described in Results of Phylogenetic Analysis, our EW analysis placed Coronodonidae and *Mystacodon* within Mysticeti. Character support for these "traditional" placements have been thoroughly discussed in previous studies (Geisler et al., 2017; Muizon et al., 2019), but with our unconventional IW trees in hand, we can reexamine some of these characters, explore characters that support exclusion of Coronodon and Mystacodon from Mysticeti, and compare the degree that these osteological characters support or contradict alternative placements of these genera. Our EW trees support Coronodonidae and *Mystacodon* as mysticetes, and there are nine characters that are synapomorphies of Mysticeti that have a shorter length as compared to the IW trees, including maxilla lateral to premaxillae and nasals (20:0>2; 1 to 3 steps shorter), maxilla/premaxilla suture marked by a deep groove (52:0>1; 1 step shorter), anteromedial corner of frontal is a triangular projection (81:0>1; 2 steps shorter), orbitotemporal crest extends onto frontals (98:0>1; 2 to 3 steps shorter), frontoparietal suture pointed posteriorly on sagittal plane (101:0>1; 1 step shorter), paroccipital process swollen with pit for stylohyoid (112:0>2; 1 to 4 steps shorter), triangular supraoccipital (114:0>1; 2 to 3 steps shorter), and bulbous basioccipital crest (153:0>1; 1 step shorter). Somewhat surprisingly, a traditional mysticete synapomorphy, the antorbital process (Barnes, 1990; Sanders and Barnes, 2002B), is the same length on the EW and IW trees. We coded the antorbital process as present in Olympicetus, mainly based on CCNHM 1000 (Racicot et al. 2019). As a result, in the EW trees, where coronodonids are mysticetes, its presence in *Olympicetus* is optimized as convergent (2) steps), whereas in the IW trees, where coronodonids are outside of Mysticeti, this character state





2546

2547

2548

2549

2550

2551

2552

2553

2554

2555

2556

2557

2558

2559

2560

2561

2562

2563

2564

2565

is a synapomorphy of all neocetes and its absence in most odontocetes is considered a reversal (also 2 steps).

A Neoceti that excludes Coronodonidae, *Mystacodon*, *Borealodon*, and *Metasqualodon*, as was found in our IW trees, is diagnosed by eight synapomorphies. The eight characters that include these synapomorphies also require less steps (i.e. support) than this more restrictive concept for Neoceti, including absence of embrasure pits anterior to p1/P1 (53:0>1; 2 to 3 steps shorter), parietals are wider than long in dorsal view (93:0>2; 1 step shorter), posterior bullar facet of periotic lacks longitudinal grooves (183:1>0; 1 step shorter), largest tooth is of medium size (319:2 or 3>1; 4 steps shorter), and elevated transverse process of C7 (339:0>1; 2 steps shorter). For each of these characters, coronodonids share the same morphology as basilosaurids but differ from the morphology in many basal odontocetes. Thus, repositioning coronodonids outside of crown Neoceti requires less steps. The largest decrease in length occurs in the character that codes for tooth size relative to bizygomatic width (character 319). Under the IW trees, there is a clear trend for decreasing tooth size among stem neocetes; the first reduction occurs at Neoceti and then a second reduction at the base of Mysticeti. This trend co-occurs with a more complicated pattern of tooth simplification and reduction in heterodonty in cetaceans (Gatesy et al., 2013; Peredo et al., 2018A), as seen in the differences between the teeth of basilosaurids as compared to those of Aetiocetus cotylalveus or Echovenator sandersi. A reduction in tooth size is consistent with the hypothesis that suction feeding evolved before the origin of Neoceti (Johnston and Berta, 2011); once this behavior developed, teeth played less of a role in prey capture.

Another clade in the IW trees includes coronodonids and neocetes, but excludes Mystacodon, Kekenodon, and basilosaurids. This result conflicts with previous studies that



2567

2568

2569

2570

2571

2572

2573

2574

2575

2576

2577

2578

2579

2580

2581

2582

2583

2584

2585

2586

2587

2588

supported a sister-group relationship between *Mystacodon* and *Llanocetus* (Fordyce and Marx, 2018), other studies that placed *Mystacodon* as the most basal mysticete (Lambert et al., 2017; Peredo et al., 2018B), and our EW trees. There are four characters that diagnose the clade that excludes Mystacodon and also require less steps, as compared to the EW trees: maxilla and premaxilla lack a scalloped edge (55:0>1; 1 step shorter), lacrimal foramina and/or channels absent (60:0>1; 1 step shorter), small anterior teeth (298:0>1; 1 step shorter), and scapular blade rapidly widens (349:0>1; 1 step shorter). The holotype of *Coronodon newtoni* is the only specimen in this family to preserve the lacrimal bone, and it lacks all traces of the lacrimal canal. This contrasts sharply with the morphology of *Mystacodon*, which has a primary and accessory lacrimal canal (Muizon et al., 2019), the same morphology as seen in basilosaurids (Uhen, 2004). *Llanocetus*, which is positioned as a basal mysticete in the IW trees, appears to have a shallow groove on the lacrimal (Fordyce and Marx, 2018: supplemental description), thus interpreted as a reversal to the primitive condition. One new character in the present study, the size of the anterior teeth relative to bizygomatic width, mirrors the previously discussed decrease in largest tooth size (character 319). This is interesting because whereas reductions in the largest tooth size among basal neocetes likely reflect a reduction in mastication and prey processing (Gatesy et al., 2013), a reduction in the anterior teeth is important evidence for a decreased reliance on raptorial feeding (Werth, 2000). The holotype skull (CCNHM 108) of Coronodon havensteini preserves a single lower canine but none of the incisors. The discovery of referred specimen CCNHM 164 reveals that the incisors, and canines, are all surprisingly small. The anteroposterior diameter of these teeth is only 3-4% of bizygomatic width, comparing well with odontocetes. In contrast, basilosaurid and protocetid archaeocetes possess anterior teeth (i3/I3 or c/C) with an anteroposterior crown length between 6 and 10% of bizygomatic width. Mystacodon selenensis



has an upper I3 and C that are 8-9% of the bizygomatic width, similar in size to these teeth in basilosaurids. Muizon et al. (2019) calculated the sum of the mesiodistal lengths of the anterior dentition for *Mystacodon* and three cetaceans straddling the archaeocete/neocete transition, and they too found *Mystacodon* to have larger anterior teeth than *Coronodon*. However, when calculated in this way, the anterior teeth of *Mystacodon* are more intermediate in size between those of archaeocetes and *Coronodon*, rather than being within the archaeocete range of variation. Finally, the distal end of the scapula of *Mystacodon* is quite narrow, resembling those of archaeocetes and likely convergent with the morphology of balaenids (Benke, 1993). By contrast, a specimen of *Coronodon havensteini* (CCNHM 164) has a partial scapula, which although incomplete, clearly had a blade that rapidly increased in width. Scapulae of basal neocetes are very rare, and it is important that additional specimens are found to test whether an abruptly widening scapular blade is characteristic of all neocetes.

Although not differing in length among trees from our two hypotheses, two other characters that are optimized as synapomorphies of the clade that excludes *Mystacodon* merit discussion. The first is the occurrence of 12 mandibular teeth (292:4>5) and the second is the presence seven upper postcanine teeth (299:0>1). Having 12 mandibular teeth is an instance of polydonty; where there are more teeth than the highly conserved tooth limit, at least within Mammalia, of 11 teeth per dental quadrant. Polydonty was proposed, with caveats, as a potential synapomorphy for the Neoceti by Fordyce and Muizon (2001). All extant odontocetes are polydont or evolved from a polydont ancestor, and the embryonic dentition of most extant mysticetes is polydont (Karlsen, 1962; Thewissen et al., 2017; Lanzetti et al., 2018). However, as noted by Fordyce and Muizon (2001), many stem mysticetes and stem odontocetes possess a tooth count identical with basilosaurid whales (ten uppers and eleven lowers), such as the



2613

2614

2615

2616

2617

2618

2619

2620

2621

2622

2623

2624

2625

2626

2627

2628

2629

2630

2631

2632

2633

2634

mysticetes Janjucetus, Mammalodon, Mystacodon, and the odontocete Simocetus (Fordyce, 2002, Fitzgerald, 2006, 2010; Muizon et al., 2019). Aetiocetid toothed mysticetes, including Aetiocetus spp., Salishicetus meadi, and Morawanocetus vabukii, as well as most Xenorophidae (except the toothless *Inermorostrum*), *Ankylorhiza*, and *Waipatia* among stem odontocetes have minimal (8-9 postcanines) to moderate (10-15+ postcanines) polydonty, perhaps suggesting that the common ancestor of mysticetes and odontocetes had the developmental capacity for polydonty. Our IW trees support a small degree of polydonty (i.e. 12 mandibular teeth) as a neocete synapomorphy and that the presence of only 11 teeth in *Simocetus* is considered a reversal to the primitive condition. The morphology in coronodonids is based on the holotype of C. havensteini, which as explained above is now interpreted to have four lower molars and 12 lower teeth in total. Under our EW trees, the occurrence of 12 mandibular teeth in coronodonids is best interpreted as convergent with the presence of 12 or more teeth in other neocetes, such as Aetiocetus weltoni or Echovenator sandersi. For the second character, the number of upper postcanine teeth (character 299), the primitive condition for our EW and IW trees is six postcanine teeth, consistent with this feature being a synapomorphy of Pelagiceti (Martínez-Cáceras and Muizon, 2017). The optimization on our trees is driven by the inclusion of the basilosaurids Zygorhiza, Dorudon, and Basilosaurus, which lack M3 and only have four premolars and two molars. More basal cetaceans, such as pakicetids and protocetids, have three upper molars and seven postcanine teeth (Hulbert et al., 1998; Cooper et al., 2009). Thus, the optimization of seven postcanine teeth at the node that excludes Mystacodon raises two important questions: is the presence of seven postcanine the plesiomorphic state, with the loss of the M3 a synapomorphy of Basilosauridae, or are last molars in coronodonids not homologous to M3 of protocetids? If the answer to the latter question is yes, then the occurrence of seven





2636

2637

2638

2639

2640

2641

2642

2643

2644

2645

2646

2647

2648

2649

2650

2651

2652

2653

2654

2655

2656

2657

postcanine teeth in early neocetes could mark concurrent polydonty in the upper and lower dentition; the lowers going from 11 to 12 teeth and the uppers from 10 to 11 (6 to 7 postcanines).

Returning to the question that headed this section: "Do Neoceti and Mysticeti include Coronodonidae and *Mystacodon*?" we tentatively suggest that that the answer to both is yes, based on our EW analyses. This is the traditional view of these taxa, and although implied weighting can be more efficient in yielding the shortest trees (Goloboff et al., 2008), it can become problematic when different partitions have very different amount of missing data, such as a morphological partition with many fossils as compared to a molecular partition where fossils cannot be coded (Goloboff, 2014). Although there are some analytical techniques that address these complexities (Goboloff, 2014), they often require substantial more computing time and additional assumptions of weights among partitions, which can be difficult to justify. In the present study, one of the characters that supports the IW over the EW trees is a rapidly widening scapular blade; Mystacodon has a narrow blade and this the character supports exclusion of this genus from Mysticeti and Neoceti. However, most extinct mysticetes are not represented by scapulae, and thus the homoplasy of this character is likely undercounted, as compared to many cranial characters, which are better represented in the fossil record. This undercounted homoplasy likely leads to higher weights in the implied weighting analysis. That said bootstrap values for the conflicting nodes between the EW and IW trees are poorly supported, and we can easily envision that one or two new fossil species, as well as careful evaluation of known characters, could more clearly tip the balance in favor of one topology over the other.

We encourage future studies to include more protocetids into this dataset, which should help polarize characters and ensure that the root is accurately identified. In addition, we encourage more detailed study of two character-rich regions. The first is the anterior edge of the



orbit, including the antorbital process, antorbital notch, zygomatic process of the maxilla, posteriormost dentition (in some taxa), lacrimal, and lacrimal foramina and/or canals. This region of the skull is quite different in odontocetes and mysticetes, and both are also unique as compared to basilosaurids. Careful comparison of basal odontocetes and mysticetes would help ensure that characters are coded consistently and that individual changes are not "upweighted" by the inclusion of logically separate, but clearly related and non-independent morphological characters. The second area we think would be fruitful would be direct comparisons of the teeth of basal mysticetes and odontocetes, with an eye to improving existing characters and developing new ones. One challenge in this undertaking would be the basic homology statements needed to code characters, including whether the teeth in basal neocetes are homologous to the deciduous or adult teeth of archaeocetes as well as the homology of teeth among taxa with very different tooth counts.

Synapomorphies for Neoceti Revisited

Neoceti is the taxon that refers to the crown group including Odontoceti and Mysticeti (Fordyce, 2009). It is equivalent to Autoceta, an older, rarely used, and imprecisely defined name with a similar taxonomic composition (Geisler and Sanders, 2003; Fordyce, 2009). The phylogeny and origin of the clade Neoceti has come into focus in recent years with many studies reporting ever-more plesiomorphic stem mysticete and stem odontocete fossils, resulting in continual reevaluation of character transformations across the archaeocete-neocete transition (Fordyce, 2002; Geisler and Sanders, 2003; Fitzgerald, 2006, 2010; Uhen, 2008; Sanders and Geisler, 2015; Geisler et al., 2014, 2017; Lambert et al., 2017; Velez-Juarbe, 2017; Fordyce and Marx, 2018; Corrie and Fordyce, 2022). Although many synapomorphies proposed in the 1990s prior to the detailed study of Oligocene stem odontocetes and mysticetes have been challenged or





refuted through the discovery of plesiomorphic fossils (Geisler and Sanders, 2003), a few reliable synapomorphies have remained. However, what are, or are not, neocete synapomorphies should be revisited given the recent redescription of *Kekenodon onamata*, which Corrie and Fordyce (2022) placed as the sole sister-group to Neoceti, as well the possibility that several taxa traditionally considered to represent toothed mysticetes might fall outside Neoceti.

One character frequently cited as a neocete synapomorphy, an immobile elbow joint (Barnes, 1990; Boessenecker et al., 2020), results from separate, flat facets for the radius and ulna on the distal humerus. Sanders and Geisler (2015) suggested the archaic odontocete *Mirocetus* had a mobile element joint, but the holotype and only known skeleton is not well preserved, and the second author of that study now believes the morphology of this taxon is uncertain. This character was included in the present study (character 358) and it is a synapomorphy of Neoceti or Kekenodon + Neoceti on the EW trees or is a synapomorphy of one of two clades of the IW trees (Mystacodon + Coronodonidae + Neoceti or this clade + Kekenodon) Determining which inference is correct will require the elbow of *Kekenodon*, or a close relative, to be described.

Geisler and Sanders (2003) stated that a posterior position of the ascending process of the premaxillae, specifically one where this bone terminates in line with the orbit, is a synapomorphy of Neoceti. In most mammals the premaxilla typically terminates on the rostrum between the nasal and maxilla, but in cetaceans, the nasals migrate posteriorly along with the bony nares (Churchill et al., 2018; Roston and Roth, 2019; Coombs et al., 2022). In protocetids, the premaxilla typically terminates around the middle of the rostrum whereas in basilosaurids it extends further posteriorly along the posterior quarter of the rostrum (Geisler et al., 2005). In the EW and IW trees of the present study, premaxillae terminating in line with the orbits is not a



synapomorphy of Neoceti, but instead diagnoses a larger clade that includes *Kekenodon*, *Coronodon*, and Neoceti. However, it should be noted the terminal ends of the premaxillae are not preserved in the holotype skull of *Kekenodon onamata*, and this inference is based on an interpretation of the sutural surfaces on the frontal (Corrie and Fordyce, 2022). If this inference is incorrect, then premaxillae reaching the level of the orbits would still be a neocete synapomorphy on the EW trees.

Loss of the sagittal crest was identified by Martinez-Caceres et al. (2017) as a possible synapomorphy of Neoceti. However, this was a result of the limited sample of mysticete and odontocete OTUs, which did not include *Coronodon* or *Mystacodon*, both of which have a sagittal crest. Tall basilosaurid-like sagittal crests are not yet known in Odontoceti, though *Xenorophus* possesses a low sagittal crest and an ovoid cross-section of the intertemporal constriction (Boessenecker and Geisler, unpublished data). We also evaluated this character in the present study (character 97) and found multiple, equally parsimonious states for Neoceti, reflecting the variability of this trait in stem odontocetes and mysticetes.

Extant mysticetes and odontocetes are distinctive in possessing a loss of the bony articulation of the premaxillae dorsally and anterior to the bony nares, forming an open mesorostral groove floored by the vomer. In protocetids and basilosaurids the medial surface of the premaxilla is flat and articulates directly with the opposite premaxilla along a planar joint. Based on this distribution, Fordyce and Muizon (2001) suggested that a continuous mesorostral groove was a neocete synapomorphy, a result corroborated by Fitzgerald (2010). In *Coronodon* and other toothed mysticetes like *Mystacodon*, *Janjucetus* and *Aetiocetus*, the premaxillae are separate along most of their length, but articulate anteriorly; this articulation is quite reduced relative to basilosaurids. Unpublished skulls of *Xenorophus* possess a thin ascending flange of



2728

2729

2730

2731

2732

2733

2734

2735

2736

2737

2738

2739

2740

2741

2742

2743

2744

2745

2746

2747

2748

2749

the premaxilla that slightly roofs over the mesorostral groove, and although the premaxillae nearly contact, there is no articular surface (Boessenecker, pers. obs.). In *Echovenator*, the ascending premaxillae completely roof over the canal and may be fused dorsally at the anterior tip (Churchill et al., 2016), though fracturing may obscure these details. The extent of a mesorostral groove was included in the present study (character 13), and it was not consistently optimized as a synapomorphy of Neoceti or adjacent node on our EW or IW trees, presumably because of anterior articulation of the premaxillae in several stem odontocetes and mysticetes.

A posterodorsally facing occipital shield, along with a supraoccipital apex shifted anteriorly relative to the occipital condyles, was proposed as a neocete synapomorphy by Martinez-Caceres et al. (2017). In contrast, the occipital shield faces posteroventrally in protocetids and posteriorly in most basilosaurids. In early odontocetes (Xenorophidae, Agorophius, Simocetus, Ashleycetus, Mirocetus, Ankylorhiza) and all toothed mysticetes (Llanocetus, Mystacodon, Mammalodontidae, Aetiocetidae, and Coronodon) the occipital shield is subvertical and faces at least somewhat posterodorsally. Martinez-Caceres et al. (2017) also proposed that a transverse constriction of the occipital shield at mid-depth as a synapomorphy of Neoceti. In general, most Neoceti possess a rectangular, semicircular, or triangular occipital shield when viewed in posterodorsal view. However, some basilosaurids also possess a rectangular occipital shield that is not constricted, including Basilosaurus cetoides, Cynthiacetus spp., and some specimens of *Dorudon atrox* (Kellogg, 1936; Uhen, 2005; Martinez-Caceres et al., 2017). Neither character was included in the present study, but a related one, the anteriormost extent of the supraoccipital (character 107) was. A supraoccipital that is extended anteriorly will also face posterodorsally, one not extended will be vertical, and one extended posteriorly will face posteroventrally. In our EW trees, a supraoccipital that extends anteriorly beyond the level



2751

2752

2753

2754

2755

2756

2757

2758

2759

2760

2761

2762

2763

2764

2765

2766

2767

2768

2769

2770

2771

2772

of the posterior margin of the temporal fossae is a synapomorphy of Mysticeti, not Neoceti. By contrast, on our IW trees, it is equally parsimonious that this state is a synapomorphy of Neoceti or for it to have evolved convergently in coronodonids, some basal odontocetes, and other toothed mysticetes.

Possession of three or more dorsal infraorbital foramina was proposed by Barnes (1990) as a synapomorphy of Neoceti, later confirmed by the phylogenetic analysis of Geisler and Sanders (2003) and Fitzgerald (2010). Like terrestrial mammals, protocetids and earlier cetaceans only have a single dorsal infraorbital foramen. By contrast, some basilosaurids possess two (e.g. some specimens of Zygorhiza), and all mysticetes and odontocetes possess three or more (Geisler and Sanders, 2003), though their position and size vary considerably. This character was included in the present study (character 36) and is important for resolving the origin of Neoceti. On our EW trees, three dorsal infraorbital foramina diagnosis Neoceti or the clade of Neoceti + Kekenodon. Multiple equally parsimonious optimizations occur on our IW trees for this character, and it is difficult to easily summarize them. Two or three infraorbital foramina is a synapomorphy for Kekenodon + Coronodonidae + Mystacodon + Neoceti; and some optimizations have three foramina evolving on multiple occasions (e.g. Chaeomysticeti, Coronodonidae and kin, and Odontoceti). Fordyce and Muizon (2001) suggested that an antorbital notch incised into the maxilla, which transmits the facial nerve, was a synapomorphy of Neoceti. In basilosaurids, there is a shallow furrow that faces ventrally, although this furrow is more a consequence of the zygomatic arch extending laterally beyond the alveolar portion of the maxilla, as is common to many mammals. In Coronodon, most other toothed mysticetes, and some stem odontocetes (e.g. Simocetus), the antorbital notch is a deeply incised, laterally facing furrow that curves anteriorly to become more dorsally or anteriorly facing. In Xenorophidae the



antorbital notch is vertical and forms a transversely broad embayment lacking a clear groove; in most later diverging stem odontocetes (*Squalodon*, *Prosqualodon*, "Waipatiidae") and crown Odontoceti the notch is clearly incised and vertically oriented, forming a gap between the base of the rostrum and the antorbital process. In other stem odontocetes like *Ankylorhiza* and *Agorophius*, an intermediate condition is present where the notch is dorsolaterally facing and developed between the preorbital process of the frontal and the maxilla. An antorbital notch was also evaluated in the present study (character 22) and it diagnoses one of two clades on our EW trees (Neoceti + *Kekenodon*) or one of two clades on our IW trees (Neoceti + *Mystacodon* + *Kekenodon*). The discovery of a more complete skull of *Kekenodon*, or a close relative, with this region preserved will allow the node that this synapomorphy applies to be determined.

Fordyce and Muizon (2001) listed loss of the exposure of the posterior/mastoid process of the periotic on the external skull wall as a synapomorphy for Neoceti, which was later supported by the phylogenetic analysis of Fitzgerald (2010). In all basal Neoceti and all odontocetes, the postmeatic process or ridge of the squamosal obscures the posterior process from the lateral edge of the skull. This includes all specimens of coronodonids examined in the present study. In basilosaurids, and especially protocetids, the posterior process is exposed laterally (Luo and Gingerich, 1999). Reversals to this plesiomorphic condition occur in cetotheriid baleen whales (Bouetel and Muizon, 2006) and most, if not all, extant mysticetes (Luo and Gingerich, 1999), though the posterior process of the bulla and periotic are fused within Crown Mysticeti and the degree of exposure of the periotic is uncertain and possibly completely obscured by the posterior process of the bulla in many taxa. The derived 'amastoid' condition appears in at least one unpublished kekenodontid whale (Fordyce, 2004), although the



2797

2798

2799

2800

2801

2802

2803

2804

2805

2806

2807

2808

2809

2810

2811

2812

2813

2814

2815

2816

2817

2818

condition of this character is unknown for *Kekenodon onamata* (Corrie and Fordyce, 2022).

Thus, although this character supports a clade of neocetes to the exclusion of basilosaurids and other archaeocetes, it diagnoses one of two clades on our EW trees (Neoceti or Neoceti + *Kekenodon*) or one of two clades on our IW trees (Neoceti + *Mystacodon* or Neoceti + *Mystacodon* + *Kekenodon*).

Extant cetaceans are highly distinctive in possessing a monophyodont dentition (Fordyce and Muizon, 2001; Uhen and Gingerich, 2001); odontocetes only possess a single set of teeth, and extant mysticetes develop and resorb a single set during fetal development (Karlsen, 1962; Thewissen et al., 2017; Lanzetti et al., 2020). This is a difficult character to evaluate as a sample of juveniles of the same species is needed to confirm the presence of deciduous and permanent teeth (Uhen, 2004A, 2004B); at present, few, if any, stem odontocetes or mysticetes are known from such samples. Coronodon havensteini is now known from four individuals, the largest available sample of any toothed mysticete species. At present, ChM PV 4745 possesses teeth that are as large as those of the holotype skull of *Coronodon havensteini*, indicating ontogenetically early eruption of permanent teeth as in some extant odontocetes (Perrin, 1975). However, it is possible that deciduous teeth could have been present and shed in utero as in extant pinnipeds (Scheffer and Kraus, 1964), given that ChM PV 4745 is a relatively large juvenile. At present it is unclear whether cetaceans have lost the permanent teeth and retained the deciduous teeth or vice versa, or even some combination of both sets (Fordyce, 1982; Uhen and Gingerich, 2001). Similarly, the holotype specimen of the small basilosaurid archaeocete *Chrysocetus healeyorum*, hypothesized as one of the most crownward basilosaurids, possesses relatively large (presumed) permanent teeth despite being a subadult, suggesting that monophyodonty may have evolved prior to the origin of Neoceti and within the Basilosauridae (Uhen and Gingerich, 2001), given



that *Zygorhiza* and *Dorudon* both preserve juveniles with a mix of deciduous and permanent teeth (Kellogg, 1936; Uhen, 2004A, 2004B). However, the premolars in *Coronodon* more closely resemble the deciduous teeth of basilosaurids in having relatively smooth enamel and accessory cusps that are nearly as large as the primary cusp, suggesting the evolution of monophyodonty through the loss of the permanent dentition (Geisler et al., 2017). Evaluation of these varying hypotheses will require the discovery of ontogenetically younger neonatal toothed mysticetes and stem odontocetes, dental histology, or geochemical study of early neocete teeth. Although this character was not included in the current data matrix, we infer that it is a synapomorphy of one of two clades on our EW trees (Neoceti or Neoceti + *Kekenodon*) or one of four clades on our IW trees (Neoceti, Neoceti + *Coronodon*, Neoceti + *Coronodon* + *Mystacodon*, Neoceti + *Coronodon* + *Mystacodon*, Neoceti + *Coronodon* + *Mystacodon* + *Kekenodon*).

Embrasure pits are deep pits formed through remodeling of bone in the rostrum and mandible in order to permit occlusion of large, greatly erupted teeth characteristic of archaeocetes (Uhen, 2004). Loss of these embrasure pits was proposed as a synapomorphy of Neoceti by Fordyce and Muizon (2001). However, *Coronodon havensteini* possesses embrasure pits along the entire upper toothrow and the anterior half of the lower toothrow; likewise, embrasure pits are present in the toothed mysticete *Mystacodon* as well as stem odontocetes including adult Xenorophidae and the anterior dentition of *Ankylorhiza* (Geisler et al., 2014; Muizon et al., 2019; Boessenecker et al., 2020). As described in the previous section, loss of the embrasure pits anterior to p1/P1 is a synapomorphy of Neoceti on our IW trees, where *Coronodon* and *Mystacodon* are excluded from this clade. On the EW trees, the presence of these anterior pits in those taxa, as well as in some basal odontocetes, leads to multiple, equally parsimonious optimizations for the basal nodes straddling the archaeocete/neocete transition. By





2843

2844

2845

2846

2847

2848

2849

2850

2851

2852

2853

2854

2855

2856

2857

2858

2859

2860

2861

2862

2863

2864

contrast, the loss of the posterior embrasure pits is either a synapomorphy of Neoceti or the clade of Neoceti + *Kekenodon* (both EW and IW trees). This optimization occurs, in part, because Metasqualodon lacks posterior embrasure pits, and we consistently recovered it the sister-group to Coronodonidae. Thus, under the EW trees, the presence of the posterior embrasure pits is best interpreted as a reversal to the primitive condition.

Postcranial morphology is typically underreported for early Neoceti, especially in comparison to the level of attention given to that of basilosaurids (Boessenecker et al., 2020). Surprisingly, a possible postcranial synapomorphy of Neoceti was recently proposed by Davydenko et al. (2021): a ventral median keel on the lumbar vertebrae. This condition seems to characterize all modern cetaceans we examined and differs from the ventrally rounded condition in the lumbar vertebrae of Basilosauridae. We found that a ventral median keel was present on all preserved lumbar vertebrae of Coronodon, and further found that such keels are present in other toothed mysticetes such as Aetiocetus cotylalveus and Fucaia goedertorum, the eomysticetids *Eomysticetus*, *Maiabalaena*, *Micromysticetus*, and many stem odontocetes including Xenorophus, Albertocetus, Ankylorhiza, and waipatiid-grade dolphins (Boessenecker, pers. obs.). We included a new phylogenetic character for this feature in our phylogenetic matrix (character 343), and it is indeed a synapomorphy of Neoceti or Neoceti + Kekenodon on our EW trees or a synapomorphy of one of four, nested clades on our IW trees (Neoceti, Neoceti + Coronodon, Neoceti + Coronodon + Mystacodon, Neoceti + Coronodon + Mystacodon + *Kekenodon*). Gatesy et al. (2013) proposed loss of external hindlimbs as another neocete synapomorphy, based largely on the morphology seen in extant cetaceans. Basilosaurids retain small, but partially functional hindlimbs (Gingerich et al., 1990), but it is unclear of the absence of similar lower limb bones on stem odontocetes and mysticetes is due to true absence or non-





preservation. Although not included in the present study, we can infer that this feature could still be a synapomorphy of Neoceti, Neoceti + *Kekenodon*, or one of the same clades mentioned above for the ventral keel character.

Like Corrie and Fordyce (2022), we found a clade comprised of various toothed mysticetes (including *Coronodon* and *Mystacodon*), all odontocetes, but excluding *Kekenodon*. This clade is diagnosed four unambiguous synapomorphies in our EW and IW trees, including supraorbital process of frontal is as long as wide (79:0>1), upper premolars entirely lack a third root (303:0>1), central cusp of cheekteeth subequal in size to accessory cusps (311:0>1), and lower molars and premolars are subequal in height (312: 0>1). To our knowledge, none of these characters has ever been suggested as a neocete synapomorphy, despite the fact that prior to the redescription and phylogenetic analysis of *Kekenodon*, this clade had the same content as Neoceti. The next node towards the base of our cladograms (both EW and IW trees) includes *Kekenodon* and all taxa traditionally considered neocetes, but excludes basilosaurids. The characters that diagnose this node are listed in Result of Phylogenetic Analysis, but one of them, a rounded anteromedial corner of pars cochlearis (184:0>1), was listed as a neocete synapomorphy by Fitzgerald (2010), The presence of this morphology in *Kekenodon onamata* shifts this feature to the next more inclusive clade.

CONCLUSIONS

The initial discovery and description of the toothed mysticete whale *Coronodon havensteini* focused only on the holotype specimen, with an emphasis on its feeding morphology and adaptations. New specimens from the Ashley Formation (Rupelian, early Oligocene) expand



2888

2889

2890

2891

2892

2893

2894

2895

2896

2897

2898

2899

2900

2901

2902

2903

2904

2905

2906

2907

2908

2909

the hypodigm of Coronodon havensteini, permitting the first evaluation of ontogenetic changes within a toothed mysticete. Chief among these are the continued postnatal eruption of the long roots of the cheek teeth, loss of juvenile, upper, postcanine overlap in adults, increase in size of the bulla, lengthening of the intertemporal constriction and sagittal crest, inflation of the anterior process and body of the periotic, and lengthening of the posterior process of the periotic. Additional specimens represent the first records of the genus from the overlying Chandler Bridge Formation (Chattian, late Oligocene) and further represent two new presumed sympatric species named herein: Coronodon newtoni, characterized by a concave up alveolar profile and a periotic resembling juveniles of Coronodon havensteini, and Coronodon planifrons, characterized by a horizontal frontal and small upper molars. This large collection of new specimens permits naming and diagnosing the family Coronodonidae as well as providing a new generic diagnosis for Coronodon. New specimens and observations of the dentition of Coronodon indicate the development of incipient polydonty, with the addition of at least one mandibular (and possibly a maxillary) tooth relative to archaeocete whales. Disarticulated rostra of Coronodon havensteini and Coronodon planifrons reveal a lightly or loosely articulated maxilla-premaxilla suture on the rostrum and a loose maxillofrontal suture, suggesting early evolution of rostral kinesis, paralleling a loose mandibular symphysis. Newly referred specimens of Coronodon preserve much of the vertebral column, indicating a vertebral formula of C7/T9/L10/L20+, presence of a caudal fluke, and a body length of about 4.9-5 meters. Phylogenetic analysis revealed widely different topologies of Cetacea, with analyses under equal weighting highlighting a traditional placement of Coronodon as the earliest diverging lineage of Mysticeti and implied weighting analyses placing Coronodon, Mystacodon, and Kekenodon just outside Neoceti, but more crownward than Basilosauridae. Traditional synapomorphies supporting Coronodon within



2911

2912

2913

2914

2915

2916

Mysticeti (and Neoceti) generally require fewer steps than the alternative topology from the implied weighting analysis. Regardless, these differing results prompted a preliminary review of synapomorphies of Neoceti and their presence (or absence) in *Coronodon* and other early presumptive Neoceti. Future studies of the late Paleogene radiation of early Mysticeti, early Neoceti, and Pelagiceti will require greater taxon and character sampling, with matrices including more archaeocete (e.g. Basilosauridae, Protocetidae, Remingtonocetidae) and odontocete taxa.

2917

2918

ACKNOWLEDGEMENTS

First and foremost we wish to thank K. Mace Brown for acquiring, preparing, and 2919 donating many of the specimens described in this study. We also wish to thank the following 2920 collectors who collected and/or donated specimens described in this study: P. Bailey, T. 2921 Chapman, P. Coleman, S. Faust, M. Havenstein, C. Kaufman, J. Kiser, A. Newton, C. Newton, 2922 A. Sanders, and especially J. Volcko. Thanks to S. Boessenecker (CCNHM), M. Gibson (ChM), 2923 J. Peragine (ChM), and A. Sanders (ChM) for facilitating access to specimens under their care. S. 2924 Boessenecker also assisted with collecting measurements. Thanks to M. Churchill and F. Marx 2925 2926 for sharing scan data and photographs of fossil cetaceans. Thanks to discussions with L.G. Barnes, E. Buchholtz, M. Churchill, J. Corrie, T.A. Deméré, R.E. Fordyce, J. Gatesy, F.G. Marx, 2927 and C.-H. Tsai on the anatomy, functional morphology, feeding ecology, and phylogeny of early 2928 2929 mysticetes. Thanks to M. Brown, M. Havenstein, and R. Weems for discussions of specimen 2930 provenience and stratigraphic origin.

REFERENCES

2931



2932 2933 2934	Albright LB, III,, Sanders AE, and Geisler JH. 2018. An unexpectedly derived odontocete from the Ashley Formation (upper Rupelian) of South Carolina, U.S.A. <i>Journal of Vertebrate Paleontology</i> 38:1-15.
2935 2936 2937	Albright LB, III,, Sanders AE, Weems RE, Cicimurri DJ, and Knight JL. 2019. Cenozoic vertebrate biostratigraphy of South Carolina, U.S.A., and additions to the fauna. <i>Bulletin of the Florida Museum</i> 57:77-236.
2938 2939	Barnes LG. 1990. The fossil record and evolutionary relationships of the genus <i>Tursiops</i> . In: Leatherwood S, and Reeves RR, eds. <i>The Bottlenose Dolphin</i> : Academic Press, 3-26.
2940 2941 2942 2943 2944	Barnes LG, Goedert JL, and Furusawa H. 2001. The earliest known echolocating toothed whales (Mammalia; Odontoceti): preliminary observations of fossils from Washington State. In: McCord RD, and Boaz D, editors. Western Association of Vertebrate Paleontologists And Southwest Paleontological Symposium-Proceedings Mesa Southwest Museum Bulletin. p 91-100.
2945 2946 2947	Barnes LG, Kimura M, Furusawa H, and Sawamura H. 1995. Classification and distribution of Oligocene Aetiocetidae (Mammalia; Cetacea; Mysticeti) from western North America and Japan. <i>The Island Arc</i> 3:392-431.
2948 2949 2950	Barnes LG, and Sanders AE. 1996a. The transition from archaeocetes to mysticetes: late Oligocene toothed mysticetes from near Charleston, South Carolina. <i>Paleontological Society Special publication</i> 8: Sixth North American Paleontological Congress:24.
2951 2952 2953	Barnes LG, and Sanders AE. 1996b. The transition from Archaeoceti to Mysticeti: late Oligocene toothed mysticetes from South Carolina, U.S.A. <i>Journal of Vertebrate Paleontology</i> 16:21A.
2954 2955	Benke H. 1993. Investigations on the osteology and the functional morphology of whales and dolphins (Cetacea). <i>Investigations on Cetacea</i> 24:9-252.
2956 2957	Bisconti M. 2001. Morphology and postnatal growth trajectory of rorqual petrosal. <i>Italian Journal of Zoology</i> 68:87-93.
2958 2959 2960	Bisconti M, Munsterman DK, and Post K. 2019. A new balaenopterid whale from the late Miocene of the southern North Sea basin and the evolution of balaenopterid diversity (Cetacea, Mysticeti). <i>PeerJ</i> 7:e6915.
2961 2962 2963 2964	Boessenecker RW, Ahmed E, and Geisler JH. 2017a. New records of the dolphin <i>Albertocetus meffordorum</i> (Odontoceti: Xenorophidae) from the lower Oligocene of South Carolina: encephalization, sensory anatomy, postcranial morphology, and ontogeny of early odontocetes. <i>PLoS ONE</i> 12:e0186476.
2965 2966 2967	Boessenecker RW, Churchill M, Buchholtz EA, Beatty BL, and Geisler JH. 2020. Convergent evolution of swimming adaptations in modern whales revealed by a large macrophagous dolphin from the Oligocene of South Carolina. <i>Current Biology</i> 30:3267-3273.



2968 2969 2970	transitional baleen whale: a new genus and species of Eomysticetidae (Mammalia: Cetacea) from the Oligocene of New Zealand. <i>PeerJ</i> 3:e1129.
2971 2972 2973	Boessenecker RW, and Fordyce RE. 2015b. A new eomysticetid (Mammalia: Cetacea) from the late Oligocene of New Zealand and a re-evaluation of 'Mauicetus' waitakiensis. Papers in Palaeontology 1:107-140.
2974 2975 2976 2977	Boessenecker RW, and Fordyce RE. 2015c. A new genus and species of eomysticetid (Cetacea: Mysticeti) and a reinterpretation of " <i>Mauicetus</i> " <i>lophocephalus</i> Marples, 1956: transitional baleen whales from the upper Oligocene of New Zealand. <i>Zoological Journal of the Linnaean Society</i> 175:607-660.
2978 2979 2980	Boessenecker RW, and Fordyce RE. 2017. A new eomysticetid from the Oligocene Kokoamu Greensand of New Zealand and a review of the Eomysticetidae (Mammalia, Cetacea). <i>Journal of Systematic Palaeontology</i> 15:429-469.
2981 2982 2983	Boessenecker RW, Fraser D, Churchill M, and Geisler JH. 2017b. A toothless dwarf dolphin (Odontoceti: Xenorophidae) points to explosive feeding diversification of modern whales (Neoceti) <i>Proceedings of the Royal Society B</i> 284:20170531. 10.1098/rspb.2017.0531
2984 2985 2986	Boessenecker RW, and Geisler JH. 2018. New records of the archaic dolphin <i>Agorophius</i> (Mammalia: Cetacea) from the upper Oligocene Chandler Bridge Formation of South Carolina, USA. <i>PeerJ</i> 6:e5290.
2987 2988	Bouetel V. 2005. Phylogenetic implications of skull structure and feeding behavior in balaenopterids (Cetacea, Mysticeti). <i>Journal of Mammalogy</i> 86:139-146.
2989 2990	Buchholtz EA. 2001. Vertebral osteology and swimming style in living and fossil whales (Order: Cetacea). <i>Journal of the Zoological Society of London</i> 253:175-190.
2991 2992	Buchholtz EA, and Gee JK. 2017. Finding sacral: developmental evolution of the axial skeleton of odontocetes (Cetacea). <i>Evolution & Development</i> 19:190-204.
2993 2994	Buffrenil Vd, Dabin W, and Zylberberg L. 2004. Histology and growth of the cetacean petro-tympanic bone complex. <i>Journal of the Zoological Society of London</i> 262.
2995 2996	Churchill M, Geisler JH, Beatty BL, and Goswami A. 2018. Evolution of cranial telescoping in echolocating whales (Cetacea: Odontoceti). <i>Evolution</i> 72:1092-1108.
2997 2998	Churchill M, Martinez-Caceres M, Muizon Cd, Mnieckowski J, and Geisler JH. 2016. The origin of high-frequency hearing in whales. <i>Current Biology</i> 26:2144-2149.
2999 3000 3001	Cicimurri DJ, and Knight JL. 2009. Late Oligocene sharks and rays from the Chandler Bridge Formation, Dorchester County, South Carolina, USA. <i>Acta Palaeontologica Polonica</i> 54:627-647.



3002 3003 3004	Goswami A. 2022. The tempo of cetacean cranial evolution. <i>Current Biology</i> 32:2233-2247.
3005 3006 3007	Cooper LN, Thewissen JGM, and Hussain ST. 2009. New middle Eocene archaeocetes (Cetacea: Mammalia) from the Kuldana Formation of Northern Pakistan. <i>Journal of Vertebrate Paleontology</i> 29:1289-1299.
3008 3009 3010	Corrie JE, and Fordyce RE. 2022. A redescription and re-evaluation of <i>Kekenodon onamata</i> (Mammalia: Cetacea), a late-surviving archaeocete from the late Oligocene of New Zealand. <i>Zoological Journal of the Linnaean Society</i> Online Early.
3011 3012	Davydenko S, Mörs T, and Gol'Din P. 2021. A small whale reveals diversity of the Eocene cetacean fauna of Antarctica. <i>Antarctic Science</i> 33:81-88.
3013 3014 3015	Deméré TA, and Berta A. 2008. Skull anatomy of the Oligocene toothed mysticete <i>Aetiocetus weltoni</i> (Mammalia; Cetacea): implications for mysticete evolution and functional anatomy. <i>Zoological Journal of the Linnaean Society</i> 154:308-352.
3016 3017 3018	Deméré TA, McGowen MR, Berta A, and Gatesy J. 2008. Morphological and molecular evidence for a stepwise evolutionary transition from teeth to baleen in mysticete whales. <i>Systematic Biology</i> 57:15-37.
3019 3020	Domning DP. 1989. Fossil Sirenia of the West Atlantic and Caribbean Region. III. <i>Xenosiren yucateca</i> , gen. et sp. nov. <i>Journal of Vertebrate Paleontology</i> 9:429-437.
3021 3022	Domning DP. 1997. Fossil Sirenia of the West Atlantic and Caribbean Region. IV. <i>Crenatosiren olseni</i> (Reinhardt, 1976). <i>Journal of Vertebrate Paleontology</i> 17:397-412.
3023 3024	Domning DP, and Beatty BL. 2019. Fossil sirenia of the west Atlantic and Caribbean region. XII. <i>Stegosiren macei</i> , gen. et sp. nov. <i>Journal of Vertebrate Paleontology</i> 39:e1650369.
3025 3026 3027	Ekdale EG, and Deméré TA. 2022. Neurovascular evidence for a co-occurrence of teeth and baleen in an Oligocene mysticete and the transition to filter-feeding in baleen whales. <i>Zoological Journal of the Linnaean Society</i> 194:395-415.
3028 3029	Emlong D. 1966. A new archaic cetacean from the Oligocene of Northwest Oregon. <i>Bulletin of the Museum of Natural History, University of Oregon</i> 3:1-51.
3030 3031 3032	Fallon BR, and Boessenecker RW. 2020. Multispecies leatherback turtle assemblage from the Oligocene Chandler Bridge and Ashley formations of South Carolina, USA. <i>Acta Palaeontologica Polonica</i> 65:763-776.
3033 3034 3035	Ferreira-Cardoso S, Delsuc F, and Hautier L. 2019. Evolutionary tinkering of the mandibular canal led to convergent regression of teeth in placental mammals. <i>Current Biology</i> 29:438-475.



3036 3037 3038	masticatory myology in anteaters and its implications for interpreting morphological convergence in merymecophagous placentals. <i>PeerJ</i> 8:9690.
3039 3040 3041	Fierstine HL, and Weems RE. 2009. Paleontology of the Oligocene Ashley and Chandler Bridge Formations of South Carolina, 4: analysis and new records of billfishes (Perciformes: Ziphiodei). <i>Palaeo Ichthyologica</i> 11:43-88.
3042 3043	Fitzgerald EMG. 2006. A bizarre new toothed mysticete (Cetacea) from Australia and the early evolution of baleen whales. <i>Proceedings of the Royal Society B</i> 273:2955-2963.
3044 3045 3046	Fitzgerald EMG. 2010. The morphology and systematics of <i>Mammalodon colliveri</i> (Cetacea: Mysticeti), a toothed mysticete from the Oligocene of Australia. <i>Zoological Journal of the Linnaean Society</i> 158:367-476.
3047 3048 3049	Fordyce RE. 1982. Dental anomaly in a fossil squalodont dolphin from New Zealand, and the evolution of polydonty in whales. <i>New Zealand Journal of Geology and Geophysics</i> 9:419-426.
3050 3051 3052	Fordyce RE. 1989. Problematic early Oligocene toothed whale (Cetacea, ?Mysticeti) from Waikari, North Canterbury, New Zealand. <i>New Zealand Journal of Geology and Geophysics</i> 32:395-400.
3053 3054 3055	Fordyce RE. 2002. <i>Simocetus rayi</i> (Odontoceti, Simocetidae, new family); a bizarre new archaic Oligocene dolphin from the eastern North Pacific. <i>Smithsonian Contributions to Paleobiology</i> 93:185-222.
3056 3057	Fordyce RE. 2004. The transition from Archaeoceti to Neoceti: Oligocene archaeocetes in the Southwest Pacific. <i>Journal of Vertebrate Paleontology</i> 24:supplement to number 3, 59A.
3058 3059 3060	Fordyce RE, and Marx FG. 2016. Mysticetes baring their teeth: a new fossil whale, <i>Mammalodon hakataramea</i> , from the southwest Pacific. <i>Memoirs of Museum Victoria</i> 74:107-116.
3061 3062	Fordyce RE, and Marx FG. 2018. Gigantism precedes filter feeding in baleen whale evolution. <i>Current Biology</i> 28:1670-1676.
3063 3064 3065	Fordyce RE, and Muizon Cd. 2001. Evolutionary history of cetaceans: a review. In: Mazin JM, and Buffrenil Vd, eds. <i>Secondary Adaptations of Tetrapods to Life in Water</i> . Munich, Germany: Verlag Dr. Friedrich Pfeil, 169-233.
3066 3067 3068 3069	Gatesy J, Ekdale EG, Deméré TA, Lanzetti A, Randall J, Berta A, El Adli JJ, Springer MS, and McGowen MR. 2022. Anatomical, ontogenetic, and genomic homologies guide reconstructions of the teeth-to-baleen transition in mysticete whales. <i>Journal of Mammalian Evolution</i> Online Early.
3070 3071 3072	Gatesy J, Geisler JH, Chang J, Buell C, Berta A, Meredith RW, Springer MS, and McGowen MR. 2013. A phylogenetic blueprint for a modern whale. <i>Molecular Phylogenetics and Evolution</i> 66:479-506.

Geisler JH, and A.E. S. 2003. Morphological evidence for the phylogeny of Cetacea. *Journal of* 3073 3074 Mammalian Evolution 10:23-129. Geisler JH, Boessenecker RW, and Brown KM. 2017. The origin of filter feeding in whales. 3075 3076 Current Biology: http://dx.doi.org/10.1016/j.cub.2017.1006.1003. Geisler JH, Colbert MW, and Carew JL. 2014. A new fossil species supports an early origin for 3077 toothed whale echolocation. Nature 508:383-386. 3078 Geisler JH, McGowen MR, Yang G, and Gatesy J. 2011. A supermatrix analysis of genomic, 3079 morphological, and paleontological data from crown Cetacea. BMC Evolutionary Biology 3080 11:1-33. 3081 Geisler JH, Sanders AE, and Luo Z. 2005. A new protocetid whale (Cetacea: Archaeoceti) from 3082 the late middle Eocene of South Carolina. American Museum Novitates 2005:1-68. 3083 Gingerich PD, Haq Mu, Zalmout IS, Khan IH, and Malkani MS. 2001. Origin of whales from 3084 early artiodactyls: hands and feet of Eocene Protocetidae from Pakistan. Science 3085 293:2239-2242. 3086 Gingerich PD, Raza SM, Arif M, Anwar M, and Zhou K. 1994. New whale from the Eocene of 3087 Pakistan and the origin of cetacean swimming. *Nature* 368:844-847. 3088 Gingerich PD, Smith BH, and Simons EL. 1990. Hind limbs of Eocene Basilosaurus: evidence 3089 of feet in whales. Science 249:154-157. 3090 Gingerich PD, ul-Haq M, Koenigswald Wv, Sanders WJ, Smith BH, and Zalmout IS. 2009. New 3091 protocetid whale from the middle Eocene of Pakistan: birth on land, precocial 3092 development, and sexual dimorphism. PLoS ONE 4:e4366. 3093 Godfrey SJ, Geisler JH, and Fitzgerald EMG. 2013. On the olfactory anatomy in an archaic 3094 whale (Protocetidae, Cetacea) and the minke whale Balaenoptera acutorostrata 3095 (Balaenopteridae, Cetacea). The Anatomical Record 296:257-272. 3096 Godfrey SJ, Uhen MD, Osborne JE, and Edwards LE. 2016. A new specimen of Agorophius 3097 pygmaeus (Agorophiidae, Odontoceti, Cetacea) from the early Oligocene Ashley 3098 Formation of South Carolina, USA. *Journal of Paleontology* 90:154-169. 3099 Goldbogen JA, Pyenson ND, and Shadwick RE. 2007. Big gulps require high drag for fin whale 3100 lunge feeding. Marine Ecology Progress Series 349:289-301. 3101 Goloboff PA. 1993. Estimating character weights during tree search. *Cladistics* 9:83-91. 3102 Goloboff PA, Carpenter JM, Arias JS, and Esquivel DRM. 2008a. Weighting against homoplasy 3103 improves phylogenetic analysis of morphological data sets. *Cladistics* 24:758-773. 3104 Goloboff PA, Farris JS, and Nixon KC. 2008b. TNT, a free program for phylogenetic analysis. 3105 Cladistics 24:774-786. 3106

3107 3108	Gradstein FM, Ogg JG, Schmitz M, and Ogg G. 2012. <i>The Geologic Time Scale 2012</i> . Oxford: Elsevier.
3109 3110 3111	Hay OP. 1923. The Pleistocene of North America and its vertebrated animals from the states east of the Mississippi River and from the Canadian provinces east of longitude 95 degrees. <i>Carnegie Institution of Washington Publication</i> 322:1-499.
3112 3113 3114	Hernández-Cisneros AE, and Velez-Juarbe J. 2021. Palaeobiogeography of the North Pacific toothed mysticetes (Cetacea, Aetiocetidae): a key to Oligocene cetacean distributional patterns. <i>Palaeontology</i> 64:51-61.
3115 3116	Hernández Cisneros AE. 2022. A new aetiocetid (Cetacea, Mysticeti, Aetiocetidae) from the late Oligocene of Mexico. <i>Journal of Systematic Palaeontology</i> 20:2100725.
3117 3118 3119	Hocking DP, Evans AR, and Fitzgerald EMG. 2013. Leopard seals (<i>Hydrurga leptonyx</i>) use suction and filter feeding when hunting small prey underwater. <i>Polar Biology</i> 36:211-222.
3120 3121	Hocking DP, Marx FG, Fitzgerald EMG, and Evans AR. 2017. Ancient whales did not filter feed with their teeth. <i>Biology Letters</i> 13:20170348.
3122 3123 3124	Hulbert RC, Petkewich RM, Bishop GA, Bukry D, and Aleshire DP. 1998. A new middle Eocene protocetid whale (Mammalia: Cetacea: Archaeoceti) and associated biota from Georgia. <i>Journal of Paleontology</i> 72:907-927. 10.2307/1306667
3125 3126	Johnston C, and Berta A. 2011. Comparative anatomy and evolutionary history of suction feeding in cetaceans. <i>Marine Mammal Science</i> 27:493-513.
3127 3128	Karlsen K. 1962. Development of tooth germs and adjacent structures in the whalebone whale (<i>Balaenoptera physalus</i>) <i>Hvalrådets Skrifter</i> 45:5-56.
3129 3130 3131	Katuna MP, Geisler JH, and Colquhoun DJ. 1997. Stratigraphic correlation of Oligocene marginal marine and fluvial deposits across the middle and lower coastal plain, South Carolina. <i>Sedimentary Geology</i> 108:181-194.
3132 3133	Kellogg R. 1923. Description of an apparently new toothed cetacean from South Carolina. Smithsonian Miscellaneous Collections 76:1-7.
3134 3135	Kellogg R. 1936. A review of the Archaeoceti. <i>Carnegie Institution of Washington Publication</i> 482:1-366.
3136 3137	Ksepka DT. 2014. Flight performance of the largest volant bird. <i>Proceedings of the National Academy of Sciences</i> 111:10624-10629.
3138 3139 3140	Lambert O, Martinez-Caceres M, Bianucci G, Di Celma C, Salas-Gismondi R, Steurbaut E, Urbina M, and Muizon Cd. 2017. Earliest mysticete from the late Eocene of Peru sheds new light on the origin of baleen whales. <i>Current Biology</i> 27:1535-1541.
3141 3142	Lambertsen RH, Ulrich N, and Straley J. 1995. Frontomandibular stay of Balaenopteridae: a mechanism for momentum recapture during feeding. <i>Journal of Mammalogy</i> 76:877-899.



3143 3144	tympanoperiotic complex in cetaceans. <i>Marine Mammal Science</i> 31:369-375.
3145 3146 3147	Lanzetti A, Berta A, and Ekdale EG. 2020. Prenatal development of the humpback whale: growth rate, tooth loss and skull shape changes in an evolutionary framework. <i>The Anatomical Record</i> 303:180-204.
3148 3149	Lloyd GT, and Slater GJ. 2021. A total-group phylogenetic metatree for Cetacea and the importance of fossil data in diversification analyses. <i>Systematic Biology</i> 70:922-939.
3150 3151 3152	Luo Z, and Gingerich PD. 1999. Terrestrial Mesonychia to aquatic Cetacea: transformation of the basicranium and evolution of hearing in whales. <i>University of Michigan Papers on Paleontology</i> 31:1-98.
3153 3154	Marino L, McShea DW, and Uhen MD. 2004. Origin and evolution of large brains in toothed whales. <i>The Anatomical Record</i> 281:1247-1255.
3155 3156 3157	Martinez-Caceres M, Lambert O, and Muizon Cd. 2017. The anatomy and phylogenetic affinities of <i>Cynthiacetus peruvianus</i> , a large <i>Dorudon</i> -like basilosaurid (Cetacea, Mammalia) from the late Eocene of Peru. <i>Geodiversitas</i> 39:7-163.
3158 3159	Marx FG. 2011. The more the merrier? A large cladistic analysis of mysticetes, and comments on the transition from teeth to baleen. <i>Journal of Mammalian Evolution</i> 18:77-100.
3160 3161	Marx FG, and Fordyce RE. 2015. Baleen boom and bust: a synthesis of mysticete phylogeny, diversity and disparity. <i>Royal Society Open Science</i> 2:140434.
3162 3163 3164	Marx FG, Hocking DP, Park T, Ziegler T, Evans AR, and Fitzgerald EMG. 2016. Suction feeding preceded filtering in baleen whale evolution. <i>Memoirs of Museum Victoria</i> 75:71-82.
3165 3166 3167	Marx FG, Tsai C-H, and Fordyce RE. 2015. A new early Oligocene toothed 'baleen' whale (Mysticeti: Aetiocetidae) from western North America: one of the oldest and the smallest <i>Royal Society Open Science</i> 2:150476.
3168 3169 3170	McCuen WN, Ishimori A, and Boessenecker RW. 2021. A new specimen of <i>Xiphiorhynchus</i> cf. <i>X. aegyptiacus</i> (Istiophoriformes, Xiphiodei, Xiphiidae) and billfish diversity in the Oligocene of South Carolina. <i>Vertebrate Anatomy Morphology Paleontology</i> 8:98-104.
3171 3172	Mead JG, and Fordyce RE. 2009. The therian skull: a lexicon with emphasis on the odontocetes. <i>Smithsonian Contributions to Zoology</i> 627:1-248.
3173 3174 3175	Meredith RW, Gatesy J, Cheng J, and Springer MS. 2011. Pseudogenization of the tooth gene enamelysin (MMP20) in the common ancestor of extant baleen whales. <i>Proceedings of the Royal Society B</i> 278:993-1002.
3176 3177 3178	Meredith RW, Gatesy J, Murphy WJ, Ryder OA, and Springer MS. 2009. Molecular decay of the tooth gene Enamelin (ENAM) mirrors the loss of enamel in the fossil record of placental mammals. <i>PLoS Genetics</i> 5:e1000634.

Mitchell ED. 1989. A new cetacean from the late Eocene Meseta Formation, Seymour Island, 3179 Antarctic Peninsula. Canadian Journal of Earth Sciences 46:2219-2235. 3180 Mu Y, Huang X, Liu R, Gai Y, Liang N, Yin D, Shan L, Xu S, and Yang G. 2021. ACPT gene is 3181 inactivated in mammalian lineages that lack enamel or teeth. PeerJ 9:10219. 3182 Muizon Cd, Bianucci G, Martinez-Caceres M, and Lambert O. 2019. Mystacodon selenensis, the 3183 earliest known toothed mysticete (Cetacea, Mammalia) from the late Eocene of Peru: 3184 anatomy, phylogeny, and feeding adaptations. *Geodiversitas* 41:401-499. 3185 Nummela S, Thewissen JGM, Bajpai S, Hussain T, and Kumar K. 2007. Sound transmission in 3186 archaic and modern whales: anatomical adaptations for underwater hearing. The 3187 Anatomical Record 290:716-733. 3188 Okazaki Y. 1982. A lower Miocene squalodontid from the Ashiya Group, Kyushu, Japan. 3189 Bulletin of the Kitakyushu Museum of Natural History 4:107-112. 3190 Peredo CM, Peredo JS, and Pyenson ND. 2018a. Convergence on dental simplification in the 3191 evolution of whales. *Paleobiology* 44:434-443. 3192 Peredo CM, Pyenson ND, and Boersma AT. 2017. Decoupling tooth loss from the evolution of 3193 baleen in whales. Frontiers in Marine Science 4:1-11. 3194 Peredo CM, Pyenson ND, Marshall CD, and Uhen MD. 2018b. Tooth loss precedes the origin of 3195 baleen in whales. Current Biology 28:3992-4000. 3196 Peredo CM, Pyenson ND, and Uhen MD. 2022. Lateral palatal foramina do not indicate baleen 3197 in fossil whales. Scientific Reports 12:11448. 3198 Perrin WF. 1975. Variation of spotted and spinner porpoise (Genus Stenella) in the eastern 3199 Pacific and Hawaii. Bulletin of the Scripps Institute of Oceanography 21:1-206. 3200 Potvin J, Goldbogen JA, and Shadwick RE. 2009. Passive versus active engulfment: verdict from 3201 trajectory simulations of lunge-feeding fin whales Balaenoptera physalus. Journal of the 3202 3203 Royal Society Interface 6:1005-1025. Pritchard GB. 1939. On the discovery of a fossil whale in the older Tertiaries of Torquay, 3204 Victoria. Victorian Naturalist 55:155-159. 3205 Pyenson ND, and Sponberg SN. 2011. Reconstructing body size in extinct crown Cetacea 3206 (Neoceti) using allometry, phylogenetic methods and tests from the fossil record. *Journal* 3207 of Mammalian Evolution 18:269-288. 3208 Racicot R, Boessenecker RW, Darroch SAF, and Geisler JH. 2019. Evidence for convergent 3209 evolution of ultrasonic hearing in toothed whales (Cetacea: Odontoceti). Biology Letters 3210 15:20190083. 3211 3212 Randall J, Gatesy J, and Springer MS. 2022. Molecular evolutionary analyses of tooth genes 3213 support sequential loss of enamel and teeth in baleen whales (Mysticeti). *Molecular* 3214 Phylogenetics and Evolution 171:107463.

3215 3216	into focus. <i>The Anatomical Record</i> 302:1055-1073.
3217 3218	Russell S. 1968. A new cetacean from the Oligocene Sooke Formation of Vancouver Island, British Columbia. <i>Canadian Journal of Earth Sciences</i> 5:929-933.
3219	Sanders AE. 1980. Excavation of Oligocene marine fossil beds near Charleston, South Carolina
3220	National Geographic Research Reports 12:601-621.
3221 3222 3223 3224	Sanders AE, and Barnes LG. 2002a. Paleontology of the Late Oligocene Ashley and Chandler Bridge Formations of South Carolina, 2: <i>Micromysticetus rothauseni</i> , a primitive cetotheriid mysticete (Mammalia: Cetacea). <i>Smithsonian Contributions to Paleobiology</i> 93:271-293.
3225 3226 3227 3228	Sanders AE, and Barnes LG. 2002b. Paleontology of the Late Oligocene Ashley and Chandler Bridge Formations of South Carolina, 3: Eomysticetidae, a new family of primitive mysticetes (Mammalia: Cetacea). <i>Smithsonian Contributions to Paleobiology</i> 93:313-356.
3229 3230 3231	Sanders AE, and Geisler JH. 2015. A new basal odontocete from the upper Rupelian of South Carolina, U.S.A., with contributions to the systematics of <i>Xenorophus</i> and <i>Mirocetus</i> (Mammalia, Cetacea). <i>Journal of Vertebrate Paleontology</i> 35:e890107.
3232 3233 3234	Sanders AE, Weems RE, and Lemon EMj. 1982. Chandler Bridge Formation - a new Oligocene stratigraphic unit in the lower coastal plain of South Carolina. <i>US Geological Survey Bulletin</i> 1529-H:H105-H124.
3235 3236	Scheffer VB, and Kraus BS. 1964. Dentition of the Northern Fur Seal. <i>Fishery Bulletin</i> 63:293-342.
3237 3238	Schulte W. 1916. Anatomy of a foetus of <i>Balaenoptera borealis</i> . <i>Memoir of the American Museum of Natural History</i> 1:389-502.
3239 3240 3241 3242	Shipps BK, Peredo CM, and Pyenson ND. 2019. <i>Borealodon osedax</i> , a new stem mysticete (Mammalia, Cetacea) from the Oligocene of Washington State and its implications for fossil whale-fall communities. <i>Royal Society Open Science</i> 6:182168. https://doi.org/10.1098/rsos.182168
3243 3244 3245	Solis-Añorve A, González-Barba G, and Hernández-Rivera R. 2019. Description of a new toothed mysticete from the late Oligocene of San Juan de La Costa, B.C.S., México. <i>Journal of South American Earth Sciences</i> 89:337-346.
3246 3247 3248	Thewissen JGM, Hieronymus TL, George JC, Suydam R, Stimmelmayr R, and McBurney D. 2017. Evolutionary aspects of the development of teeth and baleen in the bowhead whale <i>Journal of Anatomy</i> 230:549-566. https://doi.org/10.1111/joa.12579
3249 3250	Thewissen JGM, Hussain ST, and Arif M. 1994. Fossil evidence for the origin of aquatic locomotion in archaeocete whales. <i>Science</i> 263:210-212.

3251 3252	Thewissen JGM, Williams EM, Roe LJ, and Hussain ST. 2001. Skeletons of terrestrial cetaceans and the relationship of whales to artiodactyls. <i>Nature</i> 413:277-281.
3253 3254	Tsai C-H, and Ando T. 2016. Niche partitioning in Oligocene toothed mysticetes (Mysticeti: Aetiocetidae). <i>Journal of Mammalian Evolution</i> 23:33-41.
3255 3256	Tsai C-H, and Fordyce RE. 2015. The earliest gulp-feeding mysticete (Cetacea: Mysticeti) from the Oligocene of New Zealand. <i>Journal of Mammalian Evolution</i> 22:535-560.
3257 3258 3259	Tsai C-H, and Fordyce RE. 2016. Archaic baleen whale from the Kokoamu Greensand: earbones distinguish a new late Oligocene mysticete (Cetacea: Mysticeti) from New Zealand. <i>Journal of the Royal Society of New Zealand</i> 46:117-138.
3260 3261 3262	Tsai C-H, and Fordyce RE. 2018. A new archaic baleen whale <i>Toipahautea waitaki</i> (early Late Oligocene, New Zealand) and the origins of crown Mysticeti. <i>Royal Society Open Science</i> 5.
3263 3264 3265	Uhen MD. 2004a. Form, function, and anatomy of <i>Dorudon atrox</i> (Mammalia, Cetacea): an archaeocete from the middle to late Eocene of Egypt. <i>University of Michigan Papers on Paleontology</i> 34:1-222.
3266 3267	Uhen MD. 2004b. Replacement of deciduous first premolars and dental eruption in archaeocete whales. <i>Journal of Mammalogy</i> 81:123-133.
3268 3269	Uhen MD. 2005. A new genus and species of archaeocete whale from Mississippi. <i>Southeastern Geology</i> 43:157-172.
3270 3271 3272	Uhen MD. 2008. A new <i>Xenorophus</i> -like odontocete cetacean from the Oligocene of North Carolina and a discussion of the basal odontocete radiation. <i>Journal of Systematic Palaeontology</i> 6:433-452.
3273 3274	Uhen MD. 2014. New material of <i>Natchitochia jonesi</i> and a comparison of the innominata and locomotor capabilities of Protocetidae. <i>Marine Mammal Science</i> 30:1029-1066.
3275 3276	Uhen MD, and Gingerich PD. 2001. A new genus of dorudontine archaeocete (Cetacea) from the middle-to-late Eocene of South Carolina. <i>Marine Mammal Science</i> 17:1-34.
3277 3278	Velez-Juarbe J. 2017. A new stem odontocete from the late Oligocene Pysht Formation in Washington State, USA. <i>Journal of Vertebrate Paleontology</i> 37:e1366916.
3279 3280 3281	Velez-Juarbe J, and Domning DP. 2014. Fossil Sirenia of the West Atlantic and Caribbean Region. IX. <i>Metaxytherium albifontanum</i> , sp. nov. <i>Journal of Vertebrate Paleontology</i> 34:444-464.
3282 3283 3284 3285	Weems RE, and Brown KM. 2017. More-complete remains of <i>Procolpochelys charlestonensis</i> (Oligocene, South Carolina) an occurrence of <i>Euclastes</i> (upper Eocene, South Carolina), and their bearing on Cenozoic pancheloniid sea turtle distribution and phylogeny. <i>Journal of Paleontology</i> 91:1228-1243.





3286 3287 3288 3289	Weems RE, Bybell LM, Edwards LE, Lewis WC, Self-Trail JM, Albright LB, III,, Cicimurri DJ Harris WB, Osborne JE, and Sanders AE. 2016. Stratigraphic revision of the Cooper Group and Chandler Bridge and Edisto Formations in the coastal plain of South Carolina South Carolina Geology 49:1-24.
3290 3291 3292	Weems RE, and Lemon EMj. 1993. Geology of the Cainhoy, Charleston, Fort Moultrie, and North Charleston quadrangles, Charleston and Berkeley Counties, South Carolina. <i>US Geological Survey Miscellaneous Investigations Map</i> I-1935.
3293 3294 3295	Weems RE, Lemon EMj, and McCartran L. 1985. Shallow subsurface geology of the North Charleston 7.5-minute quadrangle, South Carolina. <i>US Geological Survey Open File Report</i> 85-274:1-62.
3296 3297 3298	Weems RE, and Lewis WC. 2002. Structural and tectonic setting of the Charleston, South Carolina region: evidence from the Tertiary stratigraphic record. <i>Geological Society of America Bulletin</i> 114:24-42.
3299 3300	Weems RE, and Sanders AE. 2014. Oligocene pancheloniid sea turtles from the vicinity of Charleston, South Carolina, U.S.A. <i>Journal of Vertebrate Paleontology</i> 34:80-99.
3301 3302	Werth AJ. 2000. Feeding in marine mammals. In: Schwenk K, ed. <i>Feeding: Form, Function and Evolution in Tetrapod Vertebrates</i> . San Diego: Academic Press, 487-526.
3303 3304	Whitmore FC, and Sanders AE. 1977. A review of the Oligocene Cetacea. <i>Systematic Zoology</i> 25:304-320.
3305	Wilkinson M. 1992. Ordered versus unordered characters. Cladistics 8:375-385.
3306	

Figure 1. Geologic and stratigraphic context of Coronodon.

(A) Regional map showing location of Charleston, South Carolinal USA. (B) Simplified geologic map (after Weems and Lemon, 2002) showing the extent of the Oligocene Ashley and Chandler Bridge formations and Coronodon localities (stars). (C) Sedimentary column of the uppermost Ashley Formation and Chandler Bridge Formation in the vicinity of Summerville, South Carolina (modified from Fallon and Boessenecker, 2020), showing the stratigraphic origin of coronodonid fossils and age determinations (see Geologic Background for summary).

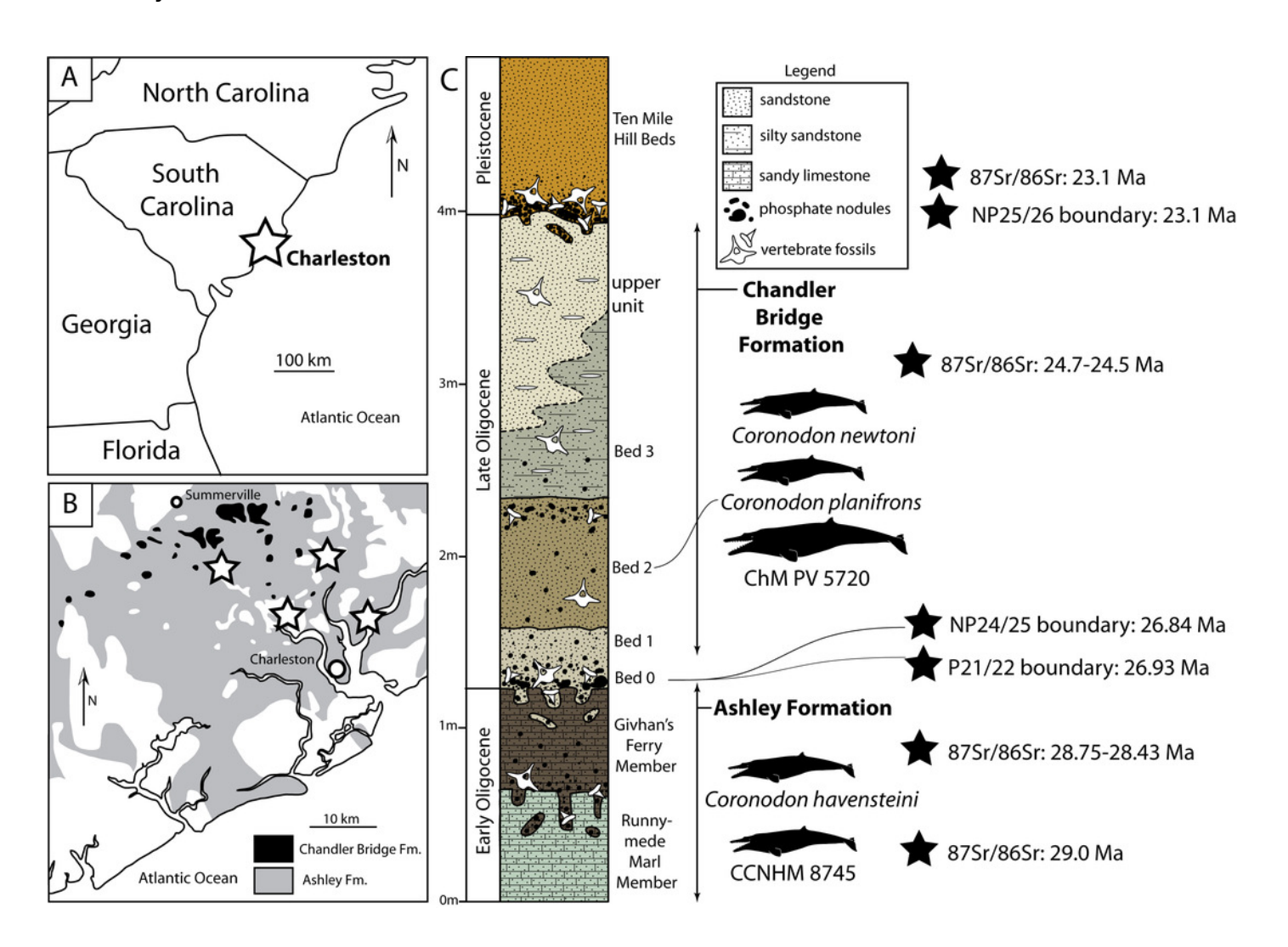


Figure 2. Skull of Coronodonidae indet., CCNHM 8745.

Skull in dorsal (A), ventral (B), lateral (C), and anterior (D) view.

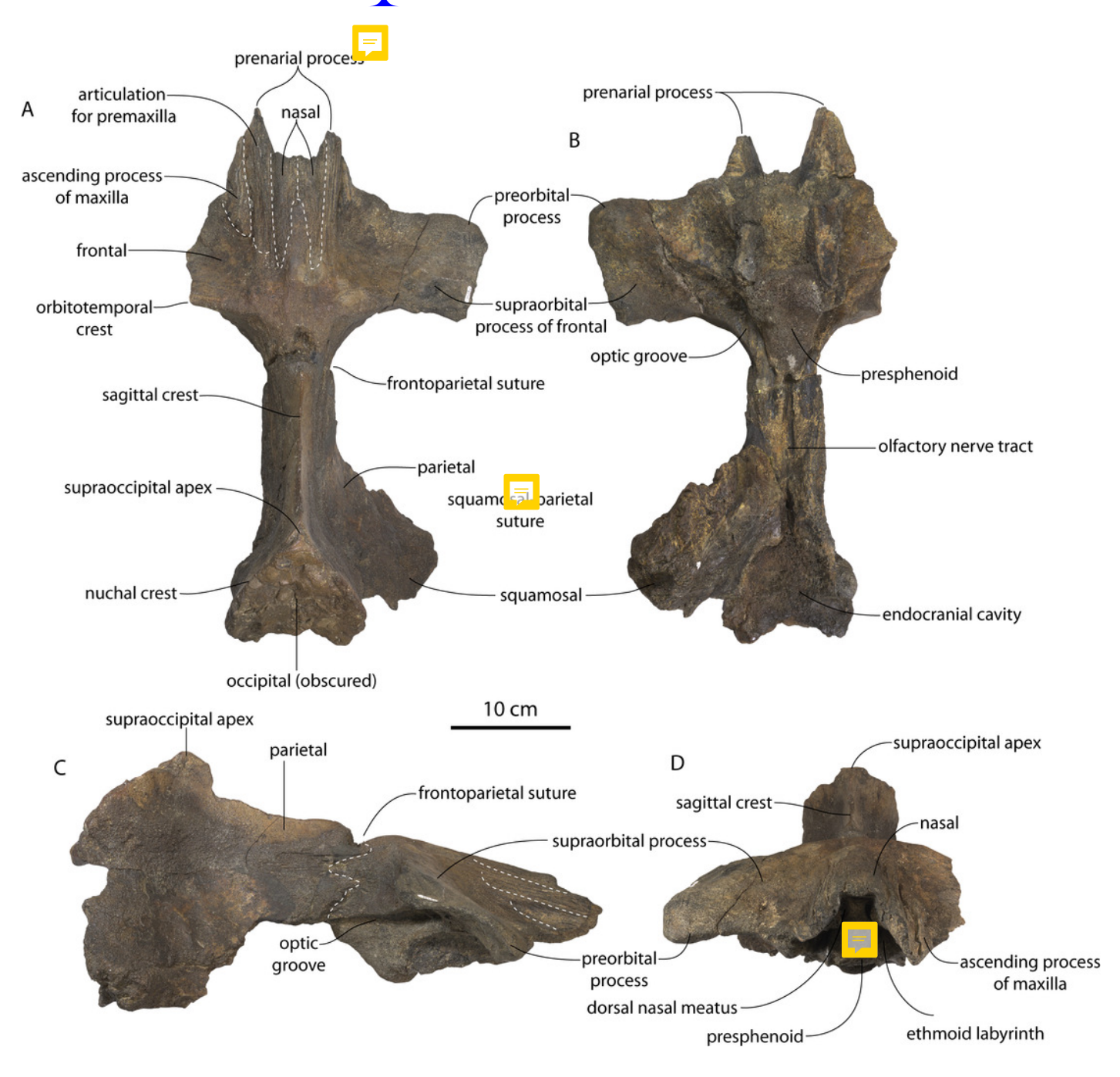


FIGURE 3. Skulls of juvenile Coronodon havensteini in dorsal view.

(A) referred specimen CCNHM 8722 and (B) referred specimen ChM PV 4745.

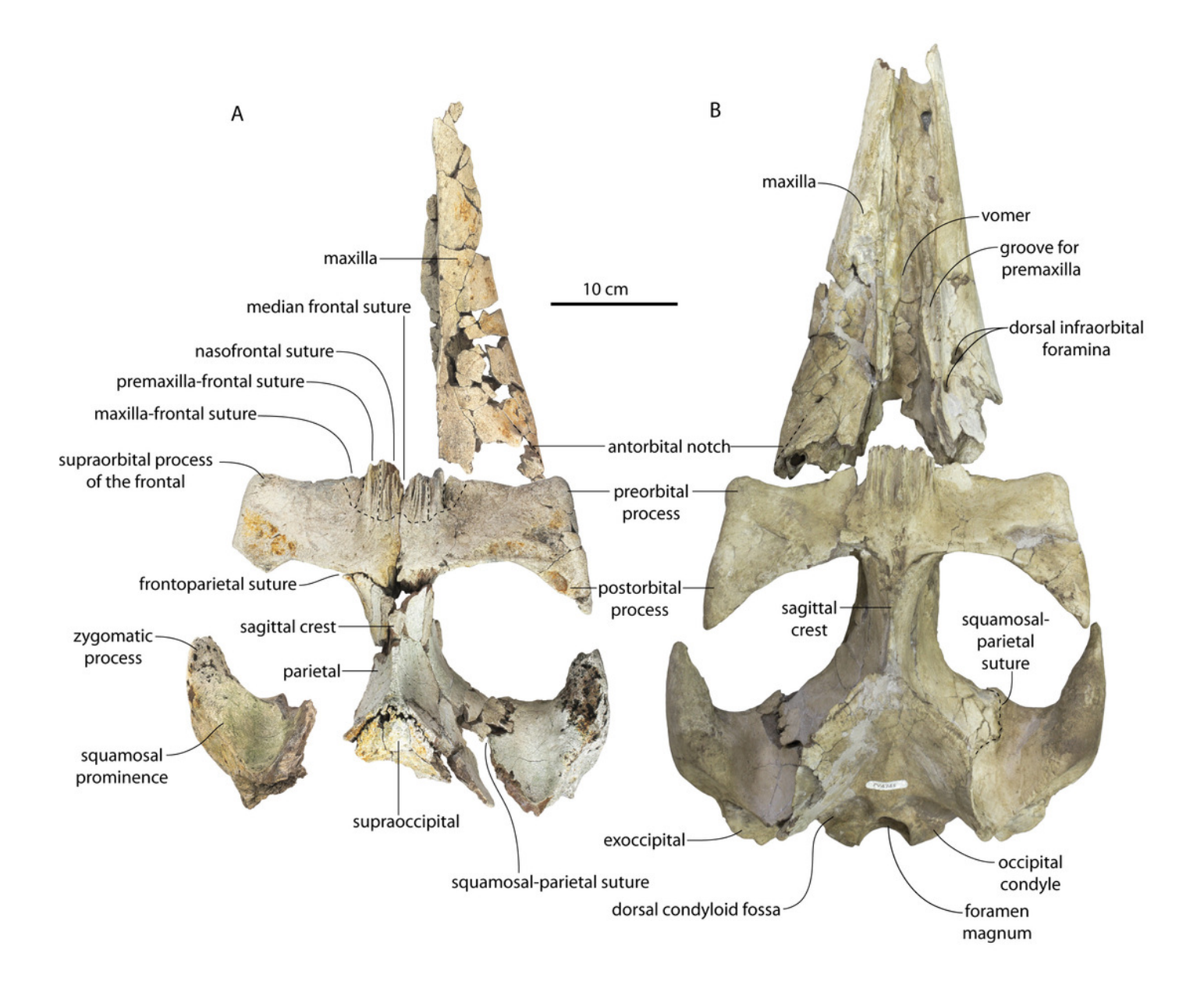




FIGURE 4. Skulls of Coronodon havensteini in ventral view.

(A) referred specimen ChM PV 4745, (B) holotype specimen CCNHM 108, and (C) referred specimen CCNHM 164.



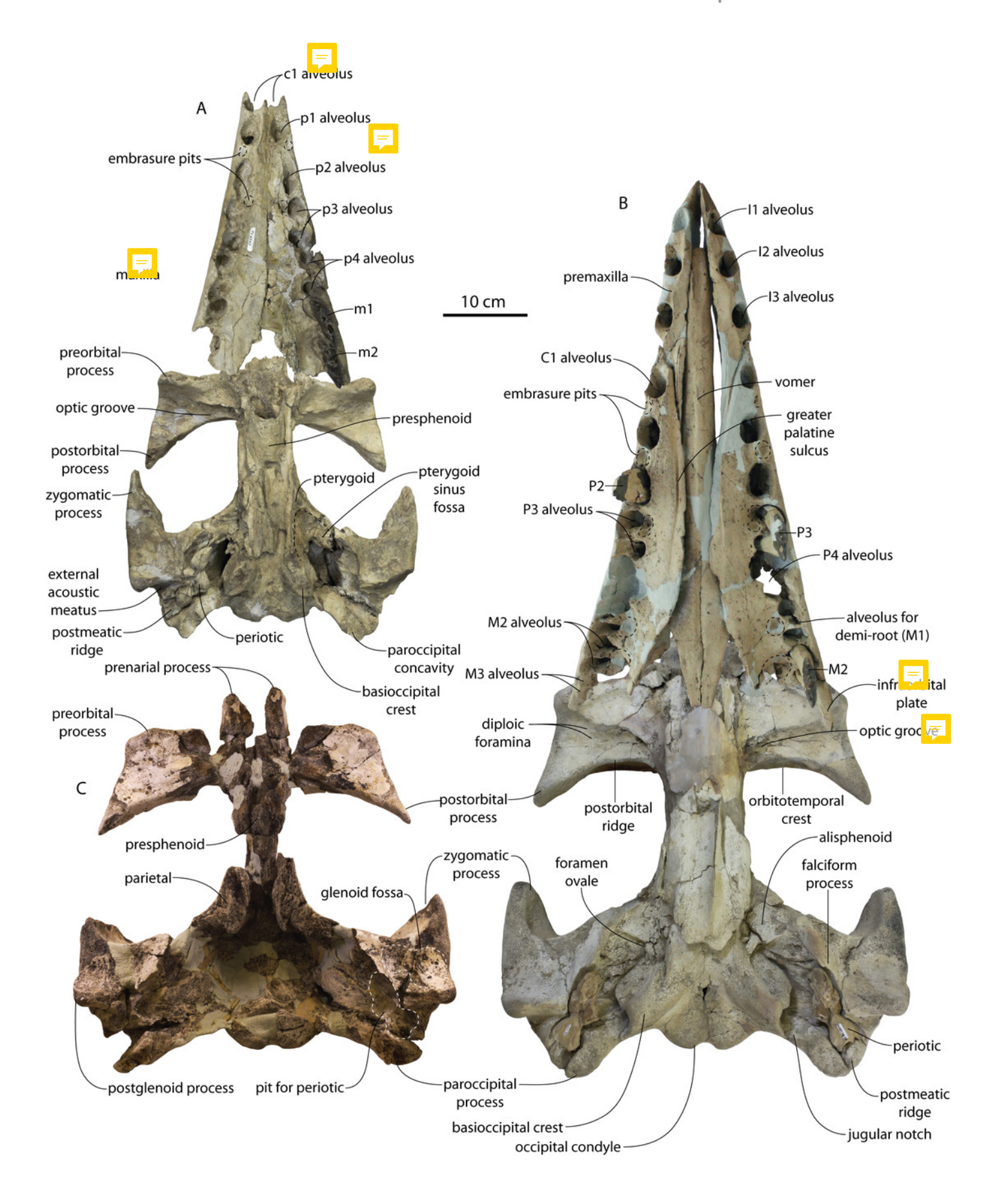


FIGURE 5. Skulls of Coronodon havensteini in lateral view.

(A) referred specimen CCNHM 8722 (right), (B) referred specimen CCNHM 164 (left), (C) referred specimen ChM PV 4745 (left), (D) rostrum of referred specimen CCNHM 164 (right), and (E) holotype specimen CCNHM 108.

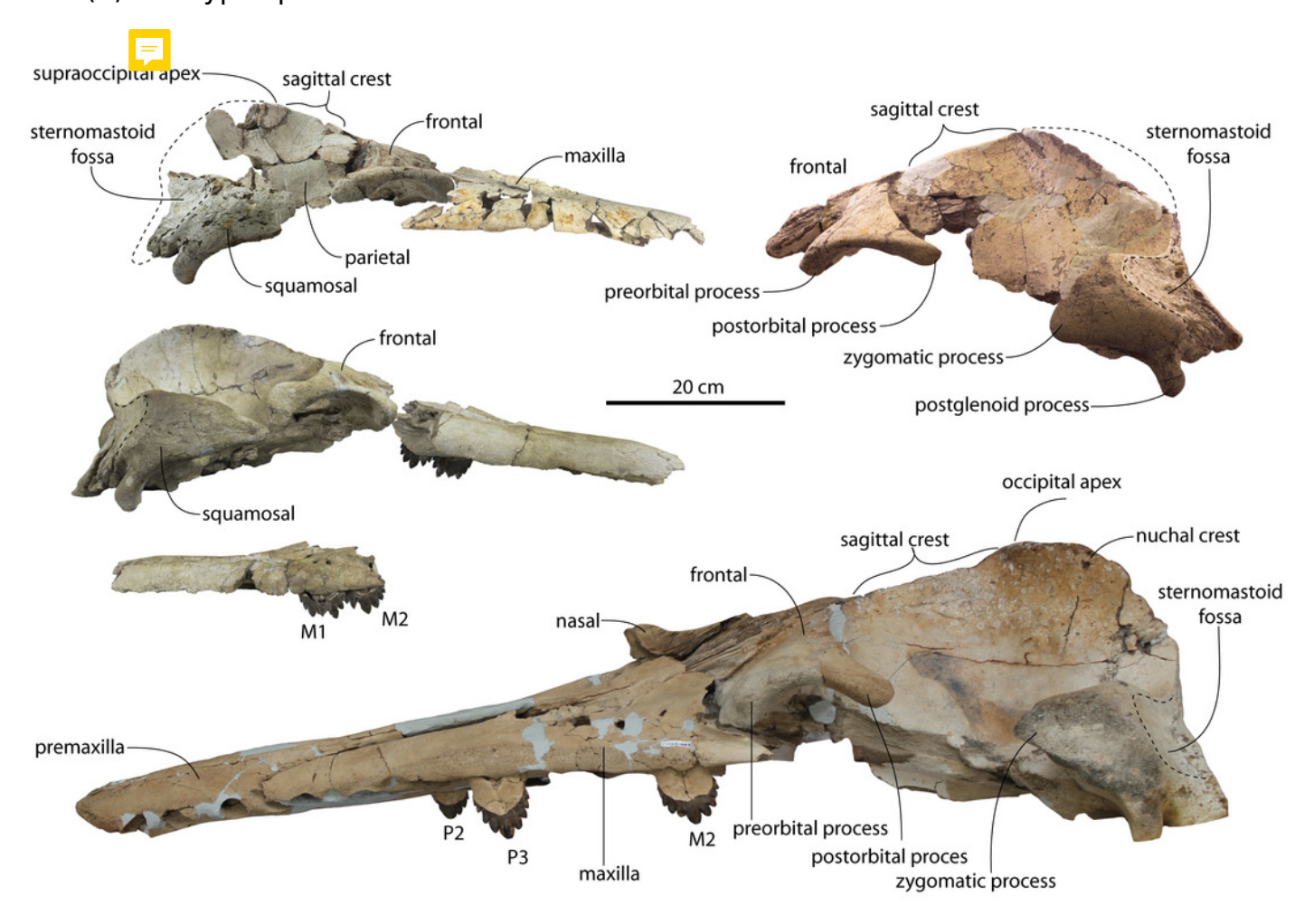


FIGURE 6. Skulls of adult Coronodon havensteini in dorsal view.

(A) referred specimen CCNHM 164 and (B) holotype specimen CCNHM 108.

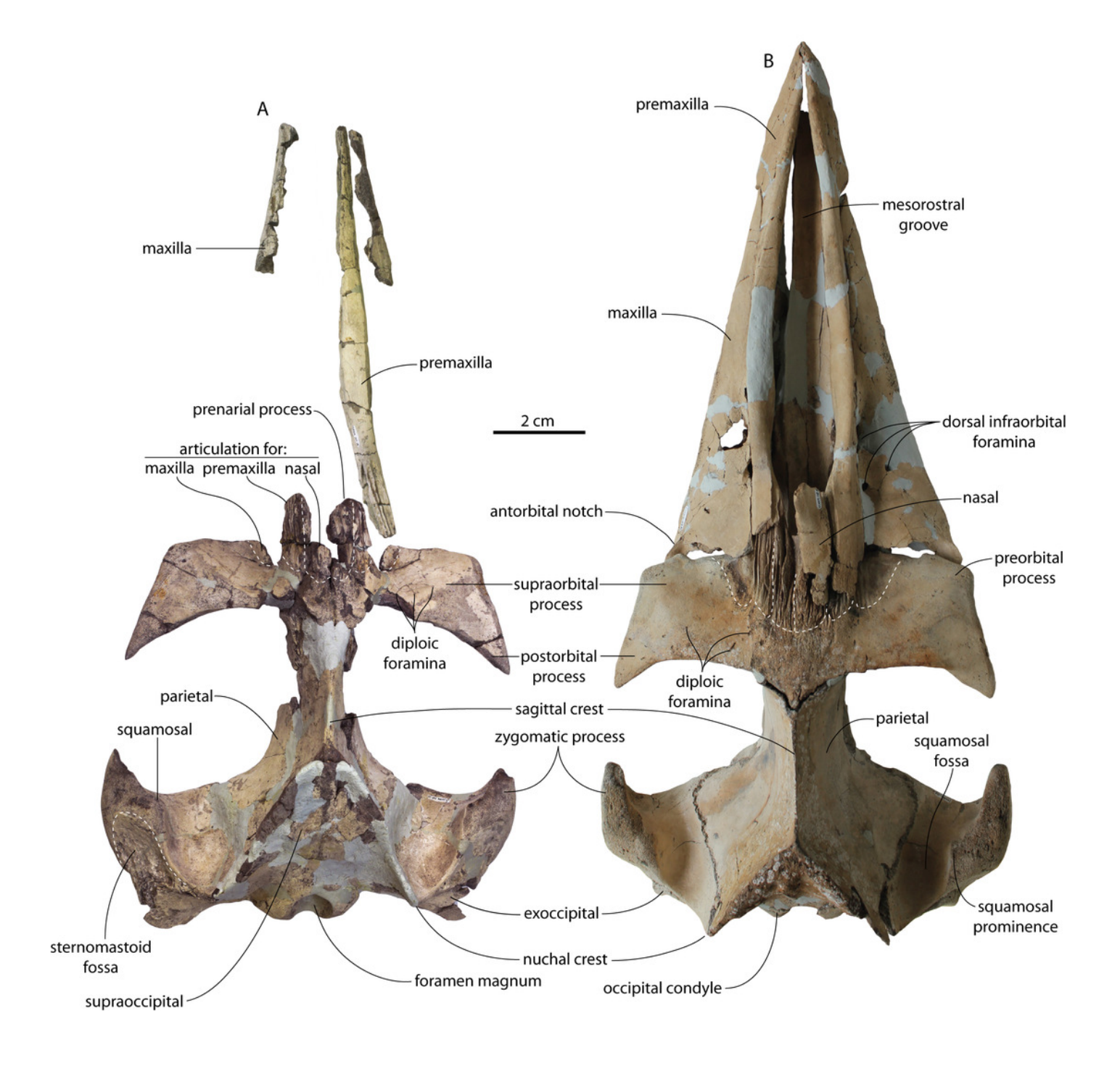


FIGURE 7. Maxilla and frontal of juvenile specimen of Coronodon havensteini.

Referred specimen CCNHM 8722 maxilla in ventral (A) and medial (B) view, and frontal in ventral view (C).

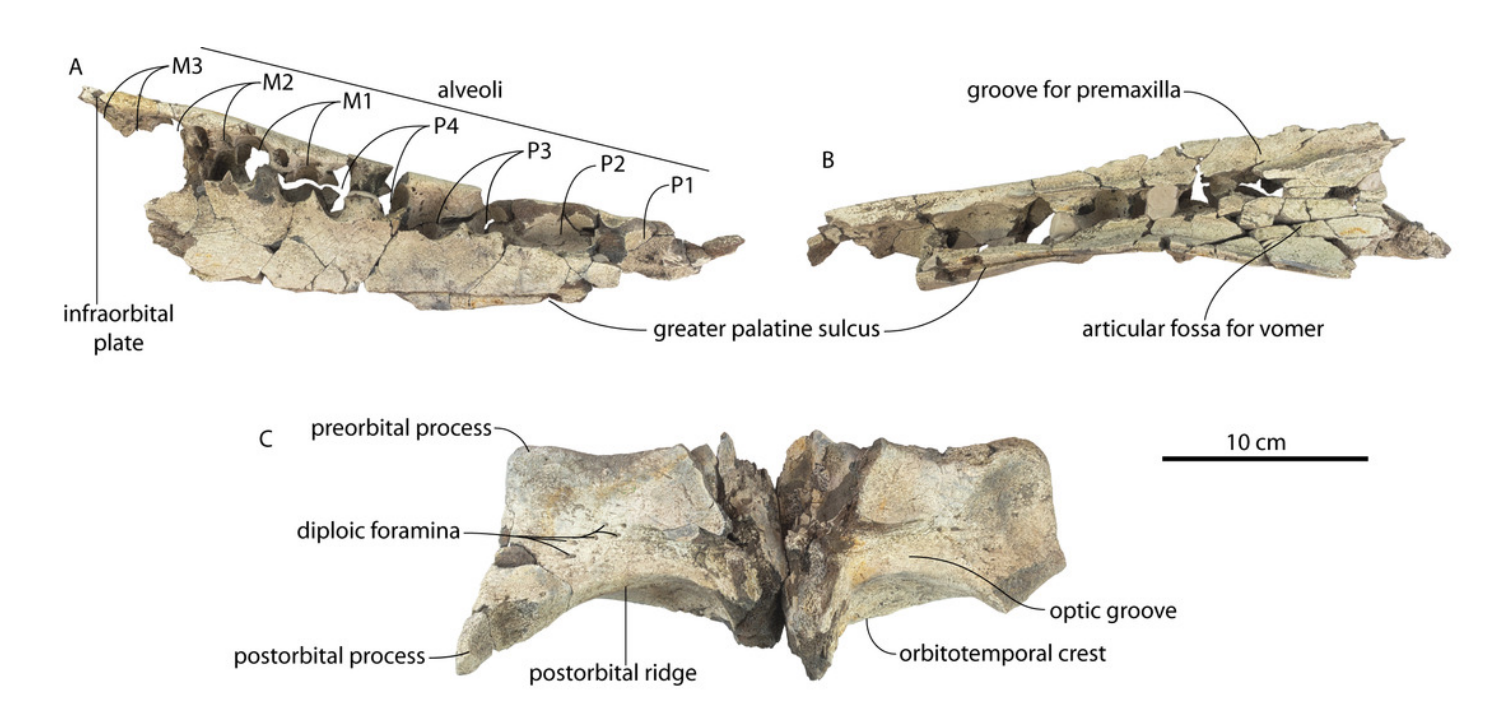


FIGURE 8. Braincases of Coronodon havensteini in anterior view.

(A) referred specimen CCNHM 8722, (B) referred specimen ChM PV 4745, (C) holotype specimen CCNHM 108 and (D) referred specimen CCNHM 164.

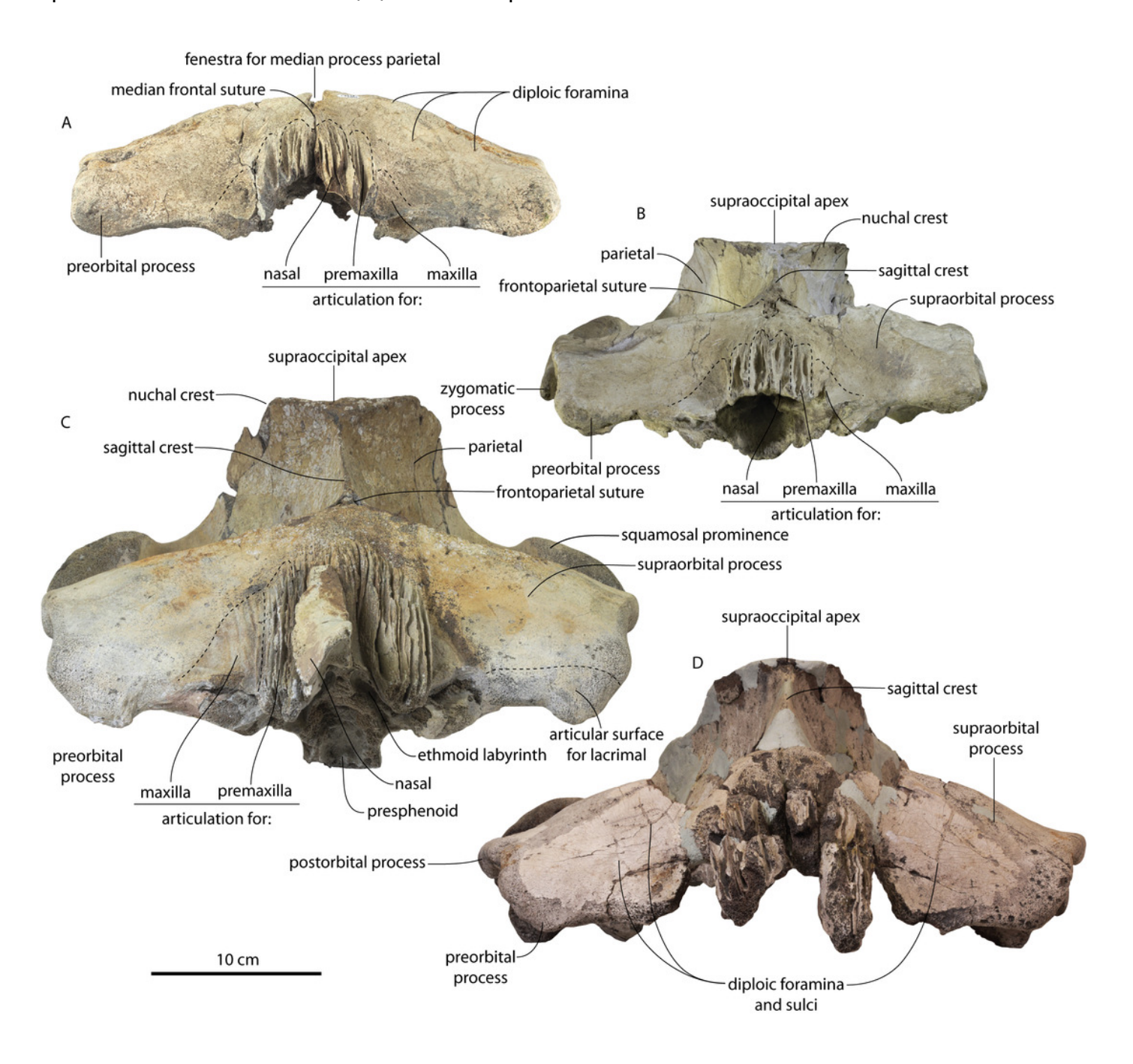
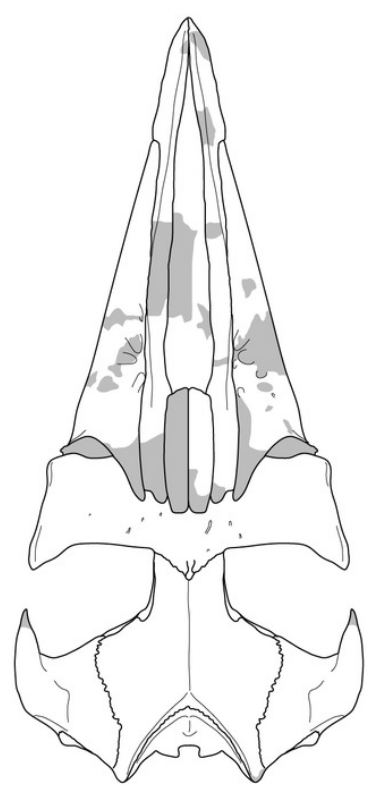


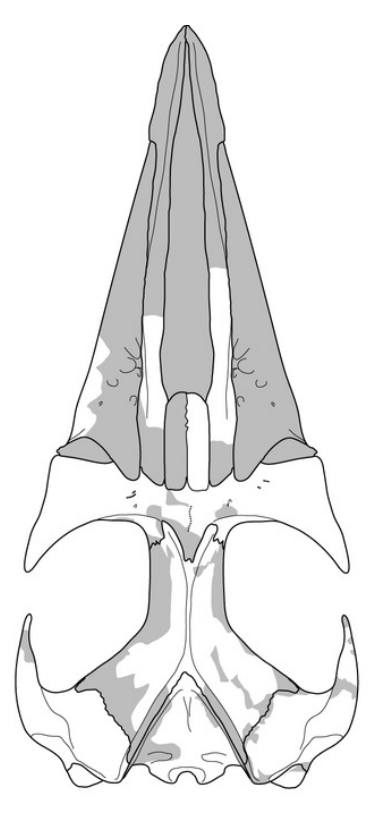


FIGURE 9. Reconstruction of holotype and referred skulls of Coronodon havensteini, Coronodon planifrons, and Coronodon newtoni.

Abbreviations: AF, Ashley Formation; CBF, Chandler Bridge Formation.

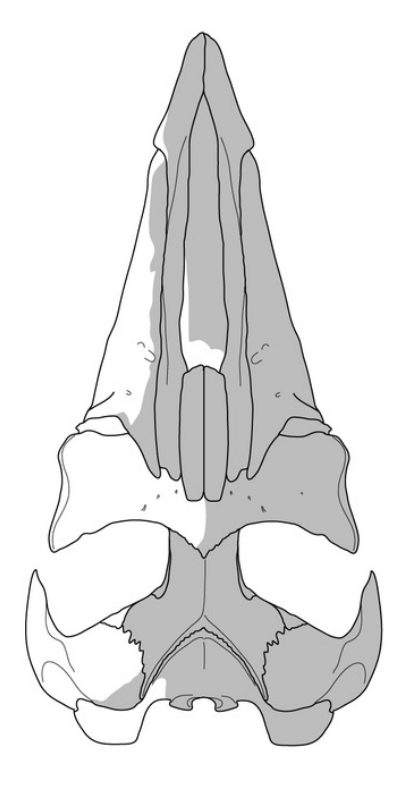


Coronodon havensteini (holotype) CCNHM 108; AF

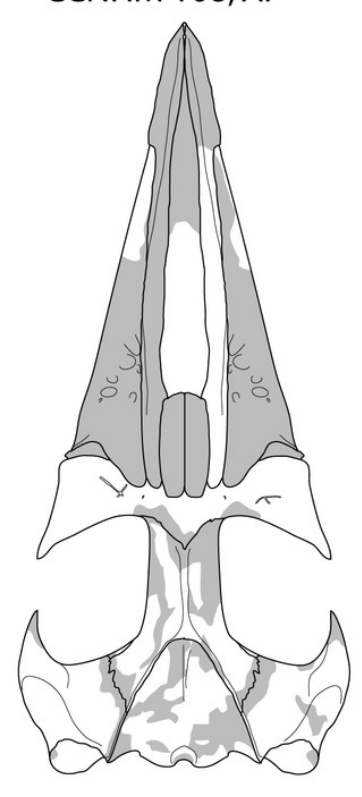


Coronodon planifrons (holotype) CCNHM 166; CBF

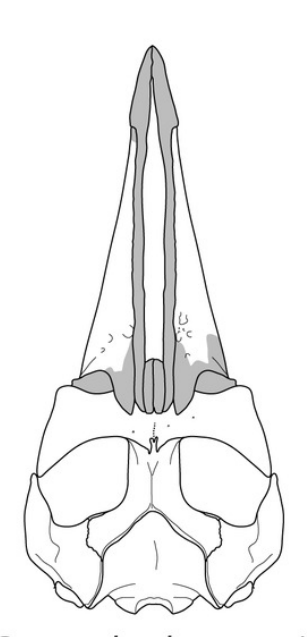
10 cm



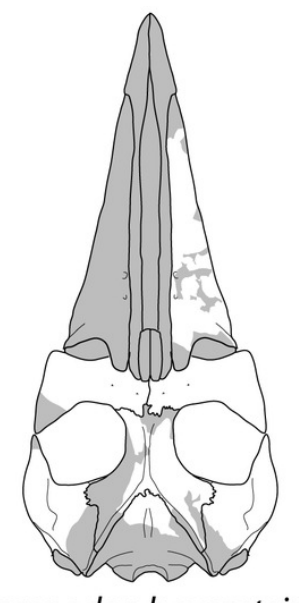
Coronodon newtoni (holotype) ChM PV 2778; CBF



Coronodon havensteini CCNHM 164; AF



Coronodon havensteini ChM PV 4745; AF



Coronodon havensteini CCNHM 8745; AF

FIGURE 10. Frontals and ethmoid region of *Coronodon havensteini* holotype (CCNHM 108) in anteroventral view.

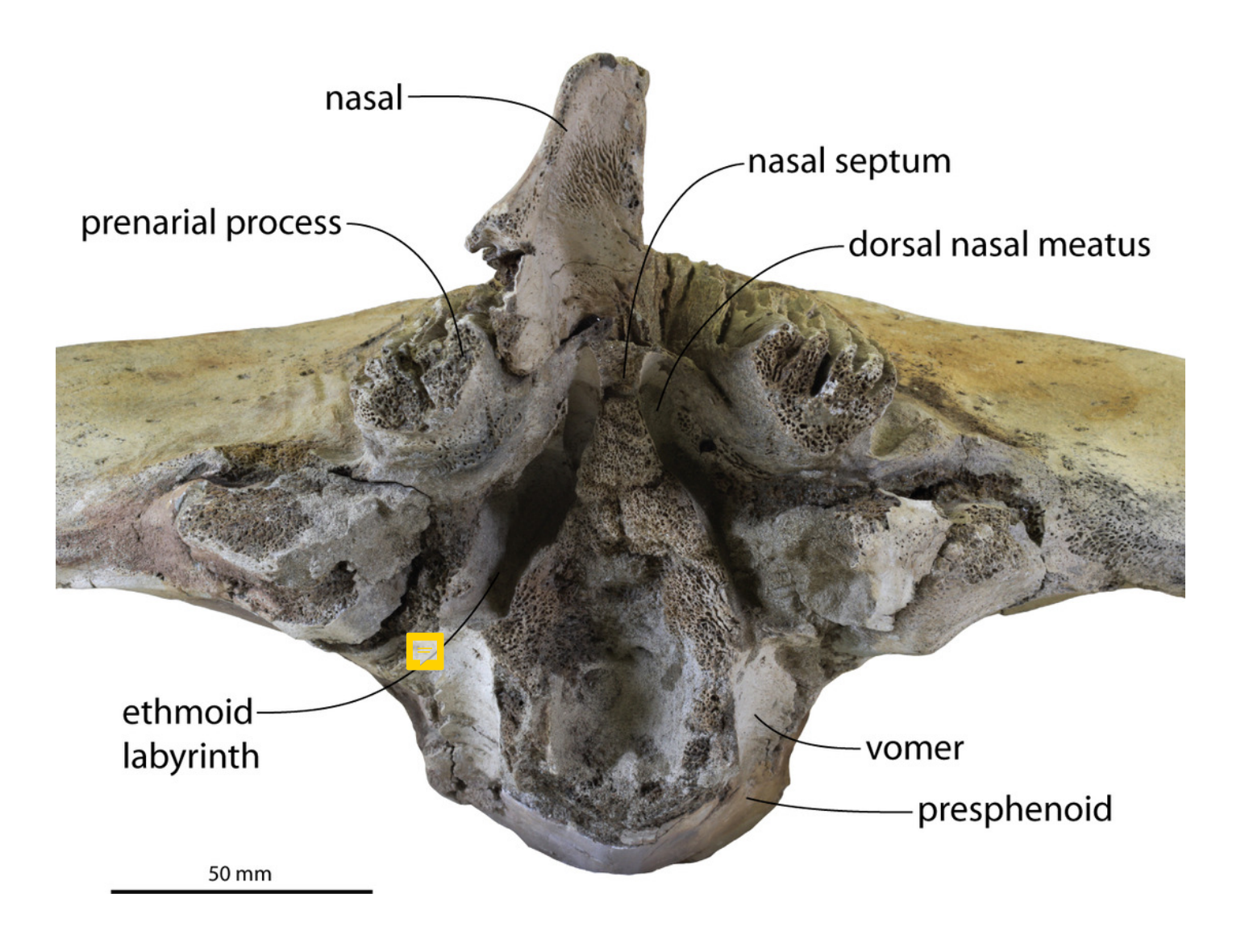


FIGURE 11. Comparison of the squamosal and sternomastoid fossae of Coronodon.

Squamosal of Coronodon planifrons (A) and Coronodon havensteini (B) in dorsolateral view,

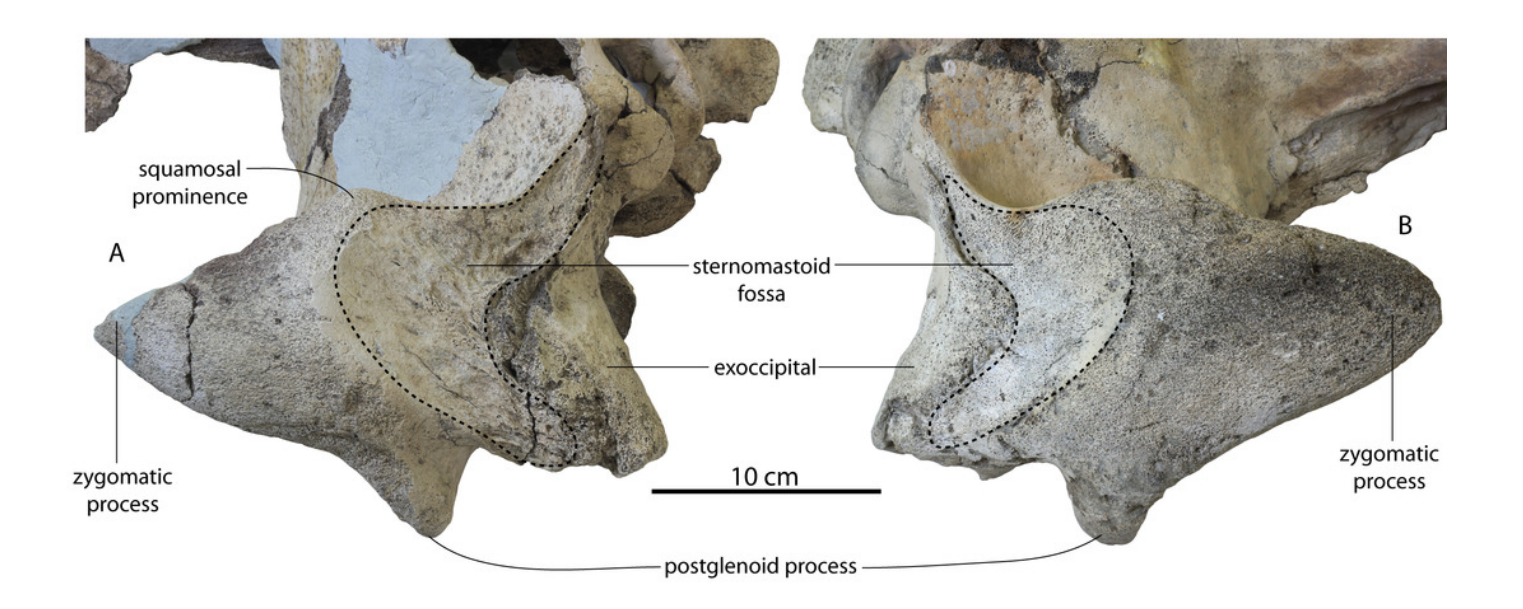


FIGURE 12. Skulls of Coronodon havensteini in posterior view.

(A) referred specimen ChM PV 4745, (B) holotype specimen CCNHM 108, and (C) referred specimen CCNHM 164.

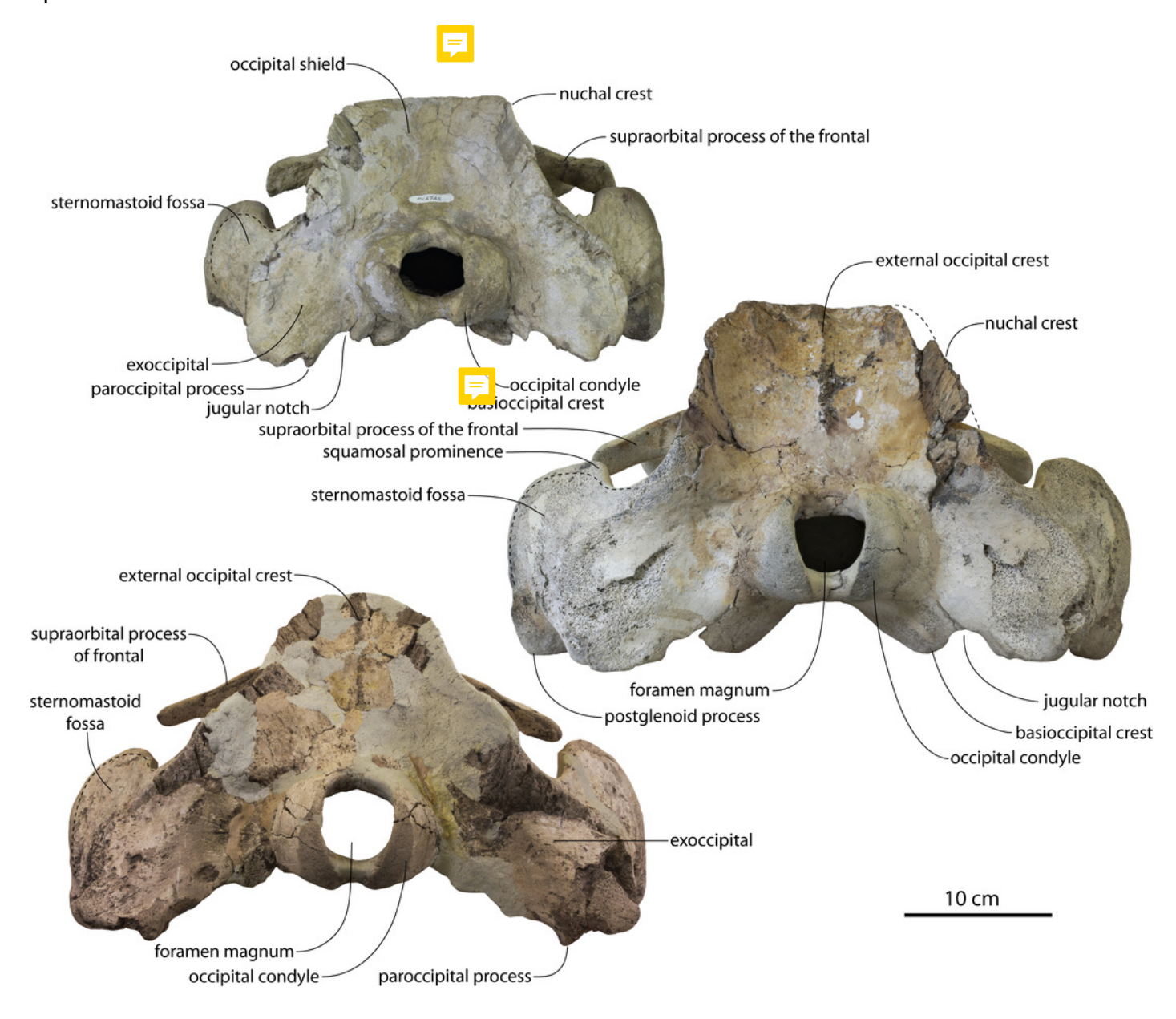




FIGURE 13. Basicranium and periotic of Coronodon havensteini.

(A) left squamosal and periotic of CCNHM 8722 in ventral view; (B) left squamosal of CCNHM 8722 in ventral view with periotic removed; (C) left squamosal of CCNHM 8722 in ventromedial view; (D) basicranium and right periotic of ChM PV 4745 in ventral view; (E) right squamosal and periotic of CCNHM 108 in ventral view; (F) right squamosal of CCNHM 108 with periotic removed.

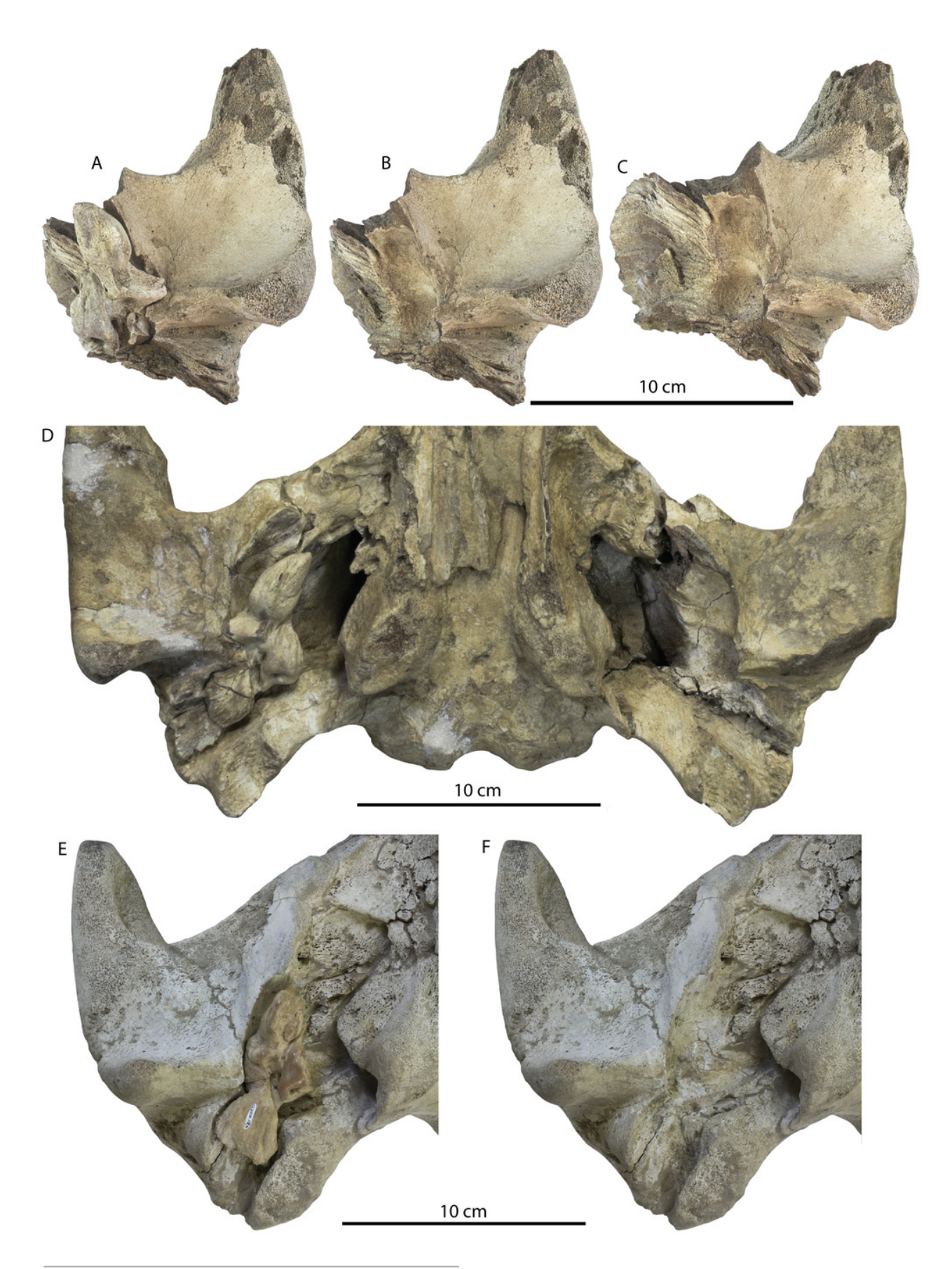




FIGURE 14. Left periotics of Coronodon havensteini.

Periotic of CCNHM 8722 in ventral (A) and dorsal (B) view; periotic of ChM PV 4745 in ventral (C) and dorsal (D) view; periotic of CCNHM 108 in ventral (E) and dorsal (F) view; periotic of CCNHM 164 in ventral (G) and dorsal (H) view.



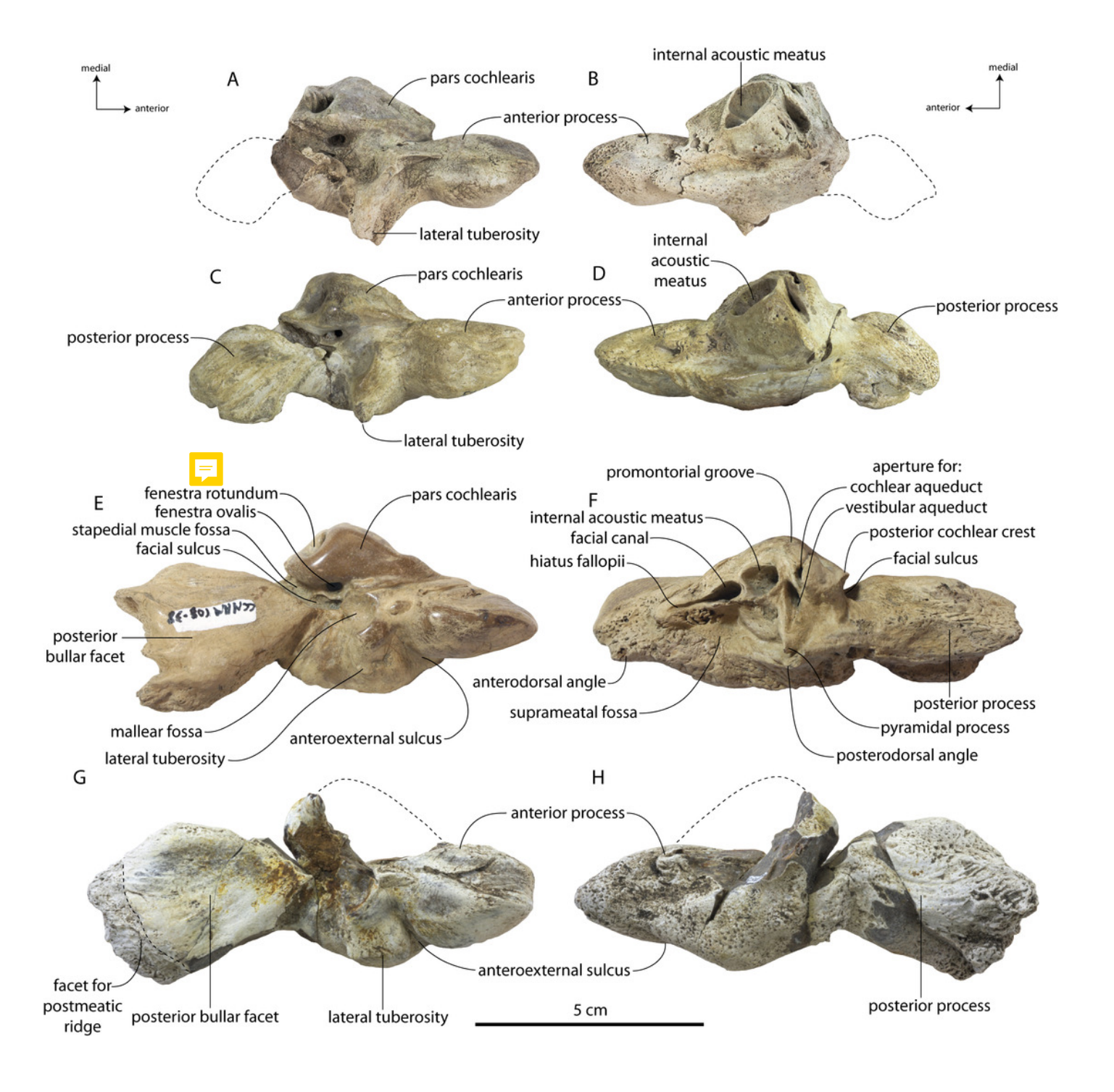




FIGURE 15. Left periotics of Coronodon havensteini.

Periotic of CCNHM 8722 in medial (A) and lateral (B) view; periotic of ChM PV 4745 in medial (C) and lateral (D) view; periotic of CCNHM 108 in medial (E) and lateral (F) view; periotic of CCNHM 164 in medial (G) and lateral (H) view.



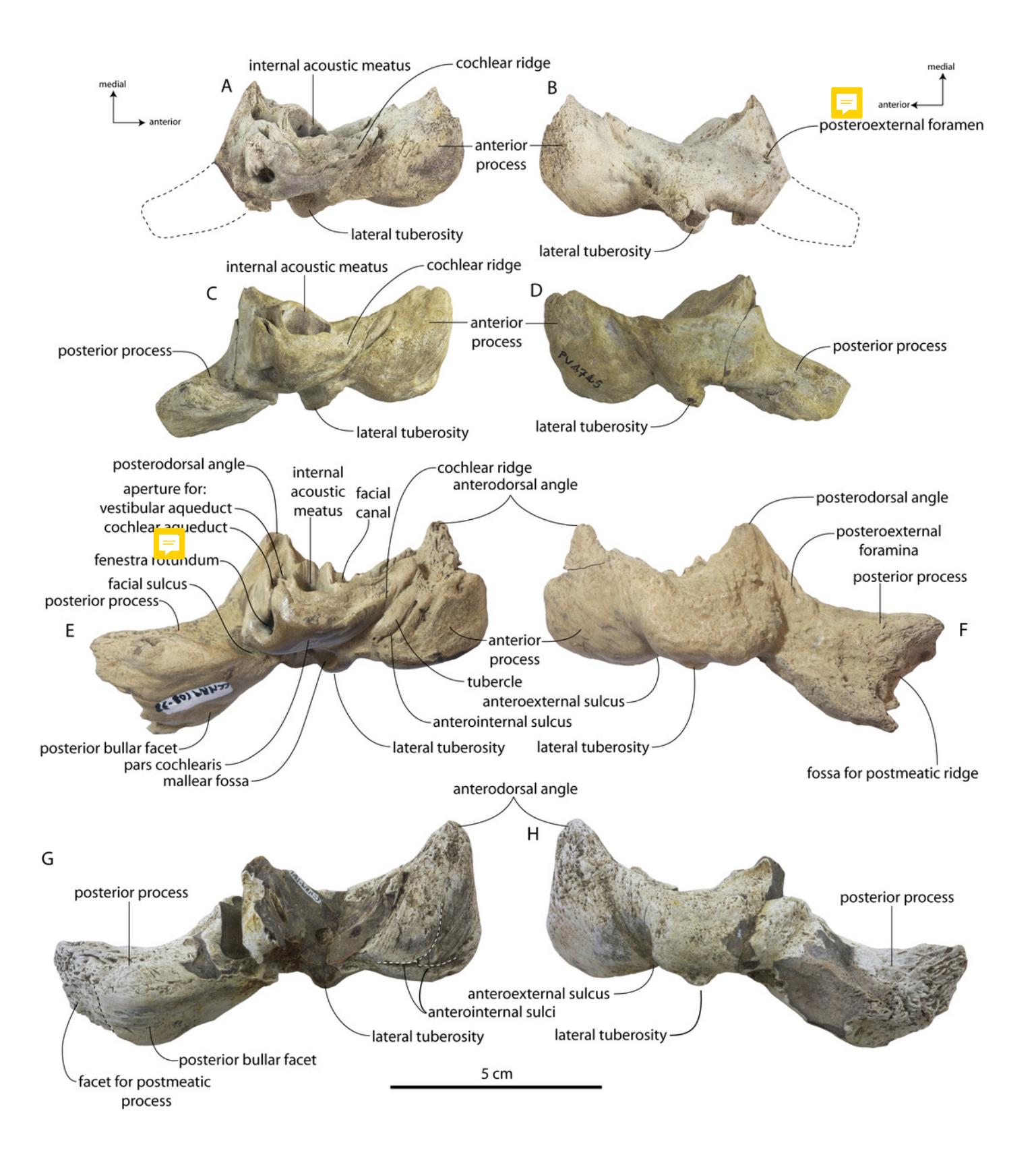


FIGURE 16. Tympanic bullae of Coronodon havensteini.

Right bulla of CCNHM 8722 in medial (A), ventral (B), and dorsal (C) view; right bulla of ChM PV 4745 in medial (D), ventral (E), and dorsal (F) view; left bulla of CCNHM 108 in medial (G), ventral (H), and dorsal (I) view.

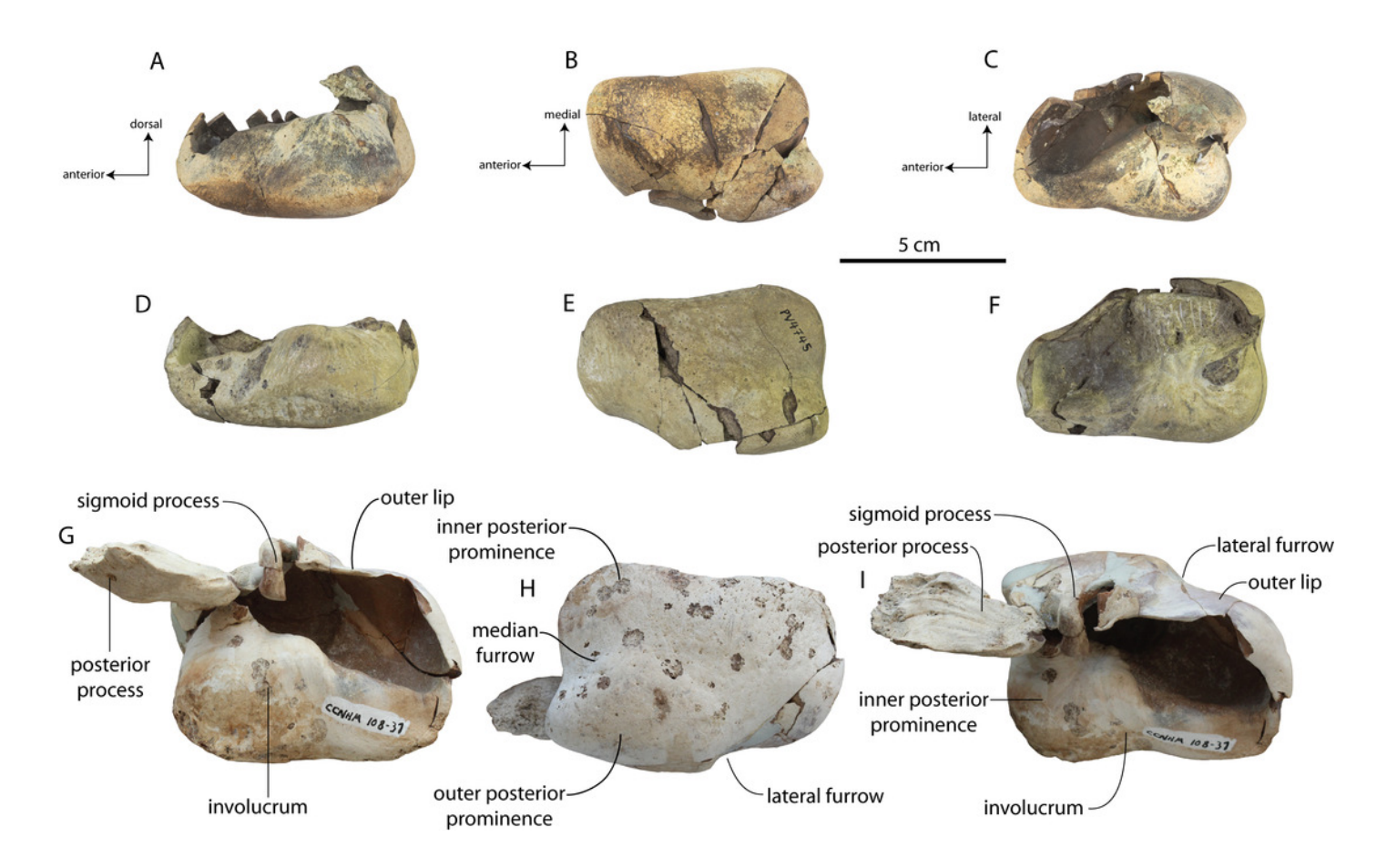
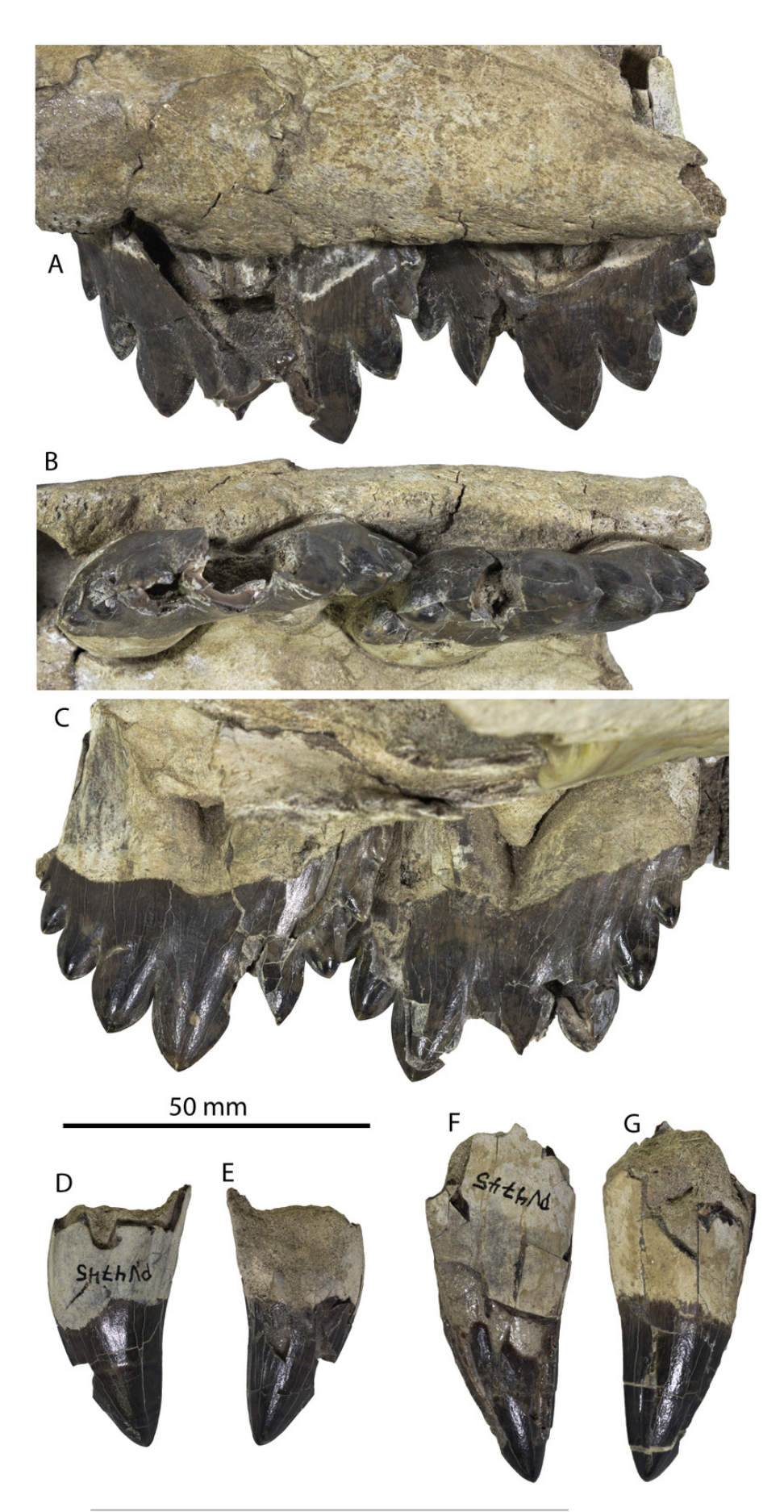




FIGURE 17. Dentition of juvenile Coronodon havensteini, ChM PV 4745.

Upper molars in labial (A), occlusal (B), and lingual (C) view; caniniform tooth in labial (D) and lingual (E) view; caniniform tooth in lingual (F) and labial (G) view.



PeerJ reviewing PDF | (2022:10:78092:0:1:NEW 6 Oct 2022)

FIGURE 18. Upper dentition of Coronodon havensteini, CCNHM 108 and 164.

Abbreviations: li, lingual; la, labial.

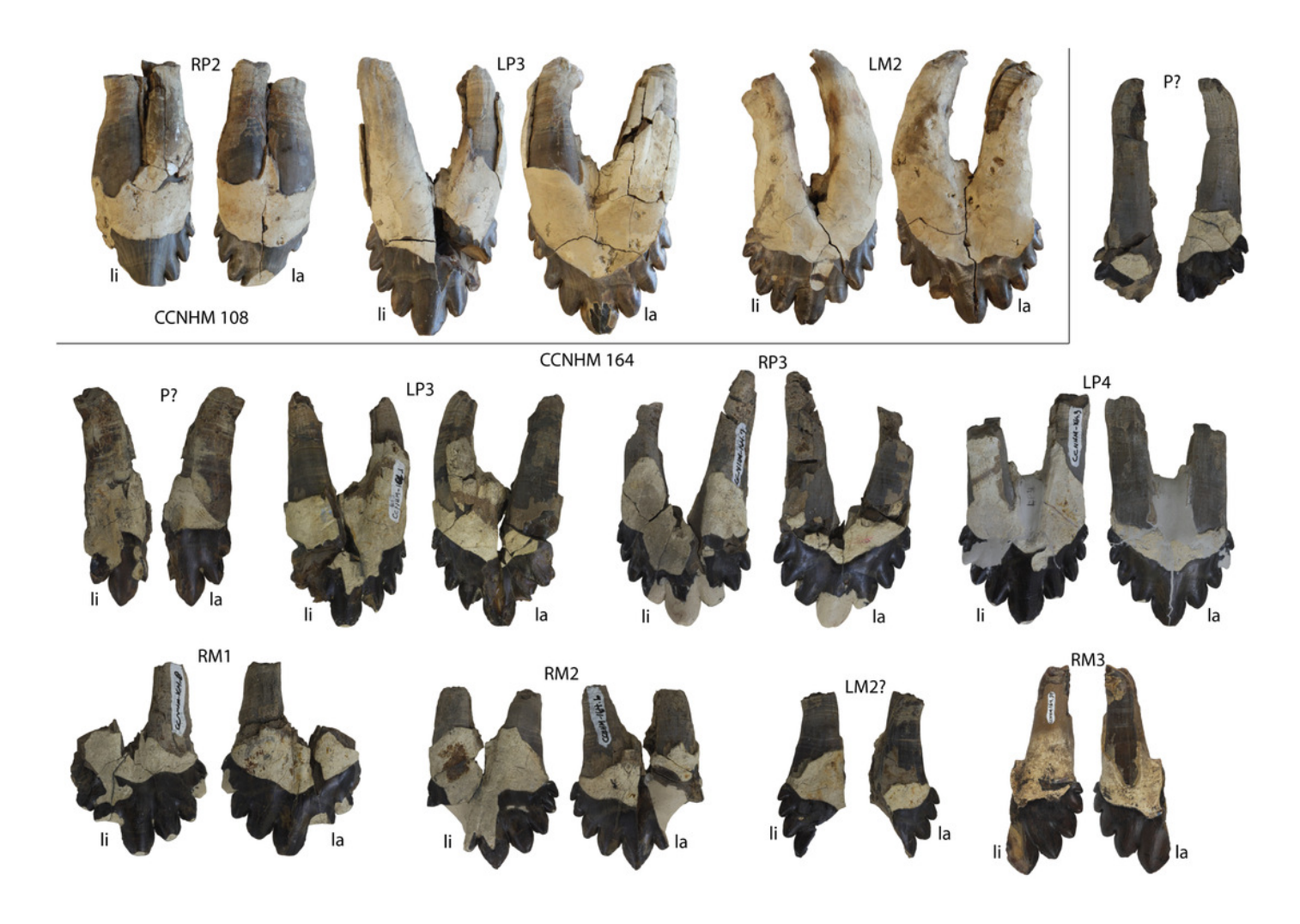




FIGURE 19. Lower dentition of Coronodon havensteini, CCNHM 108 and 164.

Abbreviations: li, lingual; la, labial.

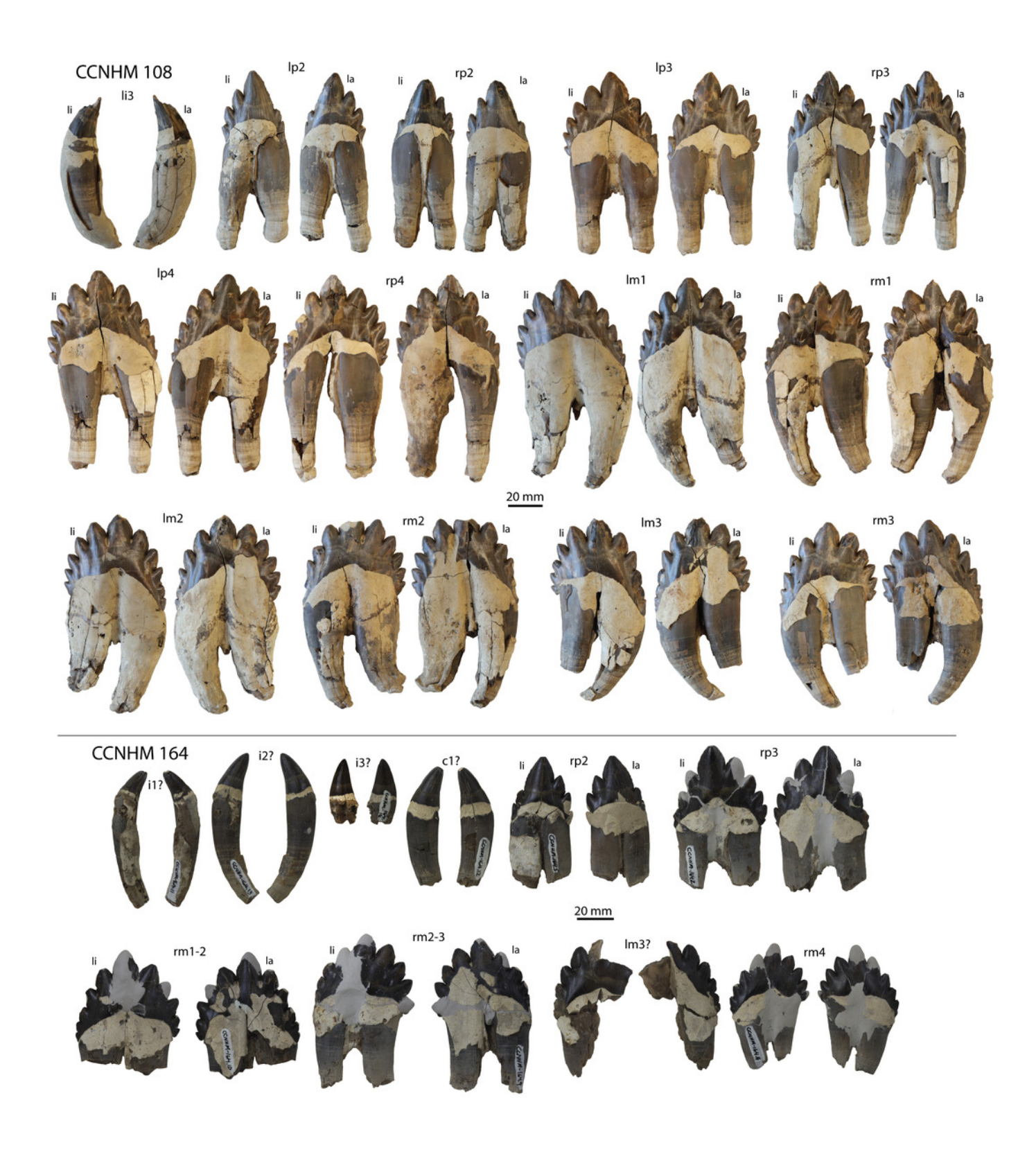




FIGURE 20. Mandibles of Coronodon havensteini.

Holotype specimen CCNHM 108 left mandible (A) and right mandible (B) in lateral view, and referred specimen CCNHM 164 right mandible in lateral view (C); holotype specimen CCNHM 108 left mandible in dorsal view (D) and referred specimen CCNHM 164 right mandible in dorsal view (E).

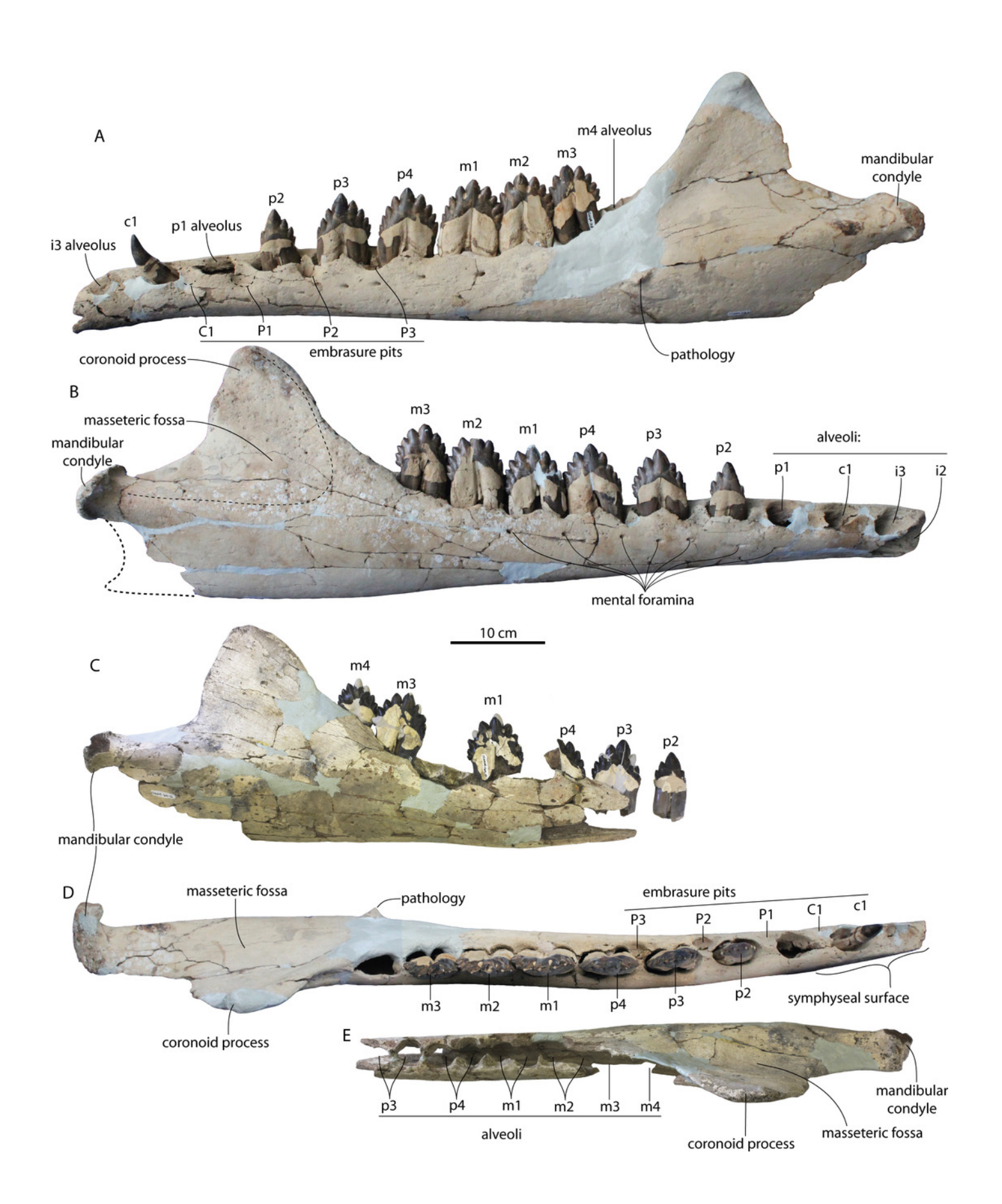


FIGURE 21. Mandibles of Coronodon havensteini.

Holotype specimen CCNHM 108 left mandible (A) and right mandible (B) in medial view; referred specimen CCNHM 164 right mandible (C) in medial view.

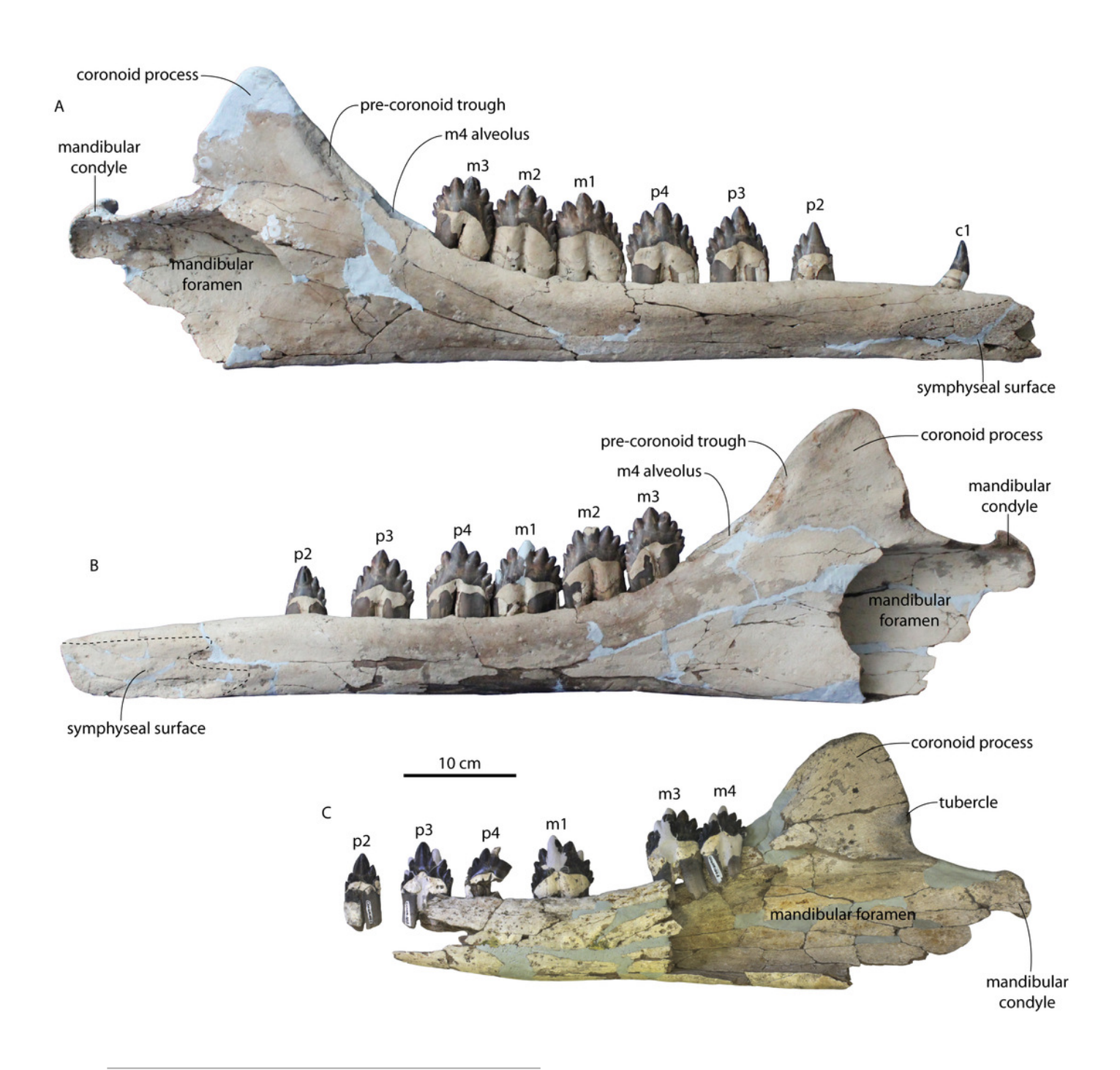




FIGURE 22. Postcranial elements of *Coronodon havensteini* holotype specimen CCNHM 108.



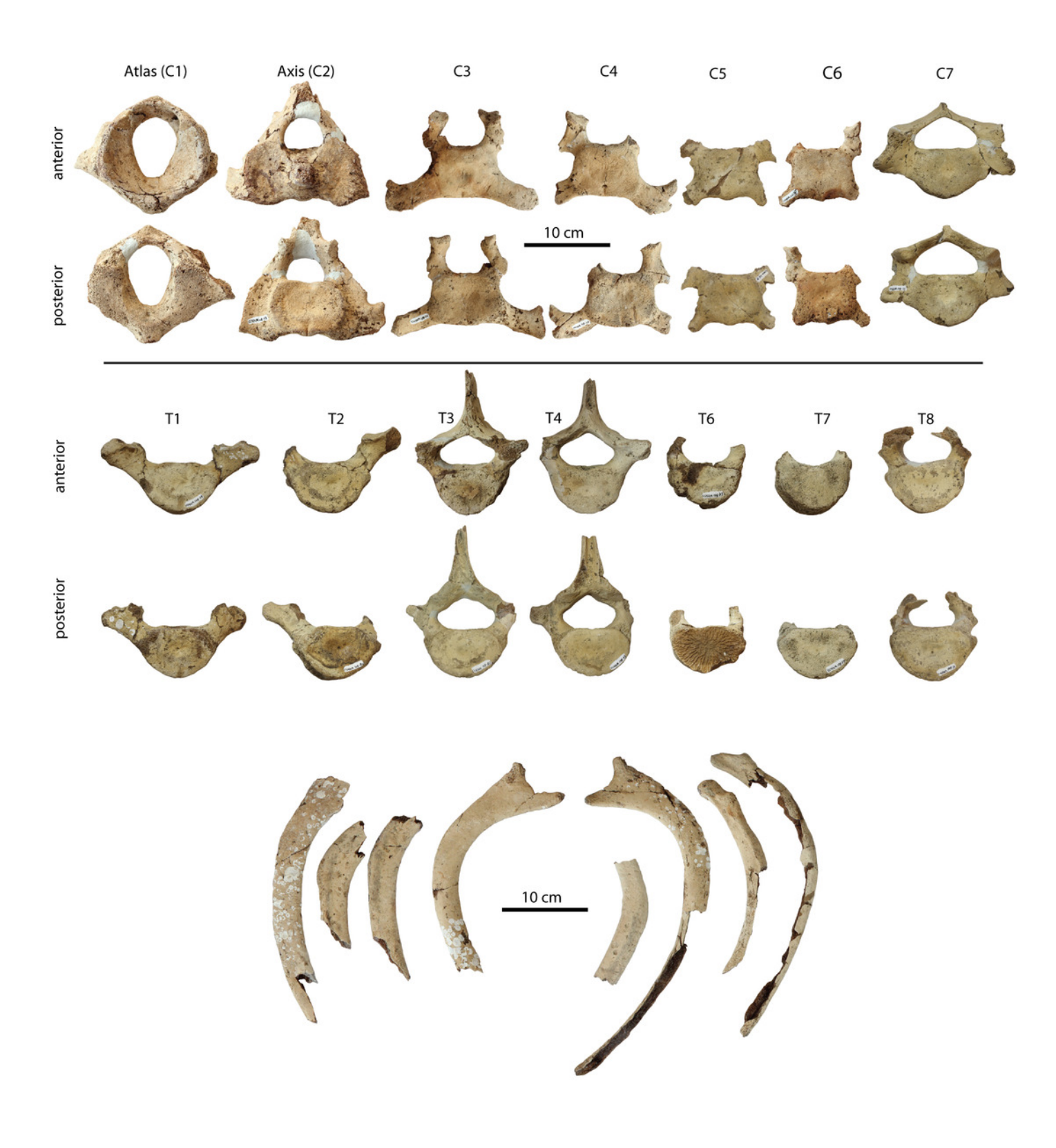




FIGURE 23. Postcranial elements of *Coronodon havensteini* referred specimen CCNHM 164.

Cervical vertebrae shown in anterior and posterior views, and thoracics, lumbars, and caudals shown in anterior view only.



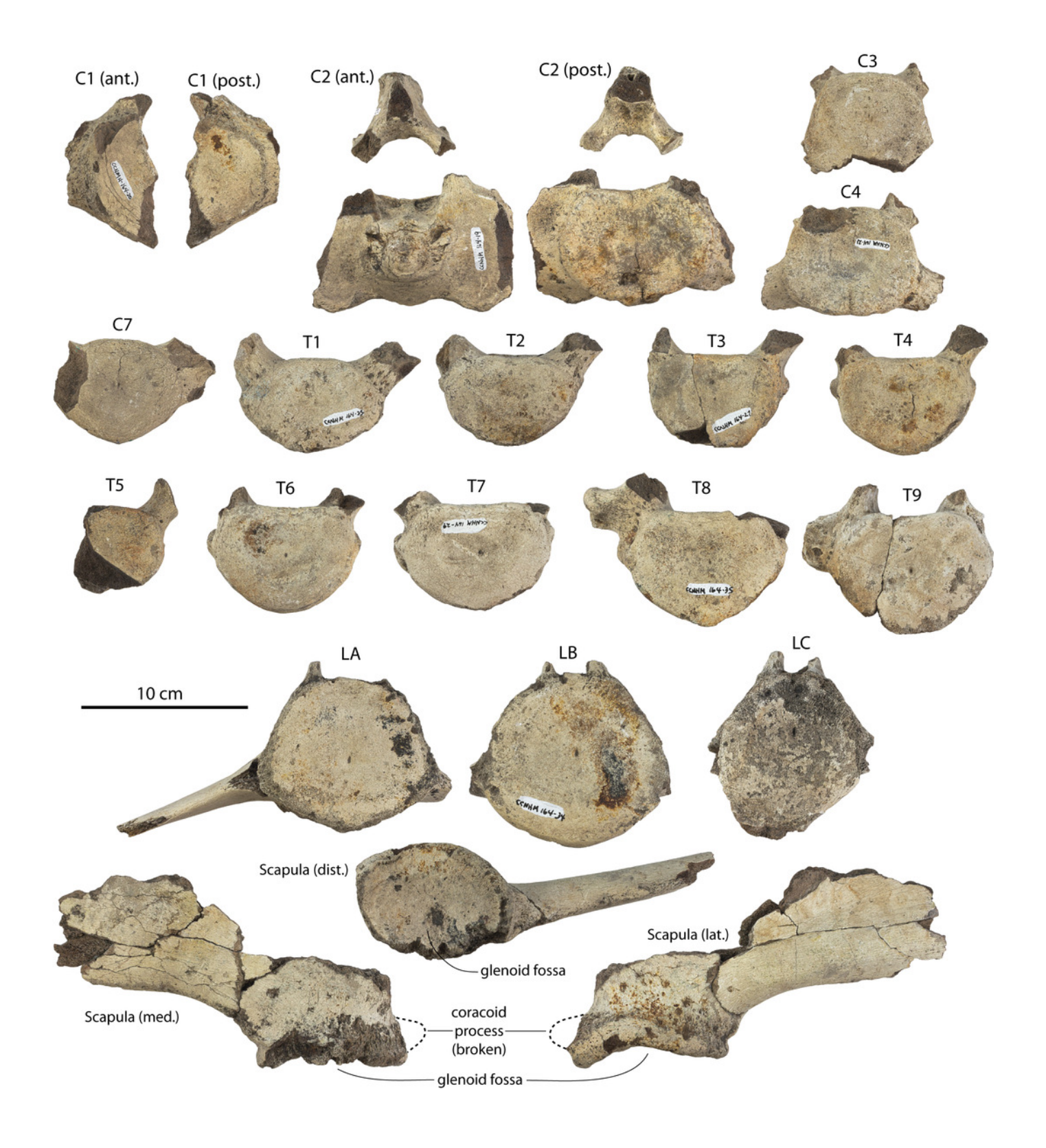


FIGURE 24. Atlas vertebra of *Coronodon havensteini* referred specimen ChM PV 4745.

Atlas in anterior (A) and posterior (B) view.

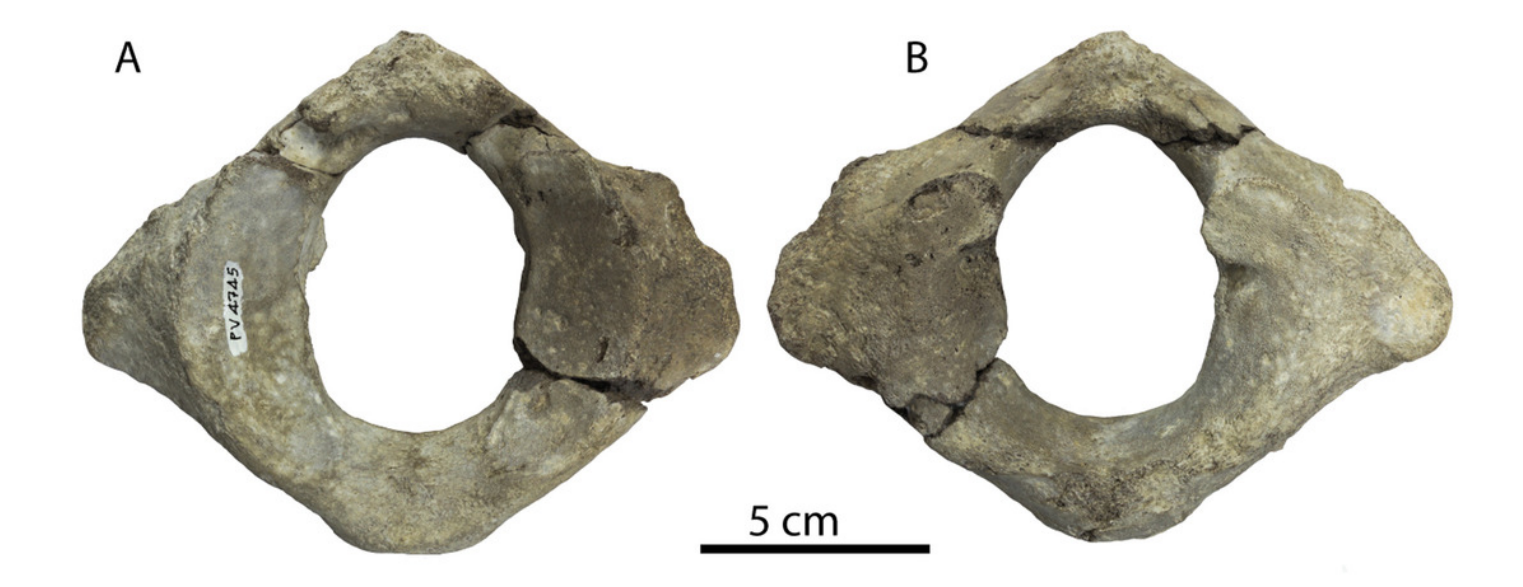




FIGURE 25. Holotype skull (ChM PV 2778) elements of Coronodon newtoni.

Antorbital notch in dorsolateral view (A), skull in dorsal view (B), premaxillae and fragment of left maxilla in ventral view (C), skull in ventral view (D), left M1 in labial (E), lingual (F) and occlusal (G) view, vomer in ventral view (H), and skull in lateral view (I).



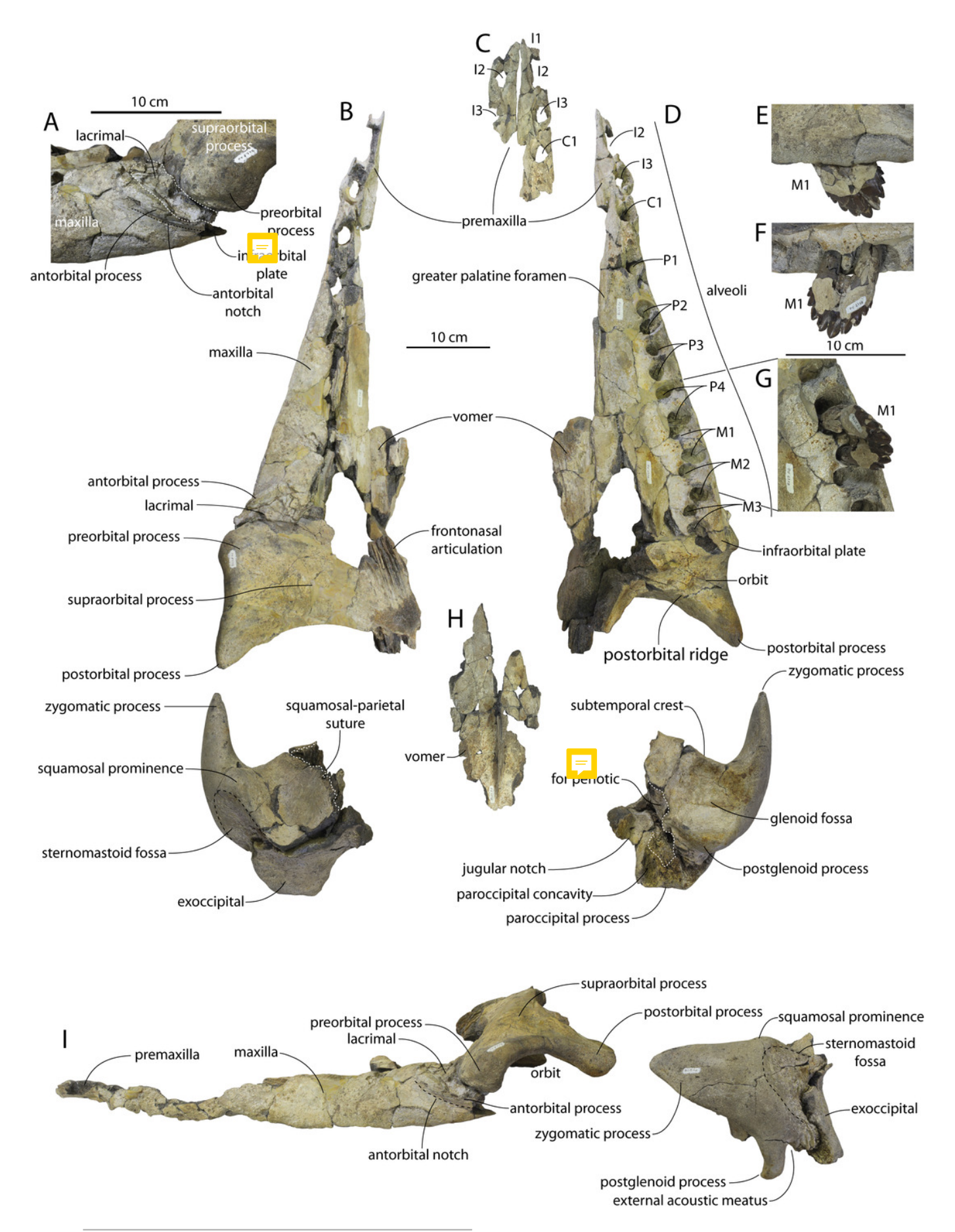


FIGURE 26. Reconstruction of the holotype skulls of *Coronodon havensteini*, *Coronodon planifrons*, and *Coronodon newtoni* in lateral view; supplementary reconstruction of alternate mandibular tooth count for *Coronodon planifrons*.

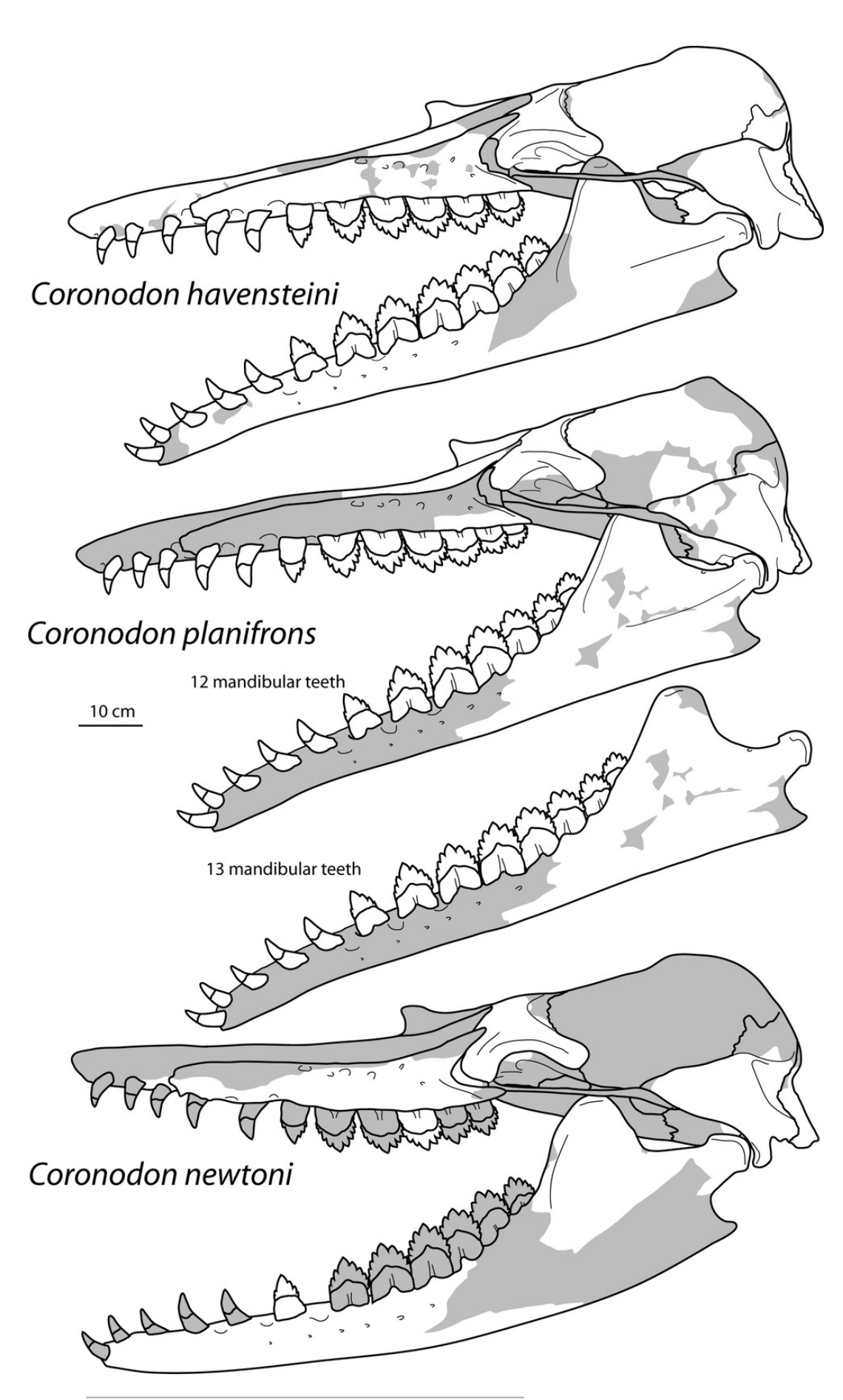




FIGURE 27. Holotype right periotic (ChM PV 2778) of Coronodon newtoni.

Periotic in dorsal (A), ventral (B), lateral (C), and medial (D) view.

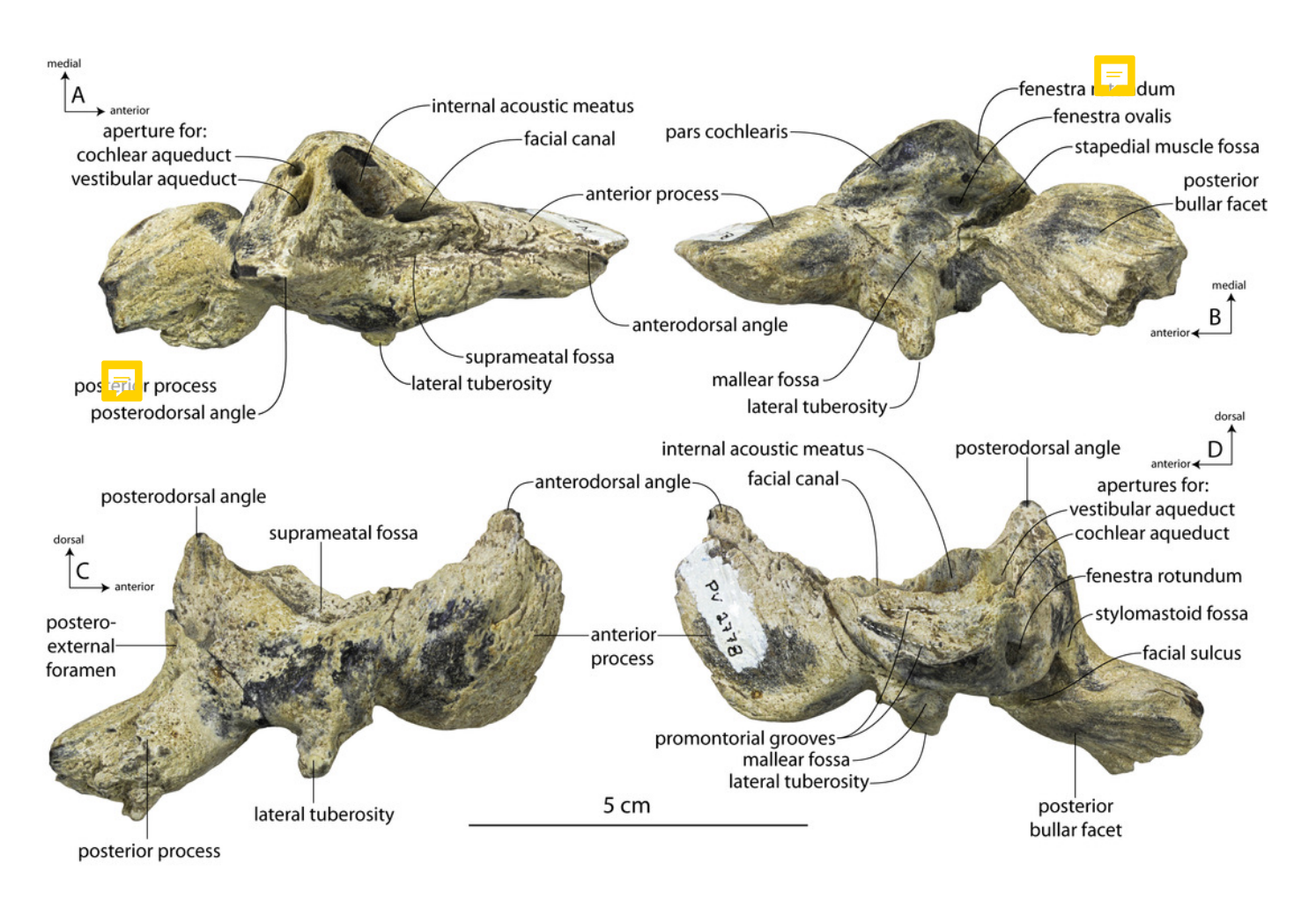


FIGURE 28. Holotype tympanic bulla (ChM PV 2778) of Coronodon newtoni.

Bulla in medial (A), lateral (B), dorsal (C), and ventral (D) view, posterior process of bulla in dorsal (E) and ventral (F) view.

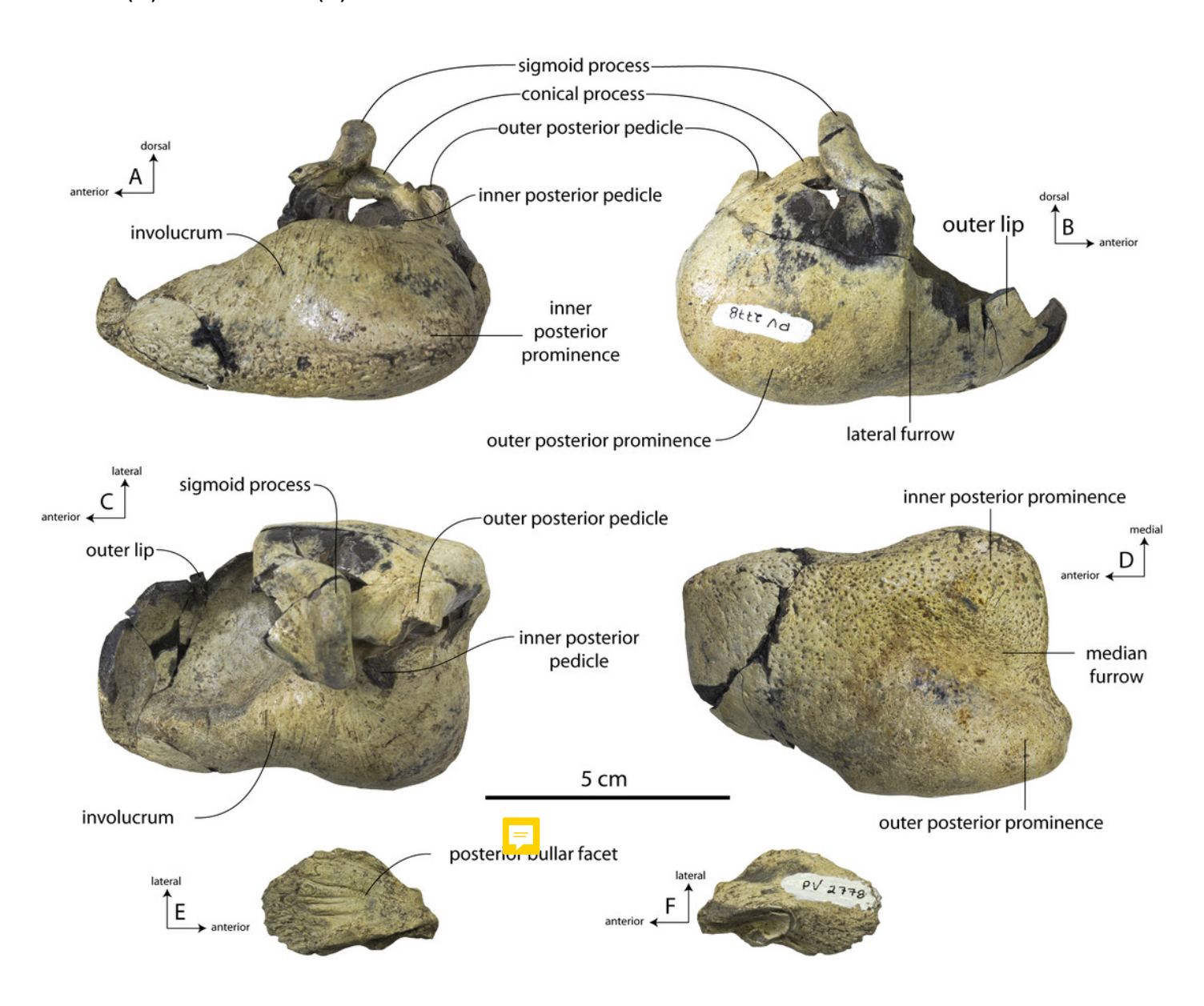




FIGURE 29. Mandible, dentition, and postcrania of holotype specimen (ChM PV 2778) of *Coronodon newtoni*.

Left M1 in labial (A) and lingual (B) view, left mandible in lateral (C), dorsal (D), and medial (E) view, upper left I1 in lingual labial (F) and lingual (G) view, lower left p2 in labial (H) and lingual (I) view; mid-thoracic vertebra in anterior (J) and posterior (K) view; posteriormost thoracic (T9) or anterior lumbar (L1) vertebra in anterior (L) and posterior (M) view; caudal vertebra (Ca 5, 6, or 7) in anterior (N) and posterior (O) view.

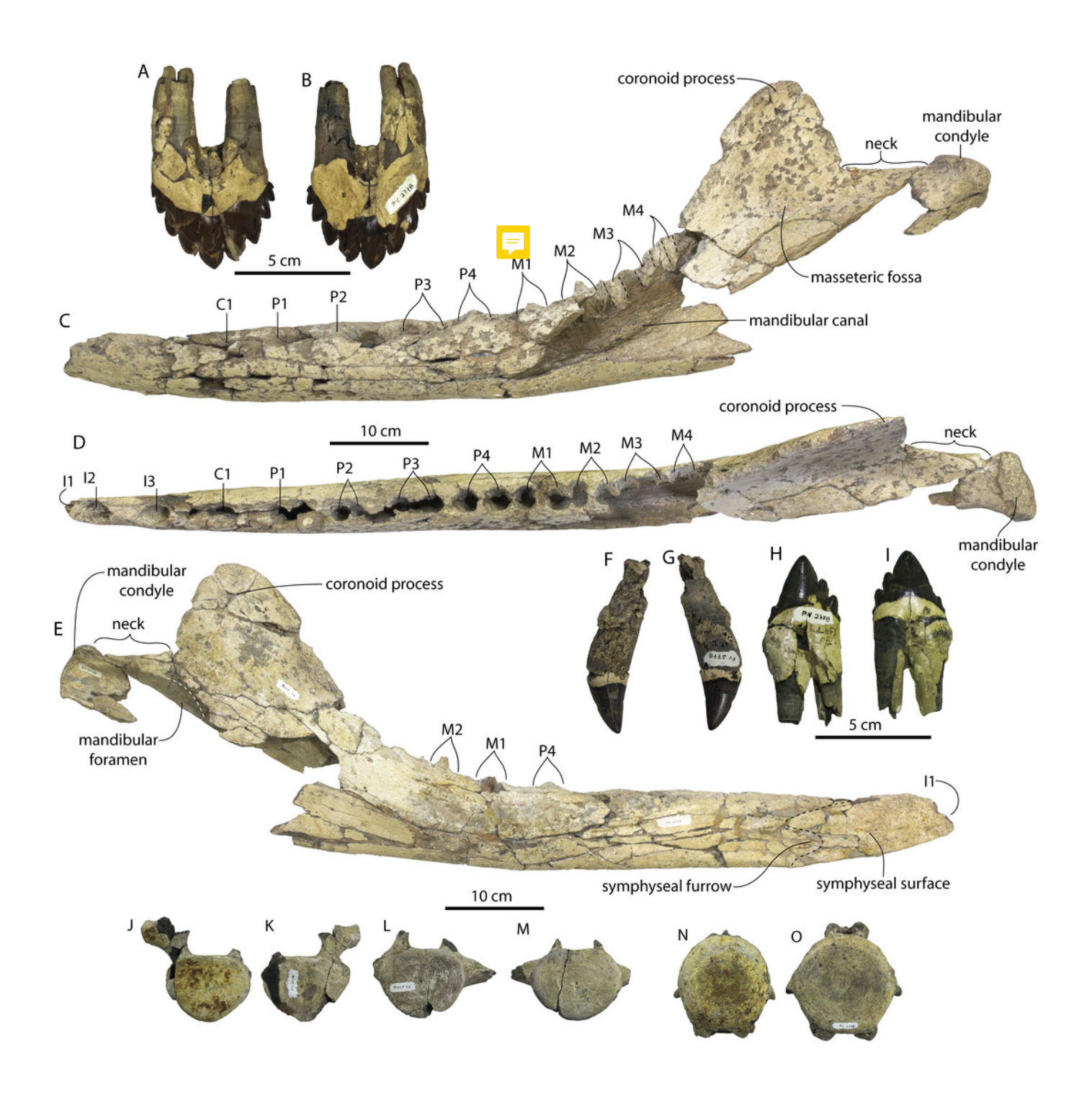




FIGURE 30. Holotype skull (CCNHM 166) of Coronodon planifrons.

Right nasal in lateral (A) and medial (B) view, right premaxilla in lateral (C), dorsal (D), and medial (E) view; skull in dorsal (F), ventral (G) and lateral (H) view.



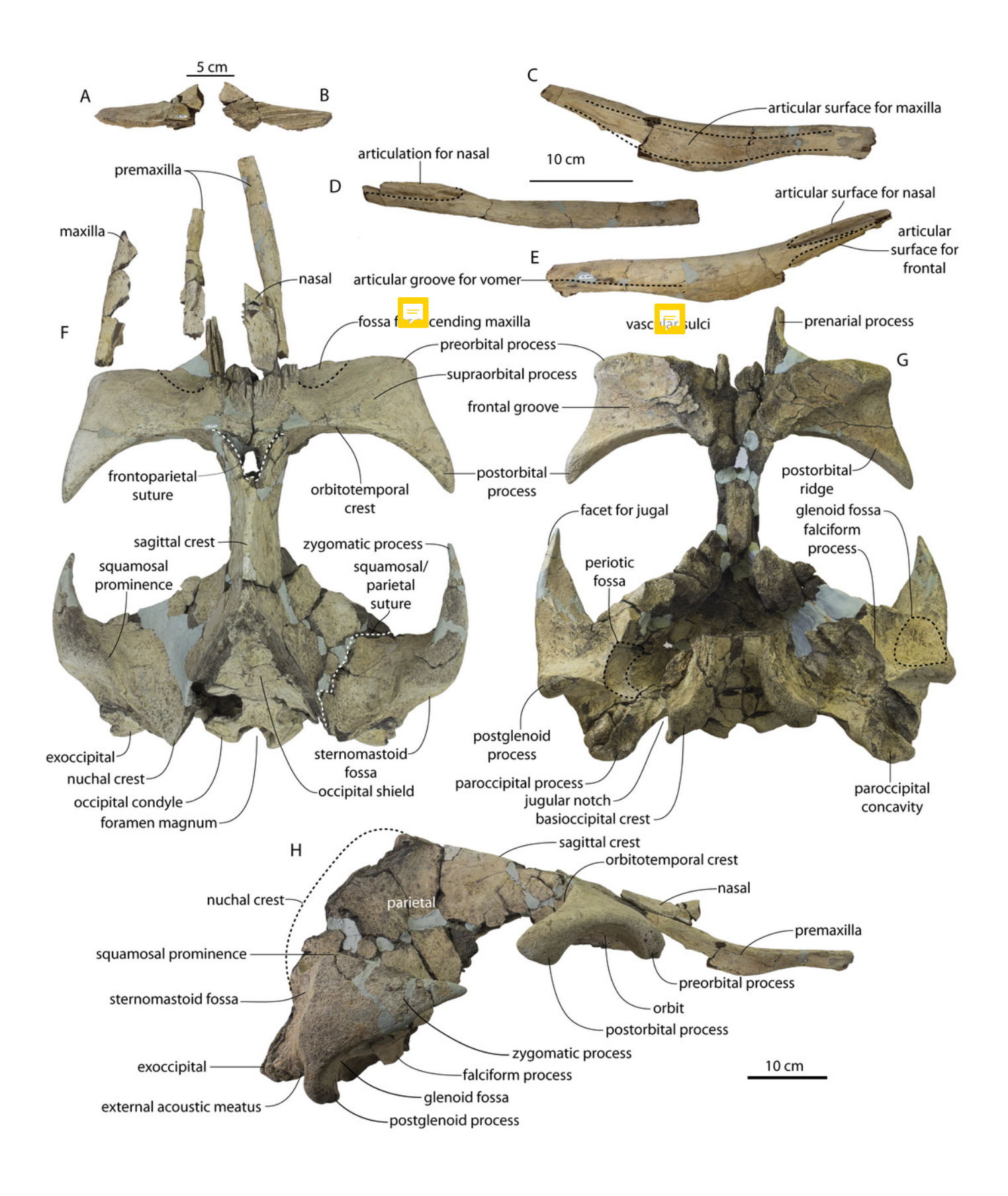




FIGURE 31. Holotype periotics and bulla (CCNHM 166) of Coronodon planifrons.

Left and right periotic in ventral (A, B) views, dorsal (C, D) views, medial (E, F) views, and lateral (G, H) views. Posterior process of right tympanic bulla in dorsal (I) and ventral (J) views.



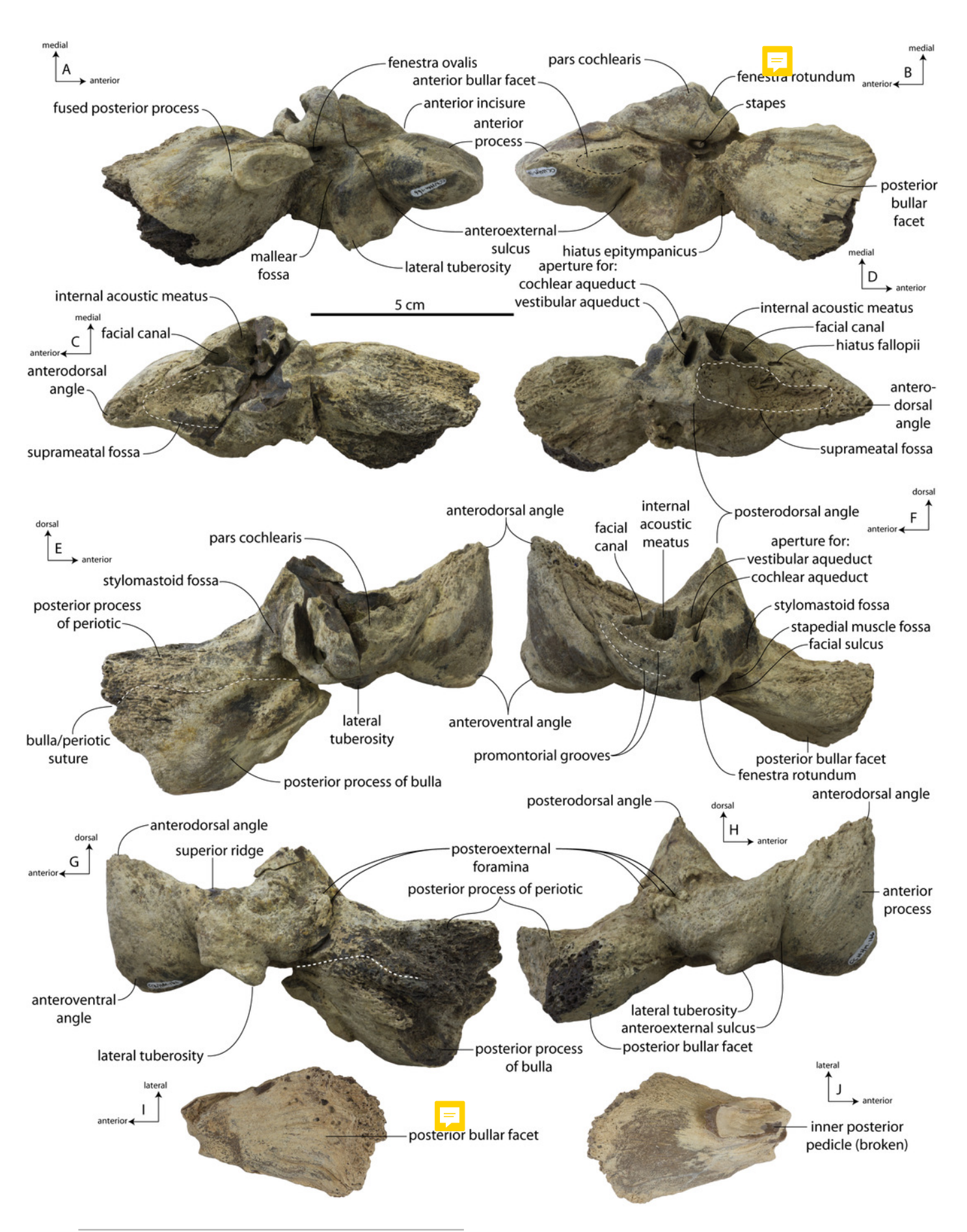




FIGURE 32. Holotype dentition (CCNHM 166) of Coronodon planifrons.

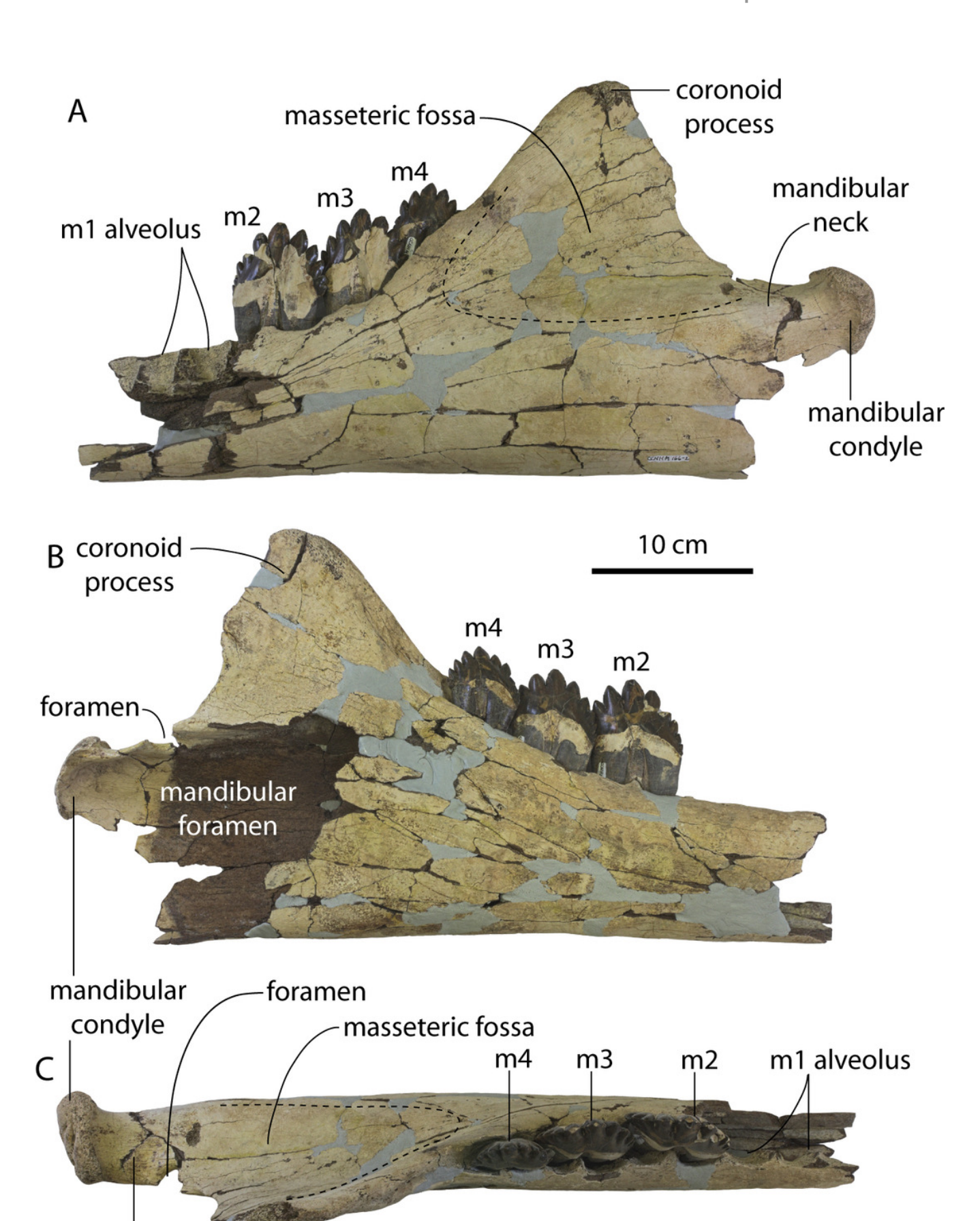
Abbreviations: li, lingual; la, labial.





FIGURE 33. Holotype mandible (CCNHM 166 of Coronodon planifrons.

Mandible in lateral (A), medial (B), and dorsal (C) view.



coronoid process

mandibular neck

FIGURE 34. Holotype vertebrae (CCNHM 166) of Coronodon planifrons.

Cervical vertebrae shown in anterior and posterior views, and thoracics, lumbars, and caudals shown in anterior view only.

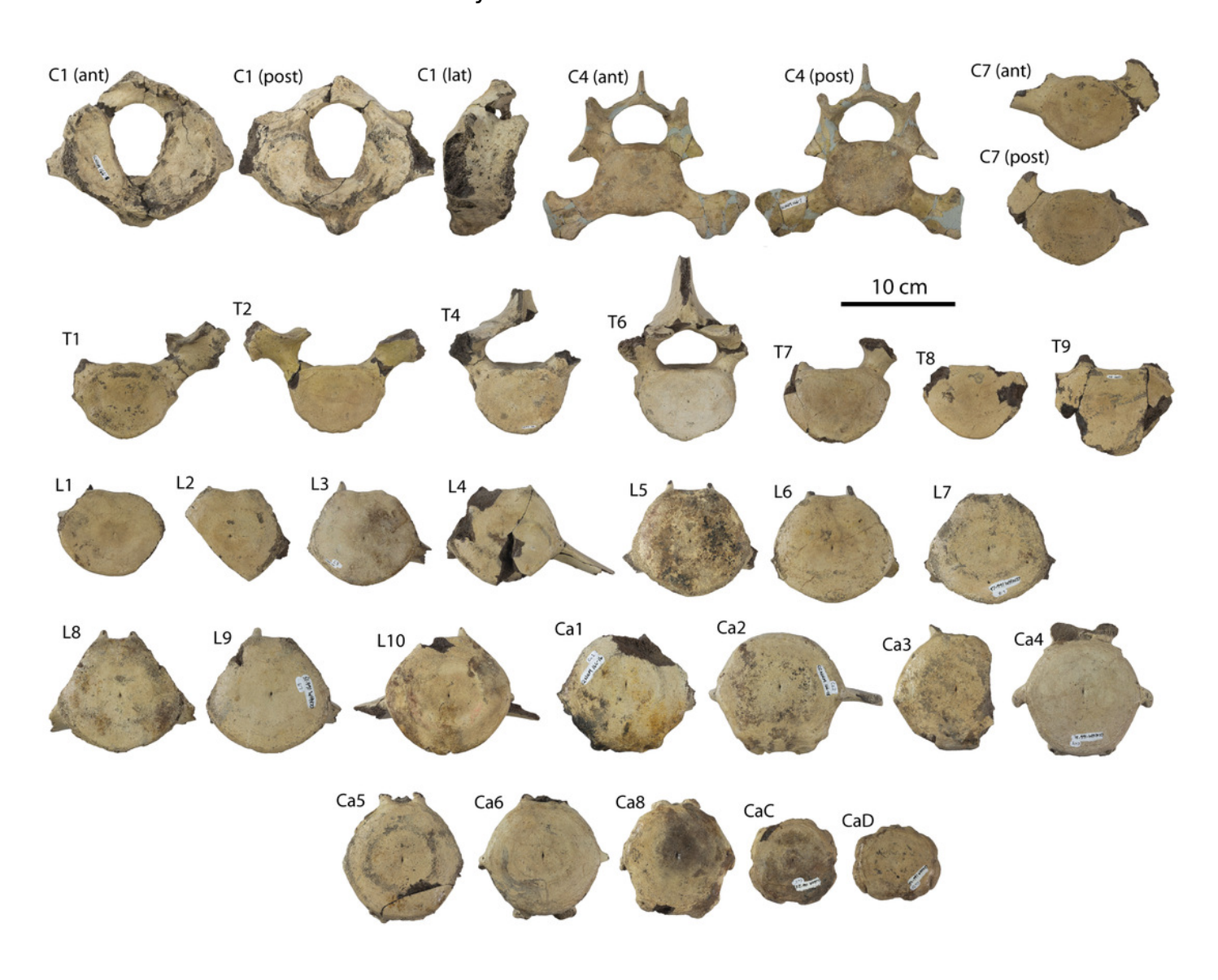


FIGURE 35. Holotype ribs (CCNHM 166) of Coronodon planifrons in anterior view.



FIGURE 36. Isolated teeth of Coronodon from the Charleston embayment

Upper left molar ChM PV 9162 in labial (A) and lingual (B) view; associated caniniform and upper left molar of ChM PV 9584 (*Coronodon* sp.) in labial (C, E) and lingual (D, F) view; isolated right upper third molar CCNHM 8732 (*Coronodon planifrons*) in labial (G) and lingual (H) view, upper left molar CCNHM 1839 (*Coronodon* sp.) in labial (I) and lingual (J) view; isolated lower left premolar ChM PV 9163/2029 (*Coronodon* sp.) in lingual (K) and labial (L) view, partial lower postcanine CCNHM 556 (*Coronodon* sp.) in lingual (M) and labial (N) view, lower molar fragment ChM PV 2029 (*Coronodon* sp.) (O, P), isolated P1 or C1 CCNHM 8729 in labial (R) and lingual (Q) view, isolated upper molar (M2-3) or lower M3 ChM PV 9161 (*Coronodon* sp.) (S, T), isolated caniniform CCNHM 8729 (*Coronodon* sp.) in labial (U) and lingual (V) view, isolated posterior left upper molar (M2-3) CCNHM 8730 (*Coronodon* sp.) in labial (W) and lingual (X) view, isolated lower left molar ChM PV 9177 in labial (Y) and lingual (Z) view.

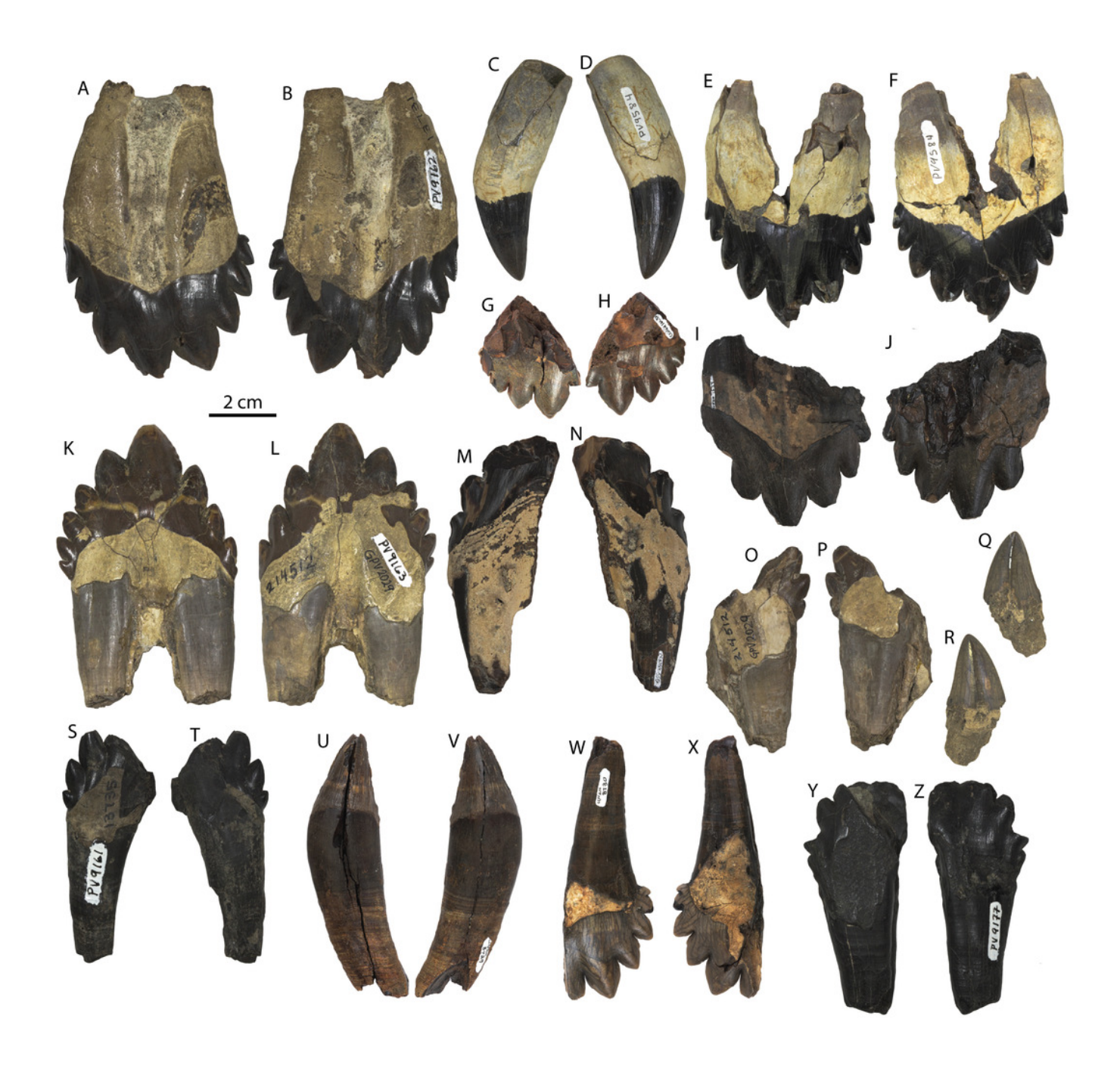




FIGURE 37. Results of phylogenetic analyses with equal weights (EW).

Strict consensus of 10,000 shortest trees (each 14013 steps in length) obtained from an analysis where all characters have equal weights, divided into three parts (A, B, C). Numbers next to nodes indicate bootstrap support values; unnumbered nodes indicate support values < 50%.







FIGURE 38. Results of phylogenetic analyses with implied weights (IW).

Strict consensus of 15 best fit trees (each with fit of 1113.20656) obtained from an analysis using implied weighting and the constant k = 3, divided into three parts (A, B, C). Numbers next to nodes indicate bootstrap support values; unnumbered nodes indicate support values < 50%. Asterisk next to *Mammalodon hakataramea* indicates that it was unresolved at the stem of Neoceti in the summary of the bootstrap analysis, inconsistent with the strict consensus and likely a result of the small percentage of characters coded for this taxon.





FIGURE 39. Composite skeletal reconstruction of Coronodon.

Skull and cervical vertebrae after *Coronodon havensteini* holotype CCNHM 108, thoracic vertebrae and scapula after referred *Coronodon havensteini* specimen CCNHM 164, and lumbocaudal vertebrae after *Coronodon planifrons* holotype CCNHM 166.

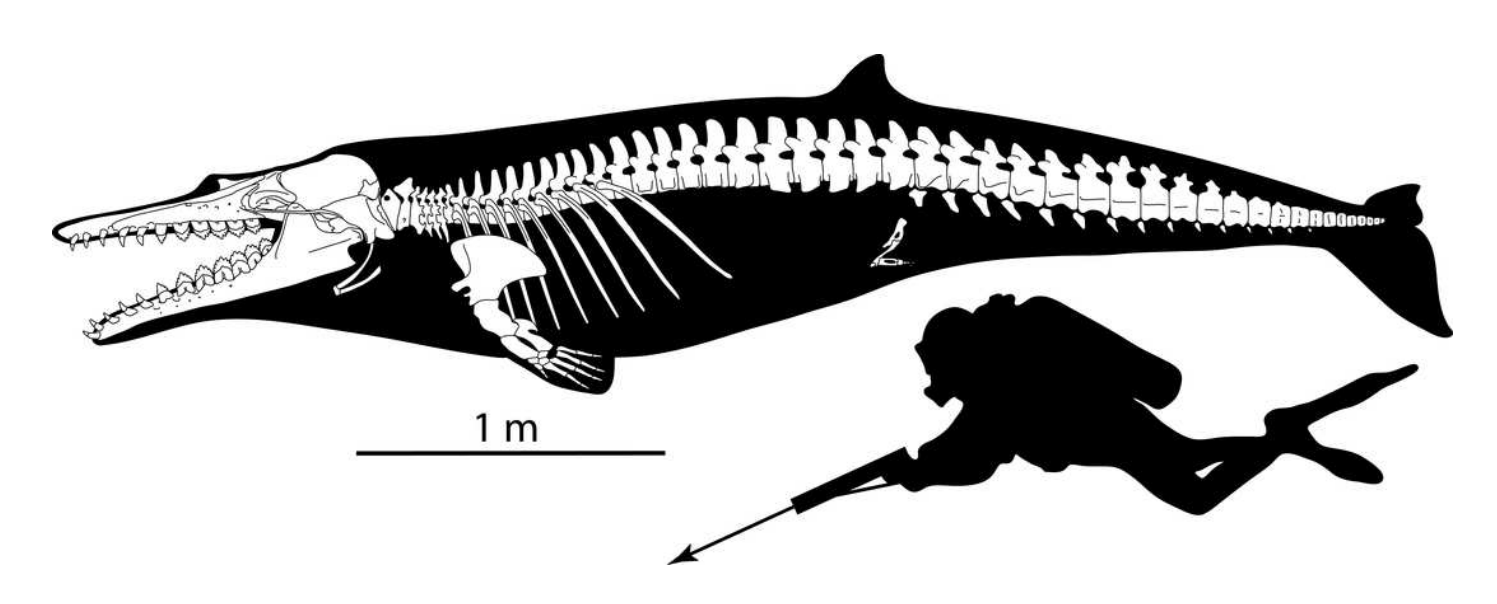




FIGURE 40. Morphology of *Coronodon* and character evidence for key clades across the archaeocete-neocete transition.

Character states in *Coronodon* supporting the Equal Weights (EW) phylogeny shown in white boxes; states supporting the Implied Weighting (IW) phylogeny shown in black boxes; states supporting both shown in grey. Colored circles show character states supporting each node on the EW and IW trees. X indicates the absence of a synapomorphic character state in *Coronodon*, chiefly synapomorphies for Neoceti B.



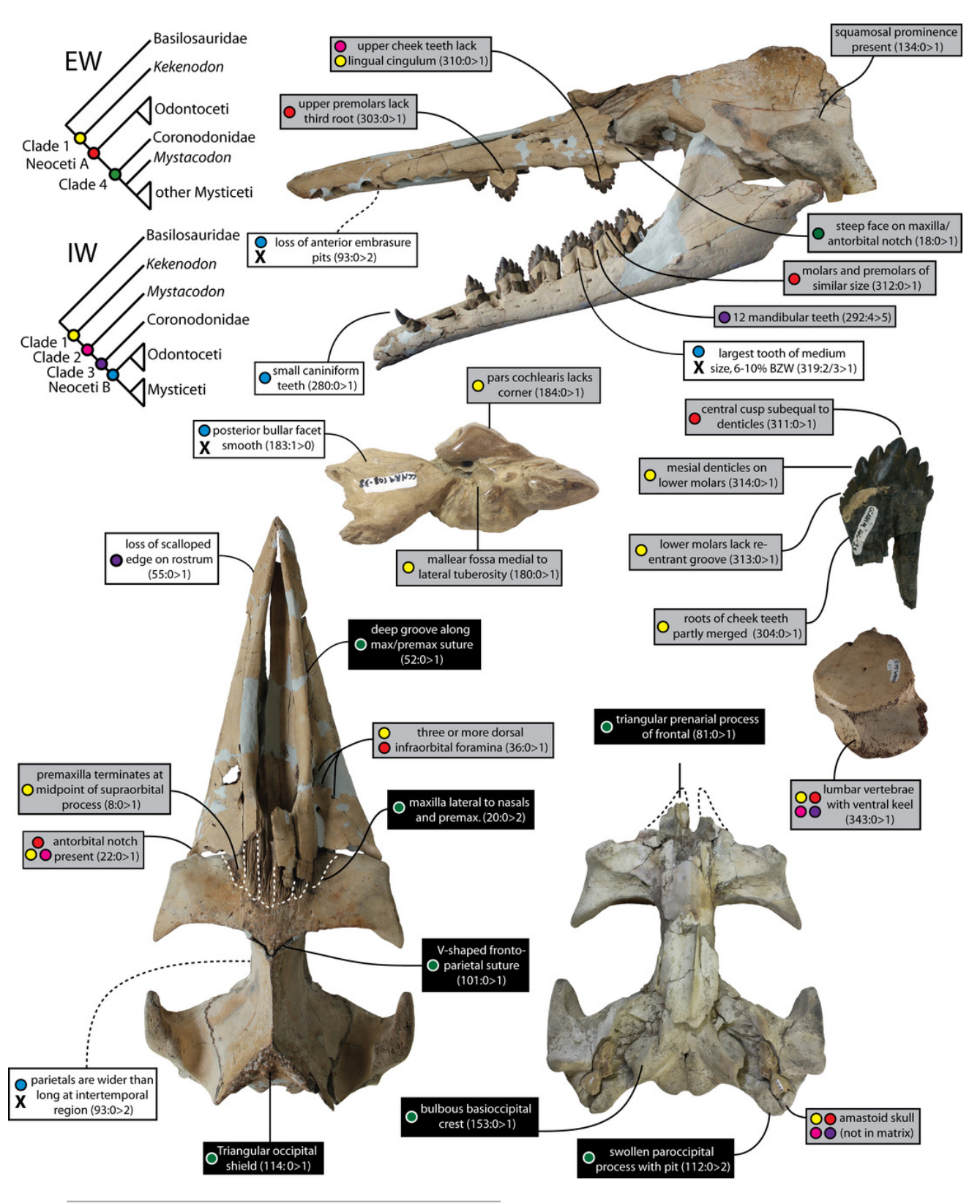




Table 1(on next page)

Table 1. Comparison of morphology among different named and unnamed Coronodonidae.



1 Table 1. Comparison of morphology among different named and unnamed Coronodonidae.

	Coronodon	Coronodon	Coronodon	ChM PV 5720	CCNHM 8745
Alignment of molars/diastemata	Anteroposterior, no diastemata	planifrons ?	newtoni Overlapping	Anteroposterior, short diastemata	?
Upper molars	Subequal	M2 and m3 successively smaller	Subequal?	Subequal?	?
Embrasure pits	Present along toothrow	?	Absent posterior to P2	Present along toothrow	?
Ventral margin of maxilla	Straight	,	Convex	Straight	,
Ventral margin of mandible	Straight	Straight	Convex	Straight	,
SOPF angle in anterior view	Ventrolateral	Horizontal	Ventrolateral	Ventrolateral	Ventrolateral
Rostrofrontal overlap v. SOPF length (ant. Frontal to ant. Orbitotemporal crest)	72.7%	64%	89.9%	100%?	65%
Dorsal profile of nasals	Upturned	Upturned	,	Upturned	Horizontal
Prenarial triangle	Absent	Absent	Absent	Present, 62% of nasal length	Present, 44% of nasal length
Preorbital v. postorbital process	Thick, subequal; postorb = 82% of preorb depth	Postorbital process thicker, postorb = 194% of preorb depth	Preorbital process thicker, postorb = 64% of preorb depth	Postorb slightly thicker, postorb = 135% preorb depth	Preorbital process thin (23 mm)
Intertemporal constriction length v. postorbital width	Long, 49%	Moderate, 40.8%	?	Short, 35%	Very long, 54%
Sternomastoid fossa	Does not ascend nuchal crest	Ascends nuchal crest	,	Does not ascend nuchal crest	,
Inflation of periotic body	Moderately to strongly inflated, 155-175%	Strongly inflated, 162%	Slightly inflated, 140%	Slightly inflated, 133%	?
Posterior process length as % of periotic length	Long, 48.2-50.3% of periotic length	Long, 44.6% of periotic length	Short, 41% of periotic length	Short, 38.5% of periotic length	?
Lateral tuberosity length	Short, does not extend beyond body (except in juvenile)	Long, extends beyond body	Long, extends beyond body	Short, does not extend beyond body	?



Table 2(on next page)

Table 2. Cranial measurements (in mm) of coronodonid specimens reported in this study. 'e' denotes estimated measurement; '+' denotes minimum measurement; measurements for bilateral structures measured from whatever side is best preserved or entered as le



- 1 Table 2. Cranial measurements (in mm) of coronodonid specimens reported in this study. 'e' denotes
- 2 estimated measurement; '+' denotes minimum measurement; measurements for bilateral structures
- 3 measured from whatever side is best preserved or entered as left/right.

	Coronodon havensteini				C. newtoni	C. planifrons	Coronodon- idae indet.
Measurement	CCNHM 8722	ChM PV 4745	CCNHM 108	CCNHM 164	ChM PV 2778	CCNHM 166	CCNHM 8745
Skull length							
without pmx	?	640 e	809	800+	820e	?	?
skull width at							
c1	3	53	118	?	100.6	?	?
skull width at							
p2	80-85e	83.2	169	?	165e	?	?
skull width at							
antorb. notch	?	200e	301	?	312e	?	?
skull width at							
preorb. Proc.	263	265.4	347	335	388e	352	330
Min. interorb.							
width	270	264.6	351	342	402e	349	324
skull width at							
postorb. Proc.	294	294.1	402	406	414e	414	?
skull width at							
zyg. proc.	330e	347	463	457	?	463	?
min intertemp.							
width	40e	66.2	88	86	?	?	65e
Exocc. width	?	258	356	380e	?	358	?
neurocranium height (basiocc. to vertex)	?	147e	237	220	?	249	?
min distance nasals to							
supraocc.	136	132	212	192	3	227	240e
dorsal length parietals (excluding interparietal)	80.9	85	129	130e	?	143	145e
dorsal length	30.0				•		1
of frontals at							
midline	64.9	53.4	70.5	80e	603	87	136.6
ant/post length of parietal/frontal overlap	57	18.7	45.5	?	32.8	63	70
anterior length from	225	221	306/290+	290+	?	330+	280+



orhitotomn		Τ		T			
orbitotemp.							
nuchal crest							
		1					
Max (diagonal) length of							
temporal fossa							
ventral view	169	166	208/210	225/230e	?	250/258	?
	109	100	200/210	223/2308	ŗ	230/236	ŗ
antpost length from							
anteriormost							
postorb ridge							
to post edge							
subtemporal							
crest	180e	139	217/212	?/185e	?	229/234	180-190
length max on	1000	133		1,1000	•	223,23 .	100 130
rostrum	320+	36e	388	?	42.3	?	?
upper		1	7			-	-
toothrow							
length	310+	?	593/595	?	58.5e	?	?
depth palate							
max-pal suture	17e	9.5	16/16	?	11 min	?	?
gap between							
premax. at							
nares	?	?	56.5	?	?	?	?
max width							
bony nares	?	?	67	70-80e	?	77e	?
depth nasals							
ant edge	?	?	4.7/?	8.3/?	?	?/6-7e	6.3
width nasals							
ant edge	?	?	29.5/?	28.6/?	?	33	45
max width							
nasals	45-55e	?	63.6	71e	?	66	25
max length							
nasals	?	?	140	?	?	130e	106.5
width post							
nasals	?	?	33.3	?	?	20e	43
max length							
frontonasal							
suture (if					100		
nasals missing)	59e	53	105e	80	min	83	106.5
min distance							
nasals to							
orbitotemp	24.5	22	22-	24.5	24.4	25	44.6
crest	31e	32	33e	31.5	21.4	35	41.6
width of pmx							
at antorbital	?	?	101.4	104.4	?	06	
notch	:	'	101.4	104.4	۱,	96	22



d/v depth							
preorb	19.7/20.5	25	35.5/41.6	28/29.2	39.9	32.5/33	25.8
d/v depth							
postorb	?/26	29	29.9/33.7	21.9/25.7	34	38.5/42.7	?
expanse of							
frontal							
anterior to							
preorb ridge	33/35	30.6	51/54	49/57	76.5	59/59	48.6
orbit length	75e	88.4	105.7/105	105/105	102.3	108/100.5	80+
depth of em							
pit post to C1	?	?	14/?	?	6.7	?	?
length of em							
pit post to C1	?	?	18/?	?	8	?	?
depth of em							
pit post to P1	?	5	19/14	3	13.5	?	?
length of em							
pit post toPC1	?	11.2	21/18	21	17e	?	?
depth of em							
pit post to p2	?	11.5	8-Oct	?	11.4	3	3
length of em							
pit post to p2	3	16	32/?	29+	17	?	Ś
depth of em							
pit post to p3	?	3.3	16/?	?	?	?	3
length of em							
pit post to p3	?	6.5	35/?	30+	?	?	?
depth of em							
pit post to p4	?	5.5	20/16+	?	?	?	?
length of em							
pit post to p4	?	16	40/40	45	?	?	?
depth of em							
pit post to m1	3	12	25/23	?	?	3	?
length of em							
pit post to m1	3	19	46/48	3	3	3	?
depth of em		_		_	_		_
pit post to m2	3	3	?	?	?	3	?
length of em							
pit post to m2	?	?	?	?	?	?	?
height or orbit							
above lat edge	50	45	60		7.6		
rostrum	58e	45e	60	?	76	?	?
width of							
squamosal lat	20-/24	27	47.2/50.6	442/2	25.	44.2/25	
to exocc	28e/21e	37	47.3/59.6	44.3/?	25e	41.2/35	?
half exoccip	1254	122	174 2/476 2	104]	170	
width	125e	132	174.2/176.3	184	?	179	?
occipital		05	115	111]	111 5	
condyle	?	95	115	111	?	111.5	?



breadth							
condyle depth	?	59.7	78.9	79	?	80e	?
foramen	•	33.7	70.5	73	•	000	•
magnum max							
width	?	41.7	46.4	46.1	?	36e	?
foramen	•	71.7	10.1	40.1		300	•
magnum max							
depth	?	33.4	46	47	?	50	?
depth of	•	33.4	10	77		30	•
squamosal							
fossa	24/24	45.1	48/46	60.1/67e	46.5	52/53	?
squamosal	24/24	45.1	46/40	00.1/076	40.5	32/33	:
fossa to							
supramastoid							
crest	35/35	33	30/26	41/38.6	39	42/38	?
width glenoid	دد ردد	33	30/20	+1/30.0	33	+4/30	:
fossa	54/52	58	70/70	/7778	88.5	77/73	?
postglenoid to	34/32	36	70/70	////0	00.3	11/13	:
1							
zyg apex, ant	?	132	151.0/2	?	151	166/196	?
post plane	ŗ	132	151.9/?	ŗ	151	100/190	ŗ
max width							
single							
basioccipital	?	22.5	F2/F2	44.754	20.4	F4.C/F2.F	2
crest	ſ	32.5	52/52	44+/51	38.4	54.6/53.5	?
max width							
across							
basioccipital							
(lateral edge in cranial hiatus)	?	111.8	190.4	?	?	147.5	?
max width	· ·	111.0	190.4	r 	· ·	147.5	ŗ
across							
basioccipital))	00.6	167.0	150.	2	167.2	3
crests	?	99.6	167.9	150+	?	167.3	?
anto/post							
length from							
anterior							
pterygoid sinus							
to							
subtemporal	?	?/23	39/38e	?	?	?	?
crest	· ·	:/23	35/38E		· ·	· ·	
max length of							
mastoid gap,							
periotic to lat							
edge of	1	10.67	22 2/24 0	22.0/2	25.4	266/40.2	3
squamosal	?	18.6/-	22.3/21.8	22.9/?	35.1	36e/40.3	?
max length	F 4 /50	47	CO- /50	02/02	F.C. 2	76/00	
sternomastoid	54/50	47	60e/58e	82/82	56.3	76/88	?



fossa							
max depth							
sternomastoid							
fossa (to							
lowest point							
supramastoid							
crest)	62/59	46.5	91/85e	76/72	96.9	95/92	?



Table 3(on next page)

Table 3. Periotic measurements (in mm) of *Coronodon* specimens reported in this study. 'e' denotes estimated measurement; '+' denotes minimum measurement; measurements for bilateral structures measured from whatever side is best preserved or entered



- 1 Table 3. Periotic measurements (in mm) of *Coronodon* specimens reported in this study. 'e' denotes
- 2 estimated measurement; '+' denotes minimum measurement; measurements for bilateral structures
- 3 measured from whatever side is best preserved or entered as left/right.

Measurement	Coronodon	havensteini			C. newtoni	C. planifrons
	CCNHM	ChM PV	CCNHM	CCNHM	ChM PV	CCNHM 166
	8722	4745	108	164	2778	
ant/post						
length periotic	?	86.3	91.3/94.6	102.6/?	78.4	102.8/93.7
ant/post						
length						
anterior						
process	25.4	22.5	22.7/22	25e/?	25.8	21.3/22.9
transverse						
width anterior						
process						
midpoint	16.4	17.1	18.1/15.4	23.4/21.9	12.8	19/20.7
dorsoventral						
depth anter.						
Proc. Midpoint	23.8	23.3	27.7/28.1	33.4/?	24	30.9/32.8
distance,						
perilymphatic						
duct to						
fenestra						
rotunda	7	8.3	7.1/4.6	?	5.7	?/8
endolymphatic						
duct to						
fenestra						
rotunda	10.6	9.8	9.3/9.2	?	8.6	?/11.5
max diameter						
of						
perilymphatic						
duct	3.4	6.1	2/2.5	?	3.1	?/3
endolymphatic						
duct max	10.1	8.5	6.4/7.1	?	9.7	?/8.6
endolymphatic						
duct min	3.6	3	2.2/2.3	?	4.1	3.4
fenestra						
rotunda max	5.6	5.8	3.2/3.3	?	5.1	5.8/5.6
fenestra						
rotunda min	3.6	3.3	5.4/5.5	?	3.1	?/4
fenestra ovalis						
max	3.9	4.6	4/3.5	?	4.2	?/4.7
fenestra ovalis						
min	2.8	3	2.8/2.7	?	2.9	?/2.7
length of						
promontorium	25.1	20	24.5/25.6	29e/?	21.1	25.7/24.8



/C		1	I	I	1	
(from fen.						
Rot.)						
greatest						
transverse						
width of pars						
coch medial to						
fen ovalis	12.6	13.7	11.4/11.9	?	11.2	12.4/15.6
IAM ant/post						
(including						
hiatus fall. If						
confluent)	13.5	12.2	25.2/24.1	?	20.1	16e/16.6
IAM						
transverse	9.1	8.2	8.3/7.8	?	8	?/8
post process						
ant/post						
length	?	28.2	37.4/42.4	51.1/?	31	52.6/38.3
post process						-
transverse						
width	?	21.3	32.9/32.8	36.5/35+	22.4	39.5/36.2
antpost			, , , , ,			,
diameter						
mallear fossa	9.5	7.5	7.7/7.7	10.8	8.7	9.3/9.8
dorsoventral	3.3	7.3	,.,,,,	10.0	0.7	3.3/3.0
depth superior						
process above						
IAM	0	0	9.3/5.1	Ş	0	?/5.6
superior	0	0	9.5/5.1	:		:/3.0
process depth						
at						
endolymphatic						
	10.0	4.1	12 6/12 1	2	2.2	2/21.2
duct	10.9	4.1	13.6/12.1	?	3.2	?/21.2
transverse						
width of fossa	2.5	2.7	2 5 /2 7	20/2.2	1.0	2/2
incudis	2.5	2.7	2.5/2.7	3e/3.3	1.9	?/?
distance						
fenestra ovalis						
to fenestra						0 - /- 6
rotunda	5.9	5.26	7.9/7.4	3	5.3	8.5/7.8
distance						
apices of						
anterodorsal						
and						
posterodorsal						
angles	42.3	10.5	40.1/35e	?	45	45.7
transverse						
diameter of						
body lateral to	15.6	16.8	22.9/22.8	28.5/?	17	23.7/22.5



fen ovalis						
transverse						
diameter of						
lateral						
tuberosity						
lateral to fen						
ovalis	20.2	18.7	19.5/18.8	24.9/?	21.5	26.2/24.2



Table 4(on next page)

Table 4. Tympanic bulla measurements (in mm) of coronodonid specimens reported in this study. 'e' denotes estimated measurement; measurements for bilateral structures measured from whatever side is best preserved or entered as left/right.



- 1 Table 4. Tympanic bulla measurements (in mm) of coronodonid specimens reported in this study. 'e'
- 2 denotes estimated measurement; measurements for bilateral structures measured from whatever side
- 3 is best preserved or entered as left/right.

	Coronodon havens	C. newtoni		
	CCNHM 8722	ChM PV 4745	CCNHM 108	ChM PV 2778
greatest length				
bulla	74.9	76.7	83.2/85	79.9
max width of				
bulla at sigmoid				
process	46.7	50.2	50.3/55.6	50.1
greatest depth of				
involucrum	33	31.7	36.5/36.4	35.6
transverse width				
of medial lobe	23.3	30.1	31.8/31.3	34
anteroposterior				
length of				
posterior lobe	?	?	50.4/48.4	46.5
dorsoventral				
depth of bulla at				
level of sigmoid	?	?	62.9/?	58.8



Table 5(on next page)

Table 5. Dental measurements (in mm) of *Coronodon*. 'e' denotes estimated measurement; '+' denotes minimum measurement; measurements for bilateral structures measured from whatever side is best preserved or entered as left/right.



- 1 Table 5. Dental measurements (in mm) of *Coronodon*. 'e' denotes estimated measurement; '+' denotes
- 2 minimum measurement; measurements for bilateral structures measured from whatever side is best
- 3 preserved or entered as left/right.

catalog tooth upper number L		1
	base W base rown	L labial
CCNHM		
C. have. 108 I2 right upper 1 17	7.05 13.6	31
CCNHM		
C. have. 108 P2 right upper 2 35	5.47 14.68	20*
CCNHM		
C. have. 108 P3 left upper 2 50	0.89 15.55	25
CCNHM		
C. have. 108 M2 left upper 2 53	1.4 14.98	24
CCNHM		
C. have. 108 p1 left lower 2 33	3.73 14.87	30
CCNHM		
C. have. 108 p2 left lower 2 52	2.13 16.27	29
CCNHM		
C. have. 108 p3 left lower 2 58	8.17 20.97	30
CCNHM		
C. have. 108 p4 left lower 2 58	8.43 17.93	29
CCNHM		
C. have. 108 m1 left lower 2 57	7.71 18.15	28
CCNHM		
C. have. 108 m2 left lower 2 52	2.21 17.66	29
CCNHM		
C. have. 108 p1 right lower 2 34	4.73 15.04	29
CCNHM		
C. have. 108 p2 right lower 2 52	2.3 16.63	29
CCNHM		
C. have. 108 p3 right lower 2 55	5.86 17.57	28
CCNHM		
C. have. 108 p4 right lower 2 59	9.54 17.79	26*
CCNHM		
C. have. 108 m1 right lower 2 56	6.38 17.91	26*
CCNHM		
C. have. 108 m2 right lower 2 53	3.03 17.03	28
CCNHM		
C. have. 164 p3 left upper 2 49	9.6+ ?	40.5+
CCNHM		
C. have. 164 p3 right upper 2 53	1.61 ?	?
CCNHM		
C. have. 164 p4 left upper 2 52	1.8 15.65	39.44
CCNHM		
C. have. 164 m1 right upper 2 ?	15.5	34.31+
C. have. CCNHM m2 right upper 2 52	2.25 13.11	34.39



	164							
	CCNHM							
C. have.	164	m2	left	upper	2	?	12.7	28+
C. Have.	CCNHM	1112	leit	ирреі		:	12.7	20+
C. have.	164	m3	right	upper	2	?	13.7	40.04
C. Have.	CCNHM	1113	rigit	иррег		•	13.7	40.04
C. have.	164	i1	?	?	1	12.35	9.9	17.9+
C. Have.	CCNHM	1±	•	•	1	12.55	J.J	17.51
C. have.	164	i2	?	?	1	15.19	12.76	21.6
C. Have.	CCNHM	12	•	•	_	13.13	12.70	21.0
C. have.	164	i3	?	?	1	12.24	11.61	21.61+
01 1101 01	CCNHM		•		_			
C. have.	164	p2	right	lower	2	34.91+	14.2	38.49+
	CCNHM	I-	0 -					
C. have.	164	p3	right	lower	2	53.26+	15.61	41.57+
	CCNHM							
C. have.	164	m1-2	right	lower	2	57.41	?	57.32
	CCNHM							
C. have.	164	m2-3	right	lower	2	57.04+	18.16	48.59+
	CCNHM							
C. have.	164	m3	left	lower	2	?	?	42.84+
	CCNHM							
C. have.	164	m4	right	lower	2	45.5+	14.59	38.05+
	CCNHM							
C. plan.	166	i?	?	?	1	18.5	13	25.1
	CCNHM							
C. plan.	166	c1	?	?	1	21.3	14e	27.2
	CCNHM							
C. plan.	166	p1/c1	?	3	1	22.6	13.8	27.3
	CCNHM	_						
C. plan.	166	p3	left	upper	2	51.5+	18.2	41.7
	CCNHM					54.0	47.4	26
C. plan.	166	p3	right	upper	2	51.2	17.1	36+
C	CCNHM	4	1-64			FF 6	16.3	44.5
C. plan.	166 CCNUM	p4	left	upper	2	55.6	16.3	41.5
Calaa	CCNHM	n/ m12	?		1	2	16:	16.
C. plan.	166 CCNHM	p4-m1?	l L	?	2	?	16+	46+
C. plan.	166	m1	right	unner	2	50+	15.9	37+
C. piaii.	CCNHM	1111	IIgIII	upper		JUT	13.3	317
C. plan.	166	m1	left	upper	2	55.2	15.9	35+
C. piaii.	CCNHM	1117	1010	ирреі		33.2	13.3	331
C. plan.	166	m2	left	upper	2	44.7	13.2	27.1+
C. piani	CCNHM		70.0	4666	-	,	15.2	
C. plan.	166	m3	right	upper	2	37.9	13e	20+
2. [2.0	CCNHM				-			
C. plan.	166	p3	right	lower	2	47.6	16.1	?



	CCNHM							
C. plan.	166	m1	left	lower	2	61.5	18.4	46+
	CCNHM							
C. plan.	166	m2	left	lower	2	61.6	18.8	47+
	CCNHM							
C. plan.	166	p3	left	lower	2	?	15.8	?



Table 6(on next page)

Table 6. Mandibular measurements (in mm) of *Coronodon* specimens reported in this study. 'e' denotes estimated measurement; '+' denotes minimum measurement; measurements for bilateral structures measured from whatever side is best preserved or entere



- 1 Table 6. Mandibular measurements (in mm) of *Coronodon* specimens reported in this study. 'e' denotes
- 2 estimated measurement; '+' denotes minimum measurement; measurements for bilateral structures
- 3 measured from whatever side is best preserved or entered as left/right.

	Coronodon havensteini		Coronodon newtoni	Coronodon planifrons
	CCNHM 108	CCNHM 164	ChM PV 2778	CCNHM 166
mandible length	848+/830+	?	700e	?
length lower				
toothrow	562/575	?	620e	?
length mand				
symphysis	?/153	?	180	?
depth at c1	63.0/65.9	?	70.7	?
depth at p4	72/74.1	?/74.9	84.6	78.9
depth at m4	134/129	?/132	129.7	139
max depth at				
coronoid	248/247	?/228	260e	244
trans width at c1	43.4/43.9	?	41	?
width at p4	50.2/51.3	48.2	55.2	52
width at m4	64.2/61.3	3	?	55
condyle width	54.9/49.1	3	60.5	51.6
condyle depth	54.3/54.3	45.6	57.7	55.6
height of				
coronoid above				
condyle	?/110	100.5	115	144
length of neck				
(coronoid-				
condyle gap)	84/86	80	70	64.5



Table 7(on next page)

Table 7. Atlas and axis measurements (in mm) of *Coronodon*. 'e' denotes estimated measurement; '+' denotes minimum measurement.



- 1 Table 7. Atlas and axis measurements (in mm) of Coronodon. 'e' denotes estimated measurement; '+'
- 2 denotes minimum measurement.

	Coronodon haven		Coronodon planifrons	
	ChM PV 4745	CCNHM 108	CCNHM 164	CCNHM 166
atlas vertebra				
max width	143.4	180	?	170+
atlas vertebra				
max depth	111.4	139	?	137.3
atlas ne for max				
width	46.2	49.7	?	49.6
atlas ne for max				
depth	63	66.9	?	64.6
atlas width				
condylar facets	105e	110e	?	128.5
atlas ant post				
length	46.7	64.6/62/2	60e	55.7
Axis, max. width	?	184	?	?
Axis, max. depth	?	135.2	?	3
Axis, max. length				
including				
odontoid	?	52.1	58.5	?



Table 8(on next page)

Table 8. Measurements (in mm) of cervical vertebrae of *Coronodon*. 'e' denotes estimated measurement; '+' denotes minimum measurement.



- 1 Table 8. Measurements (in mm) of cervical vertebrae of Coronodon. 'e' denotes estimated
- 2 measurement; '+' denotes minimum measurement.

	Coronodon havenste	eini	Coronodon planifrons
	CCNHM 108	CCNHM 164	CCNHM 166
C3 anterior width	76	73.6	66.2
C3 anterior depth	58.3	5	?
C3 length	25.2	25	23.1
C4 anterior width	70.2	81.5	77.3
C4 anterior depth	58.9	61.1	62
C4 length	22.7	24	24.1
C5 anterior width	71.4	?	·
C5 anterior depth	57	?	·
C5 length	25.6	?	·
C6 anterior width	74	?	3.
C6 anterior depth	55.1	?	3
C6 length	24.3	?	3
C7 anterior width	74.3	72	69.1
C7 anterior depth	55.4	63.2	62
C7 length	27.7	32.9	31.6



Table 9(on next page)

Table 9. Measurements (in mm) of thoracic vertebrae of *Coronodon*. 'e' denotes estimated measurement; '+' denotes minimum measurement.



- 1 Table 9. Measurements (in mm) of thoracic vertebrae of *Coronodon*. 'e' denotes estimated
- 2 measurement; '+' denotes minimum measurement.

	Coronodon havens	teini	Coronodon planifrons
	CCNHM 108	CCNHM 164	CCNHM 166
T1 anterior width	76e	83.6	86.2
T1 anterior depth	55	55.9	61.2
T1 length	40.7	40.7	40.6
T2 anterior width	89.2	77.5	80.2
T2 anterior depth	54	50.9	57.1
T2 length	46.4	44.1	44.1
T3 anterior width	76e	74.4	?
T3 anterior depth	49.2	53.5	?
T3 length	48.6	52.1	?
T4 anterior width	71.9	75.8	75.2
T4 anterior depth	48.3	55	53.6
T4 length	52.9	55	46.6
T5 anterior width	?	76	80
T5 anterior depth	?	?	55
T5 length	?	59.8	54.6
T6 anterior width	71.3	80.7	79.8
T6 anterior depth	47.3	59	58
T6 length	55e	62.5	58.4
T7 anterior width	71.6	79.1	81.6
T7 anterior depth	48.3	58.2	61
T7 length	62.2	66.5	60.9
T8 anterior width	79	86.4	94
T8 anterior depth	52.3	61.9	62.3
T8 length	62.7	10.2	64.4
T9 anterior width	?	86.6	95e
T9 anterior depth	?	32.1	65.7



Table 10(on next page)

Table 10. Measurements (in mm) of lumbar vertebrae of *Coronodon*. 'e' denotes estimated measurement; '+' denotes minimum measurement. Vertebral positions for CCNHM 164 are approximate.



- 1 Table 10. Measurements (in mm) of lumbar vertebrae of Coronodon. 'e' denotes estimated
- 2 measurement; '+' denotes minimum measurement. Vertebral positions for CCNHM 164 are
- 3 approximate.

	Coronodon havensteini, CCNHM	Coronodon planifrons, CCNHM 166
L1 anterior width	104	?
L1 anterior depth		65.9
L1 length		77.4
L2 anterior width		90
L2 anterior depth		3
L2 length		88.6
L3 anterior width		93.2
L3 anterior depth		79.8
L3 length		?
L4 anterior width	90e	94.3
L4 anterior depth	78.8	83.8
L4 length	95.6	94.2
L5 anterior width		94
L5 anterior depth		84.7
L5 length		94.8
L6 anterior width		94.2
L6 anterior depth		86.7
L6 length		95.8
L7 anterior width		98
L7 anterior depth		91
L7 length		94.9
L8 anterior width	94.5	101.2
L8 anterior depth	89	91.1
L8 length	95.3	94.2
L9 anterior width	90e	103
L9 anterior depth	96.8	91.4
L9 length	100.5	93.7
L10 anterior width		100
L10 anterior depth		95.2
L10 length		92.3



Table 11(on next page)

Table 11. Measurements (in mm) of caudal vertebrae of *Coronodon planifrons*. 'e' denotes estimated measurement; '+' denotes minimum measurement. Vertebral positions for CCNHM 164 are approximate.



- Table 11. Measurements (in mm) of caudal vertebrae of *Coronodon planifrons*. 'e' denotes estimated
- 2 measurement; '+' denotes minimum measurement. Vertebral positions for CCNHM 164 are
- 3 approximate.

Measurement	Coronodon planifrons, CCNHM 166	
Ca1 anterior width	101.5	
Ca1 anterior depth	94.8	
Ca1 length	90.3	
Ca2 anterior width	95.6	
Ca2 anterior depth	95.5	
Ca2 length	89.3	
Ca3 anterior width	103.4	
Ca3 anterior depth	96.2	
Ca3 length	88.7	
Ca4 anterior width	100.4	
Ca4 anterior depth	97.4	
Ca4 length	86.3	
Ca5 anterior width	98.9	
Ca5 anterior depth	98.2	
Ca5 length	83.6	
Ca6 anterior width	95.2	
Ca6 anterior depth	98.9	
Ca6 length	82.6	
Ca8 anterior width	94.5	
Ca8 anterior depth	98	
Ca8 length	76.3	
CaC anterior width	73.4	
CaC anterior depth	78.1	
CaC length	47.1	
CaD anterior width	64.3	
CaD anterior depth	59	
CaD length	34	